Methods in Molecular Biology 1372

Springer Protocols

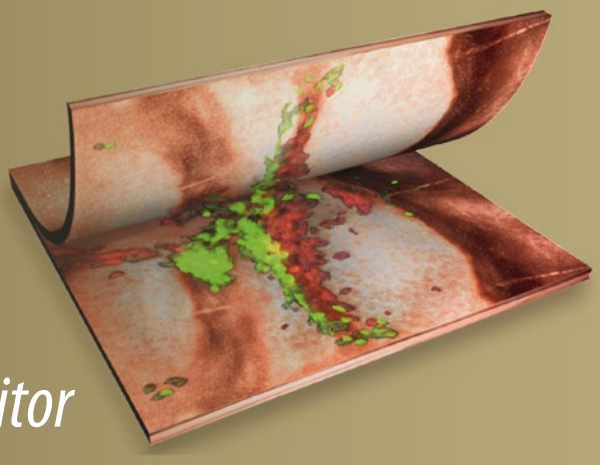

Zdravka Medarova *Editor*

RNA Imaging

Methods and Protocols

Humana Press

METHODS IN MOLECULAR BIOLOGY

Series Editor
John M. Walker
School of Life and Medical Sciences
University of Hertfordshire
Hatfield, Hertfordshire, AL10 9AB, UK

For further volumes:
http://www.springer.com/series/7651

RNA Imaging

Methods and Protocols

Edited by

Zdravka Medarova

Molecular Imaging Laboratory, MGH/MIT/HMS Athinoula A. Martinos Center for Biomedical Imaging, Massachusetts General Hospital and Harvard Medical School, Charlestown, MA, USA; Department of Radiology, Massachusetts General Hospital and Harvard Medical School, Charlestown, MA, USA

Humana Press

Editor
Zdravka Medarova
Molecular Imaging Laboratory, MGH/MIT/HMS
Athinoula A. Martinos Center for Biomedical Imaging
Massachusetts General Hospital
and Harvard Medical School
Charlestown, MA, USA

Department of Radiology
Massachusetts General Hospital
and Harvard Medical School
Charlestown, MA, USA

ISSN 1064-3745 ISSN 1940-6029 (electronic)
Methods in Molecular Biology
ISBN 978-1-4939-3147-7 ISBN 978-1-4939-3148-4 (eBook)
DOI 10.1007/978-1-4939-3148-4

Library of Congress Control Number: 2015955553

Springer New York Heidelberg Dordrecht London

Printed on acid-free paper

Humana Press is a brand of Springer
Springer Science+Business Media LLC New York is part of Springer Science+Business Media (www.springer.com)

Preface

This book is intended for physicians, scientists, and graduate students who are either new to the field of RNA-based imaging and its associated therapeutic applications or who wish to be apprised of recent advances in the state of the art.

This volume will focus on the phenomenon of RNA interference. RNA interference (RNAi) is a normal endogenous cellular mechanism for posttranscriptional regulation of gene expression in which double-stranded ribonucleic acid inhibits the expression of genes with complementary nucleotide sequences. Its potential as a tool for therapy is unlimited, considering that one can use this mechanism to modulate the expression of virtually any gene.

RNAi is mediated by small noncoding RNA molecules that are either endogenous to the cell (microRNA, miRNA) or introduced exogenously (small interfering RNA, siRNA). miRNA is positioned at the center of gene regulatory networks. A single miRNA can influence the expression of multiple gene targets. Consequently, miRNA reprogramming using inhibitory oligonucleotides or miRNA mimics can be a very powerful tool for the "normalization" of cellular phenotype and eliminating pathology. By contrast, siRNA can be designed to inhibit a given gene with single-nucleotide specificity. As such, siRNA delivers the capability of "correcting" the levels of individual proteins that predispose to disease.

An essential element in the development and optimization of these therapies is the ability to measure the bioavailability and functionality of the RNA/oligonucleotide molecule after administration into the body. Noninvasive imaging provides the necessary set of tools to accomplish this in authentic physiologic environments and across time. This book focuses on providing comprehensive coverage of various techniques for in vivo micro/siRNA imaging including the design and synthesis of specific imaging agents and tools, the development of imaging methodologies, and their interpretation.

Charlestown, MA, USA *Zdravka Medarova*

Contents

Contributors

Yukihiko Aramaki • *Department of Drug Delivery and Molecular Biopharmaceutics, School of Pharmacy, Tokyo University of Pharmacy and Life Sciences, Tokyo, Japan*

Mustafa Balcioglu • *Department of Chemistry, University at Albany, SUNY, Albany, NY, USA*

Patrick Baril • *Centre de Biophysique Moléculaire, CNRS UPR4301, Université d'Orléans France, Orléans, France*

Iwan Beuvink • *Novartis Institutes for Biomedical Research (NIBR), Novartis Pharma AG, Basel, Switzerland*

Zaver M. Bhujwalla • *Division of Cancer Imaging Research, The Russell H. Morgan Department of Radiology and Radiological Science, The Johns Hopkins University School of Medicine, Baltimore, MD, USA; Sidney Kimmel Comprehensive Cancer Center, The Johns Hopkins University School of Medicine, Baltimore, MD, USA*

Swati Biswas • *Center for Pharmaceutical Biotechnology and Nanomedicine, School of Pharmacy, Bouve College of Health Sciences, Northeastern University, Boston, MA, USA; Department of Pharmaceutical Sciences, School of Pharmacy, Bouve College of Health Sciences, Northeastern University, Boston, MA, USA*

Julien A. Boos • *Novartis Institutes for Biomedical Research (NIBR), Novartis Pharma AG, Basel, Switzerland*

Frances L. Byrne • *School of Biotechnology and Biomolecular Sciences, University of New South Wales, Sydney, NSW, Australia*

Wei Chen • *Department of Surgery, Emory University School of Medicine, Atlanta, GA, USA; Department of Gastrointestinal Surgery, First Affiliated Hospital of Sun Yat-Sen University, Guangzhou, China*

Zhihang Chen • *Division of Cancer Imaging Research, The Russell H. Morgan Department of Radiology and Radiological Science, The Johns Hopkins University School of Medicine, Baltimore, MD, USA*

Christopher H. Contag • *Molecular Imaging Program at Stanford (MIPS), Stanford University School of Medicine, Stanford, CA, USA; Department of Pediatrics, Stanford University School of Medicine, Stanford, CA, USA; Department of Radiology, Stanford University School of Medicine, Stanford, CA, USA; Department of Microbiology and Immunology, Stanford University School of Medicine, Stanford, CA, USA*

Yoko Endo-Takahashi • *Department of Drug Delivery and Molecular Biopharmaceutics, School of Pharmacy, Tokyo University of Pharmacy and Life Sciences, Tokyo, Japan*

Manuel A. Flores • *TransDerm Inc., Santa Cruz, CA, USA*

Muriel Golzio • *IPBS (Institut de Pharmacologie et de Biologie Structurale), CNRS, Toulouse, France; IPBS (Institut de Pharmacologie et de Biologie Structurale), Université de Toulouse and UPS (Université Paul Sabatier), Toulouse, France*

Emilio González-González • *Canvax Biotech S.L., Cordoba, Spain*

Robyn P. Hickerson • *Centre for Dermatology and Genetic Medicine, University of Dundee, Dundee, UK*

Steven Jones • *Department of Oncology, Wayne State University School of Medicine, Detroit, MI, USA*

Roger L. Kaspar • *TransDerm Inc., Santa Cruz, CA, USA*
Maria Kavallaris • *Tumour Biology and Targeting Program, Children's Cancer Institute, Lowy Cancer Research Centre, University of New South Wales, Randwick, NSW, Australia; ARC Centre of Excellence in Convergent Bio-Nano Science, Australian Centre for Nanomedicine, University of New South Wales, Randwick, NSW, Australia*
Amol Kavishwar • *Molecular Imaging Laboratory, MGH/MIT/HMS Athinoula A. Martinos Center for Biomedical Imaging, Department of Radiology, Massachusetts General Hospital, Harvard Medical School, Charlestown, MA, USA*
Soonhag Kim • *Institute for Bio-Medical Convergence, College of Medicine, Catholic Kwandong University, Gangneung-si, Gangwon-do, Republic of Korea; Catholic Kwandong University International St. Mary's Hospital, Incheon Metropolitan City, Republic of Korea*
Balaji Krishnamachary • *Division of Cancer Imaging Research, The Russell H. Morgan Department of Radiology and Radiological Science, The Johns Hopkins University School of Medicine, Baltimore, MD, USA*
Fernando Lecanda • *Division of Oncology, Adhesion and Metastasis Laboratory, Center for Applied Medical Research (CIMA), University of Navarra, Pamplona, Spain; IdiSNA, Navarra Institute for Health Research, Pamplona, Spain*
Jonghwan Lee • *Institute for Bio-Medical Convergence, College of Medicine, Catholic Kwandong University, Gangneung-si, Gangwon-do, Republic of Korea; Catholic Kwandong University International St. Mary's Hospital, Incheon Metropolitan City, Republic of Korea*
Seung Koo Lee • *Department of Radiology, Molecular Imaging Innovations Institute, Weill Cornell Medical College, New York, NY, USA*
Kazuo Maruyama • *Laboratory of Drug and Gene Delivery Research, Faculty of Pharma-Sciences, Teikyo University, Tokyo, Japan*
Joshua A. McCarroll • *Tumour Biology and Targeting Program, Children's Cancer Institute, Lowy Cancer Research Centre, University of New South Wales, Randwick, NSW, Australia; ARC Centre of Excellence in Convergent Bio-Nano Science, Australian Centre for Nanomedicine, University of New South Wales, Randwick, NSW, Australia*
Zdravka Medarova • *Molecular Imaging Laboratory, MGH/MIT/HMS Athinoula A. Martinos Center for Biomedical Imaging, Massachusetts General Hospital and Harvard Medical School, Charlestown, MA, USA; Department of Radiology, Massachusetts General Hospital and Harvard Medical School, Charlestown, MA, USA*
Olivia Merkel • *Department of Oncology, Wayne State University School of Medicine, Detroit, MI, USA; Department of Pharmaceutical Sciences, Eugene Applebaum College of Pharmacy and Health Sciences, Wayne State University, Detroit, MI, USA*
Leonard M. Milstone • *Department of Dermatology, Yale University School of Medicine, New Haven, CT, USA*
Anna Moore • *Molecular Imaging Laboratory, MGH/MIT/HMS Athinoula A. Martinos Center for Biomedical Imaging, Massachusetts General Hospital, Harvard Medical School, Charlestown, MA, USA; Department of Radiology, Massachusetts General Hospital, Harvard Medical School, Charlestown, MA, USA*
Noriko Mori • *Division of Cancer Imaging Research, The Russell H. Morgan Department of Radiology and Radiological Science, The Johns Hopkins University School of Medicine, Baltimore, MD, USA*
Yoichi Negishi • *Department of Drug Delivery and Molecular Biopharmaceutics, School of Pharmacy, Tokyo University of Pharmacy and Life Sciences, Tokyo, Japan*

Niravkumar R. Patel • *Center for Pharmaceutical Biotechnology and Nanomedicine, School of Pharmacy, Bouve College of Health Sciences, Northeastern University, Boston, MA, USA; Department of Pharmaceutical Sciences, School of Pharmacy, Bouve College of Health Sciences, Northeastern University, Boston, MA, USA*

Marie-France Penet • *Division of Cancer Imaging Research, The Russell H. Morgan Department of Radiology and Radiological Science, The Johns Hopkins University School of Medicine, Baltimore, MD, USA; Sidney Kimmel Comprehensive Cancer Center, The Johns Hopkins University School of Medicine, Baltimore, MD, USA*

Federico Perche • *Center for Pharmaceutical Biotechnology and Nanomedicine, School of Pharmacy, Bouve College of Health Sciences, Northeastern University, Boston, MA, USA; Department of Pharmaceutical Sciences, School of Pharmacy, Bouve College of Health Sciences, Northeastern University, Boston, MA, USA*

Chantal Pichon • *Centre de Biophysique Moléculaire, CNRS UPR4301, Université d'Orléans France, Orléans, France*

Faye A. Rogers • *Department of Therapeutic Radiology, Yale University School of Medicine, New Haven, CT, USA*

Tycho P. Speaker • *TransDerm Inc., Santa Cruz, CA, USA*

Ryo Suzuki • *Laboratory of Drug and Gene Delivery Research, Faculty of Pharma-Sciences, Teikyo University, Tokyo, Japan*

Justin Teissié • *IPBS (Institut de Pharmacologie et de Biologie Structurale), CNRS, Toulouse, France; IPBS (Institut de Pharmacologie et de Biologie Structurale), Université de Toulouse and UPS (Université Paul Sabatier), Toulouse, France*

Vladimir P. Torchilin • *Center for Pharmaceutical Biotechnology and Nanomedicine, School of Pharmacy, Bouve College of Health Sciences, Northeastern University, Boston, MA, USA; Department of Pharmaceutical Sciences, School of Pharmacy, Bouve College of Health Sciences, Northeastern University, Boston, MA, USA*

Ching-Hsuan Tung • *Department of Radiology, Molecular Imaging Innovations Institute, Weill Cornell Medical College, New York, NY, USA*

Karmele Valencia • *Division of Oncology, Adhesion and Metastasis Laboratory, Center for Applied Medical Research (CIMA), University of Navarra, Pamplona, Spain*

Ping Wang • *Molecular Imaging Laboratory, MGH/MIT/HMS Athinoula A. Martinos Center for Biomedical Imaging, Harvard Medical School, Charlestown, MA, USA; Department of Radiology, Massachusetts General Hospital, Harvard Medical School, Charlestown, MA, USA*

Lily Yang • *Department of Surgery, Emory University School of Medicine, Atlanta, GA, USA*

Mehmet V. Yigit • *Department of Chemistry, University at Albany, SUNY, Albany, NY, USA; The RNA Institute, University at Albany, SUNY, Albany, NY, USA*

Chapter 1

Imaging Functional Nucleic Acid Delivery to Skin

Roger L. Kaspar, Robyn P. Hickerson, Emilio González-González, Manuel A. Flores, Tycho P. Speaker, Faye A. Rogers, Leonard M. Milstone, and Christopher H. Contag

Abstract

Monogenic skin diseases arise from well-defined single gene mutations, and in some cases a single point mutation. As the target cells are superficial, these diseases are ideally suited for treatment by nucleic acid-based therapies as well as monitoring through a variety of noninvasive imaging technologies. Despite the accessibility of the skin, there remain formidable barriers for functional delivery of nucleic acids to the target cells within the dermis and epidermis. These barriers include the stratum corneum and the layered structure of the skin, as well as more locally, the cellular, endosomal and nuclear membranes. A wide range of technologies for traversing these barriers has been described and moderate success has been reported for several approaches. The lessons learned from these studies include the need for combinations of approaches to facilitate nucleic acid delivery across these skin barriers and then functional delivery across the cellular and nuclear membranes for expression (e.g., reporter genes, DNA oligonucleotides or shRNA) or into the cytoplasm for regulation (e.g., siRNA, miRNA, antisense oligos). The tools for topical delivery that have been evaluated include chemical, physical and electrical methods, and the development and testing of each of these approaches has been greatly enabled by imaging tools. These techniques allow delivery and real time monitoring of reporter genes, therapeutic nucleic acids and also triplex nucleic acids for gene editing. Optical imaging is comprised of a number of modalities based on properties of light-tissue interaction (e.g., scattering, autofluorescence, and reflectance), the interaction of light with specific molecules (e.g., absorbtion, fluorescence), or enzymatic reactions that produce light (bioluminescence). Optical imaging technologies operate over a range of scales from macroscopic to microscopic and if necessary, nanoscopic, and thus can be used to assess nucleic acid delivery to organs, regions, cells and even subcellular structures. Here we describe the animal models, reporter genes, imaging approaches and general strategies for delivery of nucleic acids to cells in the skin for local expression (e.g., plasmid DNA) or gene silencing (e.g., siRNA) with the intent of developing nucleic acid-based therapies to treat diseases of the skin.

Key words siRNA, Topical delivery, Nucleic acid, Skin, Monogenic, Pachyonychia congenita, Optical imaging, Biophotonic, Bioluminescence, Fluorescence, Keratin, GFP, Genetherapy

1 Introduction

Delivery of nucleic acids to cells in culture has been routine in biology laboratories for over 30 years, and has enabled thorough studies of gene expression and regulation in single cells and in

Zdravka Medarova (ed.), *RNA Imaging: Methods and Protocols*, Methods in Molecular Biology, vol. 1372,
DOI 10.1007/978-1-4939-3148-4_1,

populations of cultured cells. These delivery tools have been modified, and in some cases optimized, for delivery of specific lengths, or composition, of nucleic acids even to primary cells taken directly from animals or humans. Nucleic acid transfer to cells can be accomplished by physical methods (e.g., electroporation, microinjection, ultrasound, and laserfection) that transiently compromise the barriers, or via chemical methods that integrate nucleic acid such as incorporation into liposomes, nanoparticles, cationic polymers, dendrimers, and magnetic beads. Alternatively, chemical modifications of the nucleic acid that create self-delivery nucleic acids, or viral vectors that target cells of the skin, could be used. Physical methods may be needed to overcome the tissue barriers and it may be necessary to combine methods to both cross the tissue barriers and traverse cellular membranes [1]. Self-delivery nucleic acids have been described that confer reasonable cellular uptake in the absence of transfection reagents in cultured cells [2]. Yet nucleic acid transfer to cells in the complex environments of tissues and organs has not been as facile, and the broad potential of using nucleic acids to treat human disease is still in its infancy. Naturally occurring physical and biochemical barriers have been selected through evolution to prevent transfer of genetic material from the environment into the organs, tissues and cells of our bodies, and these comprise the primary challenge to the effective development of nucleic acid-based therapies to treat human disease.

Among the diseases that could be treated with nucleic acids, monogenic skin diseases offer unique opportunities to develop new tools with potential for clinical impact [3–5]. The skin is an accessible organ and the single gene target in monogenic diseases simplifies the requirements for the therapeutic nucleic acid [6]. We have been developing nucleic acid therapeutics to treat the rare inherited skin disease, pachyonychia congenita (PC) [4, 7]. This keratinization disorder is a result of dominant mutations, including single nucleotide changes, in one of the inducible keratin genes, resulting in aberrant intermediate filament formation. The dominant nature of the mutation, coupled with the apparent redundancy of keratins (i.e., selective inhibition of the mutant keratin preserves wild type expression and the lowered amount can be compensated by other keratins [8, 9]) and the apparent ability to achieve a therapeutic effect when only 50 % inhibition of mutant keratin expression achieved [10, 11], make this and similar keratin disorders ideal for siRNA therapeutics. However, our experience confirms that of others, that it is extremely difficult to get biologically active nucleic acids into epidermal cells at therapeutically relevant levels.

Nucleic acid–based vaccines have been developed using skin delivery and are being considered for clinical use [12–14]. Moreover, the fact that there is an amplification through transcription and translation and potentially more engagement of the immune

response through the frontline skin immune defenses including Langerhans and dendritic cells, this application tolerates inefficient delivery. Delivery of therapeutically relevant levels of siRNA to a significant number of cells in the skin presents significant challenges over what can be done with nucleic acid based vaccines. We have demonstrated effective gene silencing of the keratin target gene in cultured cells, human skin equivalents and also in a limited clinical study using multiple injections into affected areas of the foot [2, 4, 7]. The fact that we observed partial resolution of the PC lesion injected with mutant-specific siRNA suggests that injections do deliver nucleic acids to epidermal cells and indicates that skin delivery is feasible; however, the injections are inefficient and the delivery is likely facilitated by the pressure generated, exacerbating the associated pain to a clinically unacceptable level [15]. We have attempted to overcome this obstacle using a variety of delivery tools and comparing and combining delivery technologies in mouse models. Here we summarize the lessons learned and the advances to date. Despite the advances by us and many others in this field, nucleic acid delivery remains a major hurdle to the development of effective nucleic acid therapeutics for skin.

We reasoned that we could further advance this field by developing and using imaging technologies that would enable visualization of delivery of the therapeutic, or mimics of the therapeutic, as a means of improving nucleic acid transfer. We further reasoned that if we linked the therapeutic target to expression of optical reporter genes, we could also visualize effective, and in many cases ineffective, delivery of the therapeutic nucleic acid to the target cells in the skin [16]. Here we summarize these technologies as well as the imaging tools available for assessing nucleic acid delivery with a focus on the skin applications.

1.1 Problem and Possible Solution: Monogenic Skin Diseases and siRNA as a Therapeutic Strategy

Pachyonychia congenita is a dominant negative monogenic skin disorder caused by mutations, including single nucleotide mutations, in the inducible keratin genes encoding K6a, K6b, K16, and K17, resulting in dystrophic nails and exquisitely painful palmoplantar keratoderma [17, 18]. An siRNA has been developed that has the ability to target the K6a N171K single nt mutation with little or no effect on wild type expression [3, 7]. This siRNA has been successfully evaluated in a small clinical trial in which injected siRNA resulted in localized keratoderma clearing and reduction of pain [4]. Unfortunately, the mode of administration, intralesional injection, was unacceptably painful and required oral pain medications and a regional pain block. PC is one of many rare dominant negative skin disorders with unmet clinical needs (largely due to small patient populations and the reluctance of the pharmaceutical industry to develop small molecule inhibitors for small markets) [19], which could benefit from development of a patient-friendly siRNA delivery platform. Specific and potent siRNA agents are the most promising therapeutics for this class of skin disorders [3].

1.2 Imaging Nucleic Acid Delivery and Function to Accelerate Development of Therapeutics

Given the large number of variables associated with effective delivery of functional nucleic acids to the skin, tools that enable visualization of each step in the process would have tremendous benefit in the optimization process. Therefore, we have spent time developing, and using, tools to enable imaging delivery of the therapeutic, assessing distribution in the tissue and determining the effects on the genetic target. These tools are largely based on imaging of optically active dyes and proteins over a range of scales from macroscopic to microscopic imaging (Table 1). Optical imaging offers the potential to multiplex the analysis such that the therapeutic can be imaged with one optical signature and the expression of the target gene with a separate optical feature. The devices are typically able to collect a reference image of the anatomy—either macroscopic or microscopic—and an image of the optical marker can be superimposed on this image for reference. Since the background is typically shown in black and white we refer to these images as grayscale reference images.

In vivo bioluminescence imaging was developed for the purpose of enabling the study of biological processes in the context of organs and tissues of living subjects where the contextual influences remain intact and has been applied to imaging of infection, cancer, stem cell biology and many other biological processes [25]. The basis of this preclinical imaging modality is a class of light emitting enzymes call luciferases that are used as reporters of biological function [25]. In vivo bioluminescence imaging has been used to assess nucleic acid delivery to many different organ systems in small animal models. Optical imaging tools can image over a range of scales such that nucleic acid delivery can be assessed at the level of the organ or the cell in vivo and then validated using the

Table 1
In vivo optical imaging tools to assess gene delivery to skin

	Mode(s)	Imaging scale	Status of clinical approval	References
Cell-vizio	Fluorescence	Microscopic	Approved for GI and in clinical use	[20]
Dual-axis microscope	Fluorescence	Microscopic	Tested in humans for GI cancer and in dermatology	[21]
Caliber ID VivaScope	Fluorescence and reflectance	Microscopic	In clinical use in dermatology	[16, 22, 23]
Dermatoscope	Fluorescence, polarized light, and reflectance	Microscopic	In clinical use in dermatology	[24]
IVIS	Wide-field fluorescence and bioluminescence	Macroscopic	Preclinical device for a variety of organ systems	[5, 7, 9]

same optical tags in excised organs. Once excised, the tissue can be subjected to a multitude of imaging and molecular assays to validate the in vivo image and multiplex the analysis.

There are a number of architectures of confocal microscopes that vary with illumination and collection paths (Fig. 1) and one of these uses a dual axis architecture that increases signal to noise and

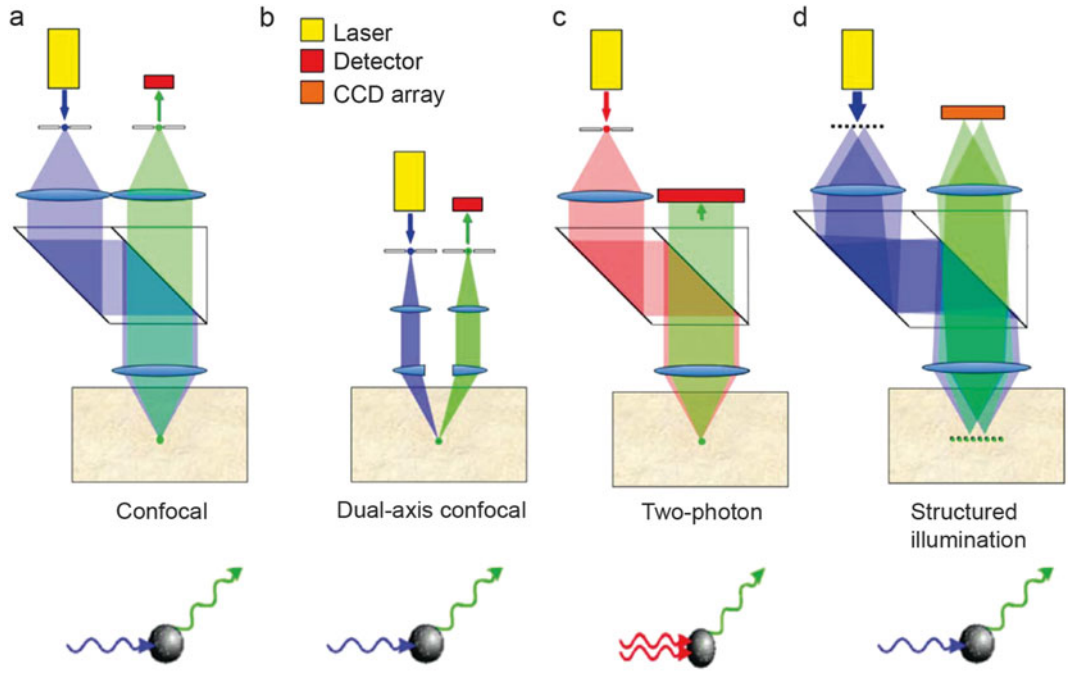

Fig. 1 Microscope designs. (**a**) The conventional confocal microscope, using a high-NA (0.8–1.4) objective and two pinholes to provide a point source and point detector (figure and text from Liu et al. [57, 58]). Images are collected by scanning the focal spot within the specimen in either reflectance or fluorescence (shown) modes. Excitation light (*blue*) is absorbed by the fluorescent molecules in the specimen and fluorescence emission (*green*) is collected by the point detector. (**b**) The dual-axis confocal microscope, using two low-NA (0.1–0.2) objective lenses and two pinholes to provide a point source and point detector. The excitation (*blue*) and emission (*green*) beams are spatially separated within the specimen, except where they overlap at the focus. (**c**) The multiphoton microscope using a high-NA (0.8–1.4) objective and a single pinhole to provide a point source. The *red* beam represents the long-wavelength excitation light (high-peak-power pulsed laser), which is nonlinearly absorbed by the fluorescent molecules in the specimen. The efficiency of two-photon absorption, for example, scales as the square of the intensity of the light, and is therefore confined to just the focus of the excitation beam. The *green* beam represents the shorter-wavelength fluorescence emission light collected by a large area detector. (**d**) The structured illumination microscope can be used to gather full-field (single-shot) 2-D images by a photodetector array (CCD) in either reflectance or fluorescence (shown) modes. The images are quasi-optically sectioned due to the fact that the structured pattern is only imaged with high contrast at the focal plane within the specimen. By spatially modulating the illumination pattern, out-of-focus (low-contrast) light may be distinguished from, and digitally filtered away from the in-focus light that is modulated with high contrast. The multiple *blue* beams represent a pattern of excitation light beams emanating from a structured light source, which is absorbed by the fluorescent molecules in the specimen. The respective green beams represent the fluorescence emission light collected by the CCD

enables radical miniaturization [26–29]. Handheld microscopes of this type were used to assess effective delivery of siRNA to the skin of mice and humans [21, 30]. The core of these miniature microscopes are microelectromechanical systems (MEMS) scanners [31] that can enable 2-D *en face* imaging at four frames per second. Three-dimensional images can also be acquired by translating the MEMS scanner in the depth direction with a piezoelectric actuator to sequentially save image stacks. This tool was initially developed for imaging in the gastrointestinal tract [32], but its potential in dermatology was recognized early in its development [26].

1.3 In Vivo Microscopy with the VivaScope 2500

The VivaScope is based on a standard confocal architecture but has been designed for in vivo use—both clinical and preclinical versions are available. Anesthetized mice can be analyzed with a modified Caliber ID VivaScope 2500 [22, 33] that has been upgraded for dual fluorescence capabilities with a blue (488 nm) and a post-manufacture addition of a green (532 nm) laser [16, 34] (Fig. 1). Briefly, *z*-stacks of images are acquired at successive 1.6 μm *z*-depths using native VivaScan software (v. VS008.01.09) and post-processed using public domain Fiji java-based image processing software [35]. Reflectance images are acquired using the 658 nm laser source with an "open" emission window. Sequential fluorescent images can be acquired using the 488 nm and 532 nm excitation laser and with the 531 and 607 nm emission filters, respectively. Figure 2 shows an example of visualizing EGFP and tdTFP following delivery of EGFP and tdTFP expression plasmids to mouse footpad skin. To increase the effective resolution of the VivaScope images, ten nominal images can be taken at each *z*-step and averaged to produce a more refined image. Because in vivo imaging is influenced by respiration and other minor subject motion, successive frames can be co-registered using an affine transform [36] (distributed with Fiji software as the StackReg plugin) prior to any frame-averaging. Images can be further intensity-scaled to maximize contrast with the Fiji software.

1.4 Evaluating siRNA Therapeutics Using Transgenic Reporter Mice with Optical Readouts

There was a need to develop a transgenic reporter mouse to enable in vivo bioluminescence imaging and fluorescence imaging of effective delivery of functional siRNA to cells in the skin along with the tools to look at the tissue microstructure (Figs. 3 and 4). The reporter transgenes in these animals were used to visualize gene silencing. To generate such a mouse, we crossed a Cre-expressing transgenic mouse with a multifunctional reporter mouse [33]. The construct in the multifunctional reporter mouse consisted of a click beetle luciferase and GFP gene fusion (CBL/hMGFP) cassette from the pCBL/hMGFP vector inserted downstream of Renilla luciferase (rLuc), with the two genes separated by a strong translation stop sequence in the following order, loxP-rLuc-stop-loxP-CBL-hMGFP. This construct, called RLG, was used to

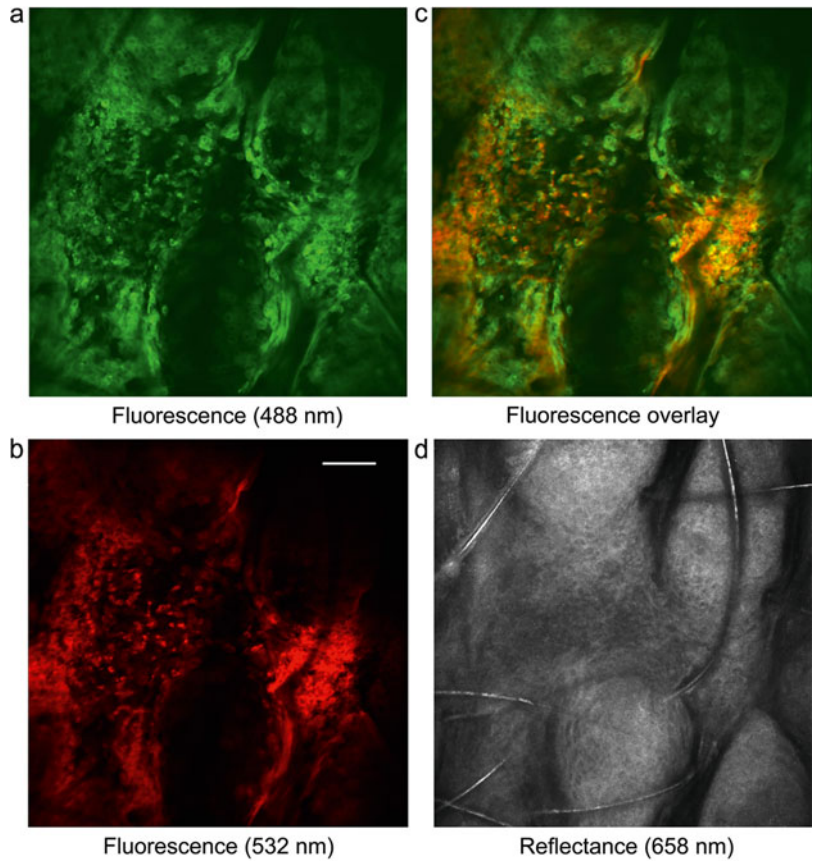

Fig. 2 Noninvasive subcellular imaging of EGFP and tdTFP expression in mouse footpad. EGFP/wt K6a (pTD241) and tdTFP/mut K6a (pTD203) UBC promoter expression plasmids (11 μg of each) were co-injected intradermally into a mouse footpad. At 36 h after injection, the footpad of the living mouse was noninvasively imaged for fluorescence using a modified Caliber ID VivaScope 2500 using 488 nm (EGFP, panel (**a**)) and 532 nm (tdTFP, panel (**b**) as well as overlay, panel (**c**)) lasers as well as with a 658 nm laser (reflectance) to determine depth and general skin structure (panel (**d**)). A z-stack of images (1.6 μM intervals) was acquired sequentially with each laser. The selected images shown from the z-stack are at 50-μm depth. Scale bar = 100 μM. A similar imaging procedure with keratin 6a (mutant and wild type)/reporter expression plasmids was used to noninvasively monitor the functional delivery and effectiveness of an siRNA specific to the keratin 6a N171K mutation that causes pachyonychia congenita [16]. Note the absence of EGFP expression in the nuclei

generate the transgenic skin reporter mouse using standard methods of pronuclear injection. The RLG transgene contains the CAG (CMV enhancer-chick β-actin) promoter [37], the coding sequence of rLuc (flanked by loxP sites) and the coding sequence of CBL fused to hMGFP. This transgenic mouse was crossed with a Tg(Krt14-cre)1Amc transgenic mouse (The Jackson Laboratory, Bar Harbor, ME) expressing Cre recombinase driven by the keratinocyte-specific K14 promoter with the intent of generating a mouse with the fusion reporter, CBL-hMGFP, expressed in keratinocytes. The use of a gene fusion containing a luciferase (CBL)

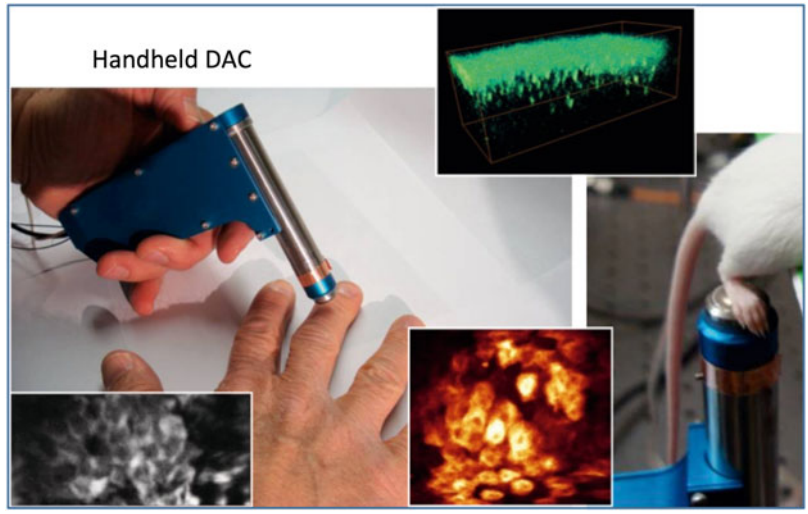

Fig. 3 DAC microscope imaging of the skin. One version of the DAC microscope is a hand-held device designed for skin imaging, and it has been used for imaging the effects of siRNA on GFP expression in the skin [21] and to image skin microanatomy. Stepping in the *z* direction is done with a piezo motor in the handle of the microscope and the *x*–*y* scan is performed with a MEMS scan mirror. The histology images are of human skin (*lower left*), GFP expression (*upper right*), and mouse skin (*lower right*)

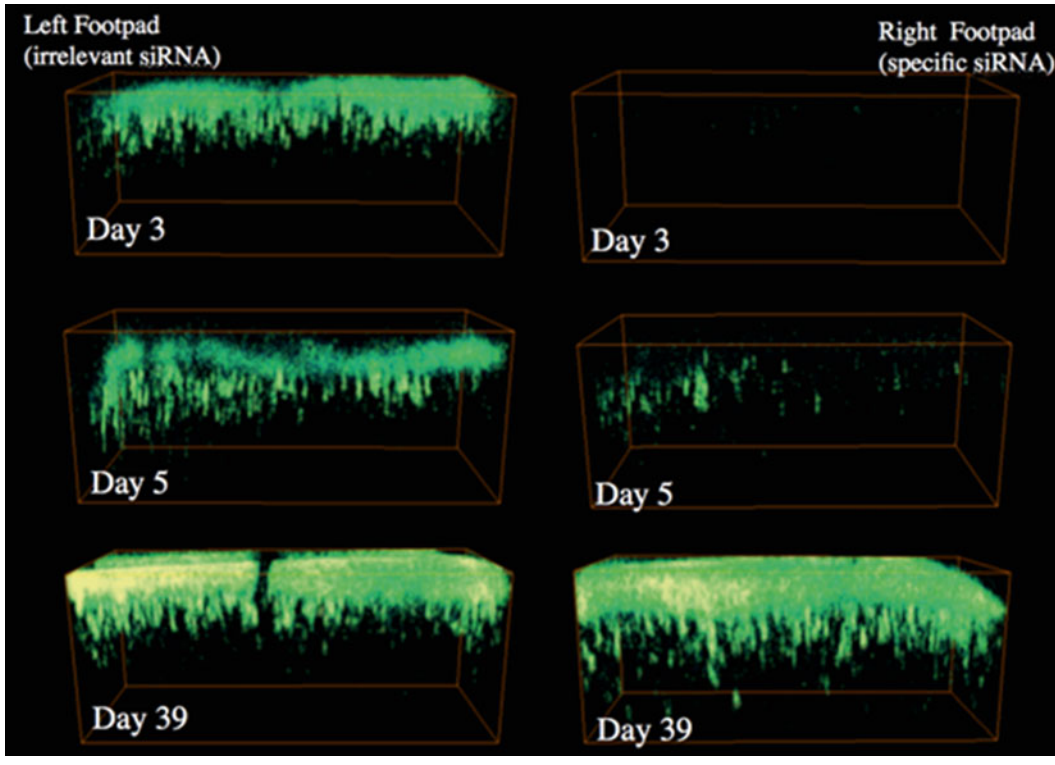

Fig. 4 Visualizing the effects of siRNA on GFP expression in the skin. Transgenic reporter mice were treated with either irrelevant siRNA (*left*) or siRNA directed at the GFP transcript (*right*) and imaged over time using a DAC microscope. The specific siRNA resulted in gene knockdown at day 3 and 5 and restoration of expression is apparent at day 39 [21]

and a fluorescent protein (hMGFP) allows use of a single siRNA (CBL3 siRNA) to silence both markers, enabling multimodal imaging of gene silencing. Mice resulting from this cross were tested for the expression of CBL by bioluminescence imaging in an IVIS 200 Imaging System after intraperitoneal injection of luciferin (30 mg/kg body weight). To improve optical imaging analyses, Tg CBL/hMGFP mice were bred with Balb/c mice (a white strain) in order to obtain a white background to facilitate in vivo detection of hMGFP signal using confocal microscopy. Subsequently, the CBL/hMGFP mice were crossed with skh1 hairless mice to enable experiments to be performed on the back of the mice using topical formulations and microneedle devices without interference of the autofluorescence and scatter from the hair. GFP expression in the skin of this mouse was validated using frozen sections [33] and then used to evaluate delivery of siRNA targeting the reporter construct (CBL3 siRNA) by looking for silencing of luciferase and/or GFP expression using either macroscopic or microscopic imaging [33, 34, 38, 39].

Treatment of some skin diseases will require long-term genetic modifications to correct mutations. Epidermal gene editing has been enabled by advances in nucleic acid biochemistry, and these strategies require that editing molecules reach keratinocyte nuclei. We have employed fluorescently tagged molecules that form triplexes with chromosomal *supFG1* DNA to monitor transfer into cell nuclei in the skin [23]. These studies demonstrated that a deoxyoligonucleotide, FITC-AG30, accumulated in keratinocyte nuclei after topical application to stratum corneum-stripped skin (Fig. 5) or intradermal injection [23]. Similarly, a clamp-forming peptide-nucleic acid conjugated to the transduction peptide antennapedia, FITC-PNA-Antp, accumulated in epidermal keratinocyte nuclei after intradermal injection (Fig. 5) [23]. Most critically, we have demonstrated that these triplex forming molecules induce sequence-specific modifications in epidermal DNA in a *supFG1* transgene after intradermal or intraperitoneal injection [23].

1.5 Technologies for Nucleic Acid Delivery

A number of technologies, including chemical and mechanical, have been developed and evaluated for nucleic acid skin delivery (Table 2). Beginning in 2008, we were part of an NIH-funded consortium formed to develop validated systems to evaluate methodologies for nucleic acid delivery including siRNAs [22, 40]. As part of this consortium, a number of delivery technologies were evaluated using the Tg CBL/hMGFP mouse reporter skin model in which a dual reporter consisting of Monster GFP (hMGFP) and click beetle luciferase (CBL) is expressed in the epidermis [33]. This model had previously been utilized to demonstrate that dissolvable microneedles, manufactured with polyvinyl alcohol (PVA) and loaded with a target-specific self-delivery siRNA cargo, were able to inhibit reporter expression in mouse footpad skin

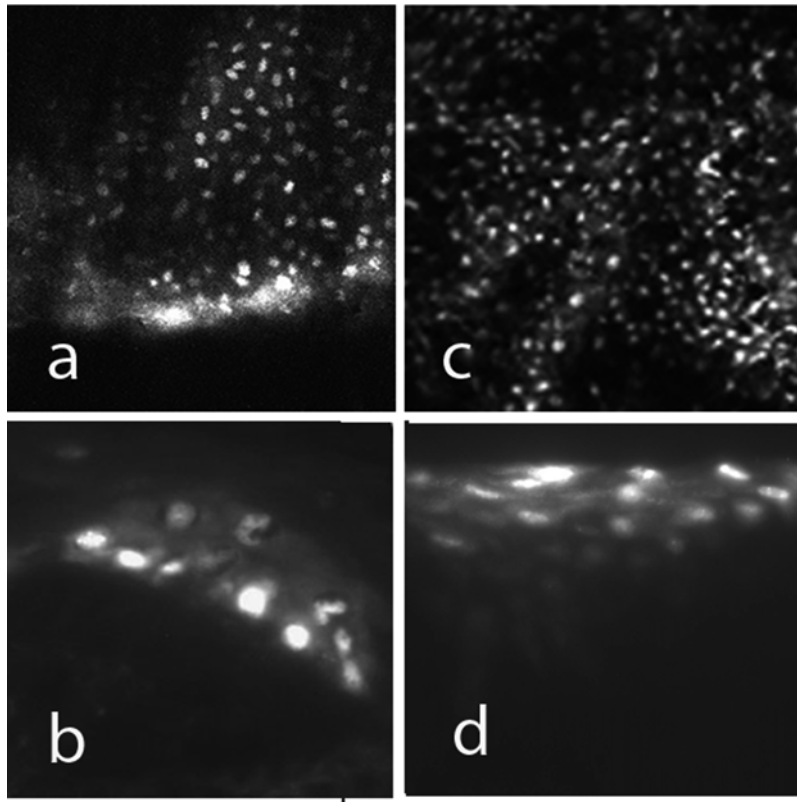

Fig. 5 FITC-tagged triplex forming molecules (TFM) accumulate in keratinocyte nuclei [23]. Fluorescent TFM capable of initiating editing of chromosomal DNA were delivered to the skin of mice. These mice had a *supFG1* transgene. The peptide nucleic acid (PNA) and the single-stranded deoxyoligonucleotide (AG30) had previously been shown to form triplex structures with the *supFG1*. Each molecule was conjugated to FITC for imaging, and the PNA was conjugated to antennapedia peptide (Antp) to facilitate delivery across membranes. After 1–2 h, live skin was imaged *en face* using the VivaScope 2500 in fluorescence mode, and then vertical sections of frozen skin samples were viewed by epifluorescence microscopy. (**a**) *En face* confocal fluorescence image of tail epidermis 2 h after intradermal injection of FITC-PNA-Antp. (**b**) Vertical section through epidermis showing FITC-PNA-Antp in nuclei of all epidermal layers. (**c**) *En Face* confocal fluorescence image of epidermis 1 h after application of aqueous buffer of FITC-AG30 to stratum corneum-stripped back skin. (**d**) Vertical section through epidermis showing FITC-AG30 in nuclei of all epidermal layers

(Fig. 6) [38]. The most promising technologies resulting from the consortium evaluation were microneedles [22, 39], including steel and dissolvable, which mechanically pierce through the stratum corneum outer barrier and deposit the siRNA cargo in the live skin layers. Following completion of that study, we reported the ability of a motorized microneedle array system to also deliver functional siRNA to skin and inhibit expression in the same mouse model [34]. This is an excellent demonstration of a combination of

Table 2
Published technologies for delivery of functional siRNA to skin

Delivery methodology	Targeted gene	% Target inhibition	Model system	References
Intradermal injection				
Hypodermic needle	EGFP/fLuc	97[a]	Mouse footpad skin	[47]
ID injection/ electroporation	COX-1	51	Atopic dermatitis mouse model	[48]
Topical formulations				
Aquaphor/PG	Luc2p	48	PPK reporter transgenic mouse	[42]
GeneCream	Osteopontin	89	Rheumatoid arthritis mouse model	[41]
Cream-based ointment	CD86	80	Mouse ear skin	[49]
SNA nanoparticles	EGFR	65/75	Mouse skin/human skin equivalent	[46]
Microneedles				
Steel	hMGFP/CBL	29	Skin reporter transgenic mouse	[39]
Dissolvable (PAD)	hMGFP/CBL	50	Skin reporter transgenic mouse	[38]
Dissolvable (PAD)	CD44	52	Human skin grafted on mouse flank	[50]
Motorized (MMNA)	hMGFP/CBL	78	Skin reporter transgenic mouse	[34]
Penetrating peptides				
SPACE peptide	IL-10/GAPDH	28/42	Mouse skin	[44]
SPACE/DOTAP	GAPDH	63	Mouse skin	[45]
TD1-R8 peptide cream	MITF	52	Mouse skin	[43]
TD-1 peptide	GAPDH	51	Rat footpad skin	[51]

[a]Target gene and siRNA were co-delivered

approaches, the motorized microneedle array, a physical method for crossing the stratum corneum, and a chemical approach in which the siRNA is modified to improve delivery across the cell membrane—these are called self-delivery siRNAs (sd-siRNA).

A number of research groups have also reported the ability of topical formulations to deliver functional siRNA to skin (Table 2). In a mouse rheumatoid arthritis model, Takanashi et al. were able to achieve dermal and subdermal siRNA delivery with a topical cream formulation and inhibit osteopontin mRNA levels, preventing irreversible damage to cartilage and bone [41]. Using a modified Aquaphor/propylene glycol (PG) formulation containing high levels of siRNA (approximately 10 μM), Hegde and coworkers

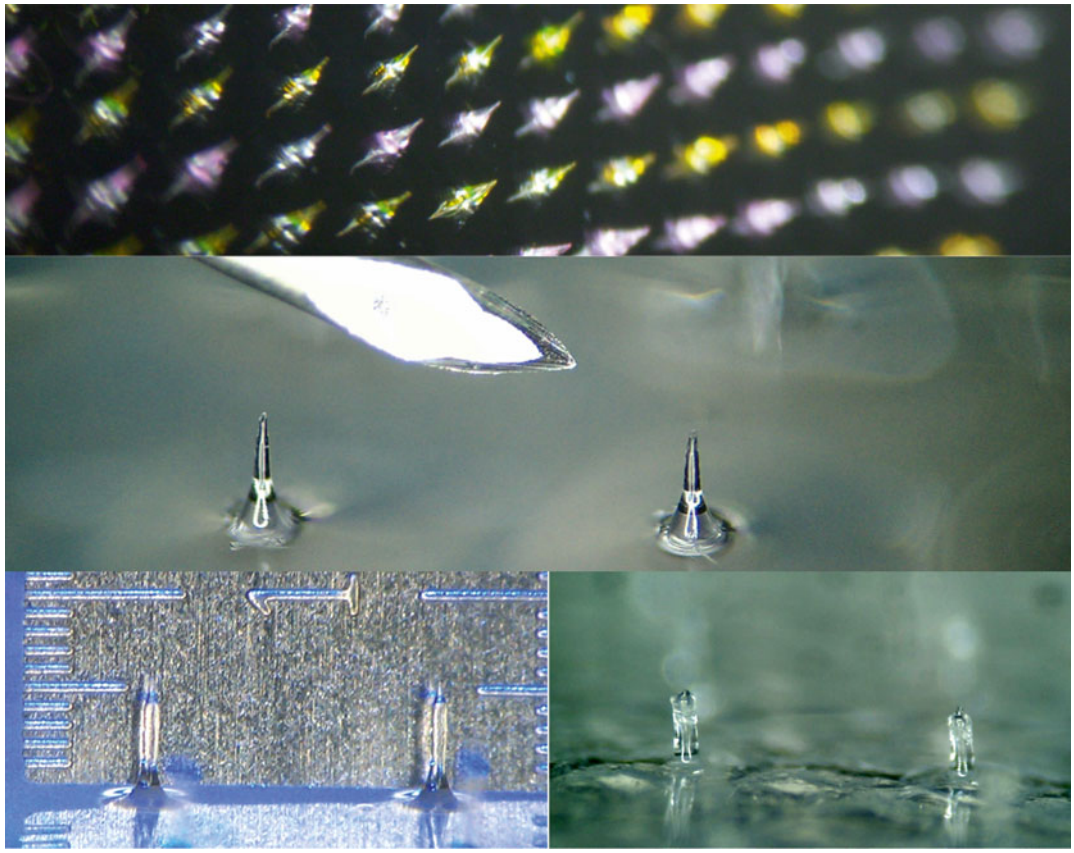

Fig. 6 Soluble polyvinyl alcohol (PVA) microneedles. *Top panel*. Microneedle array showing alternate row loading of fluorescently labeled siRNA mimics. *Middle*. 36 G stainless hypodermic needle vs. microneedle dimensions. *Lower left*. 600 μm microneedles shown against a micro ruler. *Lower right*. Erosion of top portion of microneedles is observed after skin application

inhibited luciferase expression in a palmoplantar skin reporter mouse [42]. A number of groups have used peptides to facilitate stratum corneum penetration and cellular uptake, with one of them Yi et al. [43], moving to human use to treat melasma. Indeed, this technology has now been approved in China as a cosmetic product (www.biomics.cn/en/br1.htm). The Mitragotri laboratory has used a proprietary Skin Permeating And Cell Entering (SPACE) peptide alone [44] or with DOTAP [45] to topically deliver siRNA to skin. As a final example, the Mirkin and Paller groups have demonstrated that spherical nucleic acid (SNA) nanoparticles, initially formed around gold particles but subsequently manufactured without, can deliver siRNA to mouse skin and human skin equivalents [46].

2 Materials

2.1 In Vivo Bioluminescence Imaging

1. Low light imaging system such as an IVIS (Perkin Elmer; previously CRi Inc., Woburn, MA).
2. Substrates:
   (a) Luciferin (Biosynth, International, Inc., Naperville, IL, cat. no. L-8220; 1 g). Stock concentration 30 mg/mL in PBS, aliquot, and store at −20 °C.
   (b) Coelenterazine (Nanolight, cat. no. NFCTZFB; 5 mg). Stock concentration 10 mg/mL in ethanol, aliquot, and store at −80 °C. For working stock, dilute frozen stock 10 μL into 1.5 mL of PBS (working stock concentration 67 μg/mL). Do not store.
3. Anesthetic agent (e.g., isoflurane at 2–3 %).

2.2 In Vivo Fluorescence Imaging

1. Low light imaging system such as an IVIS or Maestro or intravital microscope such as the Caliber ID VivaScope 2500 (formerly Lucid Inc., Rochester, NY).
2. Anesthetic agent (e.g., isofluorane at 2–3 %).
3. Aquasonic® 100 ultrasound transmission gel (Parker laboratories, INC. Fairfield, NJ).
4. Crodamol™ STS as index matching fluid (Croda Inc., Edison, NJ).

2.3 Plasmid Expression Constructs [22, 33]

1. Reporter gene plasmids—multifunctional (Fig. 7).
   (a) pTD138—hMGFP/CBL driven by the CMV immediate early promoter.
   (b) pTD166—Luc2/eGFP driven by the ubiquitin C (UbiC) promoter.
   (c) pTD239—K6a(wt)/eGFP driven by the CMV promoter.
   (d) pTD240—K6a(N171K)/eGFP driven by the CMV promoter.
   (e) pTD128—K6a(wt)/tdTFP driven by the CMV promoter.
   (f) pTD129—K6a(N171K)/tdTFP driven by the CMV promoter.
   (g) pTD241—K6a(wt)/eGFP driven by the UBC promoter.
   (h) pTD242—K6a(N171K)/eGFP driven by the UBC promoter.
   (i) pTD202—K6a(wt)/tdTFP driven by the UBC promoter.
   (j) pTD203—K6a(N171K)/tdTFP driven by the UBC promoter.

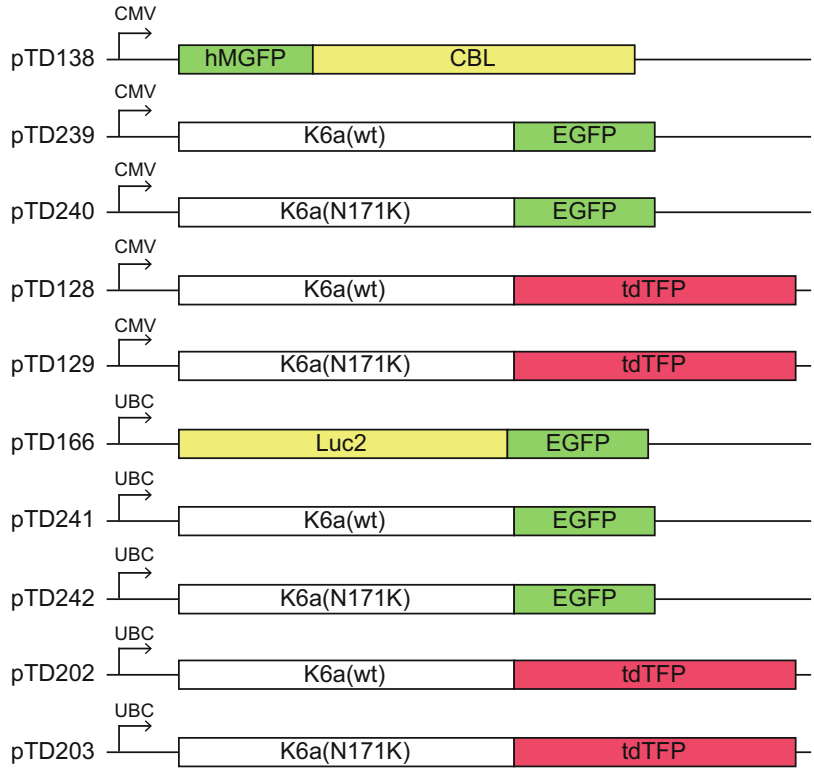

Fig. 7 Schematic representation of expression plasmids used for in vivo fluorescence and bioluminescence imaging of reporter proteins

2.4 siRNAs (Unmodified and Accell-Modified) [16, 22, 33] Were Provided by Dharmacon Products GE Healthcare (Lafayette, CO)

1. CBL3 siRNA (targets the dual function reporter construct in the RLG reporter mouse and pTD138).
   Sense: 5′-UUUACGUCGUGGAUCGUUAuu.
   Antisense: 5′-P-UAACGAUCCACGACGUAAAuu.
2. K6a_513a.12 siRNA [7] (targets the human keratin 6a N171K mutant allele containing a single point mutation in plasmids pTD240, pTD129, pTD242, and pTD203; wt plasmids pTD239, pTD128, pTD241, and pTD202 are used as controls; see Notes for design).
   Sense: 5′-CCCUCAAaAACAAGUUUGCuu.
   Antisense: 5′-P-GCAAACUUGUUUUUGAGGGuu.
3. K6a_3′UTR.1 (targets the 3′ UTR of K6a).
   Sense: 5′-GCACAAGUGACUAGUCCUAuu.
   Antisense: 5′-P-GCAAACUUGUUUUUGAGGGuu.
4. CD44 siRNA (targets exon 1 of CD44).
   Sense: 5′-GGCGCAGAUCGAUUUGAAUuu.
   Antisense: 5′-P-AUUCAAAUCGAUCUGCGCC.

5. NSC4 siRNA (targets inverted betagalactosidase sequence).
   Sense: 5′-UAGCGACUAAACACAUCAAuu.
   Antisense: 5′-P-UUGAUGUGUUUAGUCGCUAuu.
6. Unmodified eGFP siRNA (or Accell modified).
   Sense: 5′-GCACCAUCUUCUUCAAGGAuu.
   Antisense: 5′-P-UCCUUGAAGAAGAUGGUGCuu.
7. An siRNA of your choosing.

2.5 Plasmid DNA Injections

1. A 1 mL syringe with a 28-G needle is used to deliver 50–75 μL of plasmid solution intradermally to mouse footpads. A bleb is formed if the injection is performed properly. Note that large volumes are needed to generate pressure, which facilitates nucleic acid delivery to keratinocytes [15].
2. Endotoxin-free plasmids encoding reporter genes expressed from strong constitutive mammalian promoters (*see* Subheading 2.3).

2.6 Meso-Assisted Delivery of sd-siRNA

1. A Motorized Meso Machine (Triple-M from Bomtech Electronics Co., Seoul, Korea) [34].

2.7 Generation and Evaluation of Human Skin Equivalents

1. Epidermal skin equivalents [2].
2. Full thickness skin equivalents grafted onto immunocompromised mice.
   (a) Humanized mouse model [50].
   (b) Pachyonychia congenita humanized disease mouse model [52].

2.8 In Vivo Confocal Microscopy with the VivaScope or DAC Microscopes

1. Caliber ID VivaScope 2500 System [22].
2. Alternatively a DAC microscope could be used [30].
3. Aquasonic® 100 ultrasound transmission gel (Parker laboratories, INC. Fairfield, NJ).
4. Crodamol™ STS as index matching fluid.
5. Amira® software (Visage Imaging, Carlsbad, CA).

3 Methods

3.1 Plasmid Delivery Models of Gene Silencing

Plasmids encoding reporter genes can be used as the target for siRNA therapy or as a means of assessing nucleic acid transfer to tissues. There are a wide variety of plasmids encoding single and combination reporter genes (Fig. 7). Each of these could be used to evaluate siRNA gene silencing provided that an siRNA has been developed and tested for that specific reporter gene sequence.

1. Inject the reporter plasmid into the footpad skin of anesthetized Swiss Webster mice at concentrations of 10–20 μg of DNA in 50–75 μL PBS intradermally using a 1 mL insulin

syringe. 60–80 μg (4.5 nmol) of the siRNA could be mixed with the plasmid, or alternatively the siRNA could be injected separately [24]. The siRNA can be used alone or in combination with pUC19 (5 μg) as a "carrier" nucleic acid. The positive control for experimental gene delivery tools can be direct intradermal injection (10–20 daily injections of 60–80 μg per treatment) of specific CBL3 siRNA into the control footpad of white mice with reporter expression in the skin. Use an equal amount of irrelevant siRNA (K6a_513a.12) as a negative control injected intradermally into the contralateral footpad.

2. If the siRNA is to be injected separately, load the syringe with CBL3 siRNA (or siRNA of choice) and inject at 60–80 μg (4.5 nanomoles) per footpad in 50–75 μL PBS alone or in combination with pUC19 (5 μg) as a potential "carrier" [47] and at the site of plasmid injection.
3. Set up the control with an equivalent quantity of irrelevant siRNA (e.g., K6a_513a.12) [7] and inject intradermally into the counterpart footpad.
4. Follow gene expression using in vivo bioluminescence or fluorescence imaging as determined by the reporter gene used.

3.2 Testing of siRNA in Human Skin Equivalents in Mice

1. Full-thickness 3-D human skin equivalents can be obtained from a commercial source or prepared by a variety of methods whereby keratinocytes are embedded in a matrix of fibroblasts and cultured to generate a 3-D human skin equivalent (*see* Garcia et al. [52] for an example).
2. Graft human skin equivalent on to an anesthetized immunocompromised mouse by inserting a square region (2 × 2 cm) of skin equivalent into the back of the mouse (mouse skin previously removed) carefully aligning both mouse and human skin [22]. Cover the grafted area with Vaseline gauze and bandages and leave the dressing for 14 days.
3. Administer siRNA to the human skin equivalents (ID injection, microneedle arrays, etc.) about 1–2 month after the skin graft procedure. Microneedle application methods vary depending on the type of microneedle array, and can include manual application using forceps (steel microneedles) or by finger flicking, vacuum or spring-loaded application devices for application of dissolvable microneedle arrays [50].
4. Monitor gene expression using in vivo bioluminescence or fluorescence imaging as determined by the reporter gene used.
5. Harvest skin and prepare for histologic examination [50].

3.3 In Vivo Bioluminescence Imaging (BLI)

1. Anesthetize mice with 2–3 % isoflurane.
    1. Inject 100 μL of d-luciferin (Biosynth) at a concentration of 30 mg/mL solution (~150 mg/kg body weight) into the peritoneal cavity of mice under isoflurane anesthesia.

2. Wait 10 min for the luciferin to distribute throughout the body of the mouse.
3. Image live anesthetized mice using the IVIS Spectrum Imaging System (Xenogen product from Caliper LifeSciences, Alameda, CA) [53] or equivalent device.
4. Quantify light emission using LivingImage software 3.1 (Caliper LifeSciences, Alameda, CA).

3.4 Fluorescence Imaging with the VivaScope 2500 [21, 33]

1. Anesthetize mice with 2–3 % isoflurane.
2. Apply Aquasonic® 100 ultrasound transmission gel, as an immersion medium, between the objective lens of the Calilber ID VivaScope 2500 System and the glass window of the tissue cassette [21, 33].
3. Place the mouse paw to be imaged over the glass window of the tissue cassette after adding Crodamol™ STS as index matching fluid (index of refraction = 1.47).
4. Image GFP and/or RFP reporter expression in paws using the Calilber ID VivaScope 2500 [21, 33].
5. Adjust the z-depth position of the VivaScope by identifying the surface of the tissue using the 658 nm reflectance laser. Using this same laser, the position in the skin (e.g., stratum corneum, granulosum, spinal layer, basal layer) can be identified [54].
6. After switching to the 488 nm fluorescence excitation laser, generate VivaBlocks (*xy* position map) to screen the tissue to locate GFP-positive cells (the signal displays as white colored over a black background) at the selected depth.
7. Once cells expressing eGFP or hMGFP are found, generate VivaStack (*z*-axis map) images, first in fluorescence mode, and then in reflectance mode (40 slices with a *z* separation of 1.6–8 μm between slices. The field of view is 750 × 750 μm and the images are collected at nine frames per second. Image files are processed and 3-D volumes and video files reconstructed using ImageJ (National Institutes of Health, Bethesda, MD).
8. Can be repeated with the 532 nm fluorescence excitation laser to capture red (e.g., tdTFP reporter expression) fluorescence.

3.5 Intravital Microscopy with the DAC Microscope

1. Perform intravital imaging on anesthetized mice. Use isoflurane anesthesia, or alternative anesthetic following institutional guidelines.
2. Use optical gel (NyoGel® OC-431A-LVP, Nye Lubricants Inc., Fairhaven, MA, index of refraction = 1.46) as a coupling agent between the footpad skin and the microscope.
3. Analyze the footpads by intravital imaging at various time-points during and after treatment using a DAC microscope equipped with a fiber-coupled 488 nm wavelength laser [27].

4. Scan the footpads at a single depth of ~20 μm to localize both those regions expressing EGFP or hMGFP and those where the signals were absent.
5. Once the signal is found, collect image stacks at these sites.
6. Process and reconstruct the stacks into volumes and video files using Amira® software [30].

3.6 Image Processing

1. Export VivaScope native grayscale image stacks as TIF images for processing using NIH ImageJ and FIJI public domain image-processing software.
2. Image stacks can be despeckled to remove outlier noise pixels, processed with an unsharp mask filter algorithm (Sigma = 1.0, Weight = 0.7), and false-colored in the case of fluorescence data.
3. Image intensity distributions (window and level) can be set to common standard values across respective image sets to normalize intensities for comparison.
4. 3-D representations can be derived from these data (Fig. 8).

3.7 In Vivo Fluorescence Imaging with Wide Field System

1. Anesthetize mice with isoflurane and image using the Maestro Optical imaging system or IVIS imaging system if equipped with spectral unmixing capabilities as previously described [55].
2. Acquire images with an excitation filter of 445–490 nm and a long-pass emission filter (515 nm).
3. Capture Images at 10 nm windows from 500 to 700 nm using the Maestro software (exposure times are automatically calculated).

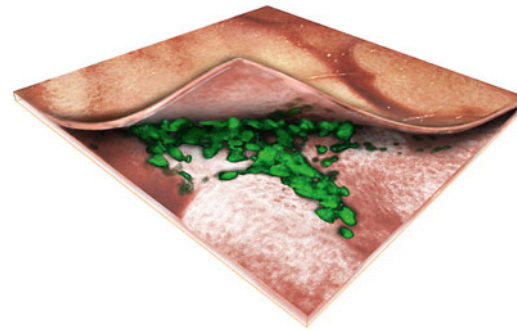

Fig. 8 A virtual peeled-back representation of noninvasive visualization of reporter expression in keratinocytes of mouse skin. This stylized representation of EGFP reporter expression was used to demonstrate imaging of EGFP expression in mouse skin. An EGFP expression plasmid was injected intradermally into a mouse footpad. At 36 h after injection, the footpad of the living mouse was imaged noninvasively with the VivaScope as described in Fig. 1. The colorized stacks corresponding to EGFP (*green*) and reflectance (total skin morphology, skin tones) were manipulated using Editable Poly with a Bend modifier (3ds Max, Auto Desk) to represent the ability to noninvasively image and monitor reporter gene expression beneath the skin surface

4. Use spectral unmixing of the resulting cube images with a user-defined GFP protocol.
5. Set the spectrum manually by unmixing autofluorescence from a negative non-hMGFP expressing mouse analyzed in parallel with a Tg CBL/hMGFP positive mouse.
6. Draw regions of interest around the palm of each paw and calculate the average signal (counts/s/mm^2).
7. Calculate the ratio of average signals in right (CBL3) versus left (nonspecific control) paws for each mouse and normalize with respect to the pretreatment analysis data.
8. For presentation, the unmixed GFP signal can be pseudo-colored green, etc.

3.8 Histological Analysis of Fluorescently Labeled sd-siRNA Distribution in Murine and Human Skin to Validate In Vivo Images

1. After sacrificing of the mouse remove the skin tissues from the footpad.
2. For cryosections, embed skin in OCT compound and freeze directly on dry ice.
3. Cut vertical section at 10 μm.
4. Mount sections with Hydromount™ (National Diagnostic, Highland Park, NJ) containing DAPI for nuclear staining.
5. Image sections using a Zeiss Axio Observer Inverted Fluorescence Microscope equipped with Cy3 and DAPI filter sets, or equivalent microscope.
6. Stitch images together using Microsoft Image Composite Editor (ICE).

3.9 Plasmid Delivery via Dissolvable Microneedle Arrays

1. Coat microneedle (also known as protrusion array devices, PAD [38]) arrays (3 × 5 needles per array), with pUbc-luc2/eGFP or pCMV-hMGFP/CBL expression plasmids.
2. Flick the array with a finger to seat the needle tips into the paw and hold the PAD in contact with the skin for 1 min.
3. Apply control PADs, loaded with β-gal expression plasmid DNA (pCMVsport-β-gal, Invitrogen), to the contralateral paws.
4. After removal, PAD arrays can be observed under an inspection Amscope SM1-BZ microscope (Iscope Corp, Chino, CA) to assess skin penetration and needle dissolution (Fig. 6). In our hands, the post-insertion inspection of the array confirmed penetration of ~5 needles per array per application, as determined by the absence of a tip at the end of the needle due to dissolution upon insertion and removal.
5. Treated paws can be analyzed by in vivo bioluminescence imaging, fluorescence imaging using the VivaScope system or by traditional microscopy of frozen skin sections.

3.10 Plasmid Delivery via Steel Microneedle Arrays

1. Coat metal microneedle arrays (1 × 5 needles per array) with pUbc-luc2/eGFP or pCMV-hMGFP/CBL.
2. Hold the coated arrays tightly with a forceps and insert the array into the skin of the paw by pushing until full penetration is achieved.
3. As a negative control, treat the contralateral paw of each with metal microneedle arrays coated with salmon sperm or other non-coding DNA.
4. Leave the arrays seated in the skin for 20 min to give the DNA payloads the opportunity to dissolve inside the skin.
5. Treated paws can be analyzed by in vivo bioluminescence imaging, fluorescence imaging using the VivaScope system or by traditional microscopy of frozen skin sections.

3.11 Evaluating the Arrays in Human Skin Equivalents

1. Apply PAD arrays (5 × 5 microneedles) to human skin equivalents [50] using a vacuum channel plate made from a modified 0.2 μm sterile syringe filter (Whatman, Florham Park, NJ), with one face and filter removed, leaving a channeled plate with an exhaust port. The vacuum is an alternative to flicking the array as mentioned above or spring-loaded application.
2. Attach the exhaust port to a vacuum pressure station (Bernant Company, Barrington, IL) providing a stable flat surface with sufficient airflow to hold a PAD over the skin surface.
3. Upon contact with the plate, seat the mouse skin immediately against the channeled plate and then insert the needles into the skin.
4. Continue the vacuum for 1 min and then remove the channeled plate.
5. Leave PADs for 20 min in the skin to allow needle dissolution and then remove the PAD.
6. Coated metal microneedles can be applied to human skin equivalents in a similar fashion as described above for mouse paws.

3.12 Meso-Assisted Delivery of sd-siRNA to Mouse and Human Skin Using a MOTORIZED Meso Machine (Triple-M) [34]

1. Load unlabeled or labeled siRNA of interest such as Cy3-Accell Non-Targeting siRNA (Dharmacon Products) into the chamber of the disposable Meso needle cartridge of the Meso device (50–300 μL at 0.1 mg/mL).
2. Set the device to a depth of 0.1 mm.
3. Lay a fold of skin on a rigid support positioned under the tip of the Meso device. Once the Meso device is oriented vertically and is perpendicular to the fold of skin, turn on the device set at the highest speed and hold in place for 10 s.
4. To treat fresh human abdominal skin (obtained immediately following surgical procedures), manually stretch and pin the skin to a cork platform and treat was with mouse skin (above).

5. Image with an IVIS Lumina imaging system, or equivalent, using the 535 nm excitation and DsRed emissions settings (1–10 s acquisition time).
6. Quantify the data using LivingImage software (Perkin Elmer).
7. Subtract the fluorescent background from an untreated area of the same animal or tissue sample and report values reported as radiant efficiency.
8. Present pseudocolored image as an overlay over the grayscale reference image.

3.13 Meso-Assisted Delivery of sd-siRNAs and Analysis of Gene Silencing [34]

1. Anesthetize hairless (SKH1) tg-CBL/hMGFP mice and treat, every other day, with 100 μL of 5 mg/mL solution in PBS of either CBL3 sd-siRNA or a nonspecific control sd-siRNA (CD44 or TD101) for 11 days (six treatments total).
2. On the day following the last treatment (day 12), sacrifice the mice and excise the treated areas and analyze by both fluorescence microscopy and RTqPCR as described in [33].
3. For RTqPCR, separate the epidermis from the dermis by incubation in dispase II (Roche, Indianapolis, IN, 10 mg/mL in PBS) for 2–4 h at 21 °C prior to RNA isolation from the epidermis only.

3.14 Flourescent Triplex-Forming Molecules

1. AG30 has the sequence AGGAAGGGGGGGGTGGTGGGGGAGGGGGAG and binds to the polypurine target at positions 167–196 of *supFG1*. It was synthesized by Midland Certified reagent Company (Midland, TX) with a 3′-propylamine and FITC at the 5′ end [23, 56].
2. PNA-Antp has the sequence, JJJJJTTJJT-O-O-O-TCCTTCCCCC-O-O-KKKKKWKMRRNQFWIKIQR, where J = pseudoisocytosine and O = 8-amino-2,6,dioxaoctanoic acid. It was designed to bind as a clamp to the homopurine strand of positions 167–176 of *supFG1*. The cell penetrating peptide, antennapedia, was covalently linked to the PNA at the C-terminal lysine. FITC was conjugated to the PNA at the N-terminus via two O linkers.
3. The AV *supFG1* mice were derived in a CD1 background as described [56] and bred into the SKH hairless background [23].
4. Inject 10 μg FITC-PNA-Antp in 50 μL PBS into the tail dermis of SKH *supFG1* transgenic mice [23].
5. Prepare stratum corneum-stripped skin by sequential application and removal of d-Squame (CUDERM Co., Dallas, TX) tapes followed by a cyanoacrylate strip, in which a drop of cyanoacrylate is placed on a glass slide, inverted onto the mouse skin for 1 min and then remove quickly.
6. Apply FITC-AG30, 200 ng in 2.5 μL PBS, to 1 cm^2 of stratum corneum-stripped back skin and allow to dry.

4 Conclusions

Despite the accessibility of the skin, the barriers to nucleic acid delivery remain formidable. Imaging can be used to accelerate the study of various topical delivery methods and the images from these studies have served to inform and guide the development of new tools. Skin delivery of nucleic acids and functional delivery are distinct, and imaging has illustrated this clearly. Through the use of reporter genes that reveal the effects of a nucleic acid on the biology of the cell, we can appreciate the accomplishments in this field, and yet, they highlight the significant challenges in the creation of clinically viable transdermal gene delivery tools for treating human disease.

Acknowledgments

This work was funded in part by the NIH through a grant called the NIH NIAMS GO Delivery! consortium grant (to RLK, LMM and CHC; RC2AR058955), support from the Pachyonychia Congenita Project (RK and CHC), and a gift from the Chambers Family Foundation (CHC).

References

1. Lorenzer C et al (2015) Going beyond the liver: progress and challenges of targeted delivery of siRNA therapeutics. J Control Release 203:1–15
2. Hickerson RP et al (2011) Use of self-delivery siRNAs to inhibit gene expression in an organotypic pachyonychia congenita model. J Invest Dermatol 131:1037–1044, In press
3. Leachman SA et al (2008) Therapeutic siRNAs for dominant genetic skin disorders including pachyonychia congenita. J Dermatol Sci 51(3):151–157
4. Leachman SA et al (2010) First-in-human mutation-targeted siRNA phase Ib trial of an inherited skin disorder. Mol Ther 18(2):442–446
5. Leslie Pedrioli DM et al (2012) Generic and personalized RNAi-based therapeutics for a dominant-negative epidermal fragility disorder. J Invest Dermatol 132(6):1627–1635
6. Préat V, Dujardin N (2001) Topical delivery of nucleic acids in the skin. STP Pharma Sci 1:57–68
7. Hickerson RP et al (2008) Single-nucleotide-specific siRNA targeting in a dominant-negative skin model. J Invest Dermatol 128(3):594–605
8. Wong P, Domergue R, Coulombe PA (2005) Overcoming functional redundancy to elicit pachyonychia congenita-like nail lesions in transgenic mice. Mol Cell Biol 25(1):197–205
9. Smith FJ et al (2008) Development of therapeutic siRNAs for pachyonychia congenita. J Invest Dermatol 128(1):50–58
10. Chen J, Roop DR (2005) Mouse models in preclinical studies for pachyonychia congenita. J Investig Dermatol Symp Proc 10(1):37–46
11. Cao T et al (2001) An inducible mouse model for epidermolysis bullosa simplex: implications for gene therapy. J Cell Biol 152(3):651–656
12. Broderick KE, Humeau LM (2015) Electroporation-enhanced delivery of nucleic acid vaccines. Expert Rev Vaccines 14(2):195–204
13. Vogel FR, Sarver N (1995) Nucleic acid vaccines. Clin Microbiol Rev 8(3):406–410
14. Colluru VT et al (2013) Preclinical and clinical development of DNA vaccines for prostrate cancer. Urol Oncol. doi:10.1016/j.urolonc.2013.09.014, Pii: S1078-1439(13)00387-6
15. Gonzalez-Gonzalez E et al (2010) Increased interstitial pressure improves nucleic acid deliv-

ery to skin enabling a comparative analysis of constitutive promoters. Gene Ther 17(10): 1270–1278
16. Hickerson RP et al (2015) Non-invasive intravital imaging of siRNA-mediated mutant keratin gene repression in skin. Mol Imaging Biol. doi:10.1007/s11307-015-0875-z
17. McLean WH et al (2011) The phenotypic and molecular genetic features of pachyonychia congenita. J Invest Dermatol 131(5): 1015–1017
18. Eliason MJ et al (2012) A review of the clinical phenotype of 254 patients with genetically confirmed pachyonychia congenita. J Am Acad Dermatol 67(4):680–686
19. Kaspar RL (2005) Challenges in developing therapies for rare diseases including pachyonychia congenita. J Investig Dermatol Symp Proc 10(1):62–66
20. Sonn GA et al (2009) Fibered confocal microscopy of bladder tumors: an ex vivo study. J Endourol 23(2):197–201
21. Ra H et al (2010) Assessing delivery and quantifying efficacy of small interfering ribonucleic acid therapeutics in the skin using a dual-axis confocal microscope. J Biomed Opt 15(3):036027
22. Gonzalez-Gonzalez E et al (2011) Visualization of plasmid delivery to keratinocytes in mouse and human epidermis. Sci Rep 1:158
23. Rogers FA, Hu RH, Milstone LM (2013) Local delivery of gene-modifying triplex-forming molecules to the epidermis. J Invest Dermatol 133(3):685–691
24. Hirokawa D, Lee JB (2011) Dermatoscopy: an overview of subsurface morphology. Clin Dermatol 29(5):557–565
25. Prescher JA, Contag CH (2010) Guided by the light: visualizing biomolecular processes in living animals with bioluminescence. Curr Opin Chem Biol 14(1):80–89
26. Ra H et al (2011) In vivo imaging of human and mouse skin with a handheld dual-axis confocal fluorescence microscope. J Invest Dermatol 131(5):1061–1066
27. Ra H et al (2008) Three-dimensional in vivo imaging by a handheld dual-axes confocal microscope. Opt Express 16(10):7224–7232
28. Wang TD et al (2004) Confocal fluorescence microscope with dual-axis architecture and biaxial postobjective scanning. J Biomed Opt 9(4):735–742
29. Wang TD et al (2003) Dual-axis confocal microscope for high-resolution in vivo imaging. Opt Lett 28(6):414–416
30. Ra H et al (2010) In vivo imaging of human and mouse skin with a handheld dual-axis confocal fluorescence microscope. J Invest Dermatol 131:1061–1066
31. Ra H et al (2007) Two-dimensional MEMS scanner for dual-axes confocal microscopy. J Microelectromech Syst 16:969–976
32. Piyawattanametha W et al (2012) In vivo near-infrared dual-axis confocal microendoscopy in the human lower gastrointestinal tract. J Biomed Opt 17(2):021102
33. Gonzalez-Gonzalez E et al (2009) siRNA silencing of keratinocyte-specific GFP expression in a transgenic mouse skin model. Gene Ther 16(8):963–972
34. Hickerson RP et al (2013) Gene silencing in skin after deposition of self-delivery siRNA with a motorized microneedle array device. Mol Ther Nucleic Acids 2:e129
35. Schindelin J et al (2012) Fiji: an open-source platform for biological-image analysis. Nat Methods 9(7):676–682
36. Thevenaz P, Ruttimann UE, Unser M (1998) A pyramid approach to subpixel registration based on intensity. IEEE Trans Image Process 7(1):27–41
37. Sawicki JA et al (1998) A composite CMV-IE enhancer/beta-actin promoter is ubiquitously expressed in mouse cutaneous epithelium. Exp Cell Res 244(1):367–369
38. Gonzalez-Gonzalez E et al (2010) Silencing of reporter gene expression in skin using siRNAs and expression of plasmid DNA delivered by a soluble protrusion array device (PAD). Mol Ther 18(9):1667–1674
39. Chong RH et al (2013) Gene silencing following siRNA delivery to skin via coated steel microneedles: In vitro and in vivo proof-of-concept. J Control Release 166(3):211–219
40. Kaspar R, McLean W, Schwartz M (2009) Achieving successful delivery of nucleic acids to skin: 6th annual meeting of the international pachyonychia congenita consortium. J Invest Dermatol 129:2085–2087
41. Takanashi M et al (2009) Therapeutic silencing of an endogenous gene by siRNA cream in an arthritis model mouse. Gene Ther 16(8): 982–989
42. Hegde V et al (2014) In vivo gene silencing following non-invasive siRNA delivery into the skin using a novel topical formulation. J Control Release 196:355–362
43. Yi X et al (2010) MITF-siRNA formulation is a safe and effective therapy for human melasma. Mol Ther 19:362–371
44. Hsu T, Mitragotri S (2011) Delivery of siRNA and other macromolecules into skin and cells using a peptide enhancer. Proc Natl Acad Sci USA 108(38):15816–15821

45. Chen M et al (2014) Topical delivery of siRNA into skin using SPACE-peptide carriers. J Control Release 179:33–41
46. Zheng D et al (2012) Topical delivery of siRNA-based spherical nucleic acid nanoparticle conjugates for gene regulation. Proc Natl Acad Sci U S A 109(30):11975–11980
47. Wang Q et al (2007) Delivery and inhibition of reporter genes by small interfering RNAs in a mouse skin model. J Invest Dermatol 127(11):2577–2584
48. Inoue T et al (2007) Modulation of scratching behavior by silencing an endogenous cyclooxygenase-1 gene in the skin through the administration of siRNA. J Gene Med 9(11): 994–1001
49. Ritprajak P, Hashiguchi M, Azuma M (2008) Topical application of cream-emulsified CD86 siRNA ameliorates allergic skin disease by targeting cutaneous dendritic cells. Mol Ther 16(7):1323–1330
50. Lara MF et al (2012) Inhibition of CD44 gene expression in human skin models, using self-delivery short interfering RNA administered by dissolvable microneedle arrays. Hum Gene Ther 23(8):816–823
51. Lin CM et al (2012) A simple, noninvasive and efficient method for transdermal delivery of siRNA. Arch Dermatol Res 304(2):139–144
52. Garcia M et al (2010) Development of skin-humanized mouse models of pachyonychia congenita. J Invest Dermatol 131:1053–1060
53. Contag CH, Bachmann MH (2002) Advances in in vivo bioluminescence imaging of gene expression. Annu Rev Biomed Eng 4:235–260
54. Rajadhyaksha M et al (1995) In vivo confocal scanning laser microscopy of human skin: melanin provides strong contrast. J Invest Dermatol 104(6):946–952
55. Hickerson RP et al (2008) Stability study of unmodified siRNA and relevance to clinical use. Oligonucleotides 18(4):345–354
56. Rogers FA et al (2012) Targeted gene modification of hematopoietic progenitor cells in mice following systemic administration of a PNA-peptide conjugate. Mol Ther 20(1):109–118
57. Liu JT et al (2013) Real-time pathology through in vivo microscopy. Stud Health Technol Inform 185:235–264
58. Liu JT et al (2011) Point-of-care pathology with miniature microscopes. Anal Cell Pathol (Amst) 34(3):81–98

Chapter 2

In Vivo Magnetic Resonance Imaging of Small Interfering RNA Nanodelivery to Pancreatic Islets

Ping Wang and Anna Moore

Abstract

Pancreatic islet transplantation is a promising therapeutic approach for type 1 diabetes.

However, recent advances in islet transplantation are limited by significant graft loss after transplantation. Multiple immunological and nonimmunological factors contribute to this loss. Novel therapies that could target the core reasons for the islet graft loss are desperately needed. Small interfering RNA can be used to inhibit the expression of virtually any gene with single-nucleotide specificity including genes responsible for islet damage. Applying adequate delivery of siRNA molecules to pancreatic islets prior to transplantation holds a great potential for improving the survival of islet grafts. Noninvasive imaging provides means for monitoring the survival of transplanted islets in real time. Here, we summarize the approach that has been developed to deliver siRNA to pancreatic islets in conjunction with tracking of the graft outcome by in vivo magnetic resonance imaging (MRI). We synthesize a nano-sized theranostic agent consisting of magnetic nanoparticles (MN), a reporter for MRI, labeled with Cy5.5 dye for near-infrared fluorescence (NIRF) imaging, and conjugated to siRNA molecule targeting genes that are harmful to islet grafts. Pre-labeling of islets by MN-Cy5.5-siRNA allowed us to monitor the survival of transplanted islet grafts by MRI and NIRF imaging and resulted in efficient silencing of the target genes in vivo. This novel approach combines a therapeutic effect provided by RNA interference technology with in vivo MR imaging and is expected to significantly improve the outcome of islet transplantation in patients with type 1 diabetes.

Key words Pancreatic islet, Small interfering RNA, Molecular imaging, Magnetic nanoparticles, Diabetes

1 Introduction

Type 1 diabetes (T1D) is a severe disease that results from destruction of insulin-producing pancreatic beta cells by autoimmune attack [1]. It is established that insulin injections do not cure T1D, although they could change the clinical course of T1D from an acutely fatal disease to a chronic one with long-term complications [2]. Currently, there are two strategies for the etiological treatment of diabetes: immunoregulatory therapy and pancreas or islet transplantation [3, 4]. The toxic effect of most anti-diabetic drugs,

Zdravka Medarova (ed.), *RNA Imaging: Methods and Protocols*, Methods in Molecular Biology, vol. 1372,
DOI 10.1007/978-1-4939-3148-4_2,

combined with the risk associated with immune suppression, limits their use. Elevated risk of surgical complications and relative invasiveness of the procedure make the practice of solid organ transplantation rare in T1D patients. Islet transplantation has emerged as one of the most promising therapeutic approaches for T1D treatment during the recent decade, but its success is hampered by drastic graft loss during the first several weeks after transplantation, due to multiple immunological and nonimmunological factors [5]. Therefore, there is an urgent need for developing strategies and methods that could protect islet grafts from abovementioned damages.

Small interfering RNAs, which are molecules that mediate an innate cellular mechanism for posttranscriptional regulation of gene expression, have a great potential for islet graft protection by silencing the expression of harmful genes with single-nucleotide specificity [6]. Magnetic resonance imaging provides the necessary set of tools for in vivo monitoring of transplanted islets and assessment of protection provided by siRNA. Recent studies from our group have demonstrated the coupling of siRNA to MRI contrast agents that can be used for noninvasive imaging [7–10].

Here, we summarize the methodology of a magnetic iron oxide nanoparticle platform for the delivery of siRNA to pancreatic islets followed by monitoring of the graft outcome by MRI and near-infrared optical imaging. This theranostic complex consists of magnetic nanoparticles that serve as a reporter for MR imaging, labeled with Cy5.5 dye for NIRF imaging, and conjugated to siRNA molecule targeting model or therapeutic genes of interest. The described approach includes three major steps: (1) synthesis of the MN-Cy5.5-siRNA complex, (2) pre-labeling islets with MN-Cy5.5-siRNA complex in vitro followed by islet transplantation under the kidney capsule of diabetic mice, and (3) real-time noninvasive MRI and NIRF imaging of transplanted islet grafts and assessing their survival.

2 Materials

2.1 Synthesis of MN-NIRF-siRNA Complex

The syntheses of MN-Cy5.5 and MN-Cy5.5-siRNA have been described previously [7–10].

1. Amino-derivatized dextran-coated iron oxide magnetic nanoparticles (pH 8.5).
2. 0.5 M Sodium bicarbonate, pH 9.6.
3. Cy5.5 NHS ester, 1 mg (Amersham Biosciences, Piscataway, NJ).
4. 20 mM Sodium citrate, 150 mM sodium chloride, pH 7, 7.5, 8.
5. Sephadex G-25, PD-10 column (Amersham Biosciences, Piscataway, NJ).

6. *N*-succinimidyl 3-(2-pyridyldithio) propionate (SPDP; Pierce Biotechnology, Rockford, IL).
7. 50 mM Sodium phosphate, 10 mM EDTA, pH 7.5, 8.
8. 15 mM and 35 mM Tris-(2-carboxyethyl) phosphine hydrochloride (TCEP, Thermo Fisher Scientific, Rockford, IL).
9. Double-stranded siRNA modified with a thiol group on the 5′ end of the sense strand (Dharmacon, Lafayette, CO).
10. Quick Spin Column G-50 Sephadex column (Roche Applied Science, Indianapolis, IN).
11. The 20 μ magnetic separation columns and MACS separator (Miltenyi Biotec, Inc., Auburn, CA) (catalog number: 130-042-701).
12. Agarose gel in Tris-borate-EDTA (TBE) buffer (Invitrogen, Carlsbad, CA).
13. Ethidium bromide (Sigma-Aldrich, St. Louis, MO).
14. Bruker MQ20 Minispec NMR spectrometer (Bruker Biospin Co., Billerica, MA).
15. Sub-micron particle size analyzer (Coulter N-4, Hialeah, FL).
16. SpectraMax M2 spectrophotometer (Molecular Devices, Sunnyvale, CA).
17. Bench-top centrifuge (Thermo Scientific).
18. Molecular Imager FX scanner (Bio-Rad Laboratories, Hercules, CA).

2.2 Pre-labeling Islets In Vitro Followed by Islet Transplantation

Labeling of pancreatic islets using MN-Cy5.5-siRNA probes and islet transplantation have been described previously [11, 7, 9, 10].

1. Pancreatic islets from healthy human donors (Integrated Islet Distribution Program, IIDP Centers, National Institutes of Health and Juvenile Diabetes Research Foundation).
2. CMRL 1066 medium, fetal bovine serum (FBS), and penicillin-streptomycin (GIBCO, Grand Island, NY).
3. 24-Well nontreated plates (Nunc, Roskilde, Denmark).
4. CO_2 incubator (Thermo Scientific), Class II type A2 biological safety cabinet (Thermo Scientific).
5. 37 % formaldehyde (Fisher Scientific, Rockford, IL).
6. Tris-EDTA buffer, pH 8.0 (Fisher Scientific, Rockford, IL).
7. 1× Phosphate-buffered saline (PBS) (Sigma-Aldrich, Milwaukee, WI).
8. Normal goat serum (Vector Laboratories, Inc. Barlingame, CA).

9. Guinea pig anti-human insulin primary antibody (Abcam, Cambridge, MA) and FITC-labeled goat anti-guinea pig secondary IgG (Abcam, Cambridge, MA).
10. DAPI (Vectashield, Vector Laboratories, Inc. Barlingame, CA).
11. 5 % potassium ferrocyanide (ACROS Organics, Fairlawn, NJ)
12. 5 % hydrochloric acid (Sigma-Aldrich, Milwaukee, WI).
13. Nuclear Fast Red (Sigma-Aldrich, Milwaukee, WI)
14. Mounting medium (Permount, Fisher Scientific, Fair Lawn, NJ).
15. Ethanol and xylene (Fisher Scientific, Rockford, IL).
16. Nikon Eclipse 50i microscope, SPOT 7.4 Slider RTKE CCD camera, and iVision 4.015 version software (Diagnostic Instruments, Sterling Heights, MI).
17. 9.4-T horizontal bore imaging unit equipped with a home-built radiofrequency transmit-receive 3 × 4-cm elliptical surface coil and ParaVision 5.1 Software (Bruker, Billerica, MA).
18. Marevisi 3.5 software (Institute for Biodiagnostics, National Research Council, Canada).
19. CellTiter 96 non-radioactive cell proliferation assay kit (Promega, Madison, WI).
20. SpectraMax M2 spectrophotometer (Molecular Devices, Sunnyvale, CA).
21. Human insulin ELISA kit (Mercodia, Uppsala, Sweden).
22. 5-Week-old NOD/scid mice (The Jackson Laboratory, Bar Harbor, ME).
23. Streptozotocin (STZ; Sigma-Aldrich, St. Louis, MO).
24. Animal anesthesia system Isotec 4 (Surgivet/Anesco, Waukesha, WI).
25. Acensia Contour Blood Glucose Monitoring System (Bayer Health Care, Tarrytown, NY).
26. Standard surgery kit (scissors, forceps) (Roboz Surgical Instrument Co., Inc., Gaithersburg, MD).
27. Tuberculin syringes, 1 cc (Becton Dickinson, Franklin Lakes, NJ).

2.3 MR and NIRFImaging of Transplanted Islet Grafts

In vivo NIFR optical imaging and MRI of islet grafts under the kidney capsule of diabetic mice has been described previously [12, 13, 11, 9, 10].

1. Alfalfa-free diet (TestDiet, Richmond, IN).
2. Animal anesthesia system Isotec 4 (Surgivet/Anesco, Waukesha, WI).

3. Whole-body animal imaging system (IVIS Spectrum), equipped with 10 narrow-band excitation filters (30 nm bandwidth) and 18 narrow-band emission filters (20 nm bandwidth) (Perkin Elmer, Hopkinton, MA).
4. Living Image 4.2 software (Perkin Elmer, Hopkinton, MA).
5. 9.4-T horizontal bore imaging unit equipped with a home-built radiofrequency transmit-receive 3 × 4-cm elliptical surface coil and ParaVision 5.1 Software (Bruker, Billerica, MA).
6. Marevisi 3.5 software (Institute for Biodiagnostics, National Research Council, Canada).

3 Methods

The synthesis of siRNA-conjugated nano-probes consists of two steps: conjugation of the fluorescent dye Cy5.5-NHS ester to dextran-coated MN followed by conjugation of siRNA to MN-Cy5.5. Labeling of human islets with MN-Cy5.5-siRNA and transplantation under the kidney capsule of diabetic animals is explained in Subheading 3.2. Monitoring of transplanted islets grafts by both MRI and NIRF imaging is depicted in Subheading 3.3.

3.1 Conjugation of Cy5.5 -NHS Ester to MN and Conjugation of siRNA to MN-Cy5.5

1. The pH of amino-derivatized dextran-coated iron oxide MN is adjusted to 9.6 with 0.5 M sodium bicarbonate.
2. A solution of monoactivated Cy5.5-NHS ester (1 mg) in 100 μL DMSO is reacted with MN (~10 mg Fe) in 20 mM sodium citrate and 150 mM sodium chloride with constant agitation for 12 h at room temperature.
3. The Cy5.5-labeled aminated iron oxide (MN-Cy5.5) is purified from nonreacted dye using a Sephadex G-25, PD-10 column equilibrated with 20 mM sodium citrate, 150 mM sodium chloride, pH 7.5.
4. MN-Cy5.5 is conjugated to the heterobifunctional cross-linker SPDP via N-hydroxy succinimide ester. The intermediate is purified using a Sephadex G-25, PD-10 column in a buffer containing 50 mM sodium phosphate, 150 mM sodium chloride, 10 mM EDTA, pH 7.5.
5. Prior to labeling, the disulfide protecting group on 5′-*S*-*S*-(CH2)6 of the custom-synthesized siRNA duplex is deprotected using 35 mM TCEP. The free thiol-siRNA is then reacted with MN-Cy5.5 via the SPDP crosslinker in 50 mM sodium phosphate, 150 mM sodium chloride, 10 mM EDTA, pH 8.0 at 4 °C over night. The product is purified using a Quick Spin Column G-50 Sephadex column.
6. Free siRNAs is removed from MN-siRNA-Cy5.5 solution using a magnetic separation column. The 20 μ column is attached to a MACS separator and washed with 20 μl of 50

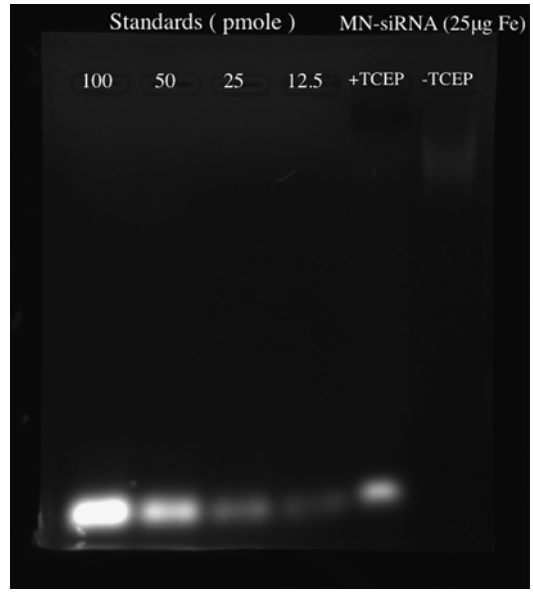

Fig. 1 Agarose gel electrophoresis shows that the siRNA molecules conjugated to the MN-Cy5.5-siRNA probes were cleaved using treatment with a reducing agent TCEP

mM sodium phosphate, 150 mM sodium chloride, 10 mM EDTA, pH 8.0. The sample is applied onto the column, and the column is rinsed with 50 μl of 50 mM sodium phosphate, 150 mM sodium chloride, 10 mM EDTA, pH 8.0, to let the free siRNA pass through. Then the column is removed from the separator. Twenty microliters of 50 mM sodium phosphate, 150 mM sodium chloride, and 10 mM EDTA, pH 8.0 is applied onto the column and the siRNA conjugated probe is flushed out and collected.

7. The labeling ratio of Cy5.5 per MN crystal is obtained spectrophotometrically. The dye-to-particle ratio is calculated from the concentrations of Cy5.5 and iron. For the Cy5.5 dye, the number of dyes per particle is obtained using absorption at 678 nm ($e = 250 \times 10^3$ M^{-1} cm^{-1}). Iron concentration is determined spectrophotometrically from absorption at 410 nm (*see* **Note 1**).
8. The number of SPDP molecules per crystal is determined based on the release of pyridine-2-thione at 343 nm ($e = 8.08 \times 10^3$ M^{-1} cm^{-1}) after the addition of 35 mM of TCEP in PBS buffer. The amount of conjugated siRNA is assayed using agarose gel electrophoresis. The amount of siRNA dissociated from the nanoparticles is assessed under reducing conditions by pretreatment with 15 mM TCEP in RNase-free PBS buffer for 30 min. siRNA standards, untreated probes, and probes treated with a reducing agent are applied to a 2 %

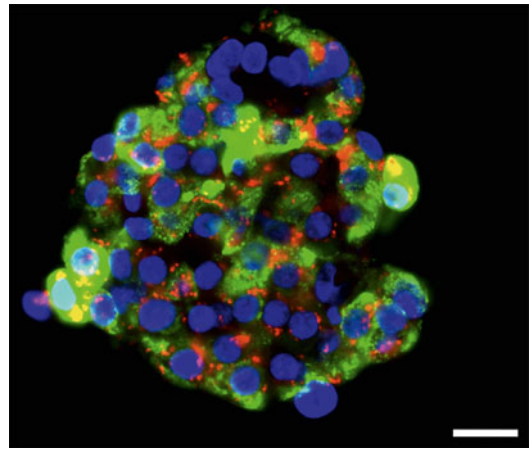

Fig. 2 Islets were treated with MN-Cy5.5-siRNA for 48 h. Fluorescence microscopy of the labeled islets shows heavy labeling of islet cells with MN-Cy5.5-siRNA probes. *Green*: insulin stain; *red*: Cy5.5 conjugated to the nanoparticles; *blue*: cell nucleus (magnification bar = 15 μm)

agarose gel in RNase-free TBE buffer and run at 145 V for 1 h. The gel is stained with 0.5 mg/mL ethidium bromide for 30 min, and visualized using a Molecular Imager FX scanner (Fig. 1) (*see* **Note 2**).

3.2 Human Islet Labeling with MN-Cy5.5-siRNA and Transplantation under the Kidney Capsule

1. Human islets are cultured in 24-well nontreated plates at 1000 islet equivalents (IEQ)/well in CMRL 1066 medium supplemented with 10 % FBS and 100 mg/mL penicillin-streptomycin (*see* **Note 3**). For labeling experiments, 1000 IEQ are incubated with MN-Cy5.5-siRNA containing cell culture medium (25 mg Fe/mL) for 48 h at 37 °C in a CO_2 incubator (*see* **Notes 4** and **5**).
2. Labeled pancreatic islets are fixed in 4 % formaldehyde for 10 min and spun down by centrifugation at 2000 rpm for 5 min. Then islet pellets are suspended in 100 μl of 1 % warm agarose/1× PBS solution at 60 °C. Next, the agarose-islet suspension is fixed with 4 % formaldehyde overnight, followed by paraffin embedding and tissue sectioning (*see* **Notes 6** and **7**).
3. Fluorescent immunostaining and Prussian Blue iron staining of the islets incubated with MN-Cy5.5-siRNA are used to identify the presence of nano-probes in the islets. The slides are deparaffinized and rehydrated. For fluorescent immunostaining (Fig. 2), after antigen retrieval with Tris-EDTA buffer (pH 8.0) in microwave oven at high for 10 min and blocking with 5 % goat serum in 1×PBS at room temperature for 1 h, the slides are incubated with guinea pig anti-human insulin primary antibody (1:50 dilution) at 4 °C overnight, followed by incubation with a FITC-labeled goat anti-guinea pig second-

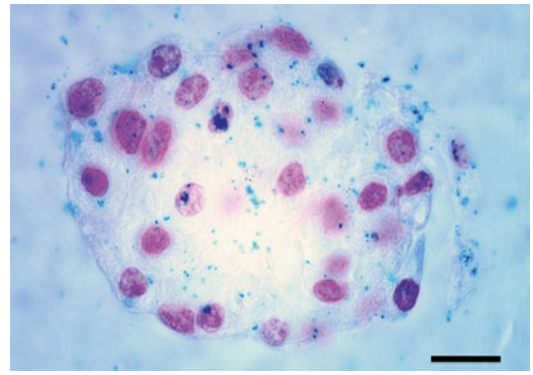

Fig. 3 Islets were treated with MN-Cy5.5-siRNA for 48 h. Prussian Blue staining demonstrates that islet cells are labeled with the iron oxide nanoparticle probes. *Blue*: iron oxide nanoparticles; *red*: cell nucleus (magnification bar = 15 μm)

ary IgG (1:100 dilution). Next, the slides are washed three times, counterstained, and mounted with mounting medium with DAPI. For Prussian Blue iron staining (Fig. 3), the sections are washed in 1×PBS for 5 min, and incubated in Prussian Blue solution containing 5 % potassium ferrocyanide and 5 % hydrochloric acid at RT for 1 h. Next, the slides are rinsed in double-distilled H_2O for 30 min followed by staining with Nuclear Fast Red for 5 min. Subsequently, the sections are dehydrated with graded ethanol and cleared with 100 % xylene. After drying overnight, the slides are mounted in 10 μl Permount mounting medium.

4. The sections stained for immunofluorescence and Prussian Blue iron stain are examined using Nikon Eclipse 50i microscope. Images are acquired using a CCD camera and analyzed with iVision 4.015 version software.
5. Islet phantoms for in vitro MRI are prepared by fixing islet pellets in 2 % formaldehyde and sedimenting them in 1 % agarose gel in Eppendorf tubes. Imaging is performed using a 9.4 T scanner equipped with ParaVision 5.1 software. The imaging protocol consisted of coronal T2-weighted spin echo (SE) pulse sequences with the following parameters: repetition time (TR)/echo time (TE) = 3000/8, 16, 24, 32, 40, 48, 56, 64 ms, field of view (FOV) = 3.2 cm^2, matrix size 128, resolution 250 mm^2, and slice thickness = 0.5 mm. T2 relaxation times are determined by T2 map analysis of regions of interest drawn around the islet pellets using Marevisi 3.5 software.
6. Diabetes in 5-week-old NOD/scid mice is induced by intraperitoneal injections of STZ (200 mg/kg body weight) freshly dissolved in sodium citrate buffer (*see* **Notes 8** and **9**). MN-Cy5.5-siRNA labeled human pancreatic islets are implanted

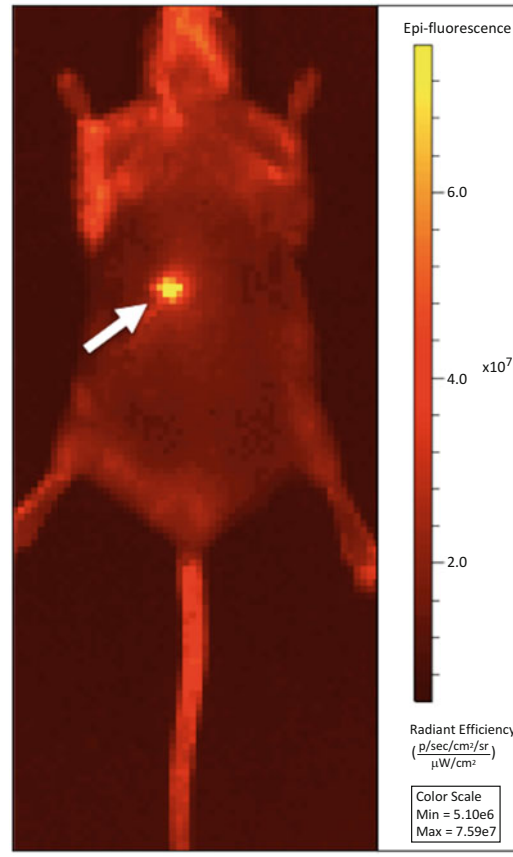

Fig. 4 In vivo near infrared optical imaging of islet grafts (*arrow*) under the left kidney capsule 3 days post-islet transplantation. The bright spot indicates the presence of Cy5.5 signal from the islet grafts labeled with MN-Cy5.5-siRNA

under the left kidney capsule (1500 IEQ/kidney) of NOD/scid mice. Normoglycemia is restored in all animals 2–3 days after transplantation (*see* **Note 10**).

3.3 In Vivo Optical and MR Imaging of Islet Grafts

1. Blood glucose levels of recipient mice are monitored using an Acensia Contour Blood Glucose Monitoring System twice weekly starting before the STZ injections and extending 7 weeks after islet transplantation.
2. In vivo optical imaging of islet grafts and 3D reconstruction

   All animals are fed with an alfalfa-free diet 2 weeks before islet transplantation (*see* **Note 11**). In vivo optical imaging is performed 7, 14, 21, 28, 35, 42, and 49 days after islet transplantation using an IVIS Spectrum whole-body animal imaging system. The Cy5.5 signal from the recipient mice is collected at 640 nm excitation and 720 nm emission (Fig. 4). The origin of

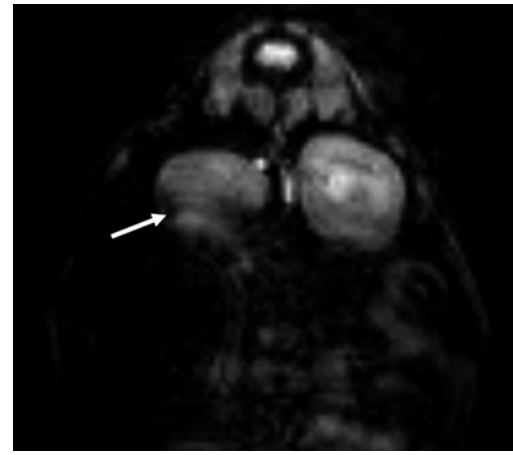

Fig. 5 T2-weightedMRI of the graft labeled with MN-Cy5.5-siRNA. MRI detects the islet grafts as a pocket-shaped signal void under the left kidney capsule (*arrow*)

the Cy5.5 signal in the animals is validated by 3D reconstruction using Living Image 4.2 software.

3. In vivoMRI of transplanted human islet grafts

   In vivo MRI of the recipient mice is performed 7, 14, 21, 28, 35, 42, and 49 days after islet transplantation using a 9.4-T scanner equipped with ParaVision 5.1 software. The imaging protocols consist of multi-slice multiecho T2-weighted map (for volume and T2 relaxivity measurement). Parameters: TR = 2000 ms and multiecho TE = 8, 16, 24, 32, 40, 48, 56, and 64; number of averages (NA) = 4; rapid acquisition with relaxation enhancement factor = 8; FOV = 4.4 cm^2, matrix size 128, spatial resolution 312 mm^2, and slice thickness = 0.5 mm. T2-weighted images are analyzed on a voxel-by-voxel basis by fitting the T2 measurements to a standard exponential decay curve, defined by the equation: [y = Aexp (-t/T2)]. Graft volumes under the kidney capsule are calculated by counting the number of voxels in each slice of a region of interest (ROI) outlining the graft and multiplying by the voxel volume (0.05 mm^3) using Marevisi 3.5 software (Fig. 5) (*see* **Note 12**).

4 Notes

1. The relaxivity values of the probes are determined at 37 °C using a Mini spec

   NMR spectrometer and the measurements of the longitudinal (R1) and transverse (R2) magnetization properties of the sample are represented as $mmol^{-1}$ s^{-1} for a given temperature.

The size and zeta potential of MN-Cy5.5-siRNA are measured using dynamic light scattering.

2. The selection of optimal magnetic separation column depends on the sample size and applications. The entire synthesis including the agarose gel electrophoresis has to be completed under RNase-free conditions.
3. Both the viability and purity of the islets used for the experiments should be higher than 85 %.
4. The viability of islets incubated with MN-Cy5.5-siRNA is determined by colorimetric (3-(4,5-dimethylthiazol-2-yl)-2,5-diphenyltetrazolium bromide assay using CellTiter 96 non-radioactive cell proliferation assay kit. After the treatment with MN-Cy5.5-siRNA probes for 48 h, islets are washed with culture medium two times, and resuspended in a 24 well non-treated plate followed by addition of 150 μl of a tetrazolium dye solution. After incubation at 37 °C for 4 h, 1 ml of solubilization solution/stop mix is added to each well to dissolve the dark blue crystals. After overnight incubation, the solution is transferred to cuvette and read on SpectraMax M2 spectrophotometer ($\lambda_{test} = 570$ nm and $\lambda_{reference} = 630$ nm).
5. Insulin secretion is evaluated by glucose-stimulated insulin secretion assay using static incubation of MN-Cy5.5-siRNA labeled islets at low (1.7 mmol/L) and high (20 mmol/L) glucose concentrations. Insulin concentrations in supernatants are measured using a human insulin ELISA kit. A stimulation index is calculated as the ratio of stimulated to basal insulin secretion normalized by the insulin content.
6. We find that frozen sections of islet agarose pellets are more easily detached from the glass slides.
7. Silencing efficacy of the target genes in islets incubated with the probe can be determined by real-time RT-PCR (at mRNA level) and Western blot (at protein level).
8. The STZ solution needs to be freshly prepared every time immediately before the injection by dissolving STZ in a sodium citrate buffer.
9. Diabetes in experimental animals is confirmed by weight loss, polyuria, and blood glucose levels higher than 250 mg/dL as assessed by an Acensia Contour Blood Glucose Monitoring System.
10. Intrahepatic islet transplantation via portal vein is an alternative transplantation site that has been found to be effective. Each of these locations has their own advantages and disadvantages. Therefore, the selection of an islet transplantation site should be determined by the objectives of the study.

11. An alfalfa-free diet can decrease the autofluorescence signal originated from the intestinal area of the animal.
12. Islet grafts can be easily identified on the surface of the recipient's kidney. To demonstrate ex vivo target gene downregulation in the islets grafts, immunostaining of tissue sections can be used. In addition, the graft tissue can be dissected from the kidney and collected for ex vivo western blot analysis and RT-PCR.

References

1. Lebastchi J, Herold KC (2012) Immunologic and metabolic biomarkers of beta-cell destruction in the diagnosis of type 1 diabetes. Cold Spring Harb Perspect Med 2(6):a007708. doi:10.1101/cshperspect.a007708
2. Azzi J, Geara AS, El-Sayegh S, Abdi R (2010) Immunological aspects of pancreatic islet cell transplantation. Expert Rev Clin Immunol 6(1):111–124
3. Kleijwegt FS, Roep BO (2013) Infectious tolerance as candidate therapy for type 1 diabetes: transfer of immunoregulatory properties from human regulatory T cells to other T cells and proinflammatory dendritic cells. Crit Rev Immunol 33(5):415–434
4. Narang AS, Mahato RI (2006) Biological and biomaterial approaches for improved islet transplantation. Pharmacol Rev 58(2):194–243. doi:10.1124/pr.58.2.6
5. Niclauss N, Morel P, Berney T (2014) Has the gap between pancreas and islet transplantation closed? Transplantation 98(6):593–599. doi:10.1097/TP.0000000000000288
6. Moore A, Medarova Z (2009) Imaging of siRNA delivery and silencing. Methods Mol Biol 487:93–110. doi:10.1007/978-1-60327-547-7_5
7. Medarova Z, Kumar M, Ng SW, Yang J, Barteneva N, Evgenov NV, Petkova V, Moore A (2008) Multifunctional magnetic nanocarriers for image-tagged SiRNA delivery to intact pancreatic islets. Transplantation 86(9):1170–1177. doi:10.1097/TP.0b013e31818a81b2
8. Medarova Z, Kumar M, Ng SW, Moore A (2009) Development and application of a dual-purpose nanoparticle platform for delivery and imaging of siRNA in tumors. Methods Mol Biol 555:1–13. doi:10.1007/978-1-60327-295-7_1
9. Wang P, Yigit MV, Medarova Z, Wei L, Dai G, Schuetz C, Moore A (2011) Combined small interfering RNA therapy and in vivo magnetic resonance imaging in islet transplantation. Diabetes 60(2):565–571. doi:10.2337/db10-1400
10. Wang P, Yigit MV, Ran C, Ross A, Wei L, Dai G, Medarova Z, Moore A (2012) A theranostic small interfering RNA nanoprobe protects pancreatic islet grafts from adoptively transferred immune rejection. Diabetes 61(12):3247–3254. doi:10.2337/db12-0441
11. Medarova Z, Evgenov NV, Dai G, Bonner-Weir S, Moore A (2006) In vivo multimodal imaging of transplanted pancreatic islets. Nat Protoc 1(1):429–435. doi:10.1038/nprot.2006.63
12. Evgenov NV, Medarova Z, Dai G, Bonner-Weir S, Moore A (2006) In vivo imaging of islet transplantation. Nat Med 12(1):144–148. doi:10.1038/nm1316
13. Evgenov NV, Medarova Z, Pratt J, Pantazopoulos P, Leyting S, Bonner-Weir S, Moore A (2006) In vivo imaging of immune rejection in transplanted pancreatic islets. Diabetes 55(9):2419–2428. doi:10.2337/db06-0484

Chapter 3

Magnetic Resonance Spectroscopy of siRNA-Based Cancer Therapy

Marie-France Penet, Zhihang Chen, Noriko Mori, Balaji Krishnamachary, and Zaver M. Bhujwalla

Abstract

Small interfering RNA (siRNA) is routinely used as a biological tool to silence specific genes, and is under active investigation in cancer treatment strategies. Noninvasive magnetic resonance spectroscopy (MRS) provides the ability to assess the functional effects of siRNA-mediated gene silencing in cultured cancer cells, and following nanoparticle-based delivery in tumors in vivo. Here we describe the use of siRNA to downregulate choline kinase, a critical enzyme in choline phospholipid metabolism of cancer cells and tumors, and the use of ^{1}H MRS of cells and ^{1}H magnetic resonance spectroscopic imaging (MRSI) of tumors to assess the efficacy of the downregulation.

Key words Choline metabolism, Dual-phase extraction, Magnetic resonance spectroscopy (MRS), Magnetic resonance spectroscopic imaging (MRSI), Nanoplex, Small interfering RNA (siRNA), Transient transfection

1 Introduction

Small interfering RNA (siRNA)-mediated silencing of specific targets has significant potential in cancer therapy to downregulate pathways that are frequently up-regulated in cancer cells, but not in normal tissue, achieving cancer cell-specific treatment [1]. A consistent metabolic hallmark observed in multiple cancers is the increase of cellular phosphocholine (PC) and total choline-containing compounds (tCho), which is closely related to malignant transformation, invasion, and metastasis [2–5]. Enzymes in choline phospholipid metabolism present attractive targets to exploit for treatment. Choline kinase-α (Chk-α) is an enzyme in the Kennedy pathway that phosphorylates free choline (Cho) to phosphocholine (PC), and its up-regulation in several cancers is a major contributor to increased PC levels. Here, we describe the use of siRNA targeting Chk-α and evaluate its functional effects on PC, phosphatidylcholine (PtdCho), and fatty acid levels using *in vitro*

Zdravka Medarova (ed.), *RNA Imaging: Methods and Protocols*, Methods in Molecular Biology, vol. 1372,
DOI 10.1007/978-1-4939-3148-4_3,

MRS and in vivo MRSI. MRS and MRSI are widely used to characterize tumor metabolism in both preclinical and clinical settings. With high-resolution ^{1}H MRS, it is possible to quantify the concentrations of free choline (Cho), PC, GPC, PtdCho and fatty acids. With ^{1}H MRSI, we can assess in vivo the efficacy of the treatment with siRNA directed against Chk-α by measuring the level of tCho that includes the PC signal. In ^{1}H MRSI, chemical information is spatially encoded, and the localized spectra can be processed to obtain images of metabolites. As MR methods are noninvasive, they can be translated easily from preclinical research to clinical applications. Here, we have described steps to downregulate Chk-α in human breast cancer MDA-MB-231 cells in culture, and in MDA-MB-231 tumors in mice.

2 Materials

2.1 Cell Culture, Transfection, and siRNA

RPMI medium (Sigma-Aldrich, St. Louis, MO).

Fetal bovine serum (FBS) (Gemini Bio-Products, West Sacramento, CA).

DharmaFECT4 (Thermo Fisher Scientific Inc., Waltham, MA).

siRNA against human Chk-α (5′-CAUGCUGUUCCAGUGCUCC-3′) (Thermo Fisher Scientific Inc., Waltham, MA).

2.2 Dual-Phase Extraction and High-Resolution ^{1}H MRS

Cold methanol, chloroform, and water.

Chelex bead (Sigma-Aldrich, St. Louis, MO).

High-speed centrifuge, rotary evaporator, lyophilizer.

5 mm NMR tubes (Wilmad Labglass, Buena, NJ).

Deuterated water (D_2O) (Sigma-Aldrich, St. Louis, MO).

3-(Trimethylsilyl) propionic 2,2,3,3-d4 acid sodium salt (TSP) (Sigma-Aldrich, St. Louis, MO).

Chloroform-D ($CDCl_3$) and methanol-D_4 (CD_3OD) (Cambrige Isotope Laboratories Inc., Tewksbury, MA).

Tetramethylsilane (TMS; Cambridge Isotope Laboratories Inc., Tewksbury, MA).

2.3 Nanoplex Synthesis

Bacterial cytosine deaminase, bCD.

Polyethyleneimine, PEI (Sigma-Aldrich, St. Louis, MO).

Poly-l-lysine, PLL (Sigma-Aldrich, St. Louis, MO).

Methyl polyethyl glycol succinimide ester (Nanocs. Inc., NY).

PEG-NHS ester (2 kDa) (Nanocs. Inc., NY).

N-succinimidyl-*S*-acetylthiopropionate, SATP (Pierce, Rockford, IL).

Rhodamine succinimide ester, rhodamine-NHS (Sigma-Aldrich, St. Louis, MO).

1,4,7,10-Tetraazacyclododecane-1,4,7,10-tetraacetic acid mono-N-hydroxysuccinimide ester, DOTA-NHS (Macrocyclics Dallas, TX).

Succinimidyl 4-formylbenzoate, SFB (Pierce, Rockford, IL).

HEPES buffer (pH 8.4).

Sodium acetate buffer (pH 4.6–5.5).

Cy5.5-NHS ester (GE Healthcare, Piscataway, NJ).

Succinimidyl 6-hydrazinonicotinamide acetone hydrazine, SANH (Pierce, Rockford, IL).

N-[e-Maleimidocaproyloxy]succinimide ester, EMCS (Pierce, Rockford, IL).

3 Methods

3.1 In Vitro Studies

3.1.1 Cell Transfection

1. Seed cells in a flask or dish. Cell density should be ~70–80 % confluent at the time of collection. In our studies, MDA-MB-231 breast cancer cells are seeded at 5×10^6 cells in 150 mm dish.
2. Twenty-four hours later, cells are transfected with 25–100 nM siRNA targeted against human Chk-α (5′-CAUGCUGUUC CAGUGCUCC-3′) using DharmaFECT4.
3. To transfect the cells, prepare two 15 mL Falcon tubes per transfection. In the first tube, add 1.8 mL of serum-free media followed by 200 μL of siRNA of desired concentration (diluted in 1× siRNA buffer) and mix well.
4. In the second tube, add 28 μL of DharmaFECT4 to 2 mL of serum-free media. Incubate both tubes for 5 min.
5. Mix the contents of both tubes and incubate this complex for an additional 20 min.
6. Add 18 mL of antibiotic free RPMI media supplemented with 10 % FBS to this complex, mix well, and add gently to the 150 mm dish containing MDA-MB-231 cells.
7. Incubate the cells at 37 °C incubator supplied with 5 % CO_2 for 48 h.

3.1.2 Dual-Phase Extraction

1. As described in Subheading 3.1.1, cells are plated, cultured for 24 h, and transfected with siRNA for 48 h.
2. Adherent cells are collected by trypsinization and counted using a hemocytometer. Trypan blue is added to cells during counting to correct for dead cells. More than 10^7 cells are needed for cell extraction to achieve good signal-to-noise ratio

(S/N) for MRS. Water-soluble as well as lipid extracts are obtained using the dual-phase extraction method. Dual phase extraction has the advantage that it does not significantly change the pH of the extracted material, and provides both the water-soluble and the lipid fractions of the cells, thereby leaving the lipids intact.

3. Pelleted cells are mixed with 4 mL of ice-cold methanol and vigorously vortexed.
4. After keeping the samples on ice for 10 min, 4 mL of chloroform are added.
5. The sample is vortexed vigorously and kept on ice for 10 min.
6. Finally, 4 mL of water are added and the sample is shaken well.
7. The sample is stored at 4 °C overnight for phase separation and then centrifuged at 20,000 × *g* at 4 °C for 30 min.
8. The water-methanol phase containing the water-soluble cellular metabolites can be treated with ~100 mg chelex beads for 10 min on ice to remove divalent cations, followed by removal of the chelex beads.
9. After removing the beads, methanol is evaporated using a rotary evaporator.
10. The remaining water phase is lyophilized and can be kept at –20 °C until analysis.
11. The chloroform phase containing the cellular lipids is dried in a stream of N_2 and stored under N_2 (i.e., the tube is "filled" with N_2) at –20 °C.

3.1.3 High-Resolution ^1H MRS

1. Water-phase cell extracts are resuspended in 0.6 mL deuterated water (D_2O) including 5 µL of 0.75 % (w/w) 3-(trimethylsilyl) propionic 2,2,3,3-d_4 acid sodium salt (TSP) in D_2O, which is used as an internal standard for concentration calculation and chemical shift assignment.
2. Lipid-phase cell extracts are resuspended in 0.4 mL of chroloform-D ($CDCl_3$) with 0.05 v/v % tetramethylsilane (TMS), as a concentration and chemical shift reference. 0.2 mL of methanol-D4 (CD_3OD) with 0.05 v/v % TMS are then added.
3. The samples are then ready to be analyzed using a high-field MR spectrometer. Conventional high-resolution ^1H MRS typically utilizes 3 mm to 5 mm probes to cover the sensitive volume of a sample size of 0.6 mL.
4. After placing the tube in the magnet, the probe is tuned and matched, the signal is then locked with D_2O for the water phase and CD_3OD for the lipid phase. Careful shimming is of utmost importance to obtain narrow line widths to resolve the peaks.

5. Fully relaxed high-resolution ^{1}H MR spectra are acquired using the following acquisition parameters: flip angle, 30°; sweep width, 10,000 Hz; repetition time, 11.2 s; time domain size, 32 K; 128 scans.
6. For metabolite quantification, the signals from fully relaxed MR spectra are integrated and the concentration of each detected metabolite of interest quantified based on the concentration standard. Signal integrals of the -*N*-$(CH_3)^3$ resonances of PC at ~3.225 ppm, GPC at ~3.235 ppm, and Cho at ~3.208 ppm are determined (Fig. 1).

In the lipid phase, the integrals of phosphatidylcholine at 3.220 ppm, and of the methylene groups in fatty acids (F_{mix}) at 1.245 to 1.364 ppm are measured, and related to the integral of the reference peak [1] (Fig. 2).

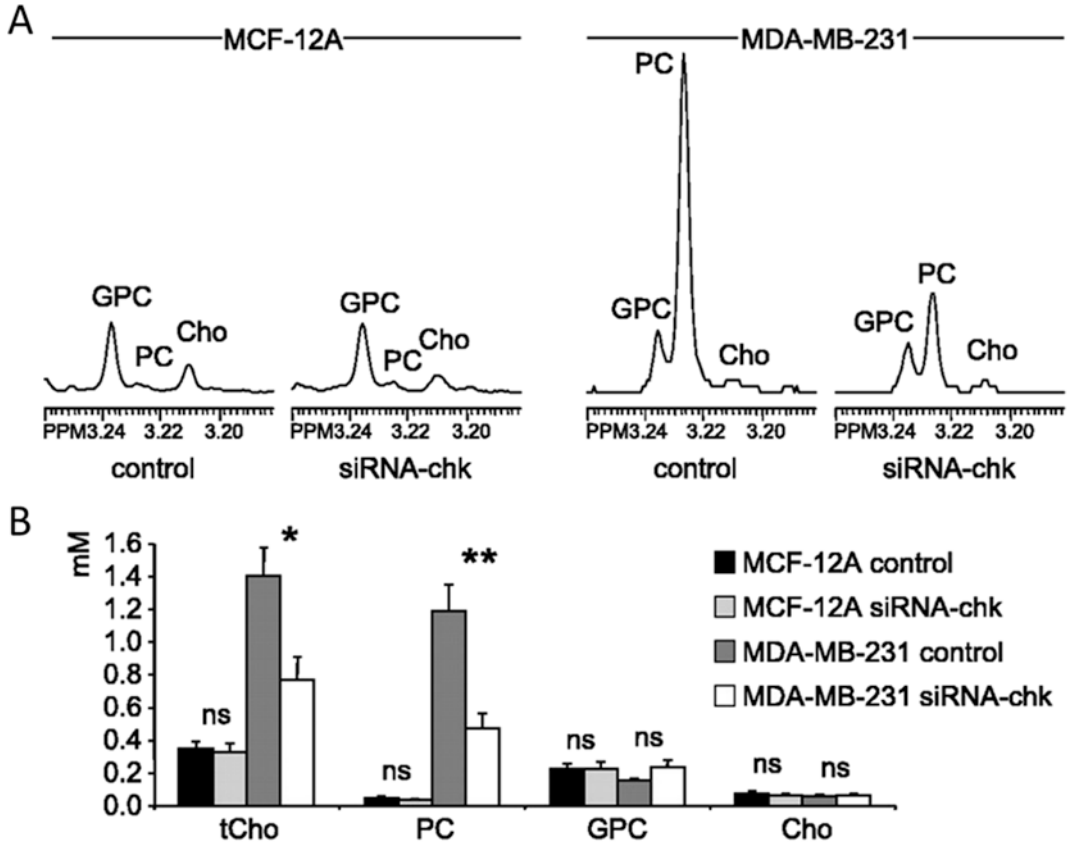

Fig. 1 (**a**) Expanded regions of ^{1}H MR spectra and (**b**) quantitation of ^{1}H MR spectra ($n=6$) from cell extracts of nonmalignant MCF-12A cells and malignant MDA-MB-231 breast cancer cells following 48 h of transient siRNA-Chk treatment. Abbreviations: Cho, free choline; GPC, glycerophosphocholine; PC, phosphocholine; tCho, total choline-containing compounds; ns, not significant. Columns, mean; bars, +/− SEM. *$P<0.05$; **$P<0.01$. Adapted with permission from ref. 1

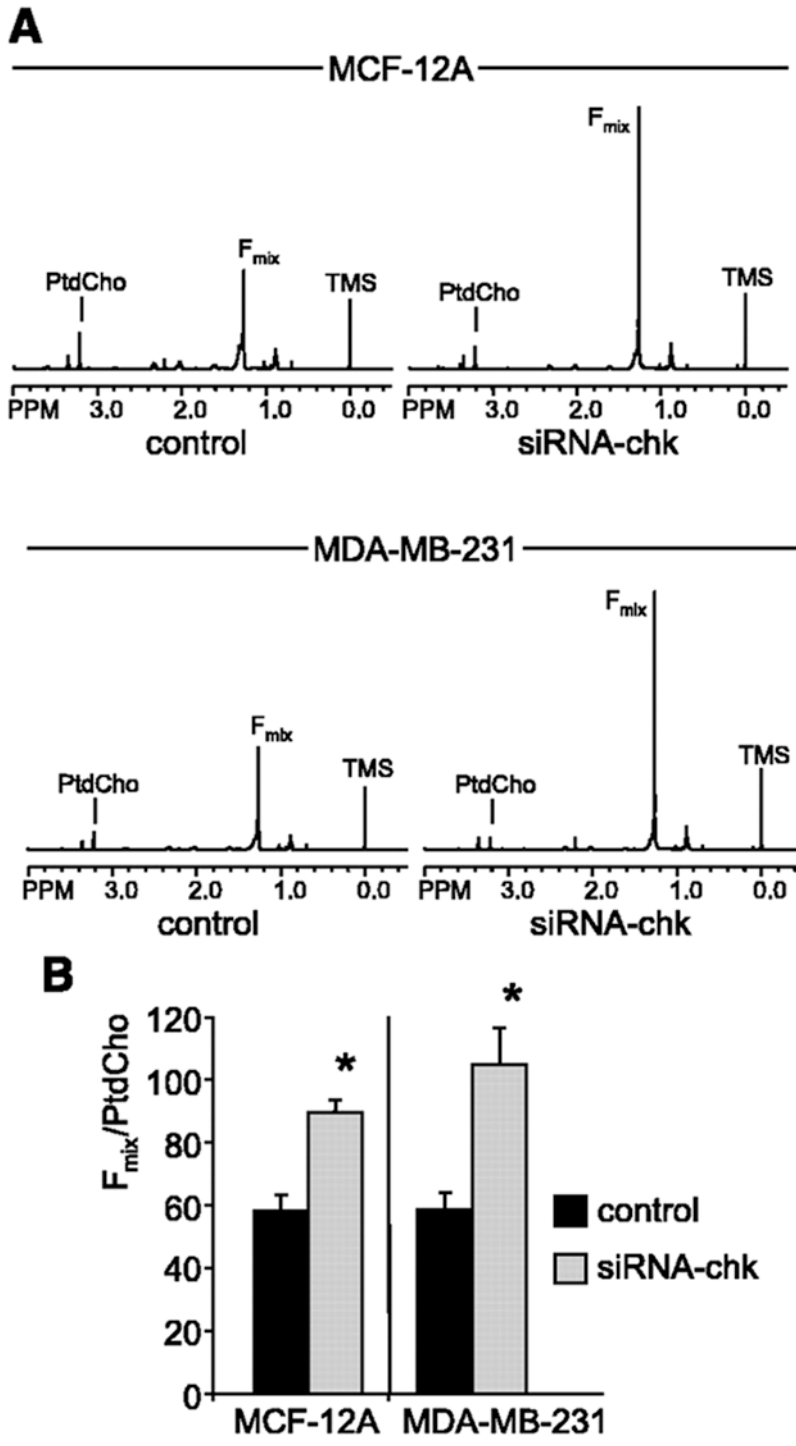

Fig. 2 (**a**) Representative ^{1}H MR spectra and (**b**) quantitation of the F_{mix}/phosphatidylcholine ratio from these ^{1}H MR spectra ($n=3$) obtained from lipid cell extract fractions of nonmalignant MCF-12A cells and malignant MDA-MB-231 breast cancer cells treated with siRNA-Chk. Abbreviation: PtdCho, phosphatidylcholine. *Columns,* mean; *bars,* +/− SEM. *$P<0.05$. Adapted with permission from ref. 1

To quantify the concentrations, the peak integration (I_{met}) from ^{1}H spectra for PC, GPC, and Cho are compared to that of the internal standard TSP (I_{TSP}) according to the equation

$$[\text{metabolite}] = A_{TSP}\frac{I_{met}}{I_{TSP}N_{cell}V_{cell}}$$

In this equation, [metabolite] represents the intracellular concentration of the metabolite of interest expressed in mmol/L (mM). A_{TSP} is the number of moles of TSP in the sample, N is the cell number, and V is cell volume. I represents the integral of the selected peak from the MR ^{1}H spectra. Because the number of protons contributing to the signals of PC, GPC, and Cho and the TSP peak is the same, a correction for differences in the number of protons is not required. The total choline (tCho) concentration is obtained by adding values for PC, GPC, and Cho. If the cell count is known, but not the cell volume, it is possible to quantify metabolites as fmol/cell. Cell volume, calculated as $[(4\pi/3)\times(d/2)^3]$, is determined by measuring the diameter (d) of 100 randomly selected cells using an optical microscope following cell trypsinization.

3.2 In Vivo Studies

3.2.1 siRNA Delivery In Vivo

We have used both non-targeted [6] and targeted [7] siRNA delivery in our in vivo studies. A brief synthesis of the non-targeted nanoplex (NP) carrying optical and MR imaging reporters is outlined in Fig. 3. In addition to choline kinase siRNA, the NP also carries a prodrug enzyme, bacterial cytosine deaminase (bCD) that converts nontoxic 5-fluorocytosine (5FC) to cytotoxic 5-fluorouracil (5FU). The non-targeted NP is delivered to the tumor through the enhanced permeability retention (EPR) effect. The targeted NP has been shown by us to act as a "theranostic agent" that binds to prostate-specific membrane antigen (PSMA) [7].

1. Initially, a *N*-hydroxysuccinamide (NHS) ester of polyethylene glycol (PEG, 2 kDa) is conjugated with polyethylenimine (PEI, 25 kDa) to form compound **2**.
2. Compound **2** is labeled with NHS-rhodamine to form compound **3**.
3. Compound **3** is conjugated with succinimidyl 4-formylbenzoate (SFB) in HEPES buffer at pH 8.4 to form compound **4**.
4. Poly-l-lysine (PLL, 6 kDa) is labeled with Cy5.5-NHS, DOTA (1,4,7,10-tetraazacyclododecane-1,4,7,10-tetraacetic acid)-NHS to produce compound **5**.
5. The DOTA on compound **5** reacts with $Gd_2(CO)_3$ to form compound **6**.
6. Compound **6** with the imaging reporter is labeled with *N-succinimidyl-S*-acetylthiopropionate (SATP) and succinimidyl 6-hydrazinonicotinamide acetone hydrazine (SANH) to produce compound **7**.

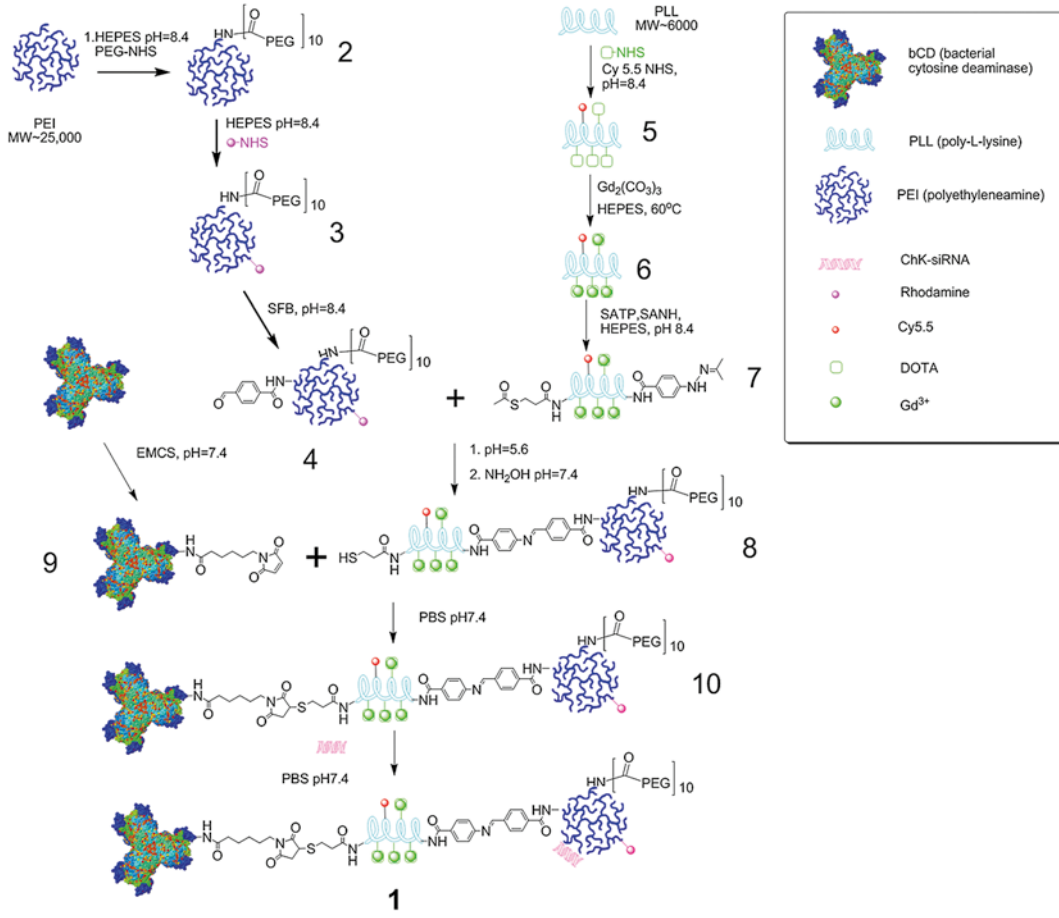

Fig. 3 Synthetic procedure to generate non-targeted NP loaded with siRNA and multiple imaging reporters

7. Conjugation of **4** and **7** at pH 7.4 produces the PEI-PLL copolymer, which is reduced to form compound **8** that contains a free sulfhydryl group.
8. Treatment of bCD with *N*-(e-maleimidocaproyloxy)-succinimide ester (EMCS) produces compound **9**.
9. Equimolar amounts of compounds **8** and **9** are cross-linked through the reaction of maleimide and sulfhydryl to provide the bCD-PLL-PEI.
10. Finally, electrostatic binding of siRNA with compound **10** gives the bCD-PLL-PEI/siRNA NP termed nanoplex **1**.
11. The NP is resuspended in 0.2 ml of PBS and injected intravenously at a concentration of 300 mg/kg.

3.2.2 Tumor Implantation

1. For the in vivo studies, 2×10^6 MDA-MB-231 human breast cancer cells are inoculated orthotopically in female severe combined immunodeficient (SCID) mice, in compliance with institutional guidelines established by the Institutional Animal Care and Use Committee of Johns Hopkins University. The mice are injected with the nanoplex and scanned when the tumors reach approximately 300 mm^3.
2. Noninvasive in vivo MRI and MRS studies are performed on a 9.4 T MR spectrometer (Bruker) using a solenoid coil placed around the tumor.
3. During the MR experiment, the animal being scanned is stably anesthetized, and the body temperature maintained by using a blanket circulating with warm water. Physiological parameters, such as body temperature, heart and breathing rates can be followed during the acquisition using specific equipment compatible with high magnetic field. Different anesthetics can be used to perform MRS studies, which are typically a gas anesthetic such as isoflurane, or injectable anesthetics such as a mixture of ketamine and acepromazine or xylazine.
4. Anatomic images are acquired using a multi slice multi echo T_1-weighted sequence, with an echo time of 15 ms, and a repetition time of 500 ms (Fig. 4). We usually acquire 8–12 consecutive 1 mm thick slices to visualize the whole tumor and a

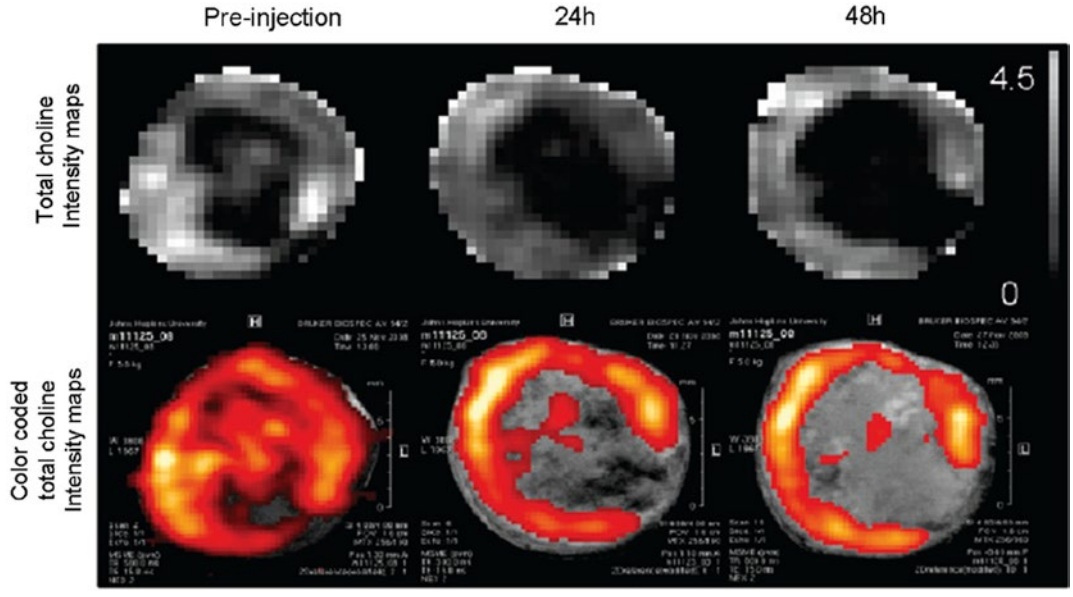

Fig. 4 Representative in vivo tCho maps and color-coded tCho intensity maps overlaid on corresponding T_1-weighted images of a tumor before and at 24 and 48 h after nanoplex injection (300 mg/kg, i.v.). Adapted with permission from ref. 6

4 mm thick slice localized generally within the center of the tumor. Before acquiring MRSI on the selected slice, we acquire first an anatomic image of the slice.

5. The geometry of the selected 4 mm thick slice is imported into a 2D chemical shift imaging (CSI) sequence. After shimming carefully, water-suppressed MRSI is performed, with an in-plane resolution of 1 mm × 1 mm per pixel with VAPOR water suppression. The following parameters are used: echo time (TE) of 120 ms, repetition time (TR) of 1000 ms, field of view of 1.6 cm × 1.6 cm, phase encode steps of 16, number of scans (NS) 8 for 2D CSI, block size 1024, and sweep width of 4000 Hz.
6. Water-unsuppressed reference MRSI is acquired from the same tumor slice as the water-suppressed MRSI, with a TE of 20 ms and an NS of 2. All other parameters are kept the same.
7. Spectroscopic images of the tCho signal at 3.2 ppm and the water signal at 4.7 ppm are generated from the MRSI data sets using an in-house IDL program and analyzed using the free-ware program ImageJ 1.37v (http://rsb.info.nih.gov/ij/).

4 Notes

To minimize spectral line width, only clear solutions should be measured as particulate matter can result in field inhomogeneities that widen line widths. Any particles left in the sample should be spun down before transferring the sample into the NMR tube.

The in vivo studies can be performed with a targeted NP as well, as shown in Fig. 5. In this example, we used a human prostate xenograft model, PC3-PIP, that overexpresses PSMA [7]. We used subcutaneously implanted male SCID mice for the study. The NP was targeted by incorporating a PSMA-specific targeting moiety, by conjugating initially a *N*-hydroxysuccinamide (NHS) ester of the low-molecular-weight urea-based PSMA inhibitor (PI) (2-(3-[1-carboxy-5-[7-(2,5-dioxo-pyrrolidin-1-yloxycarbonyl)-heptanoylamino]-pentyl]-ureido)-pentanedioic acid; MW 572.56) with maleimide-PEG-NH_2 (3.4 kDa) to form PI-PEG-maleimide. Detailed synthesis of the targeted NP can be found in [7].

Acknowledgements

Support from P50 CA103175, R01 CA82337, R01 CA73850, R01 CA136576, and R01 CA138515 is gratefully acknowledged.

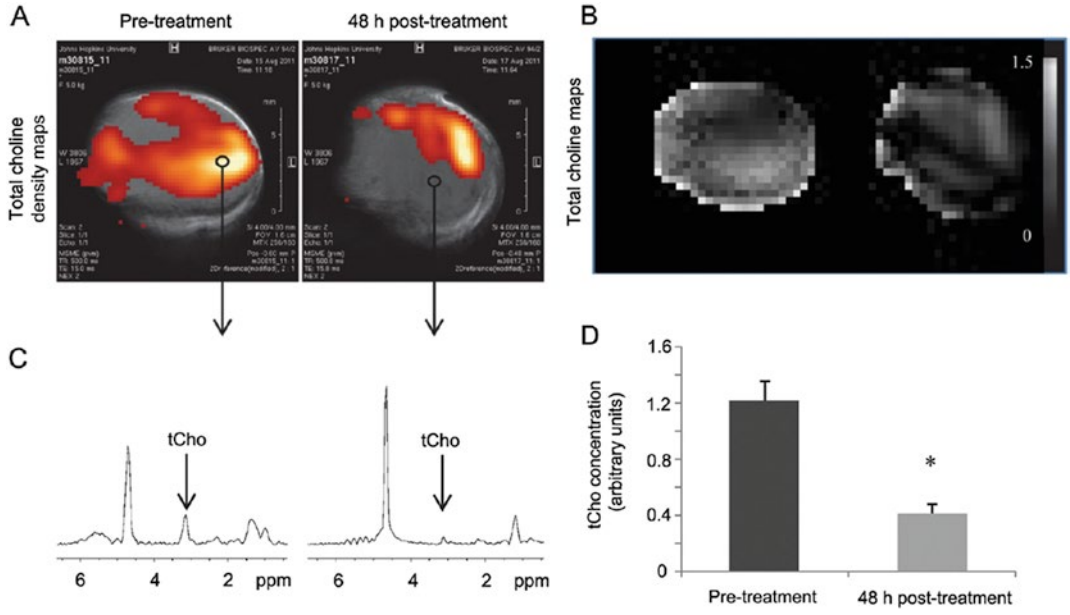

Fig. 5 (**a**) In vivotCho density maps from 2D CSI data sets acquired from a representative PC3-PIP tumor (~400 mm^3) before and 48 h after i.v. injection of the PSMA-targeted nanoplex (150 mg/kg). Parameters used were TE = 120 ms, TR = 1000 ms, 4 scans per phase encode step. CSI spectra were acquired at 9.4 T with an in-plane spatial resolution of 1 mm × 1 mm from a 4 mm thick slice. (**b**) Corresponding in vivo tCho maps from the same 2D CSI data sets. (**c**) Representative one voxel spectra from 2D CSI represented in A and B. (**d**) tCho concentration calculated in arbitrary units before and at 48 h after injection of the nanoplex. Values represent median +/− SEM ($n = 3$, $^*P < 0.05$). Adapted with permission from ref. 7

References

1. Glunde K, Raman V, Mori N, Bhujwalla ZM (2005) RNA interference-mediated choline kinase suppression in breast cancer cells induces differentiation and reduces proliferation. Cancer Res 65(23):11034–11043
2. Ramirez de Molina A, Banez-Coronel M, Gutierrez R, Rodriguez-Gonzalez A, Olmeda D, Megias D, Lacal JC (2004) Choline kinase activation is a critical requirement for the proliferation of primary human mammary epithelial cells and breast tumor progression. Cancer Res 64(18):6732–6739
3. Ramirez de Molina A, Rodriguez-Gonzalez A, Gutierrez R, Martinez-Pineiro L, Sanchez J, Bonilla F, Rosell R, Lacal J (2002) Overexpression of choline kinase is a frequent feature in human tumor-derived cell lines and in lung, prostate, and colorectal human cancers. Biochem Biophys Res Commun 296(3):580–583
4. Ramirez de Molina A, Gutierrez R, Ramos MA, Silva JM, Silva J, Bonilla F, Sanchez JJ, Lacal JC (2002) Increased choline kinase activity in human breast carcinomas: clinical evidence for a potential novel antitumor strategy. Oncogene 21(27):4317–4322
5. Nakagami K, Uchida T, Ohwada S, Koibuchi Y, Suda Y, Sekine T, Morishita Y (1999) Increased choline kinase activity and elevated phosphocholine levels in human colon cancer. Jpn J Cancer Res 90(4):419–424
6. Li C, Penet MF, Wildes F, Takagi T, Chen Z, Winnard PT, Artemov D, Bhujwalla ZM (2010) Nanoplex delivery of siRNA and prodrug enzyme for multimodality image-guided molecular pathway targeted cancer therapy. ACS Nano 4(11):6707–6716, PMCID: 2991391
7. Chen Z, Penet MF, Nimmagadda S, Li C, Banerjee SR, Winnard PT Jr, Artemov D, Glunde K, Pomper MG, Bhujwalla ZM (2012) PSMA-targeted theranostic nanoplex for prostate cancer therapy. ACS Nano 6(9): 7752–7762

Chapter 4

Targeted Delivery with Imaging Assessment of siRNA Expressing Nanocassettes into Cancer

Wei Chen and Lily Yang

Abstract

Molecular therapy using small interfering RNA (siRNA) shows great promise in the development of novel therapeutics for cancer. Although various approaches have been developed for in vivo delivery of siRNAs into tumors, stability of siRNA in blood circulation, and low efficiency of siRNA delivery into tumor cells are the major obstacles for further translation into cancer therapeutics. In this protocol, we describe methods of the production of shRNA expressing DNA nanocassettes by PCR amplification of double-stranded DNA fragments containing a U6 promoter and a shRNA gene. Those DNA nanocassettes can be conjugated to the polymer coating of nanoparticles that are targeted to cellular receptors highly expressed in tumor cells, such as urokinase plasminogen activator receptor (uPAR), for targeted delivery and receptor mediated internalization of shRNA expressing DNA nanocassettes. Methods for in vitro and in vivo evaluation of target specificity and gene-knockdown effect are also provided.

Key words Targeted nanoparticle, In vivo siRNA delivery, Imaging, Cancer therapy, shRNA expressing nanoparticle

1 Introduction

Human cancer cells are highly heterogeneous with dysfunctional signal pathways and intrinsic resistant mechanisms to stress and therapeutic agent induced cell death. To effectively treat drug resistant tumor cells, inhibition of key molecules that play the major roles in drug resistance by molecular targeted therapy using small interfering RNA (siRNA) is a promising approach in sensitizing tumor cells to therapeutic agents [1]. Although various approaches have been developed for delivering siRNAs into tumor cells, it has been very challenging to efficiently deliver sufficient amounts of siRNA into tumor cells in vivo following systemic delivery. The development of targeted siRNA delivery approaches that enable effective delivery of siRNA or siRNA producing vectors

Zdravka Medarova (ed.), *RNA Imaging: Methods and Protocols*, Methods in Molecular Biology, vol. 1372,
DOI 10.1007/978-1-4939-3148-4_4,

into tumor cells in vivo is significant for translating this molecular therapy into clinical applications [2, 3].

siRNA is a double-stranded RNA molecule with 19–23 base pairs in length and interacts with mRNA to inhibit the level of a specific gene expression. Short hairpin RNA (shRNA) is a hairpin RNA molecule that is processed by endoribonuclease (Dicer) to siRNA. shRNA can be chemically synthesized or expressed from a gene expression vector containing a U6 or H1 promoter and an shRNA gene [4]. Advantages of delivery a DNA-based shRNA expressing vector are its in vivo stability and the ability of expression of a high level of shRNA inside cells to prolong the effect of the gene knocking-down. However, the whole length shRNA plasmid or viral vector is very large (>4000 base pairs), with a large proportion of sequence supporting vector propagation and selection. Thus, to enable efficient delivery of shRNA into cells, we developed an shRNA expressing DNA cassette containing only core targeting sequence of shRNA and a U6 promoter to support its transcription inside eukaryotic cells [5].

We started by cloning the shRNA gene sequence into an shRNA expressing plasmid backbone, such as pSilencer. shRNA expressing DNA nanocassettes were then amplified by Polymerase Chain Reaction (PCR) using a pair of primers covering a short 5′-flank region of U6 promoter and a short 3′-terminal flank region following the shRNA core targeting sequence. This shRNA expressing double-stranded DNA nanocassette is around 500 base pairs (bps). It has equivalent inhibitory efficiency as the full length plasmid [5].

To deliver the shRNA cassette into targeted cells, we used quantum dots (QDs) or magnetic iron oxide nanoparticles (IONPs) to carry the shRNA cassette and serve as imaging probes for monitoring the delivery of the DNA nanocassettes. QDs produces fluorescent signal and can be used to track localization of the nanocassettes in vitro by cell imaging and in vivo by optical imaging. However, potential clinical application in humans may be limited due to a low sensitivity of optical imaging to detect signals in deep tissues and long-term toxicity concerns [6]. IONP is biocompatible and biodegradable, and produce MRI contrast for noninvasive tumor imaging [7]. The surface of the above nanoparticles has been functionalized with carboxyl residuals, which can be used for conjugation with amine containing molecules [7]. To conjugate shRNA nanocassettes to IONP, the reverse PCR primer is modified with an amine at the 5′ end, so that the PCR products can conjugate to the carboxyl group of the polymer coating by an amide bond mediated by EDAC [8].

Another advantage of these nanoparticles is that they can be decorated with many molecules simultaneously to enable multifunction, such as dyes for optical imaging, targeting ligand for tumor specific delivery, and chemotherapeutic drugs to enable

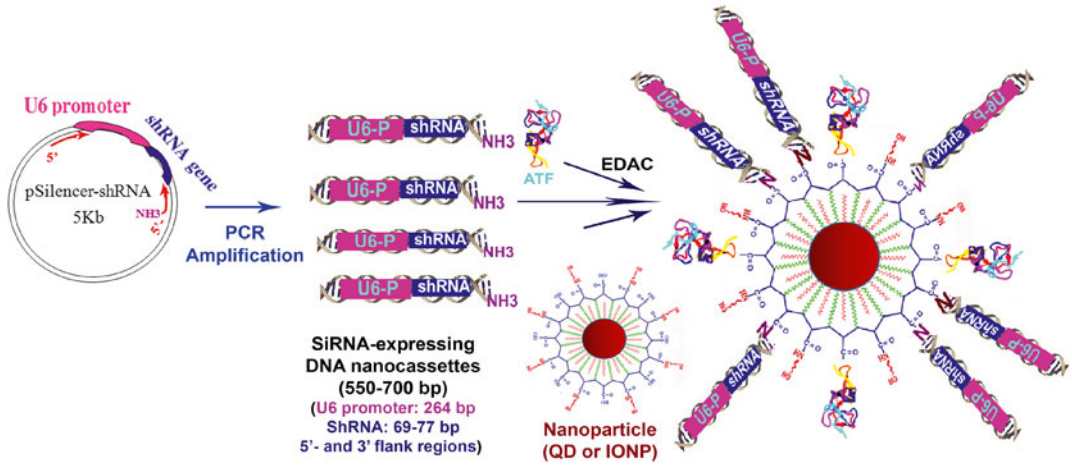

Fig. 1 Schematic illustration of the design of siRNA expression nanoparticle. siRNA expressing DNA cassette is cloned from a plasmid by PCR amplification. The PCR products encompass a U6 promoter and shRNA gene sequence, and are labeled with an amine group at one end. The shRNA cassettes and targeting ligands are then conjugated to nanoparticles using carboxyl/amine reaction. (Reprinted with permission from John Wiley & Sons, Inc. [5])

therapeutic effect [9]. In this protocol, we use amino terminal fragment (hATF) of human urokinase plasminogen activator (uPA) as a targeting ligand, which targets its receptor uPAR in tumors [10, 11]. The design of this nanoparticle is illustrated in Fig. 1. Using a LuciferaseshRNA as a model system, we show the methods of conjugation of shRNA expressing DNA nanocassettes to nanoparticles and evaluation of the effect of the nanoparticle shRNA delivery carriers in vitro in cancer cell lines and in vivo in animal tumor models. Results of our studies showed that uPAR targeted nanoparticles could efficiently deliver luciferase shRNA cassettes into cancer cells in vitro and inhibit target gene expression. In vivo administration of nanoparticles in human cancer xenograft models led to the inhibition of the level of luciferase gene expression in tumors. This protocol provides a framework for the development of targeted delivery of siRNA using shRNA expressing DNA cassettes both in vitro and in vivo, as well as method for monitoring delivery of nanoparticle-shRNA delivery carriers by noninvasive optical imaging.

2 Materials

2.1 shRNA Cloning

1. An appropriate shRNA expressing plasmid, such as pSilencer™ 2.1-U6 neo that can be purchased from Applied Biosystems (Life Technologies, Carlsbad, CA).
2. Synthesizing shRNA template sequences. The inserted shRNA fragments are chemically synthesized (Integrated DNA

Table 1
Oligonucleotides for shRNA plasmid cloning and PCR

	Name	Sequence
Cloning primers	Random control	5′-AAGAGGCTTGCAACAGTGCA-3′
	Firefly luciferase	5′-CGGATTACCAGGGATTTCA-3′
PCR primers	Forward	5′-GATGTGCTGCAAGGCGATTA-3′
	Reverse	*5′-GGAAACAGCTATGACCATGA-3′

*The reverse primer is modified at the 5′ end with an amine group for conjugation to nanoparticles

Technology, Coralville, Iowa) containing the following structure: 5′-GATCC (BamHI)-19–23 nt shRNA sense sequences-TTCAAGAGA (Loop sequence)-19–23 nt shRNA antisense sequences-TTTTTTGGAAA (Terminate sequence)-A (HindIII). The shRNA sense sequences are listed in Table 1.

3. Restriction endonucleases BamHI and HindIII, T4 DNA ligase (Sigma-Aldrich, St. Louis, MO).
4. Synthesizing PCR primers for amplification of shRNA cassettes (*see* **Note 2**). The sequences of PCR primers are listed in Table 1.
5. OneTaq® DNA Polymerase PCR kit for PCR reaction (M0480, New England Biolabs, Ipswich, MA).
6. Spectrophotometer for DNA quantification (Bio-Rad Laboratories, Inc., Hercules, CA)

2.2 Nanoparticles and Bioconjugation

1. Amphiphilic polymer coated quantum dots (QDs, emission wavelength of 620 nm) or iron oxide nanoparticles (IONPs) with 10 nm core size are provided by the Ocean Nanotech (Ocean Nanotech, San Diego, CA).
2. 6.5 mM (1 mg/mL) EDAC (Pierce, Rockford, IL) dissolved in borate buffer (pH 5.0). EDAC solution should be prepared before conjugation and used immediately.
3. 4.6 mM (1 mg/mL) sulfo-NHS (Pierce, Rockford, IL) dissolved in borate buffer (pH 5.0). sulfo-NHS solution should be prepared before conjugation and used immediately.
4. 50 mM borate buffer prepared by diluting the 20× stock solution (Pierce, Rockford, IL) with water. Adjust to pH 5.0 or pH 8.6.
5. Nanosep 100 k column (Pall Corp, Ann Arbor, MI).
6. Targeting ligands can be antibodies, antibody fragments, peptides, and recombinant natural ligands. For the uPAR targeting ligand, we use the 135 amino acids of recombinant receptor binding domain of uPA. cDNA of the recombinant amino

terminal fragment of human uPA (hATF) is cloned into pET20a plasmid (Life Technologies, Carlsbad, CA), and expressed in *E. coli* BL21 bacterial expression system [10, 11].

7. Ni-NTA agarose beads (Qiagen, Valencia, CA).
8. Bradford protein assay (Bio-Rad Laboratories, Inc., Hercules, CA).
9. Zetasizer Nano (Malvern Instruments Inc., Southborough, MA).
10. Syngene G:BOX imaging system (Syngene, Frederick, MD).
11. Centrifuge 5430 R (Eppendorf, Hamburg, Germany).

2.3 Cell Lines and Animals

1. Cancer cell lines that stably express a firefly luciferase gene can be used to establish human tumor xenograft model. We use both the MCF-10DCIS human breast cancer cell line (Asterand US, Detroit, MI) [12] and the MIAPaCa-2 human pancreatic cancer cell line (MIAPaCa-2-luc, kindly provided by Dr. Rosa Hwang, MD Anderson Cancer Center, Houston, TX) [13]. MCF-10DCIS cells are cultured in the DMEM/F12 medium supplemented with 5 % horse serum. MCF-10DCIS cell line was transfected with a lentiviral vector, LV-pUB-Fluc-eGFP that provided dual firefly luciferase and enhanced green fluorescence protein (eGFP) expression (hereafter MCF-10DCIS-luc). MIAPaCa-2-luc cells are cultured in the DMEM medium supplemented with 10 % fetal bovine serum.
2. Athymic nude mice (6–8 weeks old) for establishment of human tumor xenograft models can be purchased from qualified vendors.
3. D-Luciferin substrate (Caliper Life Sciences, Hopkinton, MA) is prepared into a fresh stock solution at 15 mg/ml in DPBS.
4. Xenogen IVIS Spectrum system (Caliper Life Sciences, Hopkinton, MA).
5. Olympus OV-100 imaging system (Olympus America Inc., Central Valley, PA) or other in vivo optical imaging systems.
6. Lipofectamine 2000 (Life Technologies, Carlsbad, CA).

3 Methods

3.1 Cloning Plasmid

1. Anneal the shRNA templates by heating the templates followed by gradually cooling.
2. Linearize pSilencer™ 2.1-U6 neo plasmid with restriction endonucleases BamHI and HindIII.
3. Ligate the annealed shRNA template sequences with the linearized plasmid using T4 DNA ligase.

4. Transform competent cells, such as DH5 alpha, with the ligation products. Plate the transformed cells on LB plates containing 100 μg/ml ampicillin and grow overnight at 37 °C.
5. Pick clones, isolate plasmid DNA, and validate the plasmid by DNA sequencing. For detailed information of cloning procedure, please check the protocol provided by the manufacturer of the plasmid.

3.2 Amplification of shRNA Expressing DNA Cassettes

1. Set up PCR reaction with the following components: 10 μl 5× One*Taq* Standard Reaction Buffer, 1 μl of 10 mM dNTPs, 10 μM of forward and reverse primers each, 0.25 μl of One*Taq* DNA Polymerase, and 1 ng of plasmid DNA. Add water to make the final volume to 50 μl.
2. Run the PCR using the following thermocycling condition: initial denaturation at 94 °C for 5 min; then 94 °C for 30 s, 58 °C for 30 s, 68 °C for 50 s for a total of 32 cycles; final extension at 68 °C for 5 min (*see* **Notes 3** and **4**).
3. Purify the PCR products by ethanol precipitation and resuspend the purified DNA in water.
4. Quantify the DNA with a spectrophotometer.
5. Test DNA by 2 % agarose electrophoresis.

3.3 Preparing hATF Protein

Recombinant hATF protein is expressed in *E. coli* BL21 and purified from bacterial extracts under native conditions using Ni-NTA agarose beads. The purified protein is then examined by 12 % SDS-PAGE, and followed by Coomassie Blue staining. The concentration of protein is quantified by Bradford protein assay.

3.4 Production of Targeted Nanoparticles

3.4.1 Conjugation of Targeting Ligand to Amphiphilic Polymer-Coated Nanoparticles, Such as QDs and IONPs

1. Spin down the buffer that is used to store nanoparticles with a Nanosep 100 k column at 2000 × *g* for 3 min.
2. Resuspend nanoparticles with 100 μl of borate buffer (pH 5.0).
3. Add fresh made EDAC and sulfo-NHS solution into nanoparticles at a molar ratio of 1:400:200 for nanoparticles:EDAC:sulfo-NHS. Mix thoroughly by vortexing. Rotate the tube at room temperature for 10 min.
4. Stop the reaction by spinning the solution in a Nanosep 100 k column at 2000 × *g* for 3 min. Thus, the total reaction time (rotation plus centrifuging) should be less than 15 min.
5. Resuspend the activated nanoparticles by adding 200 μl of borate buffer (pH 8.6). Carefully add small drops of hATF into the solution and mix by vortexing. Repeat the process until all hATF is added. The molar ratio of nanoparticles:hATF is 1:10. Rotate the solution at room temperature for an additional 4 h.

6. Transfer the solution into a 100 K Nanosep column and centrifuge at 2000 × *g* for 3 min until all the media is filtered through (longer time of centrifuging may be needed).

3.4.2 Assembling Nanoparticle-hATF and shRNA

1. Resuspend nanoparticle-hATF conjugates from the previous step with 100 μl of borate buffer (pH 5.0).
2. Conjugate nanoparticle-hATF with shRNA using the EDAC method as described in Subheading 3.4.1. The molar ratio of nanoparticles:shRNA can be adjusted based on the applications, typically in a range of 1:1 to 1:10.
3. Wash nanoparticles with sterilized water for two times, and spin down the media in a 100 K Nanosep column at 2000 × *g* for 3 min until all the media is filtered through (longer time of centrifuging may be needed).
4. Resuspend nanoparticles with desired amount of water based on nanoparticle concentrations required for specific applications and collect the products.

3.4.3 Characterizing Nanoparticles

1. Determine concentration of nanoparticles. For IONPs, read the OD at 500 nm after 50–100 times dilution of nanoparticle in water. Multiply the absorbance value with the dilution factor then divide by a factor of 4.3 to get the iron concentration in mg/ml. For QDs, read the fluorescence at emission wavelength of 620 nm. Use standard sample (like the stock QDs) to create a reference curve, and calculate the concentration of QD products based on the curve.
2. Examine the particle size distribution using Zetasizer Nano.
3. Examine the nanoparticles using electrophoresis in 2 % agarose gel at 100v for 30 min. Stain the gel with DNA dye, then examine the gel using an optical imaging system (QDs) or UV-transilluminator (IONPs) (*see* **Note 5**) (Fig. 2).

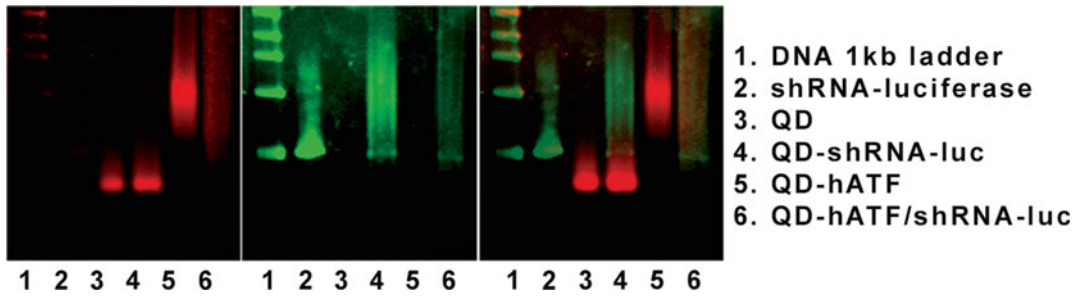

Fig. 2 Agarose gel electrophoresis of QD-hATF/shRNA nanoparticles. The *left panel* shows QDs in *red*; the *middle panel* shows DNA in green fluorescence; the *right panel* shows the overlay of QDs with DNA. QDs that conjugated with DNA nanocassettes show *orange color*. (Reprinted with permission from John Wiley & Sons, Inc. [5])

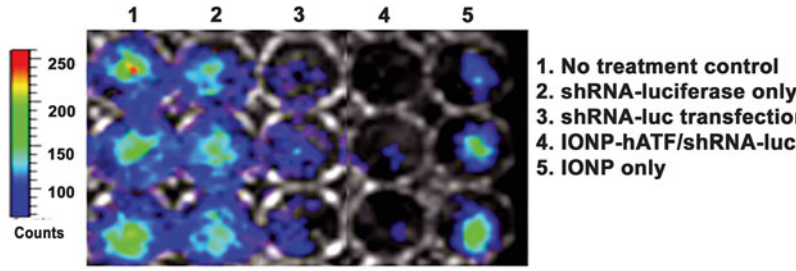

Fig. 3 Testing gene knockdown efficacy of Luciferase shRNA nanoparticle carriers in vitro. MIAPaCa-2-luc cells cultured in 96-well plates are incubated with 20 pmol of luciferase shRNA cassette (shRNA-luciferase) or IONP-hATF-luc siRNA expressing cassettes containing equivalent molar of DNA. To serve as a positive control, shRNA-luciferase cassette is also delivered into cells with a classic transfection reagent Lipofectamine 2000. Luciferase activity of cells is measured 48 h following the incubation with D-Luciferin substrate using the Xenogen IVIS system. The result shows that IONP-hATF-luc has better inhibitory efficacy of luciferase activity than the other groups. (Reprinted with permission from John Wiley & Sons, Inc. [5])

3.5 Testing the Nanoparticle In Vitro

1. A luciferase gene stably transfected cell line, such as MIAPaCa-2-luc, is added into a 96-well tissue culture plate for 24 h to grow to 50 % confluence.
2. Dilute shRNA DNA cassettes or hATF/shRNA conjugated nanoparticles containing equivalent of shRNA in RPMI-1640 media and then add 100 μl of prepared media containing 20 pmol of shRNA DNA cassettes to each well, and treat cells for 4 h.
3. Replace the media with full culture media containing 10 % FBS, and keep for 44 h.
4. To serve as a positive control, transfect the same amount of shRNA cassettes using a transfection reagent, such as Lipofectamine 2000 using the manufacturer's protocol.
5. Two days after treatment, perform bioluminescence imaging by adding 150 ug/ml D-Luciferin substrate to the culture media, and detecting luciferase activity using Xenogen IVIS Spectrum system as shown in Fig. 3 (*see* **Note 6**).

3.6 Testing the Nanoparticle In Vivo

3.6.1 Establish Human Tumor Xenograft Mode

The MCF-10DCIS-luc human breast cancer cells at 80 % confluence are trypsinized and washed with PBS. Orthotopic human breast cancer xenograft model is established by injecting 1×10^6 cells into the mammary fat pad of the nude mice.

3.6.2 Administrate Nanoparticles into Tumor Bearing Mice

One week after tumor inoculation when tumor is about 5–8 mm in diameter, inject 200–300 picomolar of nanoparticles, such as QDs, carrying hATF and luciferase siRNA-expressing DNA cassettes (about 2 nmol of DNA cassettes) into the tail vein of mice.

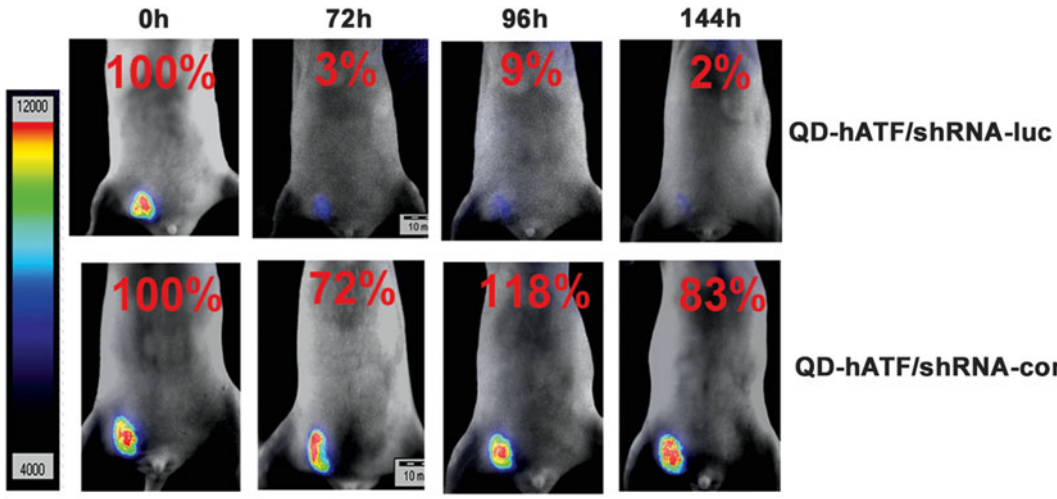

Fig. 4 Evaluation of targeted delivery and efficiency of inhibition of gene expression using uPAR targeted shRNA delivery nanoparticles in vivo in a human tumor xenograft model. QD-hATF-luc or control scrambled shRNA nanocassette are injected into nude mice bearing human breast cancer via the tail vein. Bioluminescence images are taken at different time points following the injection. Numbers in the figure show changes in the percentages of luciferase activity compared with the level in the tumor before the treatment. QD-hATF-luc nanoparticle shows substantial inhibitory effects during a 6-day observation post treatment. (Reprinted with permission from John Wiley & Sons, Inc. [5])

3.6.3 In Vivo Bioluminescence Imaging (BLI)

1. Before and at different time points following the nanoparticle administration, perform the bioluminescence imaging to assess luciferase activity of tumors. Firstly, anesthetize the mice by injecting a mixture of 95 mg/kg ketamine hydrochloride and 5 mg/kg xylazine in sterile saline intraperitoneally (i.p.).
2. Inject D-Luciferin substrate 150 mg/kg body weight i.p. into the nude mice 5 min before each bioluminescence imaging procedure.
3. Perform the bioluminescence imaging using Xenogen IVIS Spectrum system by following the instructions of the manufacturer (Fig. 4).

4 Notes

1. Use sterile water, pipette tips, and tubes in the experiment. Apply aseptic techniques as strictly as possible. This is extremely important when the conjugated nanoparticles will be used in animals.
2. To protect the DNA cassettes from digestion by deoxyribonucleases after injected into mice, the PCR primers can by modified at the 5′ end with a phosphorothioate linkage [14].

3. PCR conditions may need to be optimized according to different shRNA, PCR kit used in order to get the highest yield of PCR reaction.
4. For in vivo study, a large amount of shRNA cassettes will be needed. To generate enough shRNA cassettes, simply set up large scales of PCR reactions and run the PCR in parallel. In our experiment, about 5 μg of product can be generated after a standard PCR run with 50 μl volume.
5. Various methods can be used to assess the delivery efficacy of nanoparticles in vitro, for example RT-PCR, western blot or bioluminescence imaging for detecting the level of target gene expression.
6. For examination of IONP conjugates, nanoparticles and DNA cassettes are loaded onto agarose gel and run the electrophoresis at 100 v for 30 min. Stain the gel with DNA dye. Then the gel can be visualized using a gel imaging system, for example Syngene G:BOX imaging system. Apply the UV filter to see the fluorescence from DNA or IONP-hATF/shRNA conjugates. Switch off the UV filter to visualize IONP (brown color).

Acknowledgement

This work is supported by NIH U01 CA 151810 (Yang) grant.

References

1. Devi GR (2006) siRNA-based approaches in cancer therapy. Cancer Gene Ther 13(9):819–829
2. Kanasty R, Dorkin JR, Vegas A, Anderson D (2013) Delivery materials for siRNA therapeutics. Nat Mater 12(11):967–977
3. Whitehead KA, Langer R, Anderson DG (2009) Knocking down barriers: advances in siRNA delivery. Nat Rev Drug Discov 8(2):129–138
4. Paddison PJ, Caudy AA, Bernstein E, Hannon GJ, Conklin DS (2002) Short hairpin RNAs (shRNAs) induce sequence-specific silencing in mammalian cells. Genes Dev 16(8):948–958
5. Cho YS, Lee GY, Sajja HK, Qian W, Cao Z, He W, Karna P, Chen X, Mao H, Wang AY, Yang L (2013) Targeted Delivery of siRNA-Generating DNA Nanocassettes Using Multifunctional Nanoparticles. Small 9(11):1964–1973
6. Gao X, Cui Y, Levenson RM, Chung LW, Nie S (2004) In vivo cancer targeting and imaging with semiconductor quantum dots. Nat Biotechnol 22(8):969–976
7. Peng XH, Qian X, Mao H, Wang AY (2008) Targeted magnetic iron oxide nanoparticles for tumor imaging and therapy. Int J Nanomedicine 3(3):311
8. Hermanson GT (2008) Bioconjugate techniques (second edition). London, p.219
9. Lee GY, Qian WP, Wang L, Wang YA, Staley CA, Satpathy M, Nie S, Mao H, Yang L (2013) Theranostic nanoparticles with controlled release of gemcitabine for targeted therapy and MRI of pancreatic cancer. ACS Nano 7(3): 2078–2089
10. Yang L, Peng XH, Wang YA, Wang X, Cao Z, Ni C, Karna P, Zhang X, Wood WC, Gao X, Nie S, Mao H (2009) Receptor-targeted nanoparticles for in vivo imaging of breast cancer. Clin Cancer Res 15(14):4722–4732
11. Yang L, Mao H, Cao Z, Wang YA, Peng X, Wang X, Sajja HK, Wang L, Duan H, Ni C, Staley CA, Wood WC, Gao X, Nie S (2009) Molecular imaging of pancreatic cancer in an animal model using targeted multifunctional nanoparticles. Gastroenterology 136(5):1514–1525

12. Dohi T, Okada K, Xia F, Wilford CE, Samuel T, Welsh K, Marusawa H, Zou H, Armstrong R, Matsuzawa S, Salvesen GS, Reed JC, Altieri DC (2004) An IAP-IAP complex inhibits apoptosis. J Biol Chem 279(33):34087–34090
13. Chen Y, Zhu X, Zhang X, Liu B, Huang L (2010) Nanoparticles modified with tumor-targeting scFv deliver siRNA and miRNA for cancer therapy. Mol Ther 18(9):1650–1656
14. Spitzer S, Eckstein F (1988) Inhibition of deoxyribonucleases by phosphorothioate groups in oligodeoxyribonucleotides. Nucleic Acids Res 16(24):11691–11704

Chapter 5

Analyses of Tumor Burden In Vivo and Metastasis Ex Vivo Using Luciferase-Expressing Cancer Cells in an Orthotopic Mouse Model of Neuroblastoma

Frances L. Byrne, Joshua A. McCarroll, and Maria Kavallaris

Abstract

Cancer xenograft mouse models are useful for examining and understanding tumor growth and cancer progression in vivo. With the development of bioluminescent imaging, these parameters can now be monitored noninvasively with relative ease. Herein we describe imaging of luciferase-expressing cancer cells to quantitatively measure tumor burden in vivo and metastases ex vivo. Specifically, we detail the methodology to examine the effect of shRNA-mediated knockdown of a target gene on the growth and spread of neuroblastoma tumors in immune-deficient mice.

Key words Orthotopic, Neuroblastoma, Luciferase, Metastasis, Short hairpin RNA

1 Introduction

Metastasis is a major cause of cancer-related deaths. Understanding what drives the metastatic process is vital for the development of cancer therapies against metastatic disease. Therefore cancer xenograft mouse models that can mimic the metastatic process are valuable for understanding the biology of the disease and the preclinical evaluation of anti-metastatic targets and agents. Animal models of metastasis require injection of cancer cells either intravenously (experimental) or into the correct anatomical site of the primary tumor (orthotopic). The experimental metastasis model determines the ability of tumor cells (already in circulation) to arrest and grow at different sites. However, the route of injection, such as the lateral tail vein or portal vein, mostly determines the site of tumor growth, namely the lungs or liver [1, 2]. Additionally, other caveats to the experimental metastasis model is that many steps in the metastatic cascade, such tumor–stromal cell interactions at the primary tumor site and tumor cell intravasation (entry into

Zdravka Medarova (ed.), *RNA Imaging: Methods and Protocols*, Methods in Molecular Biology, vol. 1372,
DOI 10.1007/978-1-4939-3148-4_5,

circulation), are excluded. In orthotopic models, spontaneous metastases can arise at distant sites as a result of tumor cell dissemination from the primary tumor. This occurs via a metastatic cascade which requires tumor cell invasion of the extracellular matrix (ECM), intravasation, survival of cancer cells in the blood/lymphatic system (resistance to anoikis), extravasation, and growth of the tumor in a new microenvironment [1, 2]. It is worth noting that some cancer cells, even those of the same tumor type, have a greater capacity to metastasize than others and can preferentially hone to different organs or bones [3, 4]. Choosing which metastatic model and cancer cell to use for a particular study will depend on the experimental question to be addressed. These models are best complimented with in vitro (migration and invasion assays) and additional in vivo assays.

Bioluminescent imaging (BLI) is one method to non-invasively monitor tumor growth in vivo. Cancer cells genetically modified to express luciferase, such as that from *Photinus pyralis* (firefly), are detected in vivo via administration of luciferin (luciferase substrate). Luciferin becomes oxidized in the presence of adenosine triphosphate and oxygen upon which a visible light is emitted and detected externally (peak emission wavelength of 560 nm) [5]. When using cells with strong and stable expression of luciferase, BLI can be a very specific (only metabolically active cells are detected), sensitive, and rapid (short acquisition times) imaging tool; making this system an extremely valuable tool for preclinical oncology research [5].

In this protocol we describe methodology to address whether shRNA-mediated knockdown of a gene would influence primary tumor growth and metastasis using an orthotopic neuroblastoma mouse model, as reported [6]. Previous studies have demonstrated that the growth and spread of neuroblastoma tumors in this model simulates clinical features of the human disease and are therefore useful for studying neuroblastoma development in vivo [7–10].

2 Materials

2.1 Reagents to Make shRNA/Luciferase-Expressing Cancer Cells

1. Luciferase-expressing cancer cell lines are available commercially or can be made by transfection of a luciferase reporter construct into your cell of choice (*see* **Note 1**).
2. shRNA plasmids are available commercially from companies such as Origene Technologies Inc. (Rockville, MD, USA).
3. Plasmids can be introduced into cells using cationic lipids such as Lipofectamine® 2000 (Life Technologies, Carlsbad, CA, USE) or by viruses.
4. Phosphate buffered saline and 0.5 % Trypsin-0.2 % EDTA solution (Sigma Aldrich, St. Louis, MO, USA) for harvesting cells.

5. 0.4 % Trypan Blue solution (Sigma Aldrich) for analyzing cell viability.
6. Appropriate cell culture media.

2.2 Bioluminescent Imaging

1. Xenogen IVIS Imaging System (Perkin Elmer, Santa Clara, CA, USA) coupled with the Living Image Software (Caliper Life Sciences, Hopkinton, MA, USA). Refer to manual for equipment instructions and analyses of bioluminescent signal using the region of interest (ROI) method.
2. Isoflurane chamber (Advanced Anesthetic Specialists, Gladesville, Australia).
3. Firefly D-luciferin potassium salt (Gold Biotechnology, St. Louis, MO) diluted to 15 mg/mL in 1× Dulbecco's Phosphate Buffered Saline (DPBS) (Life Technologies) and sterile-filtered (0.22 μm).

2.3 Orthotopic Model

1. 5–8 week old immune-deficient mice (such as SCID-Beige, SCID, nude) housed under pathogen-free conditions and fed standard chow and water *ad libitum*. Mice are available from various sources such as Charles River Laboratories International Inc. Obtain relevant approvals for this procedure from appropriate institutional Animal Ethics Committees before conducting experiments involving animals.
2. Small clippers/shaver for rodents or Nair® depilatory hair removal cream.
3. Basement membrane extract (BME) can be obtained from various sources such as Trevigen, Inc. (Gaithersburg, MD, USA).
4. Stinger anesthetic machine (Advanced Anesthetic Specialists, Gladesville, Australia).
5. Isoflurane; Abbott Laboratories (Abbott Park, Illinois, USA).
6. Analgesia; buprenorphine hydrochloride (Temgesic®).
7. Ophthalmic ointment.
8. Safil 5/0 Polyglycolic acid, braided, coated, round-needle absorbable sutures (B. Braun Australia, Bella Vista, New South Wales, Australia).
9. Surgical tools (Fine Science Tools Inc., North Vancouver, B.C., Canada).
   (a) Reflex™ 7 mm stainless steel wound clips, wound clip applicator and remover
   (b) Fine scissors, curved and delicate straight (11.5 cm length)
   (c) Graefe forceps, slight curve and straight (0.8 × 0.7 mm tip, 10 cm length)
   (d) Olsen-Hegar needle holder with suture cutter (2 mm tip, 14 cm length)

10. 29ga. needles attached to 0.5 mL syringe (Terumo Medical Corporation, Elkton, MD, USA).
11. Iodine solution.
12. Alcohol swabs.
13. Sterile gauze.
14. Sterile saline (0.9 % NaCl) solution.
15. Heat pad.
16. Clean cage/s with fresh food and drinking water.

2.4 Histology

1. Aminoalkysilane-treated glass slides.
2. PBS and PBS-Tween solution (0.05 % Tween-20 in 1× PBS).
3. 10 % formalin.
4. Ethanol.
5. Xylene (Sigma Aldrich Pty. Ltd, Castle Hill, Australia).
6. Goat serum (Vector Labs, Burlingame, California, USA).
7. Antigen-retrieval citrate buffer (10 mM citrate, 0.05 % Tween-20, pH 6).
8. Peroxidase blocking solution (1 % H_2O_2, 3.3 % methanol).
9. Luciferase antibody (Fitzgerald, Acton, MA, USA).
10. Vectastain ABC Kit (Vector Labs, Burlingame, California, USA).
11. ImmPACT™ DAB substrate (Vector Labs).
12. Mayer's haematoxylin.
13. EUKITT mounting medium (O. Kindler GmbH and Co, Freiburg, Germany).
14. Aperio ScanScope XT Slide Scanner and ImageScope software (Aperio, Vista, CA, USA).
15. Histology cassettes (ProSciTech Pty. Ltd, Kirwan, QLD, Australia).
16. PAP pen (Vector Labs, Burlingame, California, USA).

3 Methods

3.1 Validation of Luciferase Expression in Cancer Cells In Vitro

1. Culture cells under normal sterile conditions at 37 °C in 5 % CO_2.
2. Seed luciferase-expressing cancer cells (*see* **Note 1**) at 20,000 cells/well (200 μL/well) into triplicate wells of a 96-well tissue culture plate.
3. Serially dilute cells across the plate by removing 100 μL/well of cells from first well and adding to 100 μL/well of cell culture media in the adjacent well.

4. Repeat **steps 1–3** until cells have been diluted across plate, from left to right (excluding outside wells).
5. After 3 h incubation, place cells in pre-warmed specimen chamber of the IVIS Imaging System.
6. Image to obtain background bioluminescent signal (*see* **Note 2**).
7. Add D-luciferin to wells at a final concentration of 150 μg/mL.
8. Return cells to specimen chamber for 3 min prior to imaging.
9. Analyze bioluminescent signal using the Living Image Software. Photon emission from the cells, calculated as total flux (photons/s), is measured using the region of interest (ROI) method as described in the Caliper Life Sciences manual.
10. Determine background luminescence of cells by measuring the total flux from the cell wells prior to the addition of the substrate (D-luciferin) and subtract this value from the total flux obtained from reciprocal wells after addition of the substrate. A representative plate of serially diluted, luciferase-expressing cells and quantitation of their bioluminescent signal is shown in Fig. 1.

3.2 Development of shRNA/Luciferase-Expressing Cancer Cells

1. Seed cells in 6 well tissue culture plates 1 day prior to transfection (*see* **Note 3**).
2. Introduce shRNA plasmids into cells using desired method. An example is to use Lipofectamine® 2000 following manufacturer's instructions for DNA transfections (*see* **Note 4**).
3. After 24 h incubation, replace media with fresh cell culture media.
4. The following day (48 h post-transfection) replace media with fresh cell culture media containing appropriate antibiotics for selection of shRNA-expressing cells (*see* **Note 5**).
5. Maintain cells in selection media for at least 10 days and ensure that all control (untransfected) cells are dead (usually within 3–4 days).
6. Confirm knockdown of target protein in selected cells by standard methods (*see* **Note 6**).
7. Cells with best knockdown of the target gene should be examined for luciferase expression to ensure they maintain the equivalent expression of luciferase as control shRNA cells (Fig. 1).
8. Make sufficient freeze-downs of cells and store in liquid or vapor-phase nitrogen until ready to thaw and culture for use in orthotopic model.
9. If possible, culture all cells for 1 month without antibiotics and harvest cell pellets at regular intervals. Examine the expression of the target gene using standard methods to determine

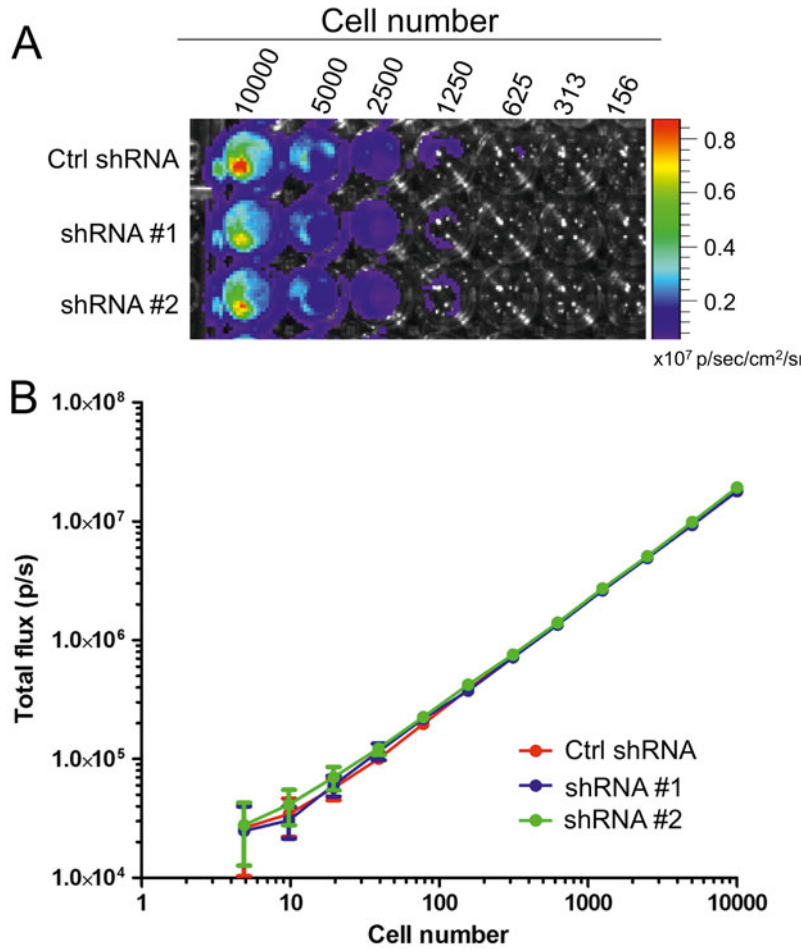

Fig. 1 Luciferase expression in shRNA-expressing neuroblastoma cells. (**a**) Representative image of bioluminescent signal from serially diluted SK-N-BE(2)/TGL cells expressing control (Ctrl) or target gene shRNA (2 independent shRNA sequences). *Colored scale bar* indicates the level of bioluminescent signal in photons/second/centimeter squared/steradian (p/s/cm^2/sr). (**b**) Bioluminescent signal, measured as total flux in photons/second (p/s) vs. number of cells. Reprinted by permission from Macmillan Publishers Ltd: Oncogene 33 (7):882–890, copyright (2014)

whether shRNA expression is maintained for this time period (1 month is the approximate time for tumors to reach 1 cm^3 in the described orthotopic model).

3.3 Orthotopic NeuroblastomaMouse Model

1. A day prior to surgery sterilize surgical equipment (e.g. autoclave).
2. Prepare surgical sites on mice by removing fur on their left flank using clippers or Nair® depilatory cream (*see* **Note 7**).
3. Weigh mice for monitoring purposes and to calculate amount of analgesia to be administered.

4. Prepare sterile hood or biological safety cabinet with all equipment required for surgery (anesthesia, analgesia, surgical equipment, heat pad etc.).
5. Harvest luciferase/shRNA-expressing cancer cells with PBS and Trypsin-EDTA solution and resuspend in standard culture media.
6. Centrifuge cells at 1500 × *g* for 5 min, remove supernatant and resuspend in PBS.
7. Count cells and determine viability using the trypan-blue dye exclusion method (*see* **Note 8**).
8. Place appropriate volume of cells required into Eppendorf tube, centrifuge at 1500 × *g*, and remove supernatant (*see* **Note 9**).
9. Place mouse in hood with nose in cone. Anesthetize mouse using 4 % isoflurane until mouse no longer responds to firm toe pinch, then reduce to 2 % isoflurane to sustain sedation (Fig. 2).
10. Place mouse on a heated pad (warm to touch) during surgery to maintain body temperature (Fig. 2).
11. Administer analgesia to mouse via subcutaneous injection at the scruff of the neck. Gently dab ophthalmic ointment on eyes to prevent eyes drying out.
12. Resuspend cell pellet in ~15–30 μL BME (*see* **Note 10**) and place tube on ice until ready for injection.
13. Prepare the surgical area by wiping once over with an alcohol swab and then iodine-soaked gauze (Fig. 2).
14. Use sterile forceps (curved) to hold up the skin layer, and sterile scissors (curved) to cut a vertical incision (~1.5 cm) into the skin on the left flank of the mouse. Use the spleen as an anatomical landmark (dark organ visible through skin layer) (Fig. 2).
15. Use sterile forceps (straight) to hold the peritoneum, and then cut with sterile scissors (straight) a small vertical incision (~1 cm) to expose the spleen, kidney, and adrenal gland (Fig. 2).
16. Move the spleen gently to the side using sterile forceps and inject the cell/BME mix (~30–50 μL) into the adipose tissue surrounding the adrenal capsule (*see* **Note 10**) (Fig. 2).
17. Close peritoneum with absorbable sutures using the Olsen-hegar needle holder.
18. Close the skin with stainless steel wound clips (or sutures if wound clips not available).
19. Administer fluid (1 mL sterile 0.9 % NaCl) and analgesia via subcutaneous injection away from surgical site.
20. Return mouse to clean, pre-warmed cage, and monitor closely during recovery. Ensure animal has easy access to clean food and water.

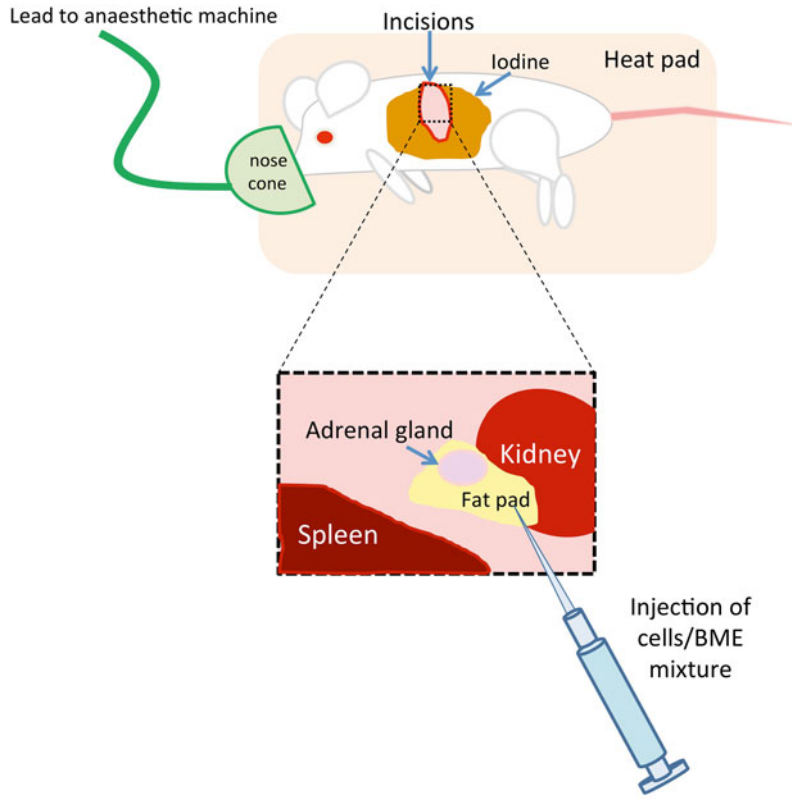

Fig. 2 Surgical method. The mouse is placed under isoflurane sedation (anesthetic administered through nose cone) and kept on a pre-warmed heat pad during the entire surgical procedure. Analgesia is administered at the scruff of the neck. The surgical site is prepared by wiping across area once with an alcohol swab then iodine-soaked gauze. Using the spleen as an anatomical landmark, cut vertical incisions in the outer skin layer (~1.5 cm) and then peritoneal layer (~1 cm) using sterile scissors. Use sterile forceps to move the spleen out of the way, and inject cells mixed with BME into the fat tissue surrounding the adrenal gland. The fat pad should inflate with injection of cells and BME will solidify at body temperature. Close incisions with absorbable sutures and wound clips

21. Repeat process for additional mice (the number of animals to be used per group should be determined prior using statistical power calculations).
22. Wound clips can be removed from mice approximately 9 days post-surgery.
23. Image animals and monitor their weight and health throughout the course of the experiment.

3.4 In Vivo and Ex Vivo Imaging of Tumors

Conduct BLI one day post-surgery if possible to ensure correct injection of cells (which will be displayed as a localized signal) (Fig. 3, and *see* **Note 11**), 1 week later, and every week thereafter to monitor tumor burden (Fig. 4).

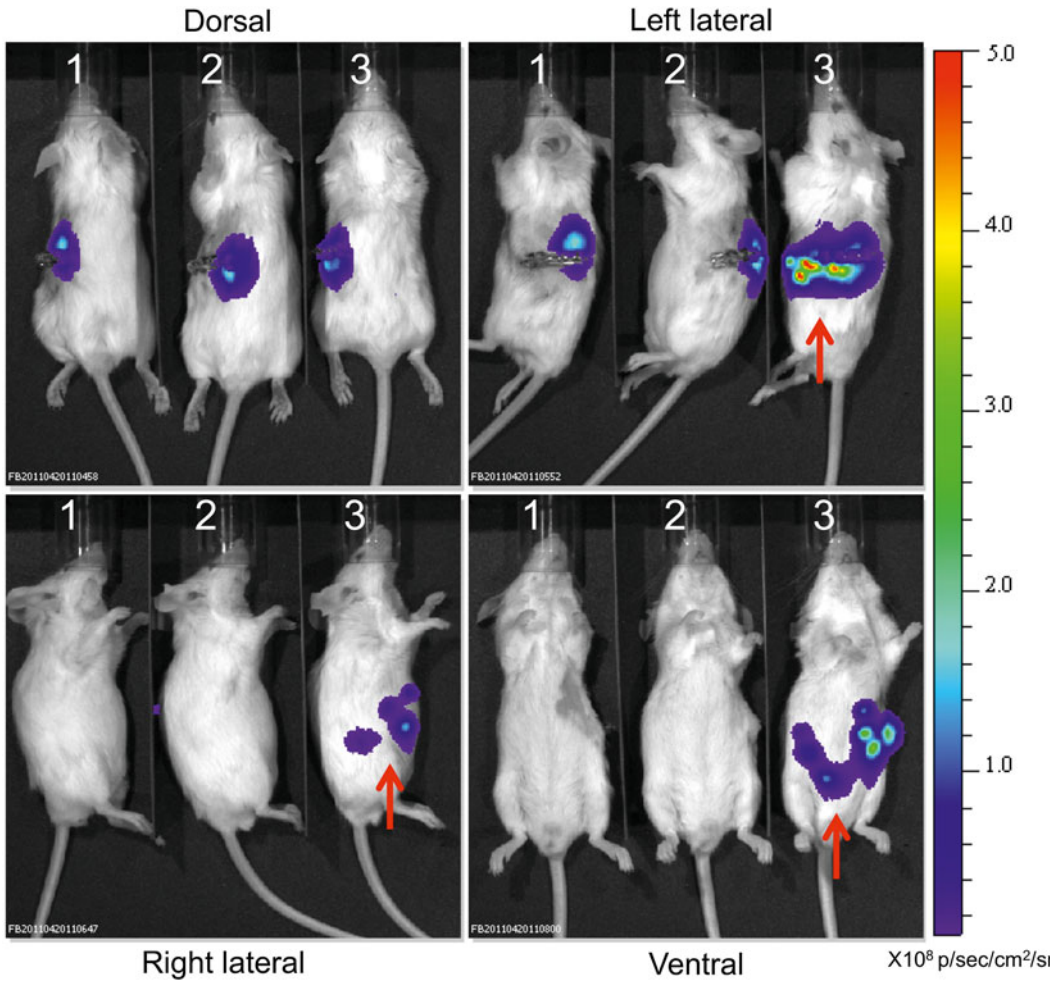

Fig. 3 Detection of adrenal fat pad injection spills by bioluminescent imaging. Representative images of 3 mice injected with luciferase-expressing neuroblastoma cells into their left adrenal fat pads. Mice were imaged on their dorsal, left lateral, right lateral, and ventral sides. Mouse #1 and mouse #2 show no cell leakage from their injection sites (localized signal). Mouse #3 shows cell leakage, as represented by the *red arrow*, on the left lateral, right lateral, and ventral sides. Mouse #3 should be excluded from the study

1. Inject mice (intraperitoneal) with D-luciferin (150 mg/kg) and anesthetize by placing in outer chamber of IVIS system with exposure to 4 % isoflurane.
2. Once mice are sedated, transfer onto the pre-warmed stage inside the IVIS Imaging System specimen chamber with continuous exposure to 2 % isoflurane to sustain sedation.
3. Approximately 10 min following injection of substrate, image mice on ventral and left lateral sides (*see* **Notes 2**, **12**, and **13**) (Fig. 3).
4. At the completion of the study (*see* **Note 14**) and before euthanizing animal, inject D-luciferin and image (as above).

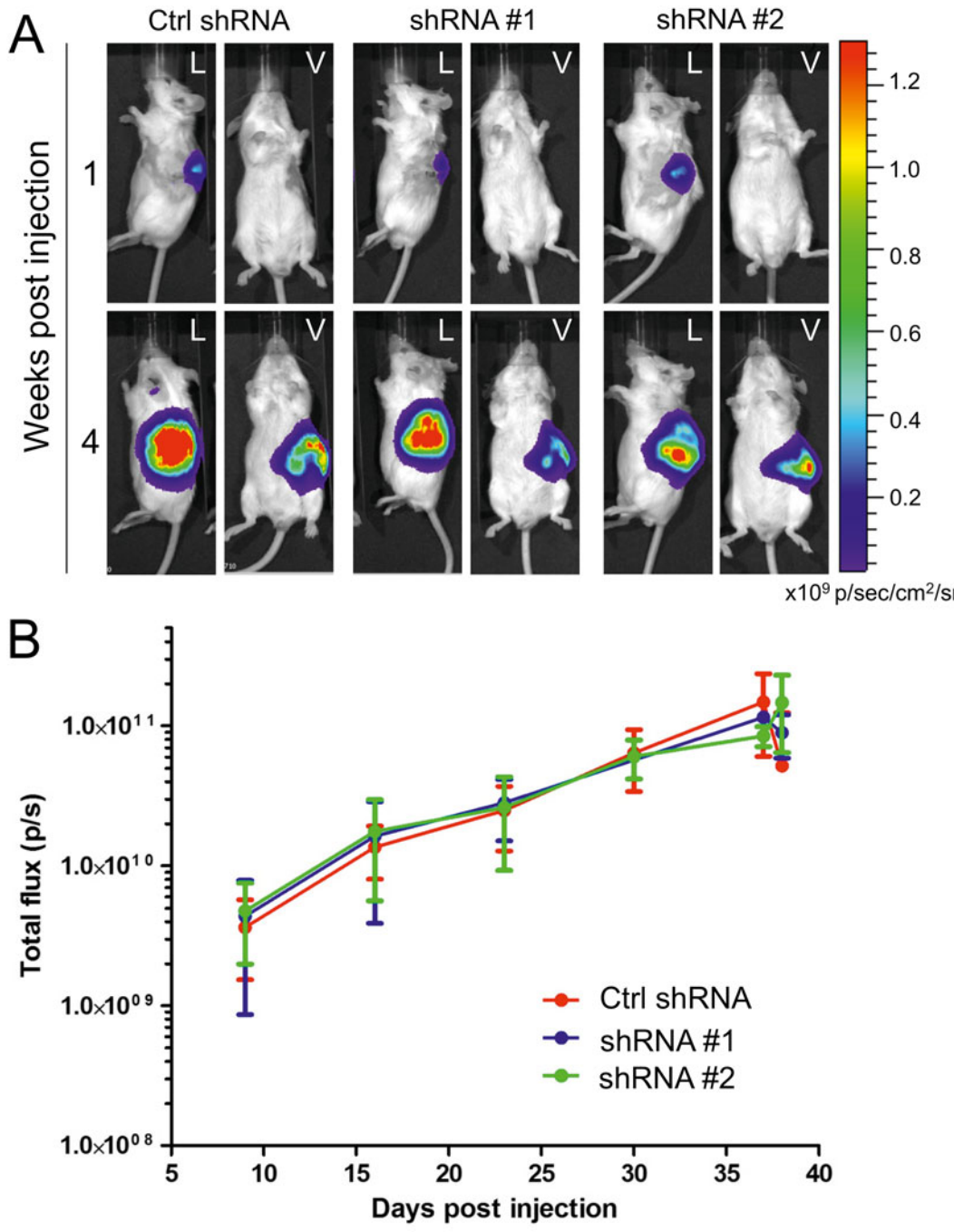

Fig. 4 Monitoring tumor burden in the orthotopic neuroblastoma mouse model. (**a**) Representative images of mice injected with SK-N-BE(2)/TGL cells expressing control (Ctrl) or target gene shRNA (2 independent shRNA sequences). *Colored scale bar indicates* the level of bioluminescent signal in photons/second/centimeter squared/steradian (p/s/cm^2/sr). Mice were imaged on their left lateral (*L*) and ventral (*V*) sides. (**b**) Total tumor burden was determined by measuring total flux (photons/second) from the left lateral sides of mice at the indicated time points, using the ROI method. Data represent the mean of ≥13 mice for each group ±SEM (error bars). Reprinted by permission from Macmillan Publishers Ltd: Oncogene 33 (7):882–890, copyright (2014)

5. Humanely euthanize the animal according to the method approved by the institutional Animal Ethics Committee immediately after imaging and remove the primary tumor.
6. Measure primary tumor weight and volume (mm^3) using calipers and place in 10 cm petri dishes on ice (*see* **Note 15**).
7. Collect organs and carcass and place in 10 cm dishes on ice.
8. Cover the tumor, organs, and carcass with D-luciferin solution (300 μg/mL) and incubate for 30 s prior to imaging using the Xenogen system (*see* **Note 16**).
9. Snap freeze a portion of primary tumor (for biochemical analyses) and place remainder in 10 % formalin, along with organs and carcass.
10. Using the bioluminescent images, quantify bioluminescent signal from the left lateral side of the animal and organs using the ROI method (Fig. 4).
11. Bioluminescent images of mice, primary tumors, and organs, can be digitized and electronically displayed as a pseudocolor overlay onto a gray scale animal image using the Living Image Software (Figs. 4 and 5).
12. Validate primary and metastatic tumors by immunohistochemistry (Fig. 6).

3.5 Immunohistochemistry to Detect Luciferase Positive Tumors

1. Place tissues in formalin for ~24–48 h and then rinse twice in PBS.
2. Place sections of tissues in histology cassettes.
3. Immerse cassettes in 70 % ethanol.
4. Embed tissues in paraffin and cut multiple 5 μm sections.
5. Stain slides with hematoxylin and eosin (H&E) and prepare concurrent sections on aminoalkysilane-treated glass slides.
6. Incubate slides at 60 °C for 30 min to assist tissue attachment to slides.
7. Deparaffinise tissues by incubating slides three times in xylene (3 min each).
8. Rehydrate section by placing slides in a graded ethanol series of 100 %, 95 %, and 70 % solution (5 min each) followed by two MQ-H_2O washes (2 min each).
9. Perform antigen retrieval by placing slides in a glass beaker with 400 mL citrate buffer.
10. Heat beaker on high for 3 min in a microwave oven followed by 15 min at 104 °C in a regular oven.
11. Remove beaker from oven and let solution cool for 1 h at room temperature.
12. Rinse slides twice with MQ-H_2O.
13. Block endogenous peroxidase activity by placing slides in peroxidase blocking solution for 10 min.

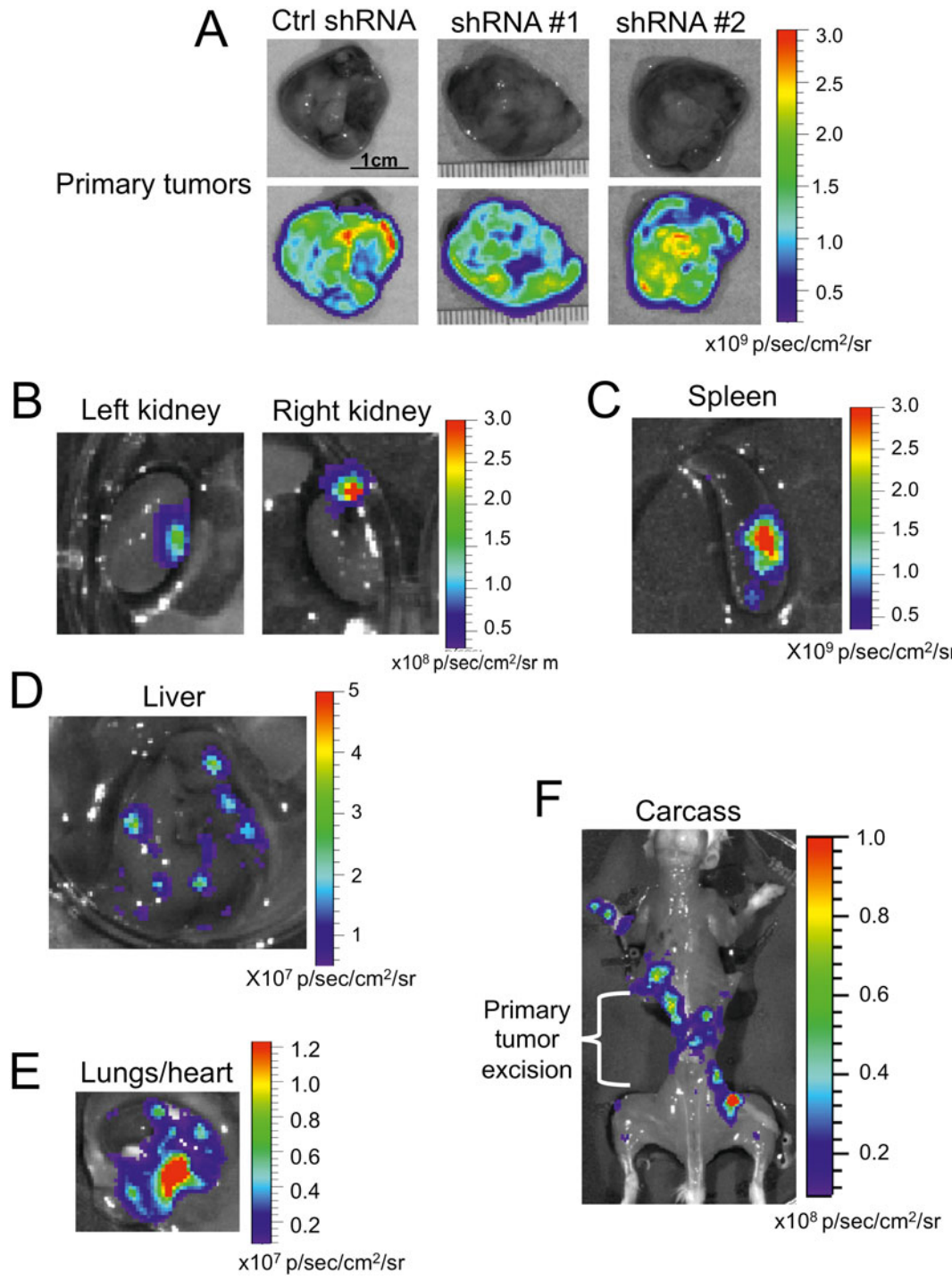

Fig. 5 Bioluminescent imaging of luciferase-expressing neuroblastoma tumors ex vivo. (**a**) Gray scale (*top images*) and bioluminescent images (*lower images*) of primary tumors removed from mice injected with SK-N-BE(2)/TGL cells expressing control (Ctrl) or target gene shRNA (2 independent sequences). Bioluminescent images of representative kidneys (**b**), spleen (**c**), liver (**d**), lungs (**e**), and entire carcass (**f**) of mice injected with SK-N-BE(2)/TGL cells expressing control (Ctrl) shRNA. *Colored scale bars indicates* the level of bioluminescent signal from tumors, in photons/second/centimeter squared/steradian (p/sec/cm^2/sr). Reprinted by permission from Macmillan Publishers Ltd: Oncogene 33 (7):882–890, copyright (2014)

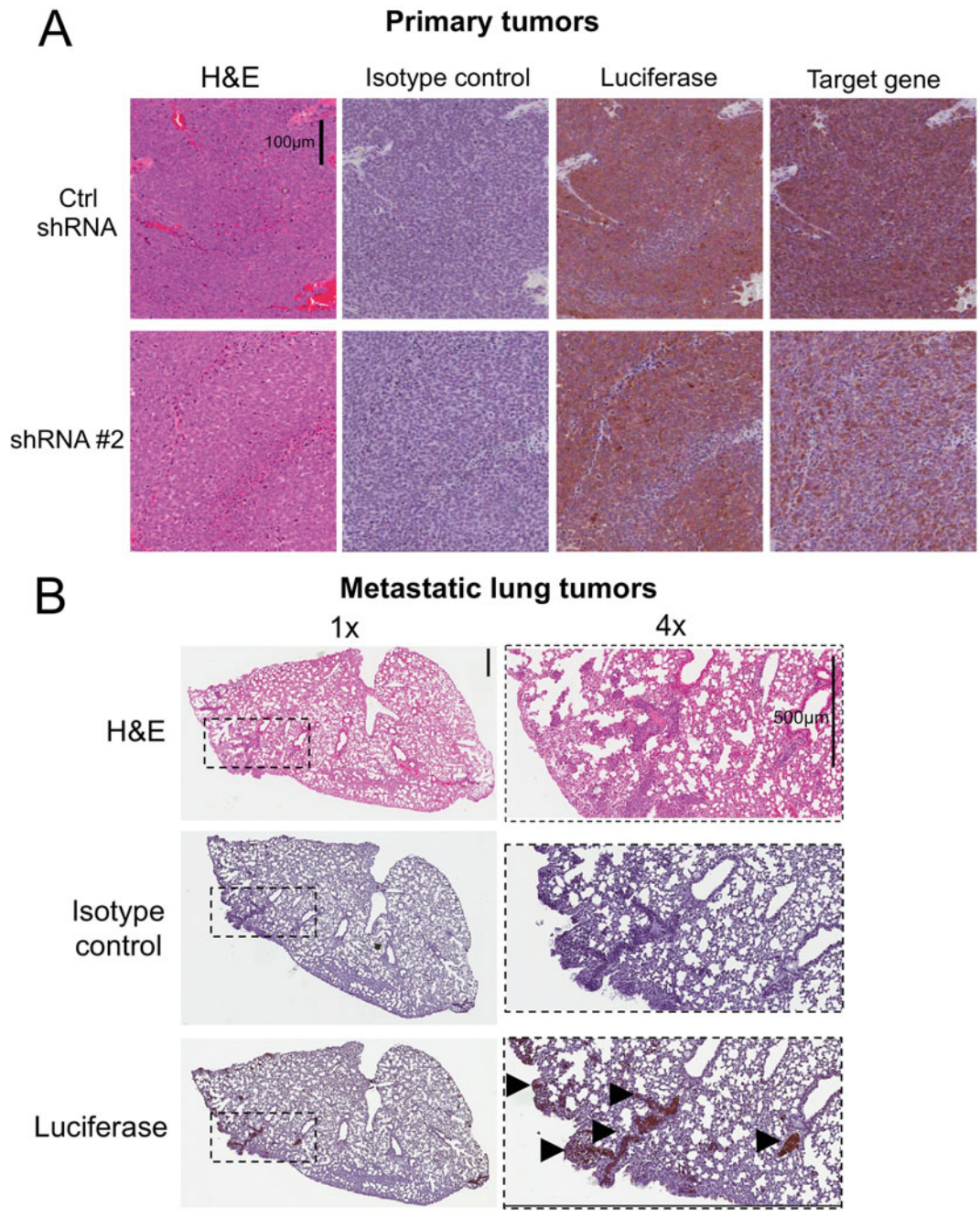

Fig. 6 Histology of luciferase-expressing neuroblastoma tumors. (**a**) Sections of primary tumors from mice injected with SK-N-BE(2)/TGL cells expressing control (Ctrl) or target gene shRNA, were stained for luciferase and the shRNA target gene/protein. Luciferase expression was similar in both control and shRNA #2 tumors. (**b**) Lungs were removed from the above-mentioned mice and metastatic neuroblastoma tumors confirmed by staining for luciferase. Reprinted by permission from Macmillan Publishers Ltd: Oncogene 33 (7):882–890, copyright (2014)

14. Outline tissue sections with a PAP pen.
15. Block slides with 10 % goat serum/PBS for 1 h.
16. Incubate tissue sections for 1 h at room temperature with rabbit polyclonal antibody against luciferase, diluted one in one hundred (1:100) in 1 % goat serum/PBS.
17. To ensure antibody specificity, incubate one slide with rabbit IgG control antibody at a concentration equivalent to the primary luciferase antibody.
18. Wash slides three times with PBS-Tween solution for 5 min followed by 1 quick wash in PBS.
19. Incubate tissue sections with biotinylated secondary antibody, diluted one in two hundred (1:200) in 1 % goat serum/PBS for 10 min.
20. Wash slides in PBS-Tween (as described above) and incubate for 5 min with avidin-biotin-peroxidase complex (2 drops each of reagent A and B in 5 mL PBS) from the Vectastain ABC Kit.
21. Wash slides twice with PBS and then incubate with ImmPACT™ DAB substrate at room temperature until the desired intensity is developed.
22. Rinse slides with MQ-H_2O, counterstain with Mayer's haematoxylin (nuclear counterstain) for 1 min.
23. Dehydrate in a graded ethanol series of 70 %, 95 %, and 100 % solution (5 min each) followed by two MQ-H_2O washes (2 min each).
24. Mount slides.
25. Slides can be scanned using an Aperio ScanScope XT Slide Scanner and images can be analyzed using ImageScope software (Aperio, Vista, CA, USA) (Fig. 6).

3.6 Final Considerations

In our in vivo model we did not observe differences in the growth of control shRNA- and target gene shRNA-expressing primary tumors. Therefore the changes we observed in lung metastasis between these groups were most likely due to perturbation of the metastatic cascade. For this reason, we performed additional experiments using in vitro and in vivo assays to 'tease out' which step/s in the cascade our target gene/protein was influencing.

4 Notes

1. For our in vivo model we used human SK-N-BE(2) neuroblastoma cells (Dr. Sylvain Baruchel, Research Institute at The Hospital for Sick Children, Toronto) [11] which were retrovirally transduced with the SFG-NESTGL triple-modality

reporter construct [12] containing genes encoding *Photinus pyralis* (firefly) luciferase, *Aequorea victoria* green fluorescent protein (GFP), and herpes simplex virus 1 thymidine kinase (HSV1-tk). GFP-expressing SK-N-BE(2) cells were selected by fluorescence-activated cell sorting and a high GFP-expressing SK-N-BE(2)/TGL population was pooled.

2. The optimum conditions for imaging will be determined by the end user and will depend on the level of luciferase expressed by the cells. For reference, we used medium binning, F-stop 1 for all imaging conditions.
3. Cells should be 70–90 % confluent on day of transfection, as recommended by Lipofectamine® 2000 protocol. For reference, SK-N-BE(2)/TGL cells were seeded at 4×10^5 in 2 mL of cell culture media per well of a 6 well cell culture plate.
4. For reference, SK-N-BE(2)/TGL cells were transfected with 4 μg of each shRNA plasmid (1 well without plasmid as a control) using 10 μL/well Lipofectamine® 2000 and 700 μL/well Opti-MEM®.
5. The optimum concentration of antibiotics should be determined for each cell line, ensuring that all untransfected cells are dead by 3–4 days. For reference, SK-N-BE(2)/TGL cells were selected in 1 μg/mL puromycin-containing media 48 h post-transfection and maintained in this media for 10 days.
6. Suppression of the target gene can be confirmed by real-time PCR (qPCR) (mRNA expression) and Western blotting (protein expression).
7. For fur removal using Nair®, apply cream with sterile cotton swabs. Remove cream with saline soaked gauze pads within 1 min to prevent skin irritation. It is preferable to do this method of fur removal 1 day prior to surgery.
8. Experiments can be continued if cell viability is high (greater than 95 % viable) as determined by Trypan Blue staining (dye exclusion) of dead cells.
9. The appropriate number of cells to inject will depend on engraftment rates and the rate at which the primary tumors grow. As a guide, 5×10^5–2×10^6 cells/mouse are good starting points for most cancer cell lines. When harvesting cells to make pellet, remove as much supernatant as possible without disrupting the cells. This is to reduce the total volume of cell/BME mix to be injected into the fat pad.
10. The orthotopic neuroblastoma model involves injection of cells into the fat pad surrounding the adrenal gland (pale pink disk). If done correctly, the fad pad should expand as it fills with the cells/BME mixture. BME will solidify at 37 °C. If BME does not solidify it may be too dilute. Refer manufacturer's instructions for preparation of BME.

11. Any mice with obvious spillage from the injection site should be humanely sacrificed according to the method approved by the institutional Animal Ethics Committee.
12. Be careful when handling mice to ensure they are not in pain following surgery.
13. The time period between injecting the substrate to imaging requires optimization. Times may vary depending on animal strain and metabolism of substrate. For reference, we waited 10 min before imaging mice following injection of D-luciferin at 150 mg/kg.
14. Euthanize mice when primary tumors reach ~1 cm^3 (estimate from palpation) or if animals lose significant weight (≥20 %) or become moribund, whichever comes first according to the method approved by the institutional Animal Ethics Committee.
15. Measure tumor size with calipers and calculate tumor volume. For reference, we used the formula: volume = (length × width × depth)/2.
16. To determine background bioluminescence for in vivo and ex vivo imaging, it is recommended that naïve mice (injected with D-luciferin) and their organs be imaged using the same method (*see* Subheading 3.4). Subtract these values from the signal obtained from similarly sized ROIs from whole animals and organs of mice injected with luciferase-expressing cancer cells.

Acknowledgement

This work was supported by the Children's Cancer Institute Australia, which is affiliated with the University of New South Wales (UNSW Australia) and Sydney Children's Hospital and by grants from The Kids Cancer Project (M. Kavallaris) and Cancer Council New South Wales (M. Kavallaris). F.L. Byrne is a Hope Funds for Cancer Research Fellow supported by the Hope Funds for Cancer Research (HFCR-14-06-04) and M. Kavallaris is an NHMRC Senior Research Fellow (MK; APP1058299). M. Kavallaris is funded by the Australian Research Council Centre of Excellence in Convergent Bio-Nano Science and Technology (project number CE140100036). This research was supported by a Cancer Institute of New South Wales infrastructure award.

References

1. Khanna C, Hunter K (2005) Modeling metastasis in vivo. Carcinogenesis 26(3):513–523. doi:10.1093/carcin/bgh261
2. Manzotti C, Audisio R, Pratesi G (1993) Importance of orthotopic implantation for human tumors as model systems: relevance to metastasis and invasion. Clin Exp Metastasis 11(1):5–14. doi:10.1007/BF00880061
3. Fidler IJ (2003) The pathogenesis of cancer metastasis: the 'seed and soil' hypothesis revisited. Nat Rev Cancer 3(6):453–458
4. Langley RR, Fidler IJ (2011) The seed and soil hypothesis revisited—The role of tumor-stroma interactions in metastasis to different organs. Int J Cancer 128(11):2527–2535. doi:10.1002/ijc.26031
5. O'Neill K, Lyons SK, Gallagher WM, Curran KM, Byrne AT (2010) Bioluminescent imaging: a critical tool in pre-clinical oncology research. J Pathol 220(3):317–327. doi:10.1002/path.2656
6. Byrne FL, Yang L, Phillips PA, Hansford LM, Fletcher JI, Ormandy CJ, McCarroll JA, Kavallaris M (2014) RNAi-mediated stathmin suppression reduces lung metastasis in an orthotopic neuroblastoma mouse model. Oncogene 33(7):882–890. doi:10.1038/onc.2013.11
7. Fuchs D, Christofferson R, Stridsberg M, Lindhagen E, Azarbayjani F (2009) Regression of orthotopic neuroblastoma in mice by targeting the endothelial and tumor cell compartments. J Transl Med 7:16. doi:10.1186/1479-5876-7-16
8. Henriksson KC, Almgren MA, Thurlow R, Varki NM, Chang CL (2004) A fluorescent orthotopic mouse model for reliable measurement and genetic modulation of human neuroblastoma metastasis. Clin Exp Metastasis 21(6):563–570
9. Khanna C, Jaboin JJ, Drakos E, Tsokos M, Thiele CJ (2002) Biologically relevant orthotopic neuroblastoma xenograft models: primary adrenal tumor growth and spontaneous distant metastasis. In Vivo 16(2):77–85
10. Nevo I, Sagi-Assif O, Edry Botzer L, Amar D, Maman S, Kariv N, Leider-Trejo LE, Savelyeva L, Schwab M, Yron I, Witz IP (2008) Generation and characterization of novel local and metastatic human neuroblastoma variants. Neoplasia 10(8):816–827
11. Zhang L, Smith KM, Chong AL, Stempak D, Yeger H, Marrano P, Thorner PS, Irwin MS, Kaplan DR, Baruchel S (2009) In vivo antitumor and antimetastatic activity of sunitinib in preclinical neuroblastoma mouse model. Neoplasia 11(5):426–435
12. Ponomarev V, Doubrovin M, Serganova I, Vider J, Shavrin A, Beresten T, Ivanova A, Ageyeva L, Tourkova V, Balatoni J, Bornmann W, Blasberg R, Gelovani Tjuvajev J (2004) A novel triple-modality reporter gene for whole-body fluorescent, bioluminescent, and nuclear noninvasive imaging. Eur J Nucl Med Mol Imaging 31(5):740–751. doi:10.1007/s00259-003-1441-5

Chapter 6

Indium-Labeling of siRNA for Small Animal SPECT Imaging

Steven Jones and Olivia Merkel

Abstract

Ever since the discovery of RNA interference (RNAi), therapeutic delivery of siRNA has attracted a lot of interest. However, due to the nature and structure of siRNA, a carrier is needed for any mode of systemic treatment. Furthermore, specific imaging techniques are required to trace where the deposition of the siRNA occurs throughout the body after treatment. Tracking in vivo siRNA biodistribution allows understanding and interpreting therapeutics effects and side effects. A great advantage of noninvasive imaging techniques such as SPECT imaging is that several time points can be assessed in the same subject. Thus, the time course of biodistribution or metabolic processes can be followed. Therefore, we have described an approach to modify siRNA with a DTPA (Diethylene Triamine Pentaacetic Acid) chelator in order to utilize an indium labeled siRNA for SPECT imaging. Here, we explain the details of the labeling and purification procedures.

Key words siRNA delivery, SPECT imaging, Indium labeling, siRNA, siRNA modification, DTPA, Purification

1 Introduction

Since the Nobel Prize in physiology was awarded in 2006 to Andrew Fire and Greg Mello for their work in RNA interference (RNAi), there has been an increase in the development of RNAi as a therapeutic tool to transiently knock down specific proteins. Unfortunately when it is delivered in vivo, naked small interfering RNA (siRNA) is taken up very poorly into the cell due to its molecular makeup [1–4]. To improve its uptake and specificity, siRNA can for example be packaged inside nanoparticles. Nanoparticle delivery offers several benefits such as increased stability, longer circulation time, capability to package multiple payloads, and specific targeting to tumor sites [5, 6].

The most common routes of nanoparticle administration for therapeutic use are intravenous, transdermal, pulmonary administration, and intraocular [7–9]. For cancer therapy, intravenous delivery of the nanoparticles is most ideal due to the ability of the nanoparticles to inherently preferentially reach the tumors directly

Zdravka Medarova (ed.), *RNA Imaging: Methods and Protocols*, Methods in Molecular Biology, vol. 1372,
DOI 10.1007/978-1-4939-3148-4_6,

from the bloodstream due to the enhanced permeation and retention (EPR) effect [10]. However, when nanoparticles are administered intravenously, several obstacles need to be overcome. Among those obstacles are the circulation profile and deposition of the nanoparticles. Both of those are key components to the success of any treatment.

In order to assess the efficacy of the nanoparticle deposition in the organ or tissue of interest, single photon emission computed tomography (SPECT) imaging can be used. SPECT imaging is often employed to detect radioactive species within the body [11]. More specifically, for siRNA delivery, this can be utilized to trace where radioactive siRNA travels throughout the bloodstream and where specifically it deposits inside the body. This approach provides useful information about the obstacles that are needed to be overcome for intravenous delivery. Consequently, SPECT imaging can illustrate whether the siRNA loaded nanoparticles are degraded in circulation before reaching the tumor site, as well as its biodistribution [12, 13]. Due to the need to overcome these hurdles for a successful treatment, siRNA imaging techniques are needed.

This chapter outlines the technique to label siRNA with a DTPA chelator. Once the siRNA is sufficiently labeled with DTPA, it can be reacted with indium and annealed in order to become radioactive. Once the indium has been chelated to the DTPA, the siRNA can then be packaged inside a nanoparticle or other nanocarriers and imaged with a SPECT scanner.

2 Materials

2.1 siRNA Formulation

Due to their increased stability, high activity, and ability to be covalently modified, 2′-*O*-methylated 25/27mer DsiRNA targeting EGFP [14] from Integrated DNA Technologies (Leuven, Belgium) was used and is recommended for use. For coupling of DTPA, amine-labeled siRNA is recommended. Here, we used a duplex with an amino-hexyl modification at the 5-prime of the antisense strand.

1. siEGFP: sense: 5′-pACCCUGAAGUUCAUCUGCACCACd CdG, antisense: 3′-mAmCmUGmGGmACmUUmCAmAGm UAmGAmCGUGGUGGC-C6H12NH2

2.2 Covalent Modification of siRNA with pBn-SCN-Bn-DTPA

1. siEGFP—described above.
2. pBn-SCN-Bn-DTPA (Macrocyclics).
3. 0.1 M $NaHCO_3$ in DEPC water—filtered through a 0.22 μm filter before use.
4. 2M NaOAc in DEPC water—filtered through a 0.22 μm filter before use.

5. Dried DMSO (about 3 mL).
6. 0.22 μm filter.
7. 2 mL centrifuge tube.
8. Metal spatula wrapped in parafilm—Used to weigh out pBn-SCN-Bn-DTPA (*see* **Note 1**).
9. Aluminum foil.
10. Vortex.

2.3 Precipitation of the siRNA–DTPA Complex

1. 2M NaOAc in RNase free water—filtered through a 0.22 μm filter before use.
2. Absolute ethanol—filtered through a 0.22 μm filter before use.
3. 15 mL conical tube.

2.4 Isolation of the siRNA–DTPA Complex

1. Ultracentrifuge (*see* **Note 6**).
2. Lysis Buffer from Absolutely RNA miRNA Kit (Agilent).
3. 2M NaOAc in RNase free water—filtered through a 0.22 μm filter before use.
4. Absolute ethanol—filtered through a 0.22 μm filter before use.
5. 5 RNeasy Midi Kit (10) columns (Qiagen).

2.5 siRNA–DTPA Purification

1. Centrifuge.
2. Low salt buffer from the Absolutely RNA miRNA Kit (Agilent).
3. RNase free water.
4. Sterile 2 mL collection centrifuge tubes.

2.6 siRNA Concentration Measurement

1. Nanodrop.
2. RNase free water.
3. 0.5 mL tubes.
4. Parafilm.
5. Dry heat bath set to 94 °C.
6. Timer.

2.7 DTPA Concentration Measurement

1. Stock solution of the yttrium(III)–arsenazo III complex containing 5 μM arsenazo(III) (Chem-Impex INT'L INC.), and 1.6 μM yttrium(III) chloride (Acros Organics) in a 0.15 M NaOAc buffer at pH 4.
2. Stock solution of 0.123 mM DTPA dissolved in DI-H_2O with 3 molar equivalents of NaOH (*see* **Note 2**).
3. UV–Vis spectrophotometer.
4. UV–Vis disposable cuvette.

2.8 Indium Labeling

1. Radioactive Indium(III) chloride (Covidien).
2. GE Healthcare Disposable PD-10 Desalting Columns.
3. RNase free water.
4. Scintillation vials (make and model to fit gamma counter).
5. Gamma counter (e.g., Packard 5005).
6. Nanodrop.

2.9 Animal Imaging

1. Mice, e.g., 6-week-old balb/c mice.
2. Sterile Insulin Syringes.
3. Sterile siRNA formulation, e.g., nanoparticles.
4. Mouse anesthesia.
5. SPECT imaging device and mouse cradle, e.g., Siemens E.CAM with custom-made collimator.

3 Methods

3.1 React siRNA with pBn-SCN-DTPA

1. Weigh out 5.11 mg of Double Stranded siRNA in a 2 mL centrifuge tube and dissolve it in 100 μL of RNase free water (*see* **Note 3**).
2. To the 2 mL tube, add 100 μL of filtered 0.1 M $NaHCO_3$.
3. Next, weigh out 9.76 mg of pBn-SCN-Bn-DTPA and dissolve it in 540 μL of dry DMSO (*see* **Notes 1** and **4**).
4. Add the 540 μL of the DTPA to siRNA mixture. The new total volume should be 740 μL (*see* **Note 5**).
5. Wrap the solution in tin foil, vortex thoroughly, and incubate for 6 h. Agitate the solution every 30 min.

3.2 Precipitation of the siRNA–DTPA Complex

1. Add 74 μL of filtered 2 M NaOAc to the mixture (10 % of the total amount of mixture).
2. Transfer the mixture to a 15 mL conical tube.
3. Add filtered absolute ethanol so that the final concentration is 80 % v/v.
4. Freeze solution overnight at –80 °C.

3.3 Isolation of the siRNA–DTPA Complex

1. Centrifuge the sample for 30 min at 12,000 × *g* in an ultracentrifuge (*see* **Note 6**).
2. Discard the supernatant.
3. Add 2.5 mL of Lysis Buffer from "Absolutely RNA miRNA Kit" (Agilent).
4. Vortex the solution.
5. Add 250 μL of filtered 2M NaOAc.

6. Add 7.25 mL of filtered absolute ethanol for a total of 10 mL (*see* **Note 7**).
7. Vortex the solution and equally distribute the 10 mL onto 5 RNeasy Midi Kit (10) Qiagen Columns (see **Note 8**).

3.4 siRNA–DTPA Purification

1. Centrifuge the columns at 4500 × *g* for 5 min, discard the flow through.
2. To each column, add 200 μL of the low salt buffer from the Absolutely RNA miRNA Kit (Agilent).
3. Centrifuge the solution at 4500 × *g* for 2 min, discard the flow through.
4. Repeat **steps 2** and **3**.
5. To dry the column, spin them down at 5000 × *g* for 5 min.
6. Transfer the columns to a new collection tube and add 200 μL of 60 °C hot RNase free water.
7. Centrifuge the solution at 5000 × *g* for 5 min to collect the purified siRNA–DTPA.
8. Add 100 μL of 60 °C hot RNase free water and centrifuge at 5000 × *g* for 5 min.
9. Combine the flow through from all of the columns into one sterile 2 mL tube.

3.5 siRNA Concentration Measurement

1. Measure the siRNA concentration on a nanodrop (Thermo Scientific—Nanodrop 2000c). Use RNase free water as your blank.
2. In a sterile environment, dilute the siRNA to a desired concentration and aliquot into 0.5 mL sterile tubes (*see* **Note 9**).
3. Filter the siRNA–DTPA solution to make it sterile.
4. Parafilm each tube and anneal the siRNA at 94 °C for exactly 2 min.
5. Let the samples cool down to room temperature.
6. Freeze the samples and keep frozen until needed.

3.6 DTPA Concentration Measurement

1. Using a UV–Vis spectrophotometer (Cary—50 Bio), you will create the standard curve for DTPA concentrations.
2. Pipette 3 mL of the Y(III)–arsenazo III complex stock solution into a cuvette and read (652 nM) this as the blank.
3. Add 5 μL of the stock DTPA solution to the cuvette, gently mix, and read the solution again (*see* **Note 10**).
4. Add another 5 μL of the stock DTPA solution, read, and repeat.
5. Do this until you have generated enough points for your standard curve.

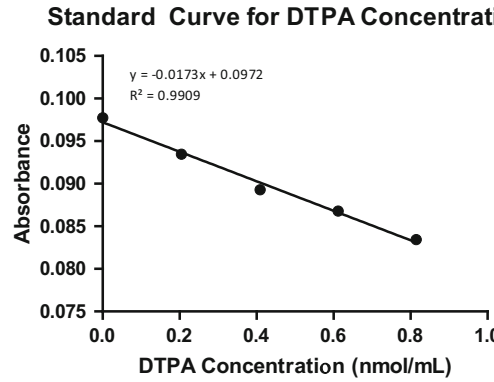

Fig. 1 Scatter plot obtained from creating the standard curve of the DTPA concentrations. As seen below, the final concentration of DTPA added to the cuvette is on the *X*-axis, and absorbance at 652 nm is on the *Y*-axis. From here, concentration of the DTPA inside the siRNA–DTPA mixture can be obtained

6. Each new data point will have an additional 5 μL added into the cuvette.
7. Once all the standards have been made and read on the spectrophotometer, discard the solution inside the cuvette and put 3 mL of fresh Y(III)–arsenazo III complex stock solution into the cuvette (*see* **Note 11**).
8. Add 5 μL of your siRNA–DTPA sample into the 3 mL and take the measurement.
9. Plot the standard curve for the DTPA concentrations versus absorbance and insert a linear line of best fit (Fig. 1).
10. Using the equation yielded from the line of best fit, plug the absorbance value obtained from your sample measurement into the *Y*-value of the equation in order to solve for *X*.
11. The *X*-value obtained will be the concentration of DTPA in your sample.
12. Now that the DTPA and siRNA concentrations have been found for the siRNA–DTPA mixture, figure out the molar amounts of the siRNA and DTPA within your sample. From here, you can determine the molar equivalency of the siRNA and DTPA (*see* **Note 12**).

3.7 Indium Labeling and Purification

1. React radioactive $^{111}InCl_3$ with siRNA. In the example shown below, 116.9 MBq $^{111}InCl_3$ were reacted with 15 nmol siRNA. Incubate for 30 min at room termperature.
2. Equilibrate a PD-10 column with RNase free water by washing it with 25 ml.

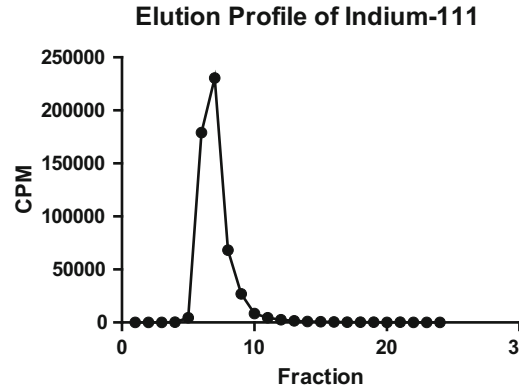

Fig. 2 Scatter plot obtained from purifying and eluting ^{111}Indium-labeled siRNA over a PD-10 column. The radioactivity as measured in counts per minute (CPM) are shown on the *Y*-axis as a function of the fraction eluted on the *X*-axis. A clear peak is shown in fraction 7

3. Prepare 24 scintillation vials in a rack and label them from 1 to 24.
4. Place vial 1 underneath the PD-10 column and start adding the siRNA–Indium mixture to the column slowly.
5. Collect 13 drops in the first vial as fraction 1 and then move on to the next vial. Collect 13 drops per fraction. Once the complete volume of the siRNA–Indium mixture is applied to the column, add RNase free water. Collect 24 fractions.
6. Close the scintillation vials and measure the counts per minute (CPM) in every vial using a gamma counter.
7. Plot the CPM versus the fraction number (Fig. 2).
8. Determine the siRNA concentration in the peak fraction using a Nanodrop (**Note 13**).

3.8 Animal Imaging

1. Prepare the siRNA formulation to be administered, e.g., nanoparticles. In the example below, micelles of polyethyleneimine-graft-polycaprolactone-block-poly(ethylene glycol) were prepared with 2 nmol siRNA per animal which was equivalent to approximately 3 MBq per animal.
2. Anesthetize the animals and administer the siRNA formulation. In the example below, injection to the tail vein was chosen.
3. Place the animals, one after the other, in the cradle and start the 360° imaging program (Fig. 3) (**Note 14**).

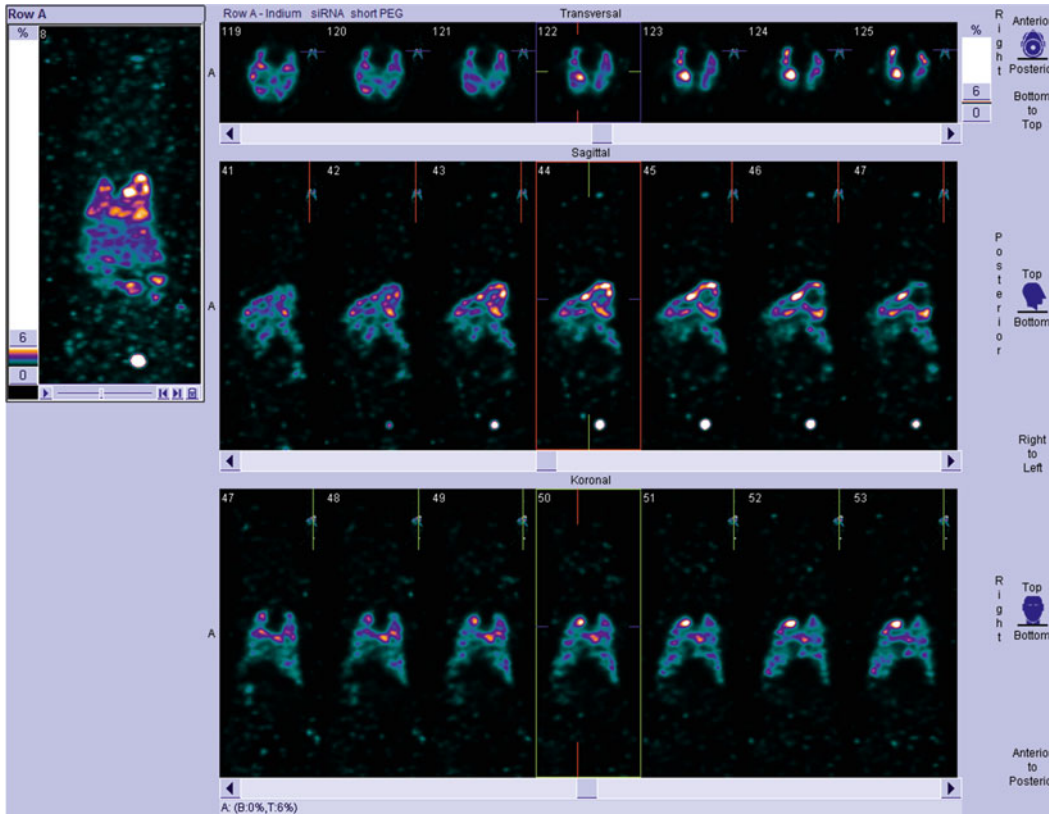

Fig. 3 SPECT images of a 6-week-old balb/c mouse i.v. injected with 2.9 MBq ^{111}Indium-labeled siRNA formulated as micelles 2 h after injection. The formulation was obtained with a polymer carrying a short, 500 Da, PEG chain which is the reason for the accumulation of the micelles in the lung. Deposition in the liver and excretion through the kidneys into the bladder can be observed as well

4 Notes

1. Wrap the metal spatula in parafilm so the DTPA does not complex to the metal ions from the spatula.
2. You should first dissolve the DTPA in DMSO before diluting in the DI-H_2O with NaOH. Make sure the DMSO is at least diluted out by a factor of 1:100.
3. Our siRNA had an MW of 17950.36 g/mol. Therefore, we use 0.285 μmol of siRNA.
4. Total pBn-SCN-DTPA (MW = 649.9 g/mol) is 15.02 μmol.
5. The solution turned cloudy upon the addition of the DTPA to the siRNA solution.
6. You should get a nice visible white pellet at the bottom of the 15 mL conical tube. A regular centrifuge that reaches a speed of 12,000 × *g* may as well be used.

7. Upon addition of the ethanol, the solution should turn slightly cloudy again.
8. You should put roughly 2 mL into each column due to the fact that each column can only retain 1 mg RNA and a limited volume. If you add too much, you may lose some during the purification steps.
9. To make calculations easier in the future, dilute the siRNA to either 100 mM or 50 mM. Aliquot the samples into small portions to prevent several freeze–thaw cycles.
10. Mix the samples by gently pipetting up and down within the cuvette. Be careful not to create any bubbles.
11. Make sure you rinse out the cuvette very well. When you read the fresh 3 mL of the complex solution, verify that the values are in line with the previous measurements.
12. Since each siRNA strand has only 1 amine group for DTPA to complex to, if performed correctly, your ratio should be approximately a 1:1 molar equivalence of DTPA and siRNA. If the ratio of DTPA per siRNA is higher than 1:1, residual free DTPA was not removed during the purification.
13. It may be necessary to combine 2 or more peak fractions based on the CPM values and RNA concentrations. If free DTPA is present in the siRNA solution when it is radiolabeled, a second small peak will appear around fraction 12, and free Indium appears around fraction 20.
14. The imaging procedure can be repeated at any given time. The half-life of ^{111}Indium is 2.6 days, and a significant amount of siRNA is typically excreted renally or even hepatically. Therefore, imaging at time points later than 48 h can become challenging.

Acknowledgements

This work was supported by the NanoIncubator grant to Olivia Merkel as well as the Ruth L. Kirschstein National Research Award T32-CA009531 fellowship to Steven Jones.

References

1. Dickerson EB, Blackburn WH, Smith MH, Kapa LB, Lyon LA, McDonald JF (2010) Chemosensitization of cancer cells by siRNA using targeted nanogel delivery. BMC Cancer 10:10
2. Huang YH, Bao Y, Peng W, Goldberg M, Love K, Bumcrot DA, Cole G, Langer R, Anderson DG, Sawicki JA (2009) Claudin-3 gene silencing with siRNA suppresses ovarian tumor growth and metastasis. Proc Natl Acad Sci U S A 106(9):3426–3430
3. Shahzad MM, Lu C, Lee JW, Stone RL, Mitra R, Mangala LS, Lu Y, Baggerly KA, Danes CG, Nick AM, Halder J, Kim HS, Vivas-Mejia P, Landen CN, Lopez-Berestein G, Coleman RL, Sood AK (2009) Dual targeting of EphA2 and FAK in ovarian carcinoma. Cancer Biol Ther 8(11):1027–1034

4. Goldberg MS, Xing D, Ren Y, Orsulic S, Bhatia SN, Sharp PA (2011) Nanoparticle-mediated delivery of siRNA targeting Parp1 extends survival of mice bearing tumors derived from Brca1-deficient ovarian cancer cells. Proc Natl Acad Sci U S A 108(2):745–750
5. Vlahov I, Leamon CP (2012) Engineering folate-drug conjugates to target cancer: from chemistry to clinic. Bioconjug Chem 23:1357–1369
6. Akhtar S (2006) Non-viral cancer gene therapy: beyond delivery. Gene Ther 13:739–740
7. Watts JK, Corey DR (2010) Clinical status of duplex RNA. Bioorg Med Chem Lett 20:3203–3207
8. Durcan N, Murphy C, Cryan SA (2008) Inhalable siRNA: potential as a therapeutic agent in the lungs. Mol Pharm 5:559–566
9. Davies LA et al (2007) Identification of transfected cell types following non-viral gene transfer to the murine lung. J Gene Med 9:184–196
10. Bertrand N, Wu J, Xu X, Kamaly N, Farokhzad O (2014) Cancer nanotechnology: the impact of passive and active targeting in the era of modern cancer biology. Adv Drug Deliv Rev 66:2–25
11. Renette T, Librizzi D, Endres T, Merkel O, Broichsitter MB, Bege N, Petersen H, Curdy C, Kissel T (2012) Poly(ethylene carbonate) nanoparticles as carrier system for chemotherapy showing prolonged in vivo circulation and anti-tumor efficacy. Macromol Biosci 12:970–978
12. Pippin CG, Parker TA, McMurry TJ, Brechbiel MW (1992) Spectrophotometric method for the determination of a bifunctional DTPA ligand in DTPA-monoclonal antibody conjugates. Bioconjug Chem 3:342–345
13. Merkel OM, Librizzi D, Pfestroff A, Schurrat T, Behe M, Kissel T (2009) In vivo SPECT and real-time gamma camera imaging of biodistribution and pharmacokinetics of siRNA delivery. Bioconjug Chem 20:174–182
14. Rose SD et al (2005) Functional polarity is introduced by Dicer processing of short substrate RNAs. Nucleic Acids Res 33:4140–4156

Chapter 7

Imaging of Electrotransferred siRNA

Muriel Golzio and Justin Teissié

Abstract

SiRNA delivery to the cytoplasm can be obtained through the application of calibrated electric field pulses to a mixture of cells and oligonucleotides. To investigate the uptake pathway, time lapse confocal fluorescence microscopy provides a direct visualization of the transfer. SiRNA is electrophoretically drifted directly to the cytoplasm during the pulse. No post pulse transfer is observed. The uploaded siRNA then freely diffuse in the cytoplasm with no access to the nuclei.

Key words Confocal fluorescence imaging, Electropulsation, Electroporation, siRNA

1 Introduction

RNAi was proposed as a useful therapeutic [1]. But the bottleneck was the delivery to the cytosol by avoiding the deep end associated to endocytotic pathways [2, 3]. This appeared as a major drawback to all nanoparticles supported delivery. As a result only a very limited fraction of the engulfed oligonucleotides was active. New delivery approaches are crucially needed.

Electric pulses are known to strongly stimulate the cell uptake of various polar molecules showing intrinsically very poor transmembrane crossing abilities [4, 5]. The exact molecular and cellular mechanism leading to enhanced intracellular nucleic acid delivery remains unclear. In vivo, electric pulses have been extensively used for drugs, siRNA and pDNA delivery (electrotransfer) into a large number of organs and tissues [6, 7]. Indeed in rodents, electrotransfer has been used to deliver siRNAs into various organs [8–11]. Their delivery led to an efficient transient specific gene silencing when transferred into a tumor where their biodistribution was found to be homogeneous throughout the cytoplasm of electropermeabilized tumor cells [12]. Due to the physics of the electric process, the delivery of molecules is restricted to the volume where the electric field is applied. Only a very few short-lived side effects

Zdravka Medarova (ed.), *RNA Imaging: Methods and Protocols*, Methods in Molecular Biology, vol. 1372,
DOI 10.1007/978-1-4939-3148-4_7,

have been reported for these treatments (muscle contraction, inflammation), emphasizing the innocuity of this physical method for clinical use [13]. Indeed, electrochemotherapy, the electrotransfer of cytotoxic drugs into tumors, is a routine clinical methodology in Europe [14]. Well-established clinical protocols are available following the recommendations of the European ESOPE project [15]. Moreover, siRNAs delivered directly into the cytoplasm by electropulsation do not induce inflammatory responses, as reported with other delivery approaches [13]. Although electropermeabilization (EP) shows promise in the field of new therapies, one major concern on its safety remains that very little is known about the molecular and cellular processes supporting RNA transfer across the plasma membrane to the cytoplasm where it has a direct access to the RNA-induced silencing complex (RISC).

In order to investigate the processes that support siRNA electrotransfer in melanoma cells, we proceeded to a direct single cell visualization of siRNA electrotransfer and followed the localization of biologically active fluorescently labeled siRNA at the single cell level along a train of electrical pulses by using time lapse fluorescence confocal microscopy [16]. We observed that the electrophoretic drag allows a direct access of siRNA across the plasma membrane into the cytoplasm where its enzymatic target is present. A diffusion of the electrotransferred oligonucleotides follows bringing a homogeneous distribution in the cytoplasm.

Alexa Fluor 546 (AF-546) labeled egfp siRNA electrotransfer (AF-546 siRNA þ EP) showed the same silencing efficiency as unlabeled siRNA on egfp expression in B16-F10 mouse melanoma cells expressing the EGFP after retroviral transduction.

We visualized the first steps of siRNA import into the cells by adding AF-546 siRNA to adherent cells and delivering the electric pulses on the microscope stage. Time lapse confocal microscopy was used in a differential approach. Confocal microscopy provides an optical slicing and an observation only on a thin layer. To eliminate the strong background signal present in the buffer bathing the cells, a differential digital method was used where that background was removed by subtracting from each image recorded during the pulse train, the image before EP. As a result, before EP, no spontaneous uptake or direct interaction with the plasma membrane can be observed. During pulse train application, labeled siRNA penetrated the cell. The penetration took place through the membrane on the side of the cell facing the cathode (Fig. 1a). The entrance of the siRNA molecules was already detected just after the first pulse. No complex between the siRNA and the cell surface was present during the EF application (no fluorescence labeling of the membrane). A light profile parallel to the electric field direction or better a surface plot allowed the quantification of fluorescence intensity (FI) due to siRNA inflow. These results

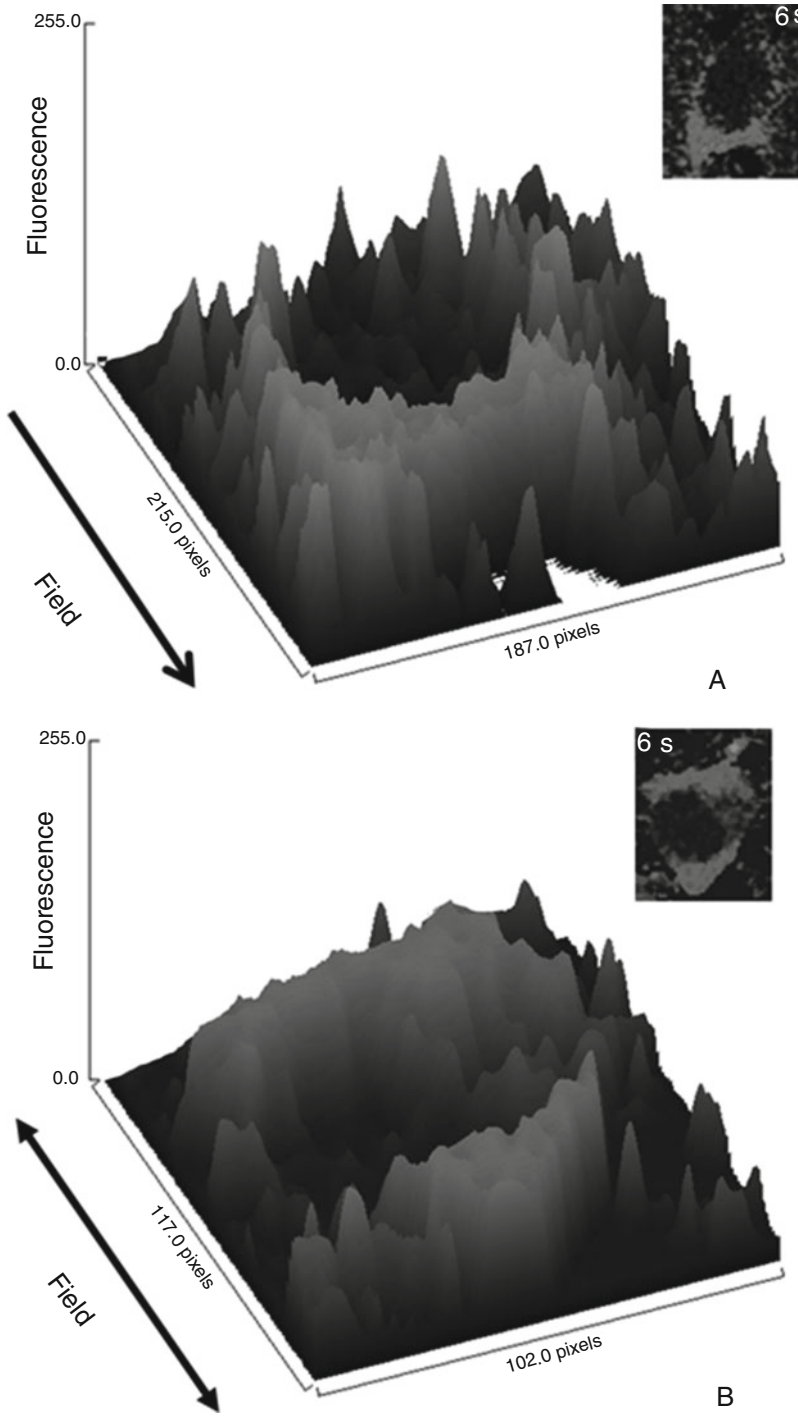

Fig. 1 Pattern of fluorescence distribution within a cell after siRNA electrotransfer. (**a**) 6 Unipolar pulses were delivered. The image is in the *upper right corner*. The field orientation is given by the *arrow*. Surface plot was obtained by using Image J. (**b**) A train of 3+3 pulses with alternating polarities was delivered. The image is in the *upper right corner*. The field orientations are given by the *arrow*. Surface plot was obtained by Image J

showed the unidirectional entrance of siRNA during the electric field application. Statistical analysis of the FI profiles confirmed that this labeling was restricted mostly to the cathode-facing side of the membrane. Almost no siRNA electrotransfer occurred on the side of the membrane facing the anode whereas the Propidium iodide (PI) uptake experiments showed that this side was permeabilized (data not shown). The polarity of the electrodes was then changed between each pulse in order to determine whether or not the electrophoretic forces could push the siRNA molecules alternatively in two opposite directions (Fig. 1b). Successive scans were acquired during the pulse train and after EP. Under a unipolar treatment, the FI always increased on the side of the cell facing the cathode during each pulse, meaning that entry of the siRNA was driven under the control of the polarity of the EF pulse (as expected). The plot profiles after the sixth pulse of the electropermeabilized cells under uni- and bipolar conditions are shown in Fig. 1a. The labeled siRNA was detected in the cytoplasm mainly on the side facing the cathode under the unipolar condition, whereas it was observed on both sides facing the electrodes under the bipolar condition (Fig. 1b).

Therefore, siRNA import occurred at the level of the membrane cap facing the negative electrode and directly reached the cell cytoplasm. These data supported the model in which the electrophoretic forces drove the negatively charged siRNA molecules inside the cell. In the seconds following the train of pulses, siRNA was observed to diffuse in the cytoplasm and a homogeneous distribution was observed. But, siRNA fluorescence was only observed in the cytoplasm of the cells. No fluorescence was seen in the nucleus (Fig. 1a). No increase in the average fluorescence intensity within the cell was detected in the post pulse period, confirming the electrophoretic drift as the cause of the siRNA uploading (Fig. 2).

2 Materials

2.1 Cells

1. B16F10 Cells are cultured in Eagle Minimum Essential Medium (EMEM) supplemented with 10 % fetal calf serum, penicillin (100 U/ml), streptomycin (100 mg/ml), and L-glutamine (0.58 mg/ml) at 37 °C under a 5 % CO_2 atmosphere.
2. B16F10 cells are passaged when confluent with trypsin/EDTA to provide new culture on a 175 cm^2 flask.
3. One day before the observation, cells are harvested by digestion with trypsin/EDTA and 5×10^4 cells are grown on a glass cover slip chamber for fluorescence microscopy observations (*see* **Note 1**).

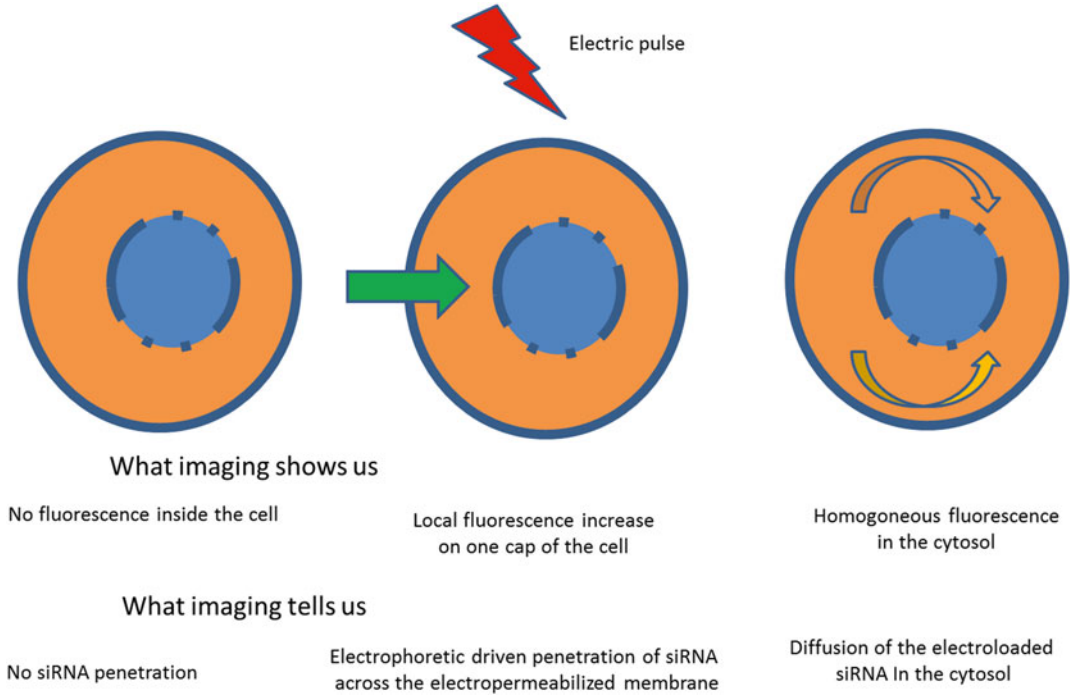

Fig. 2 This cartoon indicates the biophysical and functional informations which are obtained from the imaging observations

2.2 Solutions

1. Pulsation buffer: 10 mM Potassium phosphate; 1 mM $MgCl_2$; 250 mM sucrose; pH 7.4.
2. siRNA suspension buffer: 100 mM Potassium acetate, 30 mM HEPES–KOH, 2 mM magnesium acetate, pH 7.4.
3. Trypsin/EDTA solution: Sigma-T3924.

2.3 Molecules

1. siRNAs were purchased from Qiagen Xeragon (Germantown).
2. The egfp siRNA duplexes were designed according to Caplen and coworkers and provided labeled with Alexa Fluor 546 at the 3′ position of the sense strand [17]. The sequences of egfp22 siRNA (sense: 5′ r(GCA AGC UGA CCC UGA AGU UCA U) and antisense: 5′ r(GAA CUU CAG GGU CAG CUU GCC G)) is directed against GFPmRNA as in [12].
3. Upon receipt, lyophilized pre-annealed double-stranded siRNAs (Qiagen) are resuspended at a concentration of 100 μM in siRNA suspension buffer, heated to 90 °C for 1 min, and incubated at 37 °C for 60 min.
4. Resolubilized siRNAs are stored at –80 °C.

2.4 Equipment

1. Inverted confocal laser scanning microscope: Zeiss LMS510 (Germany).
2. Electropulsator: Beta tech B10 (St Orens, France).
3. Glass coverslip chamber for fluorescence microscopy observations: Lab-Tek™ II system (Nalge Nunc International).

3 Methods

3.1 Electrotransfer Procedure

1. Electropulsation (EP) was operated by using a CNRS cell electropulsator which delivered square-wave electric pulses.
2. All electrical parameters (voltage, pulse duration, number of pulses, and delay between each pulse) were preset on the touch screen. The touch screen monitored and stored pulse shapes (*see* **Note 2**).
3. A polarity inverter allowed the triggering of pulses with alternating (bipolar) polarities.
4. To avoid an electric drift of the cells during pulsation, adherent cells were grown on a glass coverslip chamber for fluorescence microscopy observations.
5. The EP chamber was designed using two stainless steel parallel rods (1 mm diameter, 10 mm length, 5 mm inter-electrode distance) [18]. The rods were in contact with the Labtech dish. The electrodes were connected to the pulse voltage generator and a uniform electric field was generated in the central part of the electrode gap (*see* **Note 3**).
6. The cells were washed and kept in the low ionic content pulsation buffer along the observation (*see* **Note 4**).
7. 7×10^4 adherent cells on the microscope glass coverslip chamber were treated in 400 µl of pulsation buffer in presence of 4 µg of labeled siRNA (10 µg/ml final).
8. Cell permeabilization was performed by applying the electrical pulses required to transfer macromolecules into cells, called EGT protocol [19]. Ten pulses of 5 ms, at a frequency of 1 Hz were applied at 300 V/cm (voltage to electrode gap) (*see* **Notes 5** and **6**).

3.2 Confocal Fluorescence Microscopy

1. The chamber was placed onto the stage of an inverted confocal microscope to visualize the siRNA electrotransfer. Fluorescence was detected using a Zeiss LMS510 inverted confocal laser scanning microscope equipped with a 514 nm Helium-Neon laser. A Zeiss 40× objective (1.3 numerical aperture, oil immersion) was used (*see* **Note 7**).
2. Successive scans shorter than 1 s were performed every second on the same plane to follow the transfer of the siRNA into cells (*see* **Note 8**).

3. Laser power and photomultiplier settings were kept identical for all samples to make the results comparable (*see* **Notes 9** and **10**).
4. Eight bit images were recorded using the Zeiss LMS510 software (EMBL) in the format of 864×611 pixels, i.e., 326.3×291.5 μm.
5. The laser scan was unidirectional and perpendicular to the electric field direction in order to get rid of the temporal delay during image acquisition (*see* **Note 11**).

3.3 Image Analysis

1. The LSM images were processed using ImageJ software (National Institutes of Health; http://rsb.info.nih.gov/ij/).
2. A differential method was performed. The fluorescence signal of the labeled siRNA in the cytoplasm was analyzed as follows: the first image (before EP) was subtracted from each image of the scan series. This process allowed the elimination of siRNA outside the cells and thus discriminated the labeled siRNA penetrating into the cells.
3. Either a surface plot or a light profile oriented parallel to the electric field direction was plotted across the cell in order to determine the orientation of the siRNA entrance. Then, the percentages of labeled cells on the cathode, anode, both or no sides were calculated.
4. A region of interest (ROI) was created limited by the internal periphery of each cell. The MFI of the same ROI was quantified for each image in the scan series. This gives access to the kinetic of the uptake (*see* **Note 12**).
5. Image surface plots provide a global view of the siRNA inflow.

3.4 Statistical Analysis

1. For each condition, more than 30 individual cells were analyzed (N represents the number of individual analyzed cells).
2. Differences in percentages or relative differential fluorescence levels between the different conditions were statistically compared by using unpaired two-sided Student t-tests in Microsoft Excel software (version 2003). *** $P<0.01$. The error bars represent the standard deviation of three independent measurements.

4 Notes

1. To avoid an electric drift of the cells during pulsation, adherent cells must be used.
2. A careful monitoring of the pulse time course must be recorded to avoid artifacts in the pulsing protocol.

3. Cells are observed only in the central part of the electrode gap where a uniform electric field was generated.
4. Experiments were run at room temperature, which was controlled. The pH of the pulsation buffer was stable under our experimental conditions.
5. Cells were always kept for a short period in the pulsation buffer to limit starving.
6. A low voltage to electrode gap was used as plated cells were treated. Plated cells have a large size in the direction of the field and are more sensitive to its intensity.
7. Photobleaching should be avoided by selecting a probe that is stable under illumination and using a proper setting of the confocal microscope
8. A delay is always present in the sampling between the two sides of the cell. Scanning should start on the side facing the negative electrode.
9. Laser power and photomultiplier settings are kept identical for all samples to make the results comparable.
10. No saturation should be present on the first image (before EP).
11. Scanning by the confocal microscope should be in a parallel direction to the electric field, i.e., parallel to the electrodes, to limit the delay in the acquisition.
12. Quantification of the number of uploaded nucleotides can be obtained from the fluorescence intensity only if the signal dose relationship is linear.

Acknowledgments

The authors would like to thank laboratory members for their help and comments (Elisabeth Bellard, Aurelie Paganin-Gioanni, Sophie Chabot, Sandrine Pelofy, and Marie-Pierre Rols). Financial supports were obtained from the Seventh Framework European Programme (FP7) OncomiR [grant number 201102], the "Ligue nationale contre le Cancer," and the "Région Midi-Pyrenées."

This work has been performed in collaboration with the "Toulouse Réseau Imagerie" core IPBS facility (Genotoul, Toulouse, France), which is supported by the Association Recherche Cancer (no. 5585), Region Midi Pyrenees (CPER), and Grand Toulouse cluster.

This work was conducted in the scope of the LEA-EBAM and the EU-COST Action TD1104.

References

1. Zeliadt N (2014) Big pharma shows signs of renewed interest in RNAi drugs. Nat Med 20:109
2. Juliano RL, Ming X, Carver K, Laing B (2014) Cellular uptake and intracellular trafficking of oligonucleotides: implications for oligonucleotide pharmacology. Nucleic Acid Ther 24:2
3. Wang Y, Huang L (2013) A window onto siRNA delivery. Nat Biotechnol 31:611–612
4. Mir LM (2009) Nucleic acids electrotransfer-based gene therapy (electrogenetherapy): past, current, and future. Mol Biotechnol 43:167–176
5. Cemazar M, Sersa G (2007) Electrotransfer of therapeutic molecules into tissues. Curr Opin Mol Ther 9:554–562
6. Golzio M et al (2007) In vivo gene silencing in solid tumors by targeted electrically mediated siRNA delivery. Gene Ther 14:752–759
7. Kishida T et al (2004) Sequence-specific gene silencing in murine muscle induced by electroporation-mediated transfer of short interfering RNA. J Gene Med 6:105–110
8. Akaneya Y, Jiang B, Tsumoto T (2005) RNAi-induced gene silencing by local electroporation in targeting brain region. J Neurophysiol 93:594–602
9. Takabatake Y et al (2005) Exploring RNA interference as a therapeutic strategy for renal disease. Gene Ther 12:965–973
10. Matsuda T, Cepko CL (2004) Electroporation and RNA interference in the rodent retinain vivo and in vitro. Proc Natl Acad Sci U S A 101:16–22
11. Broderick KE, Chan A, Lin F, Shen X, Kichaev G, Khan AS, Aubin J, Zimmermann TS, Sardesai NY (2012) Optimized in vivo transfer of small interfering RNA targeting dermal tissue using in vivo surface electroporation. Mol Ther Nucleic Acids 2:e11
12. Paganin-Gioanni A, Bellard E, Couderc B, Teissie J, Golzio M (2008) Tracking in vitro and in vivo siRNA electrotransfer in tumor cells. J RNAi Gene Silencing 4:281–288
13. Jackson AL, Linsley PS (2010) Recognizing and avoiding siRNA off-target effects for target identification and therapeutic application. Nat Rev Drug Discov 9:57–67
14. Hampton T (2011) Electric pulses help with chemotherapy may open new paths for other agents. JAMA 305:549–551
15. Cadossi R, Ronchetti M, Cadossi M (2014) Locally enhanced chemotherapy by electroporation: clinical experiences and perspective of use of electrochemotherapy. Future Oncol 10:877–890
16. Paganin-Gioanni A, Bellard E, Escoffre JM, Rols MP, Teissié J, Golzio M (2011) Direct visualization at the single-cell level of siRNA electrotransfer into cancer cells. Proc Natl Acad Sci U S A 108:10443–10447
17. Caplen NJ, Parrish S, Imani F, Fire A, Morgan RA (2001) Specific inhibition of gene expression by small double-stranded RNAs in invertebrate and vertebrate systems. Proc Natl Acad Sci U S A 98:9742–9747
18. Mazeres S et al (2009) Non invasive contact electrodes for in vivo localized cutaneous electropulsation and associated drug and nucleic acid delivery. J Control Release 134:125–131
19. Rols MP, Teissie J (1998) Electropermeabilization of mammalian cells to macromolecules: control by pulse duration. Biophys J 75:1415–1423

Chapter 8

Whole-Body Scanning PCR, a Tool for the Visualization of the In Vivo Biodistribution Pattern of Endogenous and Exogenous Oligonucleotides in Rodents

Julien A. Boos and Iwan Beuvink

Abstract

Characterizing the in vivo biodistribution pattern and relative expression levels of oligonucleotide-based molecules such as mRNA, miRNA, siRNA, and anti-miRNAs in animal models, could be a helpful first-step in the successful development of therapeutic oligonucleotides. Here we describe a simple procedure called "Whole-Body Scanning PCR" (WBS-PCR), which combines the power of PCR with that of imaging. WBS-PCR relies on 384 well-defined extractions across a mouse whole-body section followed by a single dilution step which renders the lysates compatible with various qPCR-based assays. The in vivo biodistribution maps are generated by deconvoluting the qPCR data and converting it into a TissueView compatible image file which can be overlaid with an image of the whole-body section used for extractions. WBS-PCR is a flexible platform that can be adapted to other detection systems and thereby further expand the use of this technology.

Key words In vivo biodistribution, Mouse, Rat, qPCR, RT-qPCR, miRNA, siRNA, Therapeutic oligonucleotides, Imaging, QWBA

1 Introduction

The interest to develop therapeutic oligonucleotides is fueled by their potential to drug the so-called "undruggable" targets [1]. However, developing oligonucleotide-based therapeutics pose many challenges. Some of the major challenges encountered concern stability, activity, tissue specific delivery, and cellular uptake. Although there are many assays available that aid in resolving some of the challenges, only a limited number of tools are available to study tissue specific delivery of oligonucleotides in animal models. Moreover, most of these tools require incorporation of tracers, such as fluorophores or radioactivity, which might generate false-positive biodistribution patterns due to altered biophysical properties of the delivery-vehicle or accumulation of tracer in secondary tissues [2, 3]. In order to eliminate the need of tracers, we set out to

Zdravka Medarova (ed.), *RNA Imaging: Methods and Protocols*, Methods in Molecular Biology, vol. 1372,
DOI 10.1007/978-1-4939-3148-4_8,

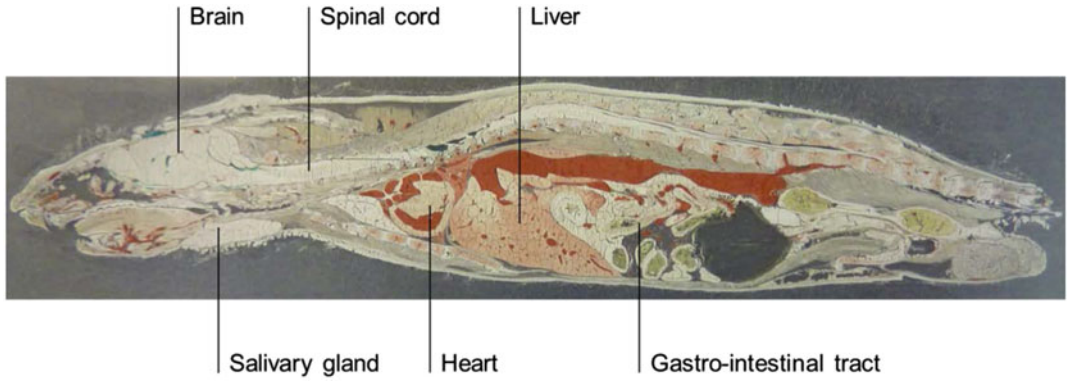

Fig. 1 Annotated Whole-Body section typically used for Whole-Body Scanning PCR

develop a qPCR-based method to visualize the in vivo biodistribution of the therapeutic oligonucleotides. The WBS-PCR procedure makes use of 40-μm sagittal cross-sections of a mouse, typically generated for biodistribution studies of novel radiolabelled therapeutic compounds involving Quantitative Whole-Body Autoradiography (QWBA) (Fig. 1) [4], the spatial resolution of a 1536 round-well plate and a potent tissue lysis buffer. By placing the mouse section on a pre-filled 1536-well plate and extracting the target from the exposed tissues by simply inverting the plate, the entire section is deconvoluted into separate tissue lysates, which can be subjected to downstream analytical assays such as RT-qPCR. Typically, a mouse section covers ~363 wells of the 1536-well plate which, when analyzed on a 384-well qPCR plate, reserves 20 wells for the inclusion of reference samples or standards. Subsequently, with the use of spreadsheets (i.e. Excel) and imaging software (i.e. Tissue View), the localization of the analyte is visualized by converting the qPCR signals into an image and overlaying them with a picture taken of the whole-body cross-section prior to the extraction procedure. The WBS-PCR method described here can be used to study the biodistribution of moderately chemically modified siRNAs (which are still recognized and transcribed into cDNA by reverse transcriptase) and endogenous oligonucleotides such as genomic DNA, ribosomal RNA, messenger RNAs, and microRNAs. Depending on the nature and the amounts of chemical modifications introduced into the therapeutic oligonucleotide, other detection methods might be required for visualization such as Chemical-Ligation qPCR [5]. Combining the principle of WBS-PCR imaging with other detection technologies could lead to novel exciting applications such as the whole-body biodistribution of peptides and proteins [6–9]

2 Materials

2.1 Whole-Body Sectioning

1. N-Hexane.
2. 2 % Carboxymethylcellulose (low viscosity).
3. Adhesive Tape (Scotch Magic Tape 810, 118 mm × 66 m).

2.2 Lysis of the Whole-Body Sections

1. 1536-Well plate Polypropylene Plate (Greiner Bio-One).
2. Clarity OTX Buffer (Phenomenex).
3. 20 mM Tris(2-carboxyethyl) phosphine hydrochloride.
4. Adhesive cover, Microseal 'B' film (Bio-Rad).
5. Rubber brayer.
6. 384-Well Hard-Shell PCR Plate.
7. Pictures of the sections were taken on a ChemiDoc XRS+ System (Bio-Rad).

2.3 Quantification of Genomic DNA

1. 384-Well Hard-Shell PCR Plate.
2. Microseal 'B' Film (Bio-Rad).
3. 100 mM dNTPs.
4. 10× PCR Buffer 1 (Applied Biosystems).
5. 25 mM $MgCl_2$.
6. Rox Reference Dye.
7. Assay On Demand (Applied Biosystems).
8. Hot Start Taq Polymerase, 5 U/μL.
9. The PCR plates were read on a 7900HT Fast Real-Time PCR System (Applied Biosystems).

2.4 Quantification of rRNA and mRNA

1. 384-Well Hard-Shell PCR Plate.
2. Microseal 'B' Film (Bio-Rad).
3. 100 mM dNTPs.
4. 10× PCR Buffer 1 (Applied Biosystems).
5. 25 mM $MgCl_2$.
6. Rox Reference Dye.
7. Assay On Demand (Applied Biosystems).
8. Multiscribe, 50 U/μL (Applied Biosystems).
9. Hot Start Taq Polymerase, 5 U/μL.
10. The PCR plates were read on a 7900HT Fast Real-Time PCR System (Applied Biosystems).

Sequence ID	Sequence	Forward primer	Reverse primer
mmu-miR-1a-3p	UGGAAUGUAAAGAAGUAUGUAU	FAM-CTCCCTCCCTCGATTTTGGAATGTAAAGAA	GCGCTGGATAATACATAC
mmu-miR-122-5p	UGGAGUGUGACAAUGGUGUUUG	FAM-CTCCCTCCCTCGATTTTGGAGTGTGACAAT	GCGCTGGATACAAACACC
mmu-miR-124-3p	UAAGGCACGCGGUGAAUGCC	FAM-CTCCCTCCCTCGATTTTAAGGCACGCGGT	GCGCTGGATAGGCATTC
mmu-miR-124-5p	CGUGUUCACAGCGGACCUUGAU	FAM-CTCCCTCCCTCGATTTCGTGTTCACAGCGG	GCGCTGGATAATCAAGGT
mmu-miR-125a-3P	ACAGGUGAGGUUCUUGGGAGCC	FAM-CTCCCTCCCTCGATTTACAGGTGAGGTTCT	GCGCTGGATAGGCTCCCA
mmu-miR-125a-5P	UCCCUGAGACCCUUUAACCUGUGA	FAM-CTCCCTCCCTCGATTTTCCCTGAGACCCTT	GCGCTGGATACACAGGTTA
mmu-miR-125b-2-3p	ACAAGUCAGGUUCUUGGGACCU	FAM-CTCCCTCCCTCGATTTACAAGTCAGGTTCT	GCGCTGGATAAGGTCCCA
mmu-miR-125b-1-3P	ACGGGUUAGGCUCUUGGGAGCU	FAM-CTCCCTCCCTCGATTTACGGGTTAGGCTCT	GCGCTGGATAAGCTCCCA
mmu-miR-125b-5P	UCCCUGAGACCCUAACUUGUGA	FAM-CTCCCTCCCTCGATTTTCCCTGAGACCCTA	GCGCTGGATATCACAAGT
mmu-miR-126-3P	UCGUACCGUGAGUAAUAAUGCG	FAM-CTCCCTCCCTCGATTTTCGTACCGTGAGTA	GCGCTGGATACGCATTAT
mmu-miR-126-5P	CAUUAUUACUUUUGGUACGCG	FAM-CTCCCTCCCTCGATTTCATTATTACTTTTG	GCGCTGGATACGCGTAC
mmu-miR-127-3p	UCGGAUCCGUCUGAGCUUGGCU	FAM-CTCCCTCCCTCGATTTTCGGATCCGTCTGA	GCGCTGGATAAGCCAAGC
mmu-miR-128-3p	UCACAGUGAACCGGUCUCUUU	FAM-CTCCCTCCCTCGATTTTCACAGTAACCGG	GCGCTGGATAAAAGAGA
mmu-miR-132-3p	UAACAGUCUACAGCCAUGGUCG	FAM-CTCCCTCCCTCGATTTTAACAGTCTACAGC	GCGCTGGATACGACCATG
mmu-miR-133a-3p	UUUGGUCCCCUUCAACCAGCUG	FAM-CTCCCTCCCTCGATTTTTTGGTCCCCTTCA	GCGCTGGATACAGCTGGT
mmu-miR-137-3p	UUAUUGCUUAAGAAUACGCGUAG	FAM-CTCCCTCCCTCGATTTTTATTGCTTAAGAA	GCGCTGGATACTACGCGTA
mmu-miR-139-3P	UGGAGACGCGGCCCUGUUGGAG	FAM-CTCCCTCCCTCGATTTTGGAGACGCGGCCC	GCGCTGGATACTCCAACA
mmu-miR-139-5P	UCUACAGUGCACGUGUCUCCAG	FAM-CTCCCTCCCTCGATTTTCTACAGTGCACG	GCGCTGGATACTGGAGAC
mmu-miR-148b-3p	UCAGUGCAUCACAGAACUUUGU	FAM-CTCCCTCCCTCGATTTTCAGTGCATCACAG	GCGCTGGATAACAAAGTT
mmu-miR-15a-5p	UAGCAGCACAUAAUGGUUUGUG	FAM-CTCCCTCCCTCGATTTTAGCAGCACATAAT	GCGCTGGATACACAAACC
mmu-miR-15b-5p	UAGCAGCACAUCAUGGUUUACA	FAM-CTCCCTCCCTCGATTTTAGCAGCACATCAT	GCGCTGGATATGTAAACC
mmu-miR-16-5p	UAGCAGCACGUAAAUAUUGGCG	ROX-CTCCCTCCCTCGATTTTAGCAGCACGTAAA	GATTTGTTCTGGTTCGCCAAT
mmu-miR-191-5p	CAACGGAAUCCCAAAAGCAGCUG	TAMRA-CTCCCTCCCTCGATTTCAACGGAATCCCA	GCGCTGGATAAGCTGCTTT
mmu-miR-208a-3p	AUAAGACGAGCAAAAAGCUUGU	FAM-CTCCCTCCCTCGATTTATAAGACGAGCAAA	CCGAGGTACAAGCTTTTTG
mmu-let-7a-5p	UGAGGUAGUAGGUUGUAUAGUU	FAM-CTCCCTCCCTCGATTTTGAGGTAGTAGGTT	GCGCTAAGGATAAACTAT
mmu-let-7b-5p	UGAGGUAGUAGGUUGUGUGGUU	FAM-CTCCCTCCCTCGATTTTGAGGTAGTAGGTT	GCGCTGGATAAACCACAC
mmu-let-7c-5p	UGAGGUAGUAGGUUGUAUGGUU	FAM-CTCCCTCCCTCGATTTTGAGGTAGTAGGTT	GCGCTAAGGATAAACCAT
mmu-let-7d-5p	AGAGGUAGUAGGUUGCAUAGUU	FAM-CTCCCTCCCTCGATTTAGAGGTAGTAGGTT	GCGCTGGATAAACTATGC
mmu-let-7e-5p	UGAGGUAGGAGGUUGUAUAGUU	FAM-CTCCCTCCCTCGATTTTGAGGTAGGAG	GCGCTGGATAAACTATAC
mmu-let-7f-5p	UGAGGUAGUAGAUUGUAUAGUU	FAM-CTCCCTCCCTCGATTTTGAGGTAGTAGATT	GCGCTGGATAAACTATAC
mmu-let-7g-5p	UGAGGUAGUAGUUUGUACAGUU	FAM-CTCCCTCCCTCGATTTTGAGGTAGTAGTTT	GCGCTGGATAAACTGTAC
mmu-let-7i-5p	UGAGGUAGUAGUUUGUGCUGUU	FAM-CTCCCTCCCTCGATTTTGAGGTAGTAGTTT	GCGCTGGATAAACAGCAC
Mrp4 siRNA	ACAGCUCCUGACACCUCUCdTdT	FAM-ACTCCCTCCCTCGATTTACAGCTCCTGACAC	CAAGCAGAAGACGAAGAGAGG

Fig. 2 Detailed sequences of RT-qPCR primers used for the detection of various miRNAs and Mrp4 siRNA

2.5 Quantification of miRNA and siRNA

1. 384-Well Hard-Shell PCR Plate.
2. Microseal 'B' Film (Bio-Rad).
3. 100 mM dNTPs.
4. 10× PCR Buffer 1 (Applied Biosystems).
5. 25 mM $MgCl_2$.
6. Rox Reference Dye.
7. RT/Reverse Primers, Forward primers, and Anti-primer (Fig. 2).
8. Multiscribe, 50 U/μL (Applied Biosystems).
9. Hot Start Taq Polymerase, 5 U/μL.
10. The PCR plates were read on a 7900HT Fast Real-Time PCR System (Applied Biosystems).

2.6 Synthetic miRNA and siRNA Standard Curves

1. Synthetic miRNA and siRNA (Fig. 2).
2. Poly(A) (polyadenylic acid).

2.7 Data Analysis and Imaging

1. SDS Software 2.2 (Applied Biosystems).
2. Excel to Analyze Conversion macro (http://maldi.ms).
3. TissueView (AB Sciex).

3 Methods

3.1 Mouse Freezing

1. Pour n-hexane in an isothermal can under a chemical hood.
2. Gently and gradually add dry-ice to the n-hexane.
3. The n-hexane/dry-ice mixture will be at the right temperature (−70 °C) when adding more dry-ice does not generate boiling of the n-hexane anymore.
4. Soak the mice right after sacrifice in the n-hexane/dry-ice mixture by sliding the mouse along the inner wall of the isothermal can, with its back facing the wall of the can.
5. Hold the mouse by its tail for 4–5 min to ensure proper and complete freezing of all tissues.
6. Take out the mouse and put it on absorbent pads to remove the excess of n-hexane solution.
7. Shave the mouse using an electric razor, being cautious that the mouse does not thaw. If the ears of the mouse begin to thaw, put the mouse back for 1–2 min in the n-hexane/dry-ice mixture. Repeat the process until the mouse is completely shaven.
8. Cut the legs and tail using scissors and label it well before putting the mouse in a plastic bag. Store immediately at −80 °C until sectioning.

3.2 Mouse Sectioning

In order to minimize the diffusion of compounds, we recommend performing the following steps at temperatures around −20 °C.

1. The frozen carcasses were embedded in a mold on a microtome stage by adding an ice-cold aqueous solution of 2 % carboxymethylcellulose.
2. Subsequent freezing took place in an n-hexane/dry-ice bath for 40 min.
3. After removal from the mold, the frozen block was stored at −20 °C until sectioning.
4. The block was put on a CM3600XP cryomacrotome and sectioning was performed in the sagittal plane (from cranial end to caudal end).
5. Several sections of 40 μm thickness were taken at varying depths throughout the body, in order to maximize the organ coverage.
6. Collected sections were mounted on a wooden frame and left for dehydration in the cryomacrotome chamber for 72 h at −23 °C.
7. The sections were stored at −80 °C until further use.

3.3 Lysis of Whole-Body Sections

1. A picture of the intact section was taken on the ChemiDoc System (Fig. 3a).

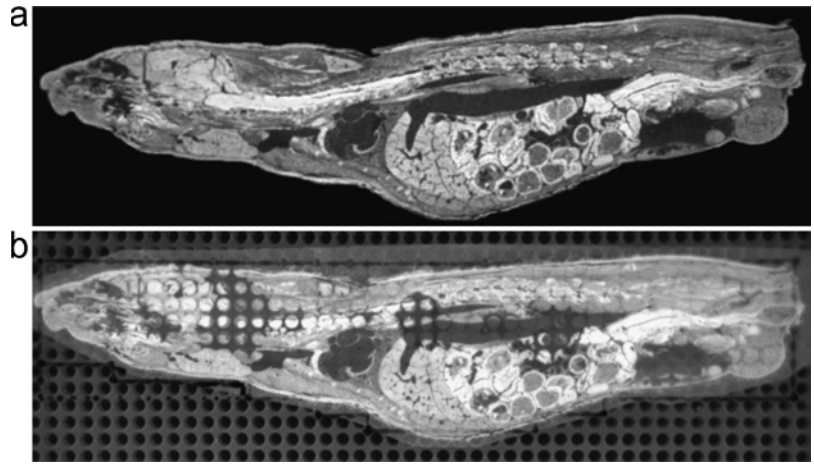

Fig. 3 Whole-body section pictures used for the imaging process. (**a**) Picture taken before the lysis of the section, used for generating biodistribution patterns. (**b**) Picture of the section once overlaid on the lysis plate, used for defining alignment parameters

2. A 1536-well plate (*see* **Note 1**) was filled with 15 µL Lysis Buffer composed of Clarity OTX Buffer supplemented with 20 mM TCEP.
3. A matrix of 363 wells was outlined on the 1536-well lysis plate with a marker pen and the section was overlaid with the whole-body section tissues facing the wells on this matrix in a way that maximizes the coverage of the section (Fig. 3b).
4. The plate was firmly sealed with Microseal 'B' Film with the help of a rubber brayer.
5. Another picture of the plate overlaid with the mouse section was taken for data analysis purposes (*see* **Note 2**).
6. The lysis buffer was put in contact with the tissues of the section by repeated inversion of the lysis plate followed by centrifugation at 1450 × *g* for 3 min.
7. After removal of the sealing foil and lysed section, the lysates were transferred to a 384-well Hard-Shell PCR plate. Keep track of the exact position each lysate originates from and the position it is transferred to.
8. To render the lysates compatible with RT-qPCR analysis, dilute 2 µL lysate in 148 µL RNase-free water.
9. Store both plates at −80 °C until further use, taking care of minimizing freeze–thawing cycles of the diluted lysates (*see* **Note 3**).

3.4 Quantification of 18S Genomic DNA by qPCR

The quantification of 18S genomic DNA has two main purposes in the data analysis process. Through its broad coverage of the mouse section (Fig. 4), the qPCR signals obtained for genomic 18S DNA

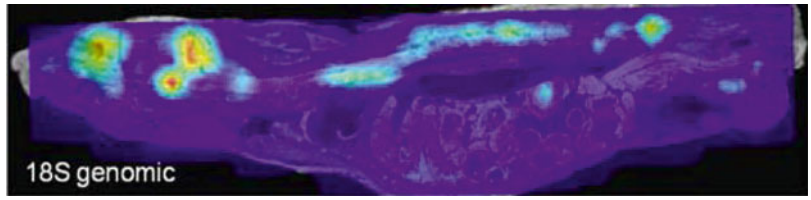

Fig. 4 Expression pattern of genomic 18S in a mouse whole-body section

can be used to define the optimal alignment parameters to generate good overlays of RT-qPCR signals and section picture. Moreover, the genomic 18S signal serves as control for efficient extraction and as normalizer for mRNA, miRNA, and siRNA RT-qPCR signals.

1. The qPCR mix was prepared in a 2 mL Eppendorf Tube. 8 μL qPCR mix contained; 5.45 μL RNase-free Water, 0.15 μL 100 mM dNTPs, 1 μL 10× PCR Buffer 1, 1 μL 25 mM $MgCl_2$, 0.1 μL Rox Reference Dye, 0.2 μL Assay on Demand (18S Genomic) and 0.1 μL Hot Start Taq Polymerase.
2. The qPCR mix was quickly vortexed and briefly centrifuged before and after adding the Hot Start Taq Polymerase to ensure proper homogenization.
3. 8 μL qPCR mix was dispensed in each well of a 384-well Hard-Shell PCR plate, and 2 μL diluted lysate was added to each well.
4. The plate was sealed using a Microseal 'B' Film and mixed by inversion.
5. Following centrifugation at 1450×*g* for 30 s, the plate was loaded in a 7900HT Fast Real-Time PCR System using the following cycling conditions: 1 cycle: 10 min/95 °C followed by 40 cycles: 3 s/95 °C; 30 s/60 °C.
6. Data acquisition and analysis was performed using the software provided by Applied Biosystems.

3.5 Quantification of rRNA and mRNA by One-Step RT-qPCR

1. The RT-qPCR mix was prepared in a 2 mL Eppendorf Tube. 8 μL RT-qPCR mix contained; 5.35 μL RNase-free Water, 0.15 μL 100 mM dNTPs, 1 μL 10× PCR Buffer 1, 1 μL 25 mM $MgCl_2$, 0.1 μL Rox Reference Dye, 0.2 μL Assay on Demand, 0.1 μL Multiscribe and 0.1 μL Hot Start Taq Polymerase.
2. The RT-qPCR mix was quickly vortexed and briefly centrifuged before and after adding the Hot Start Taq Polymerase to ensure proper homogenization.
3. 8 μL RT-qPCR mix was dispensed in each well of a 384-well Hard-Shell PCR plate, and 2 μL diluted lysate was added to each well.

4. The plate was sealed using a Microseal 'B' Film and mixed by inversion.
5. Following centrifugation at 1450×*g* for 30 s, the plate was loaded in a 7900HT Fast Real-Time PCR System using the following cycling conditions: 1 cycle: 30 min/50 °C, 1 cycle: 10 min/95 °C followed by 40 cycles: 3 s/95 °C; 30 s/60 °C.
6. Data acquisition and analysis was performed using the software provided by Applied Biosystems.

3.6 Preparation of Synthetic miRNA and siRNA Standard Curves

1. The dilution solution was prepared by diluting Poly(A) at a concentration of 10 ng/μL in RNase-free water.
2. The Poly(A) solution was dispensed in twelve 1.5 mL Eppendorf tubes. Tubes 1–11 were used for the serial dilution of synthetic miRNA and siRNA. Tube 12 contained only Poly(A) solution and was used as No Template Control.
3. Synthetic miRNAs and siRNAs were serially diluted in tenfold dilution steps to obtain a concentration ranging from 10 ng/μL to 1 zg/μL.
4. At each dilution step, the 1.5 mL Eppendorf was briefly vortexed to ensure optimal homogenization (*see* **Note 4**).
5. The dilutions were subsequently transferred to a V-Bottom 96-well plate and stored at −20 °C until further use (*see* **Note 3**).

3.7 Quantification of miRNAs and siRNAs by RT-qPCR

1. The RT mix was prepared in a 2 mL Eppendorf Tube. 8 μL RT-mix contained: 5.65 μL RNase-free Water, 0.15 μL 100 mM dNTPs, 1 μL 10× PCR Buffer 1, 1 μL 25 mM $MgCl_2$, 0.1 μL 1 μM RT-primer, and 0.1 μL Multiscribe Reverse Transcriptase.
2. The RT mix was quickly vortexed and briefly centrifuged before and after adding the Multiscribe Reverse Transcriptase to ensure proper homogenization.
3. 8 μL RT-mix was dispensed in each well of a 384-well Hard-Shell PCR plate, and 2 μL diluted lysate was added to each well. 2 μL of each dilution step of the miRNA or siRNA standard curves was also added to the 384-well Hard-Shell PCR plate.
4. The plate was sealed using a Microseal 'B' Film and mixed by inversion.
5. Following centrifugation at 1450×*g* for 30 s, the plate was loaded in a 7900HT Fast Real-Time PCR System and incubated for 10 min at 25 °C followed by 5 min at 95 °C.
6. After completion of the RT-reaction, the plate was centrifuged for 3 min at 1450×*g*.
7. The qPCR-mix was prepared in a 2 mL Eppendorf Tube. 5 μL PCR-mix contained: 3.325 μL RNase-free water, 0.15 μL 100 mM dNTPs, 0.5 μL 10× PCR Buffer 1, 0.5 μL $MgCl_2$,

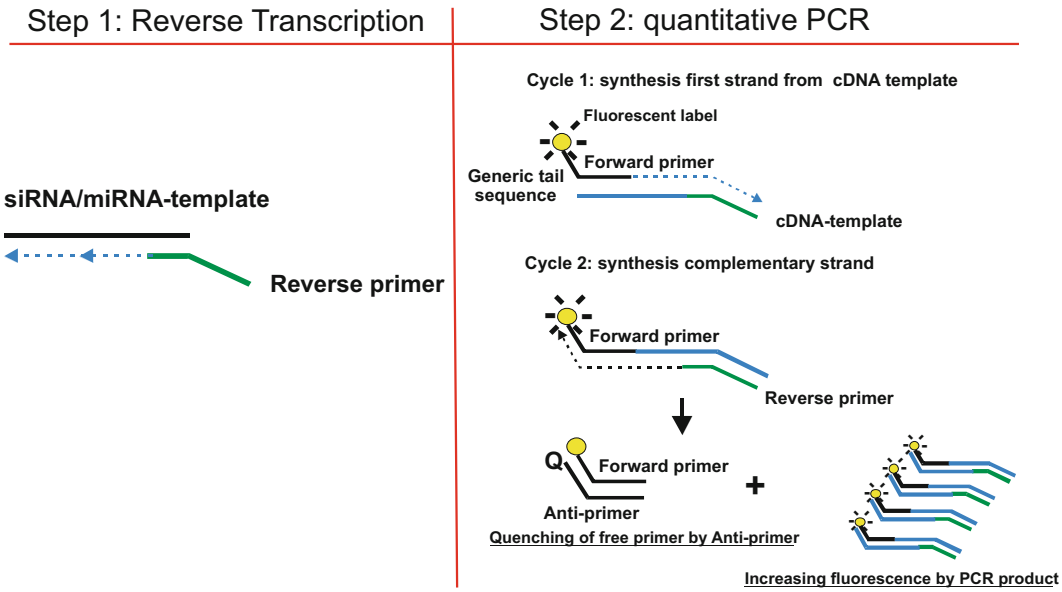

Fig. 5 Molecular mechanism of the siRNA and miRNA RT-qPCR method

0.15 µL 10 µM Forward primer, 0.15 µL 10 µM reverse primer, 0.075 µL 50 µM Anti-primer and 0.15 µL Hot Start Taq Polymerase.

8. The qPCR-mix was quickly vortexed and briefly centrifuged before and after adding the Hot Start Taq Polymerase to ensure proper homogenization.
9. The seal of the RT-plate was removed and 5 µL PCR-mix was directly added to each well of the plate.
10. After addition of the PCR-Mix, the plate was sealed with a Microseal 'B' Film, mixed by inversion and centrifuged for 30 s at 1450×*g*.
11. The PCR reaction was performed in a 7900HT Fast Real-Time PCR System and consisted of the following cycling conditions: 10 min/95 °C followed by 50 cycles: 3 s/95 °C; 30 s/55 °C. The ramping speed should not be faster than 3 °C/s (*see* **Note 5**).
12. Data acquisition and analysis was performed using the software provided by Applied Biosystems.

3.8 Design of the Primers for miRNA and siRNA RT-qPCR

The miRNA and siRNA RT-qPCR primers were designed according to the following guidelines:

1. The RT-primer is also used as reverse-primer in the qPCR reaction (Fig. 5). The primer contains a generic sequence at its 5′-end and a Target Recognition Sequence (TRS) at its 3′-end (*see* **Note 6**).

2. The typical length of the Target Recognition Sequence is 8 nucleotides but can vary from 6 to 12 nucleotides, depending on the G/C content of the TRS, and is complementary to the target-sequence.
3. If the 3′-end of the RT-primer contains a palindromic motif (i.e. –ccgg, -aatt, -ggcc, -ttaa, -atat, -tata, -cgcg, and -gcgc), the primer can be elongated or truncated by one nucleotide to disrupt the palindromic sequence.
4. The forward primer is composed of a generic sequence at its 5′-end and a Target Recognition Sequence at the 3′-end. The 5′-end is labeled with a fluorophore compatible with the quencher used in the anti-primer (*see* **step 7**).
5. Typically, the TRS of the forward primer is 13–14 nucleotides long. Depending on the GC-content of the target sequence and palindromic motives at the 3′-end of the forward primer, the length can be reduced or extended.
6. An overlap of more than 3 nucleotides between the forward and reverse primers should be avoided since this increases primer-dimer formations.
7. The generic sequence of the forward primer must be complementary to the sequence of the quencher-labeled anti-primer (5′-AAATCGAGGGAGGGAG-BHQ_2-3′)
8. In order to make sure that the designed miRNA/siRNA-primers meet the expected criteria with respect to specificity and sensitivity. We recommend extensive characterization of the primers before using them in WBS-PCR (Fig. 6). For primers designed against miRNAs, it is recommended to check the sequences for homologous miRNAs (http://www.mirbase.org/) and validate the primers using every closely-related miRNA as template.

3.9 Data Analysis and Deconvolution

The first step of the data analysis was to set up a conversion matrix. This matrix indicates the position of a sample of the qPCR plate on the lysis plate and facilitates the reconstitute of the whole-body section.

1. After analysis of the data using the SDS 2.2 software, the Ct-values were exported to spreadsheet software, such as Excel.
2. Using either the formulas provided by Applied biosystems for the analysis of mRNA, rRNA, or gDNA, or linear regression for the absolute quantification of miRNAs and siRNAs, Ct-values were converted into relative/absolute expression signals.
3. Using the conversion matrix, the signals obtained in each PCR-Plate were deconvoluted to match the positions on the lysis plate.

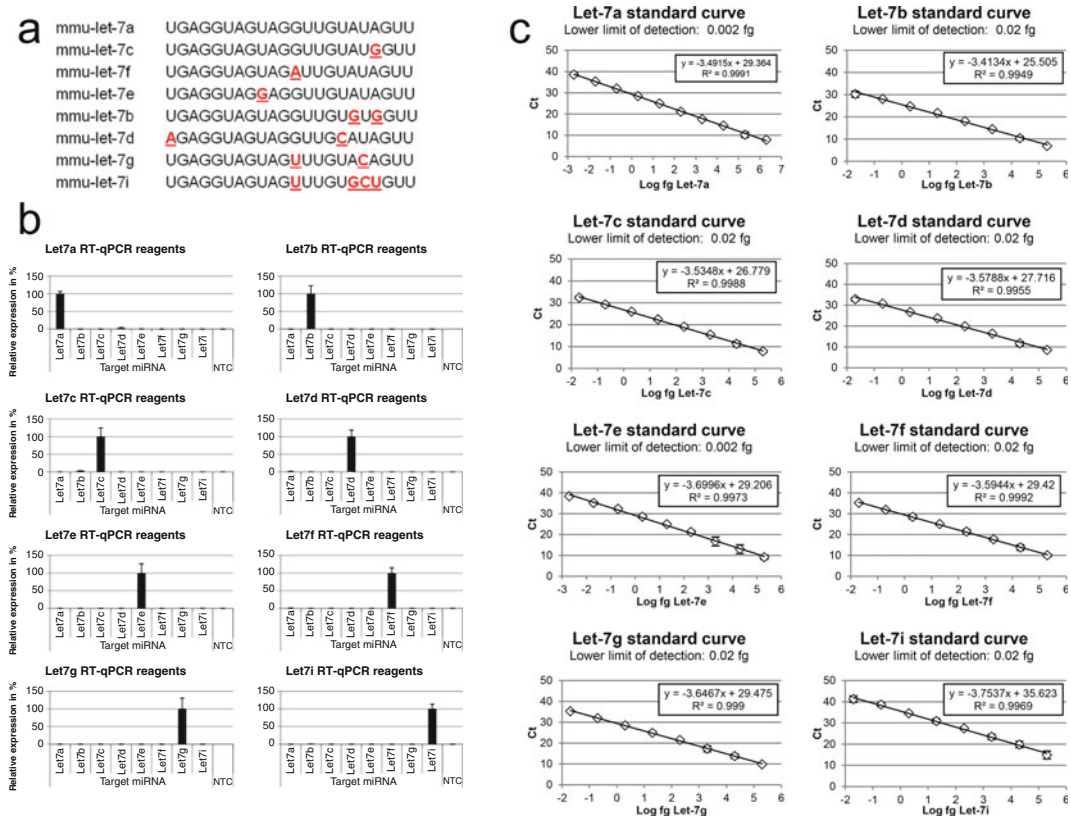

Fig. 6 Characterization of the RT-qPCR primers detecting various members of the Let-7 family of miRNAs. Sequences of the tested members of the Let-7 family of miRNAs (**a**). Cross-specificity study (**b**) and sensitivity study (**c**) of the Let-7 RT-qPCR primers

4. In order to correct for extraction efficiencies and tissue density, signals obtained for all RNA targets (mRNA, rRNA, miRNA, and siRNA) were corrected by the signals obtained for genomic 18S.
5. An Excel to Analyze Conversion macro was used to convert these data into TissueView compatible image files.
6. The images were directly loaded into TissueView and overlaid with the Whole-Body Sections taken at Subheading 3.3, **steps 1** and **5**. The signals obtained for genomic 18S can be used to fine-tune the adjustments of the alignment parameters (*see* **Note 7**).

4 Notes

1. It is crucial to use round-well 1536-well plates as lysis plates and not the square-well 1536-well plates. The round-well plates have bigger inter-well surfaces and seal better thereby preventing leakage of lysate from one well to another.

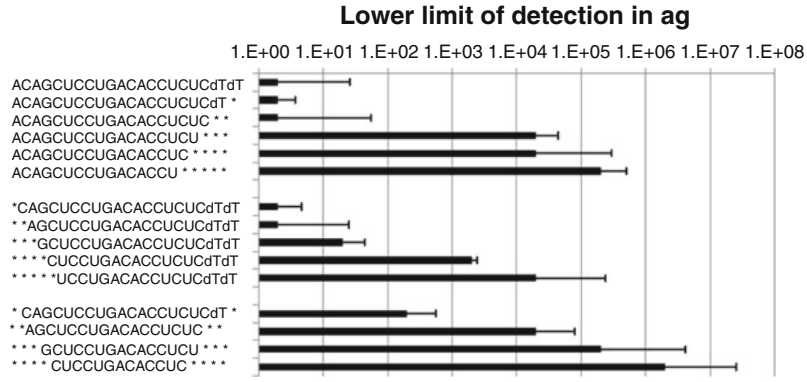

Fig. 7 Lower limit of detection obtained for the truncated version of an siRNA. Values are averages of 3 measurements. Error bars, STDEV ($n = 3$)

2. Take a picture immediately after placing the whole-body section on the lysis plate. The exposed tissue starts to disintegrate quickly when it comes into contact with the lysis buffer.
3. Keep the amount of freeze-and-thaw cycles of the lysate-plate and dilution plate to a minimum. Repeated cycles of freezing and thawing results in a weakening/loss of PCR-signals.
4. For the preparation of miRNA and siRNA standard curves, we recommend to use 1.5 mL Eppendorf Tubes for each dilution, to vortex the tubes at each dilution steps and not to pipet small volumes.
5. Some PCR-machines have very fast ramping speeds which can affect the performance of the miRNA/siRNA qPCR-assay. Lowering the ramping speed to 3 °C/s solves this issue.
6. The miRNA/siRNA RT-qPCR method is very sensitive to the truncation of its target (Fig. 7). Due to the short TRS length imposed by the target and the design of the assay, a single truncation of the target sequence can dramatically reduce the sensitivity of the assay, and can in some instances make a target undetectable.
7. In order to obtain the best alignment in TissueView, we suggest to start the overlay using a pixelated image of the 18S genomic DNA, so that each "Pixel" represents one well on the lysis plate (Fig. 8, top panel). Once aligned, change the picture-view to for example: smoothened signals (Fig. 8, bottom panel).

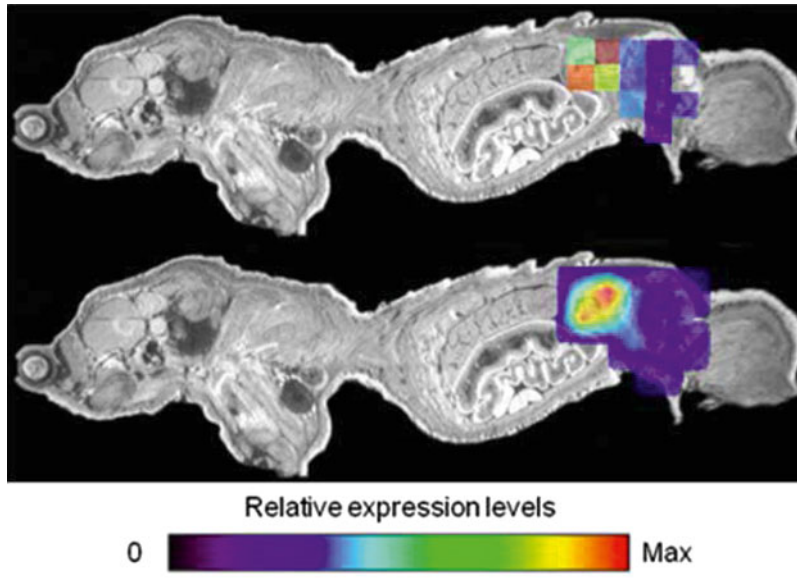

Fig. 8 Impact of the signal smoothening on the human ELAVL1 mRNA biodistribution pattern

References

1. Melnikova I (2007) RNA-based therapies. Nat Rev Drug Discov 6:863–864
2. Yoo H, Juliano RL (2000) Enhanced delivery of antisense oligonucleotides with fluorophore-conjugated PAMAM dendrimers. Nucleic Acids Res 28:4225–4231
3. Christensen J, Natt F, Hunziker J, Krauser J, Andres H, Swart P (2012) Tritium labeling of full-length small interfering RNAs. J Labelled Comp Radiopharm 55:189–196
4. Coe RA (2000) Quantitative whole-body autoradiography. Regul Toxicol Pharmacol 31: S1–S3
5. Boos JA, Kirk DW, Piccolotto M-L, Zuercher W, Gfeller S, Neuner P, Dattler A, Wishart WL, Von Arx F, Beverly M et al (2013) Whole-body scanning PCR; a highly sensitive method to study the biodistribution of mRNAs, noncoding RNAs and therapeutic oligonucleotides. Nucleic Acids Res 41(15), e145
6. Liao S, Liu Y, Zeng J, Li X, Shao N, Mao A, Wang L, Ma J, Cen H, Wang Y et al (2010) Aptamer-based sensitive detection of target molecules via RT-PCR signal amplification. Bioconjug Chem 21:2183–2189
7. Lin JS, McNatty KP (2009) Aptamer-based regionally protected PCR for protein detection. Clin Chem 55:1686–1693
8. Wang XL, Li F, Su YH, Sun X, Li XB, Schluesener HJ, Tang F, Xu SQ (2004) Ultrasensitive detection of protein using an aptamer-based exonuclease protection assay. Anal Chem 76:5605–5610
9. Zhang H, Wang Z, Li XF, Le XC (2006) Ultrasensitive detection of proteins by amplification of affinity aptamers. Angew Chem Int Ed Engl 45:1576–1580

Chapter 9

siRNA Nanoparticles for Ultra-Long Gene Silencing In Vivo

Seung Koo Lee and Ching-Hsuan Tung

Abstract

Small interfering RNA (siRNA)-mediated gene silencing has shown prominent therapeutic effects in treating various diseases. However, adequate delivery and persistent gene silencing remain challenging. A nanoparticle-based delivery system which assembled by layering siRNAs between protease degradable polypeptides to show ultra-long gene silencing effect in vivo is developed. Gold nanoparticle is used as a scaffold for its unique properties including uniform size, biocompatibility, ready synthesis, and easy functionalization. A simple layer-by-layer fabrication approach, based on the electrostatic interaction between positively and negatively charged polymers, is applied to package the therapeutic siRNAs.

Key words Small interfering RNA, Layer-by-layer, Gold nanoparticles, Poly-l-lysine, Electrostatic interaction, Ultra-long, Genesilencing, Genetherapy, In vivo

1 Introduction

Since its discovery in mammalian cells, small interfering RNA (siRNA) has been applied to silence the expression of disease-related genes. It is believed that siRNA could be a paradigmatic therapeutic agent and an ultimate cure for many acquired and inherited life-threatening diseases such as AIDS, genetic disorders, and cancer [1–4]. However, the lack of an effective siRNA delivery system has hindered the success of siRNA-based therapeutics [5, 6]. Despite various approaches such as lipids [7], cationic polymers [8, 9], and exosome nanoparticles [10] exploited to resolve this drawback, only a transient gene-silencing effect has been achieved due to the dilution of siRNA upon cell division and its nonrenewable nature [11]. For this reason, in order to obtain a consistent silencing effect in vivo, current siRNA-based therapy is dependent upon repetitive agent administrations, which result in a substantial impediment to the patient's welfare [12].

Zdravka Medarova (ed.), *RNA Imaging: Methods and Protocols*, Methods in Molecular Biology, vol. 1372,
DOI 10.1007/978-1-4939-3148-4_9,

To overcome these existing challenges, a single treatment of a complete and long gene silencing is crucially required. To achieve a controlled release and prolonged gene silencing effects, we have adopted a layer-by-layer (LbL) fabrication method [13–15] and developed multilayered siRNA delivery nanocomplex [17, 18]. The LbL fabrication method is a gentle and simple assembly procedure based on the charge–charge interactions between positively and negatively charged polymers [16].

Here, we have described the formulation of siRNA nanocarrier optimized for ultra-long gene silencing in vivo using luciferase as a model system. Using the LbL fabrication method, two layers of negatively charged siRNAs targeting luciferase gene (Table 1) and three layers of positively charged poly-l-lysine (PLL) are coated onto gold nanoparticles (AuNPs) (Fig. 1). The formulated particle carries siRNA into tumor cells and effectively silences the luciferase gene without any noticeable cytotoxicity. The cellular uptake and the release of siRNA are visualized by fluorescence microscopy (Fig. 2). The coated siRNAs are gradually and continuously released for an extended period of time following the intracellular degradation of the polyelectrolyte layers. Using this innovative construct, the in vivo gene silencing effect of siRNA is shown to be

Table 1

Sequence of siRNAs

Name	Sense strand sequence (5′ → 3′)	Antisense strand sequence (5′ → 3′)
Ba [21]	UUAAUCAGAGACUUCAGGCGGUdTdT	ACCGCCUGAAGUCUCUGAUUAAdTdT
Ba-cy5	[Cy5]UUAAUCAGAGACUUCAGGCGG UdTdT	ACCGCCUGAAGUCUCUGAUUAAdTdT
Na [1]	CGUACGCGGAAUACUUCGAdTdT	UCGAAGUAUUCCGCGUACGdTdT
Na-cy3	[Cy3]CGUACGCGGAAUACUUCGAdTdT	UCGAAGUAUUCCGCGUACGdTdT
siLuc-ctrl [1]	AGCUUCAUAAGGCGCAUGCdTdT	GCAUGCGCCUUAUGAAGCUdTdT

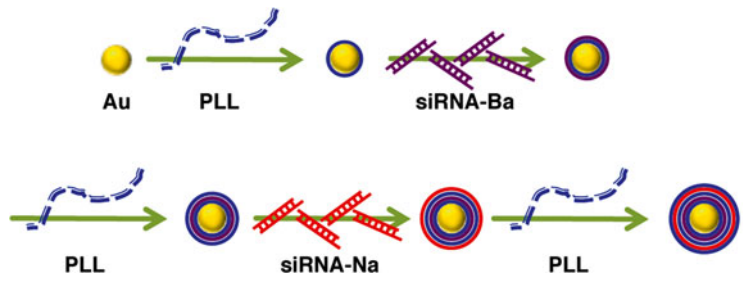

Fig. 1 The scheme for the preparation of siRNA coated gold nanoparticles (sRAuNPs) by electrostatic interaction of layer-by-layer (LbL) deposition

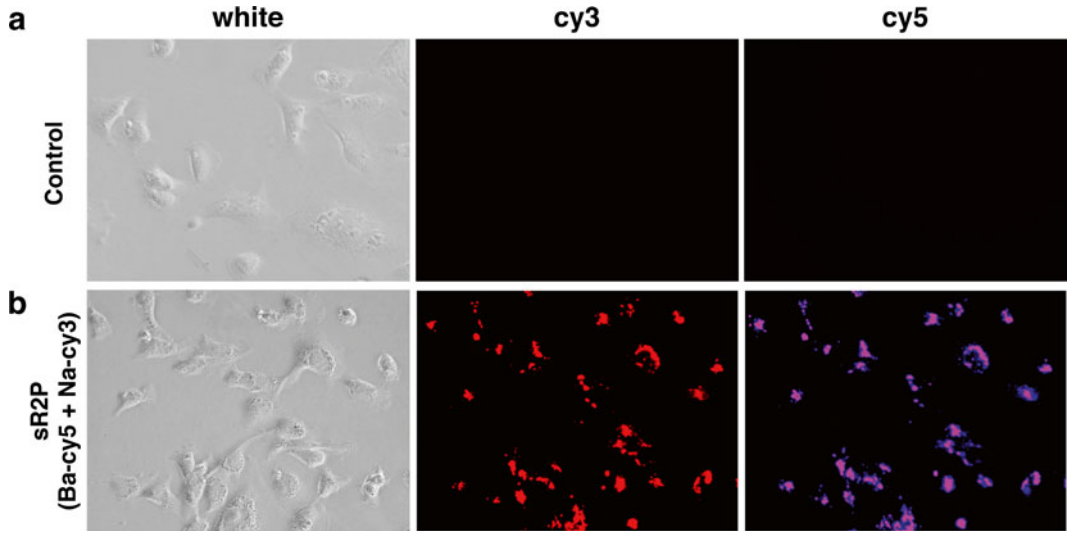

Fig. 2 Images of released siRNA after 24 h incubation (**a**) without or (**b**) with sR2P (Ba-cy5 + Na-cy3) in MDA-MB231-luc2 cells are visualized using fluorescence microscopy in different filters

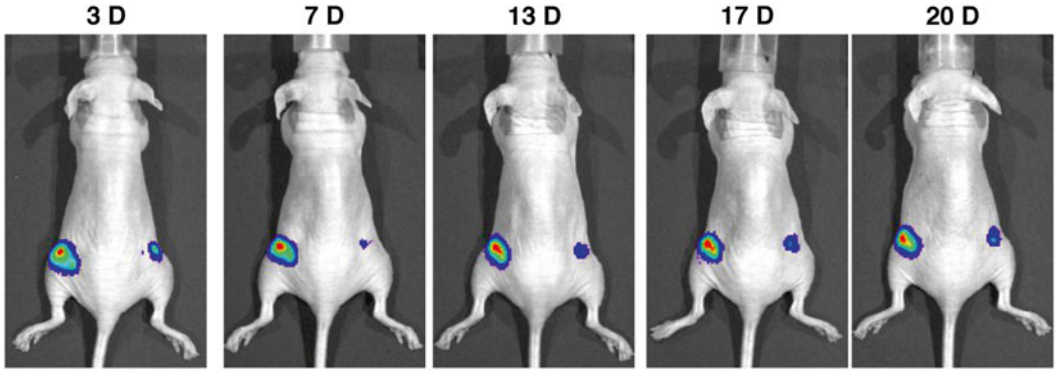

Fig. 3 In vivo gene-silencing effect of sRAuNPs. The luminescence signals from nontreated (*left flank*) or sR2P (Ba + Na) treated MDA-MB231-luc2 cells (*right flank*) are visualized by IVIS-200 until 20 days after implantation. The images are from representative one mouse ($n = 3$)

consistent for an ultra-long period of time (>3 weeks), in result over 60 % of the luciferase gene expression was inhibited even 20 days after its initial inoculation (Fig. 3). An additional advantage of this delivery system is its flexibility. Using this same fabrication protocol, different nucleic acid-based drugs could be packed. With minor modifications, this same concept was used to develop multilayered nanoprobes suitable for long-lasting fluorescent cell labeling and cell fate imaging [19, 20].

2 Materials

2.1 Fabrication of siRNA Coated Gold Nanoparticles (sRAuNPs)

Prepare all solutions using ultrapure water and store all reagents at room temperature unless otherwise specified.

1. Bare gold nanoparticles (AuNPs: 40 nm of size) (BB International, Cardiff, UK) (*see* **Note 1**).
2. Poly-l-lysine (PLL: 15,000–30,000 g/mol of molecular weight) (Sigma-Aldrich, St. Louis, MO) (*see* **Note 2**).
3. siRNA (Sigma-Aldrich) against luciferase and control nonsense siRNA (*see* **Note 3**).
4. Ultrapure distilled water (Invitrogen, Carlsbad, CA).

2.2 Cell Culture

1. Cell maintenance: MDA-MB231-luc2 (Caliper, Alameda, CA), human breast cancer cell line stably expressing firefly luciferase, is cultured in DMEM medium (Mediatech Inc., Manassas, VA) supplemented with 2 mM l-glutamine, 100 U/mL penicillin, 100 mg/mL streptomycin, and 10 % heat-inactivated fetal bovine serum (Sigma-Aldrich) in a humidified atmosphere of 5 % CO_2 at 37 °C (*see* **Note 4**).
2. Live cell imaging: Both cy5 fluorochrome tagged Ba-cy5 [21] and cy3 tagged Na-cy3 [1], which target luciferase gene, have been chosen from well-studied literatures and are used for fluorescence imaging using a fluorescence microscopy system (Olympus, Tokyo, Japan) (Table 1).
3. Genesilencing effect: For the examination of the gene silencing effect, bioluminescence measurement is performed using IVIS-200 (Caliper) immediately after the addition of d-Luciferin (Regis Technologies, Morton Grove, IL).

2.3 In Vivo GeneSilencingImaging

1. Female nude (nu/nu) mice (Charles River, Wilmington, MA) (*see* **Note 5**).
2. Nontreated or sRAuNPs pretreated MDA-MB231-luc2 cells.
3. Matrigel (BD Biosciences, San Jose, CA) (*see* **Note 6**).
4. Small animal optical imaging system (IVIS-200, Caliper).

3 Methods

3.1 Preparation and Characterization of Multilayered sRAuNPs

1. Add AuNPs solution (3.15×10^9 particles in 0.7 mL) dropwisely onto PLL solution (0.5 mL of 5 mg/mL stock solution) in pure water (*see* **Note 7**).
2. Incubate for 30 min in the dark with gentle shaking.

3. Centrifuge incubated solutions for 30 min at 16,100 × *g* using a micro centrifuge (Eppendorf, Hauppauge, NY).
4. Remove the supernatant.
5. Re-suspend the gel-like deep red pellet with pure water and centrifuge for 30 min at 16,100 × *g* using a micro centrifuge (Eppendorf).
6. Remove the supernatant.
7. Wash one more time with centrifugation (repeat **steps 5–6**).
8. Resuspend PLL-coated AuNPs in 0.5 mL of pure water.
9. Add PLL-coated AuNPs drop-wisely onto siRNA solution (4.0 nmol, 0.5 mL pure water).
10. Incubate the reaction solution in the dark for 30 min with gentle shaking.
11. Wash particles three times with pure water (repeat **steps 3–8**).
12. Repeat the deposition procedures to have total 5 layers of polyelectrolytes (3 layers of PLL and 2 layers of siRNA) (Fig. 1).
13. Measure sizes and zeta potentials of bare and multilayered AuNPs in pure water by Zetasizer Nano-ZS (Malvern, Worcestershire, UK) according to the manufacturer's instruction (*see* **Note 8**).

3.2 Live Cell Imaging for Cellular Uptake of sRAuNPs

1. Seed MDA-MB231-luc2 cells on a 96-well black clear bottom culture plate (Corning Life Sciences, Pittston, PA) at a density of 5.0×10^3 cells per well.
2. Incubate cells for 1 day at 37 °C incubator.
3. Replace the culture medium with sR1P (Ba-cy5), sR1P (Na-cy3) or sR2P (Ba-cy5 + Na-cy3) AuNPs (1.58×10^8 particles) containing medium.
4. Incubate cells for 1 day at 37 °C incubator.
5. Wash cells twice with phosphate buffered saline (PBS) and culture them in the phenol red-free DMEM medium (Mediatech).
6. Image cells with a fluorescence microscopy system (Olympus) with various filters such as cy3 and cy5 (Fig. 2).

3.3 In Vitro Gene Silencing Effect

1. Seed MDA-MB231-luc2 cells in a 96-well black clear bottom culture plate at a density of 5×10^3 cells per well.
2. Incubate cells for 1 day at 37 °C incubator.
3. Treat cells with sRAuNP (1.58×10^8 particles) or Lipofectamine 2000.
4. Culture cells for 48 h at 37 °C incubator (*see* **Note 9**).
5. Replace each well with fresh medium.

6. Add 125 μg/mL of D-Luciferin (12.5 μL of 1 mg/mL in 100 μL of medium) and measure bioluminescence using IVIS-200 (Caliper).

3.4 In Vivo Gene Silencing Effect

1. Seed MDA-MB231-luc2 cells in a 6-well culture plate (BD Falcon) at a density of 2.0×10^5 cells per well.
2. Incubate cells for 1 day at 37 °C incubator.
3. Treat cells with sR2P (Ba + Na) (1.58×10^9 particles).
4. Culture cells for 48 h at 37 °C incubator (*see* **Note 10**).
5. Collect sRAuNPs treated or nontreated MDA-MB231-luc2 cells by trypsinization and count cells of each group (*see* **Note 11**).
6. Implant bilaterally (3.5×10^6 cells in 200 μL of PBS including 50 μL of Matrigel) via subcutaneous in the posterior flanks of mice (*see* **Note 12**).
7. Measure bioluminescence of tumor-bearing mice using IVIS-200 (Caliper) immediately after injecting 2 mg (in 150 μL of PBS) of d-Luciferin (Regis) per mouse (*see* **Note 13**).
8. Continue imaging mice until 20 days after cell implantation (Fig. 3).

4 Notes

1. 20 mL of AuNPs from BB International contains 9.0×10^{10} particles.
2. PLL is dissolved with ultrapure water and stored with the concentration of 5 mg/mL at −20 °C.
3. All siRNAs are ordered as the yield of 50 OD (250 nmol) with HPLC purification and stored with the concentration of 100 μM at −80 °C.
4. Human prostate cancer cell line stably expressing firefly luciferase (LNCaP-luc2) were tested separately and showed similar results with MDA-MB231-luc2 cells [18]. LNCaP-luc2 cells (Caliper) are maintained as the same conditions with MDA-MB231-luc2 except cultured in RPMI 1640 medium (Thermo Scientific, Rockford, IL).
5. All animal studies were performed in compliance with the approved animal protocols and guidelines of Institutional Animal Care and Use Committee at the Methodist Hospital Research Institute.
6. For the optimal result in formulating tumor, growth factor reduced and phenol red-free matrigel is used.

7. The number of gold nanoparticles (AuNPs) from BB International is 4.5×10^9 particles/mL, thus the number of prepared AuNPs in 0.7 mL is 3.15×10^9.
8. The nanoparticle solution, if not in use, should be best stored at 4 °C.
9. When transfect cells with Lipofectamine 20000, due to toxicity issue, replace fresh complete medium after incubation with Lipofectamine 2000 for 4 h, and further culture for additional 44 h. No significant toxicity was detected in any sRAuNPs-treated MDA-MB231-luc2 or LNCaP-luc2 cells [18].
10. Fresh complete medium is replaced after incubation with sR2P (Ba + Na) for 24 h, and further cultured for additional 24 h.
11. Nontreated MDA-MB231-luc2 cells (control) are implanted on the left flank and sR2P (Ba + Na) treated MDA-MB231-luc2 cells are implanted on the right flank of each mouse.
12. For the optimization of cell growth, 5–6 week old female BALB/c Nu/Nu mice are used and *n* number of mice is three.
13. Bioluminescence imaging of tumor-bearing mice should be done no later than 5 min after intraperitoneal injection of D-luciferin to maintain same condition at all indicated time points among each mouse.

Acknowledgement

This study was supported in part by NIH CA135312 and DOD W81XWH-11-1-0442.

References

1. Elbashir SM, Harborth J, Lendeckel W, Yalcin A, Weber K, Tuschl T (2001) Duplexes of 21-nucleotide RNAs mediate RNA interference in cultured mammalian cells. Nature 411:494–498
2. Qin XF, An DS, Chen IS, Baltimore D (2003) Inhibiting HIV-1 infection in human T cells by lentiviral-mediated delivery of small interfering RNA against CCR5. Proc Natl Acad Sci U S A 100:183–188
3. Lee MY, Park SJ, Park K, Kim KS, Lee H, Hahn SK (2011) Target-specific gene silencing of layer-by-layer assembled gold-cysteamine/siRNA/PEI/HA nanocomplex. ACS Nano 5:6138–6147
4. Guo X, Huang L (2012) Recent advances in nonviral vectors for gene delivery. Acc Chem Res 45:971–979
5. Castanotto D, Rossi JJ (2009) The promises and pitfalls of RNA-interference-based therapeutics. Nature 457:426–433
6. Davis ME, Zuckerman JE, Choi CH, Seligson D, Tolcher A, Alabi CA et al (2010) Evidence of RNAi in humans from systemically administered siRNA via targeted nanoparticles. Nature 464:1067–1070
7. Zou S, Scarfo K, Nantz MH, Hecker JG (2010) Lipid-mediated delivery of RNA is more efficient than delivery of DNA in non-dividing cells. Int J Pharm 389:232–243
8. Boussif O, Lezoualc'h F, Zanta MA, Mergny MD, Scherman D, Demeneix B et al (1995) A versatile vector for gene and oligonucleotide transfer into cells in culture and in vivo: polyethylenimine. Proc Natl Acad Sci U S A 92:7297–7301

9. Kim HJ, Ishii A, Miyata K, Lee Y, Wu S, Oba M et al (2010) Introduction of stearoyl moieties into a biocompatible cationic polyaspartamide derivative, PAsp(DET), with endosomal escaping function for enhanced siRNA-mediated gene knockdown. J Control Release 145:141–148
10. Alvarez-Erviti L, Seow Y, Yin H, Betts C, Lakhal S, Wood MJ (2011) Delivery of siRNA to the mouse brain by systemic injection of targeted exosomes. Nat Biotechnol 29:341–345
11. Tanaka T, Mangala LS, Vivas-Mejia PE, Nieves-Alicea R, Mann AP, Mora E et al (2010) Sustained small interfering RNA delivery by mesoporous silicon particles. Cancer Res 70:3687–3696
12. Merritt WM, Lin YG, Spannuth WA, Fletcher MS, Kamat AA, Han LY et al (2008) Effect of interleukin-8 gene silencing with liposome-encapsulated small interfering RNA on ovarian cancer cell growth. J Natl Cancer Inst 100:359–372
13. Peyratout CS, Dahne L (2004) Tailor-made polyelectrolyte microcapsules: from multilayers to smart containers. Angew Chem Int Ed Engl 43:3762–3783
14. Jewell CM, Lynn DM (2008) Multilayered polyelectrolyte assemblies as platforms for the delivery of DNA and other nucleic acid-based therapeutics. Adv Drug Deliv Rev 60:979–999
15. Reum N, Fink-Straube C, Klein T, Hartmann RW, Lehr CM, Schneider M (2010) Multilayer coating of gold nanoparticles with drug-polymer coadsorbates. Langmuir 26:16901–16908
16. Chanana M, Gliozzi A, Diaspro A, Chodnevskaja I, Huewel S, Moskalenko V et al (2005) Interaction of polyelectrolytes and their composites with living cells. Nano Lett 5:2605–2612
17. Lee SK, Han MS, Asokan S, Tung CH (2011) Effective gene silencing by multilayered siRNA-coated gold nanoparticles. Small 7:364–370
18. Lee SK, Tung CH (2013) A fabricated siRNA nanoparticle for ultra-long gene silencing. Adv Funct Mater 23:3488–3493
19. Lee SK, Han MS, Tung CH (2012) Layered nanoprobe for long-lasting fluorescent cell label. Small 8:3315–3320
20. Lee SK, Mortensen LJ, Lin CP, Tung CH (2014) An authentic imaging probe to track cell fate from beginning to end. Nat Commun 5:5216
21. Chang K, Elledge SJ, Hannon GJ (2006) Lessons from Nature: microRNA-based shRNA libraries. Nat Methods 3:707–714

Chapter 10

Sensing miRNA: Signal Amplification by Cognate RISC for Intracellular Detection of miRNA in Live Cells

Amol Kavishwar and Zdravka Medarova

Abstract

The ability to detect miRNA expression in live cells would leave these cells available for further manipulation or culture. Here, we describe the design of a miRNA sensor oligonucleotide whose sequence mimics the target mRNA. The sensor has a fluorescent label on one end of the oligo and a quencher on the other. When inside the cell, the sensor is recognized by its cognate miRNA-RISC and gets cleaved, setting the fluorophore free from its quencher. This results in fluorescence "turn on." Since cleavage by the RISC complex is an enzymatic process, the described approach has a very high level of sensitivity (nM). The rate of nonspecific cleavage of the sensor is very slow permitting the collection of meaningful signal over a long period of time.

Key words miRNA, Sensor, RISC, Intracellular detection, Fluorescence, Turn on, Live cells

1 Introduction

miRNAs are powerful regulators of gene expression [1]. They function by guiding a multienzyme complex, named the RNA-induced silencing complex (RISC), to their cognate mRNA transcripts. This primes the mRNA for cleavage and degradation or translational repression, depending on the level of complementarity between the miRNA and the mRNA [2, 3]. In this work, we focus on microRNA-10b (MIR10B) because of its proven role in metastasis [4]. Chemically, the sensor represents a single-stranded RNA with a Cy5 dye molecule covalently linked to its 5′ end and an Iowa Black RQ quencher to the 3′ end [5]. Iowa Black RQ is an efficient quencher of Cy5. Thus, the sensor molecule, by itself, has very low background fluorescence. The sequence of the sensor is completely complementary to the sequence of miRNA-10b. Once inside the cell, the sensor is recognized by the MIR-10b-RISC complex and is cleaved, releasing Cy5 from its quencher.

Zdravka Medarova (ed.), *RNA Imaging: Methods and Protocols*, Methods in Molecular Biology, vol. 1372,
DOI 10.1007/978-1-4939-3148-4_10,

This results in fluorescence "turn on" that can be detected by fluorescence readers, FACS machines and confocal microscopes. Potentially, the cells detected in this manner can be sorted out for further studies. Since the sensor is chemically similar to the native mRNA and uses the same pathways of degradation as mRNA, it is expected that the sensor will not affect cell phenotype.

2 Materials

All media and solutions were prepared in DNase- and RNase-free water, aliquoted, and stored frozen. Handling was minimized to reduce contamination with RNases. Thawing was done on ice to prevent degradation. Certified DNase- and RNase-free pipette tips, tissue culture flasks and multiwell plates were used throughout this study.

1. Sensor oligo: The oligo is a single-stranded RNA whose sequence is complementary to miR10b. On its 5′ end, it is conjugated to Cy5 (fluorophore). On its 3′ end, it is conjugated to Iowa black RQ (quencher). No other chemical modification is introduced, as it might affect the cleavability of sensor. The construct was custom synthesized by Integrated DNA Technologies (Coralville, IA). The sequence of the final construct is: 5′Cy5/rCrArCrArArArUrUrCrGrGrUrUrCrUrArCrArGrGrGrUrA/IAbRQSp-3′.
2. Predesigned, pre-validated miRCURY LNA™ microRNA inhibitors (antisense oligos, ASO) of MIR10B and scrambled controls were purchased from Exiqon (Woburn, MA). These oligos are made up of locked nucleic acids (LNA) that are chemically stable in a wide variety of biological environments. The antisense oligo designed to block MIR10B-RISC activity is labeled as MIR10B-ASO and its scrambled control is labeled as SCR-ASO.
3. Human breast cancer cell line, MDA-MB-231-luc-D3H2LN: The cell line is known for its metastatic potential in an orthotopic mouse model of breast cancer and was purchased from Caliper Life Sciences (Waltham, MA).
4. Dulbecco's modified Eagles medium: The cell line was maintained in Dulbecco's modified Eagles medium supplemented with heat-inactivated fetal bovine serum (10 % final). Antibiotics (penicillin and streptomycin; 1 % final concentration) were only present during regular culture.
5. Lipofectamine LTX-plus (Invitrogen) and Lipofectamine RNAiMAX (Invitrogen): The sensor incubated with these

reagents did not exhibit any appreciable increase in fluorescence after 24 h of incubation indicating that the reagents at hand were free of nonspecific RNase activity.

6. Prolong gold (Invitrogen) mounting medium containing DAPI and an anti-fade was used to mount cells for fluorescence and confocal microscopy.

3 Methods

3.1 Preparation of Cells

1. Exponentially growing cells were collected by trypsinization and counted using a cell counter.
2. Cell concentration was adjusted to 150,000 cells/ml in DMEM. 200 μl/well were plated in 96-well clear bottom black tissue culture plates. While performing these steps, care must be taken to avoid cell rupture during trypsinization and subsequent cell culture handling steps as this may result in release of RNase activity. Plates were incubated in a CO_2 incubator.
3. After 24 h, all wells were observed under the microscope for any contamination or cell clumps. Over- or under-seeded wells were marked and excluded from the study. Also all wells on the edge of the plate were excluded from the study because of the "edge effect" that leads to uneven evaporation of media from these wells.
4. The media in the 96-well plates was replaced with 100 μl of fresh DMEM without FBS or antibiotics (*see* **Notes 1** and **2**). Care was taken to not dry the cell layer during this step. Two different multichannel pipettes were used. One for removing and one for adding media.
5. Plates were returned to the incubator and allowed to equilibrate for a few hours.

3.2 Transfection of Cells

3.2.1 Premise

Two rounds of transfections will be performed on the same cells. First, the cells will be transfected with a chemically stable (locked nucleic acid) MIR10B-ASO to block the endogenous MIR10B-RISC activity. For control, another set of cells will be transfected with SCR-ASO. After 2–4 h, a second round of transfection will be performed with the sensor oligos. Assuming 100 % efficiency, the MIR10B-ASO treated cells will not be able to bind and degrade the sensor and fluorescence activation will not occur. By contrast, in the control wells, in which the cells are treated with SCR-ASO, the MIR10B will bind and prime the sensor for degradation by the RISC, leading to fluorescence activation.

3.2.2 Transfection with Antisense Oligonucleotide

Transfection with an excess of antisense oligos (3.8 μM final concentration) was performed to ensure complete inhibition of MIR10B-RISC activity.

1. Dilutions of MIR10B-ASO and SCR-ASO were prepared by diluting 5 μl of stock (5 mM) solution into 125 μl of serum-free media.
2. Two sets of dilutions of lipofectamine were prepared by mixing 13 μl of lipofectamine in 120 μl of serum-free media (*see* **Notes 3** and **4**).
3. Next, the ASO and lipofectamine were mixed (final volume 130 + 133 = 263 μl) and allowed to incubate at room temperature for 30 min (*see* **Note 5**).
4. 10 μl of MIR10B-ASO + lipofectamine mix was added to 3 sets of 7 wells (21 wells total). Final concentration of ASO was 3.8 μM.
5. Similarly, SCR-ASO + lipofectamine mix was distributed in another set of 21 culture wells.
6. The culture plate was incubated for 2 h in a CO_2 incubator.

3.2.3 Transfection with Sensor Oligo

1. First, 140 μl of 12 μM sensor solution was prepared by mixing 11.2 μl of sensor stock solution with 110.8 μl of serum-free media and 18 μl of lipofectamine (*see* **Note 6**).
2. Then this solution was serially diluted to get 70 μl each of 12, 6, 3, 1.5, 0.75, and 0.375 μM sensor dilutions.
3. Then, 10 μl of each dilution was added in triplicate to cells pretransfected with either MIR10B-ASO or SCR-ASO. Final concentration of sensor in culture wells was 1000, 500, 250, 125, 62.5, and 31.25 nM.
4. Plates were incubated for 3 h.
5. After incubation, transfection media was replaced with 200 μl of DMEM supplemented with 10 % heat inactivated FBS. No antibiotics were added to this media.
6. After replacing media, fluorescence was immediately recorded on an IVIS-spectrum imaging station with filter sets for Cy5 dye. Wells for 125 nM sensor concentration were shown in Fig. 1a. Note that there is minimal background fluorescence at this time (Fig. 1a).
7. Fluorescence "turn on" was measured by reading the plate at specified time points (Fig. 1a). For this cell line, fluorescence peaked at 16 h after which no appreciable increase in MIR-10B-RISC-mediated fluorescence was observed (Fig. 1b).

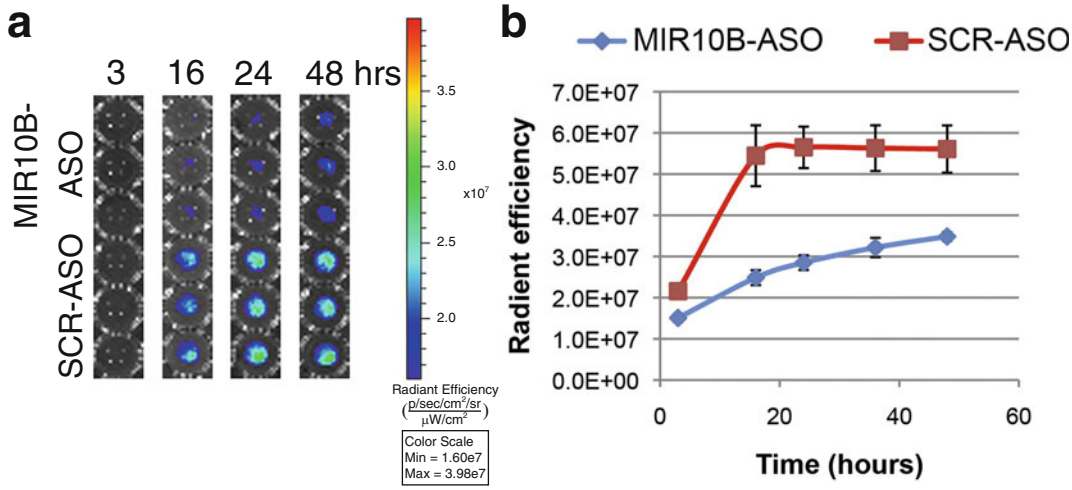

Fig. 1 Sensor activation. (**a**) Sensor activation at a fixed concentration of 150 nM was followed for 48 h on IVIS-spectrum imaging station. Data were recorded using filter sets for Cy5 dye. (**b**) Quantitative analysis of signal observed in Fig. 1a. (This figure is reproduced with permission from Elsevier. Original article appeared in Chemistry & Biology 21, 1–6, February 20, 2014)

8. Nonspecific cleavage of sensor in MIR-10B-ASO-treated cells was slow and even after 48 h of incubation, fluorescence did not reach maximum (Fig. 1b).

3.3 Fluorescence and Confocal Microscopy

1. For fluorescence microscopy, cells were grown in 8-chambered slides.
2. After 24 h of growth, they were transfected with either MIR10B-ASO or SCR-ASO as described above and incubated for 2 h.
3. After 2 h, cells were transfected with a single sensor concentration of 125 nM.
4. After 24 h, cell layers were washed with PBS, fixed in 4 % formaldehyde for 10 min, mounted in mounting medium, and observed under a fluorescence microscope with filter sets for Cy5 (Fig. 2a).

3.4 Flow Cytometry

1. For flow cytometry and sorting, cells were grown in 6-well plates. The concentrations of ASO and sensor were kept constant as described above. Volumes were increased to match the increased area of 6-well plates.
2. After 16–24 h of incubation, cell were collected by trypsinization and kept on ice for sorting or fixed with 4 % formaldehyde for FACS analysis. No further washing steps were performed (Fig. 2b).

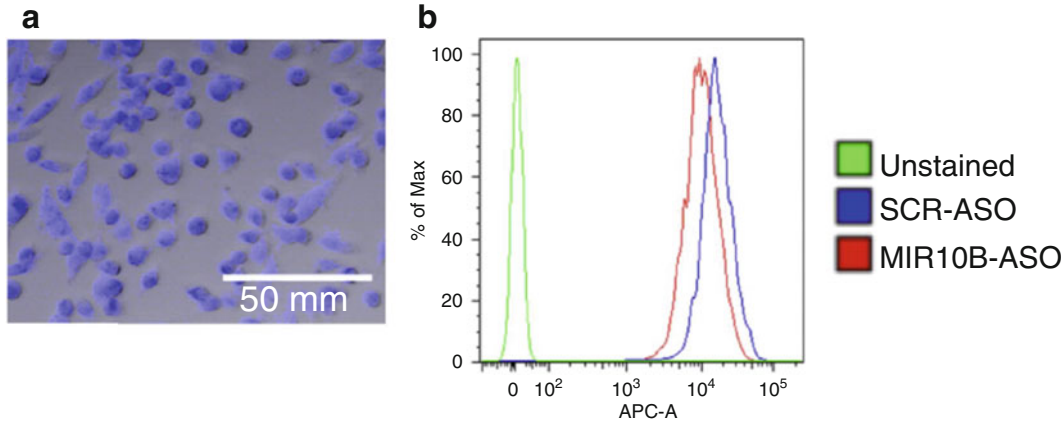

Fig. 2 Sensor activation in live cells. (**a**) MIR10B-RISC activity was first blocked by treatment with MIR10B-ASO and then cells were transfected with the sensor. Fluorescence accumulation due to sensor activation was observed after ~16 h under a confocal microscope. (**b**) Flow cytometry of intact cells. (This figure is reproduced with permission from Elsevier. Original article appeared in Chemistry & Biology 21, 1–6, February 20, 2014)

4 Notes

1. Presence of antibiotics can be detrimental to cell survival during transfection.
2. Removal of FBS during transfection ensures efficient transfection and reduces RNase activity that might be present in FBS. Keep in mind that the sensor being used in subsequent steps of this experiment is an unmodified RNA oligonucleotide. The dye and quencher present on either end do not protect the sensor oligos from nonspecific RNase activity.
3. Lipofectamine is detrimental to cell survival. Amounts tolerated vary from cell line to cell line. Hence, the researcher must have a good idea of the amounts of lipofectamine that will be tolerated by their cell line. We recommend titration of lipofectamine at hand with the cell line to be tested.
4. Ratio of oligos to lipofectamine is important for efficient uptake. Adhere to manufacturer's recommendation.
5. Since in this protocol, two rounds of transfection will be performed on the same cells, the total amount of lipofectamine that is used should be less than the dose that can be easily tolerated by the cells.
6. Once the sensor is removed from the −80 freezer, exposure to bright light must be minimized.

Acknowledgements

This work was supported by grants NCIR00CA129070, NCI-1R01CA163461-01A1 by the NIH and the Young Investigator Award by the Breast Cancer Alliance to Z.M.

References

1. Roberts TC (2014) The MicroRNA biology of the mammalian nucleus. Mol Ther Nucleic Acids 3, e188. doi:10.1038/mtna.2014.40
2. Eulalio A, Huntzinger E, Izaurralde E (2008) Getting to the root of miRNA-mediated gene silencing. Cell 132(1):9–14. doi:10.1016/j.cell.2007.12.024
3. Lewis BP, Shih IH, Jones-Rhoades MW, Bartel DP, Burge CB (2003) Prediction of mammalian microRNA targets. Cell 115(7):787–798
4. Yigit MV, Ghosh SK, Kumar M, Petkova V, Kavishwar A, Moore A, Medarova Z (2013) Context-dependent differences in miR-10b breast oncogenesis can be targeted for the prevention and arrest of lymph node metastasis. Oncogene 32(12):1530–1538. doi:10.1038/onc.2012.173
5. Yoo B, Kavishwar A, Ghosh SK, Barteneva N, Yigit MV, Moore A, Medarova Z (2014) Detection of miRNA expression in intact cells using activatable sensor oligonucleotides. Chem Biol 21(2):199–204. doi:10.1016/j.chembiol.2013.12.007

Chapter 11

Molecular Beacon-Based MicroRNA Imaging During Neurogenesis

Jonghwan Lee and Soonhag Kim

Abstract

The fluorescence monitoring system for examining endogenous microRNA (miRNA) activity in cellular level provides crucial information on not only understanding a critical role of miRNA involving a variety of biological processes, but also evaluating miRNA expression patterns in a noninvasive manner. In this protocol, we report the details of a new procedure for a molecular beacon-based miRNA monitoring system, which includes the illustration scheme for miRNA detection strategy, exogenous miRNA detection, and measurement of endogenous miRNA expression level during neurogenesis. The fluorescence signal of miR-124a beacon quenched by BHQ2 was gradually recovered as increasing concentration of the miR-124a in tube. The functional work of miR-124a beacon was examined in intracellular environment, allowing for the internalization of the miR-124a beacon by lipofectamine, which resulted in activated fluorescent signals of the miR-124a beacon in the HeLa cells after the addition of synthetic miR-124a. The endogenous miR-124a expression level was detected by miR-124a beacon system during neurogenesis, showing brighter fluorescence intensity in cytoplasmic area of P19 cells after induction of neuronal differentiation by retinoic acid. The molecular beacon based-miRNA detection technique could be applicable to the simultaneous visualization of a variety of miRNA expression patterns using different fluorescence dyes. For the study of examining endogenous miRNA expression level using miRNA-beacon system, if cellular differentiation step is already prepared, transfection step of miR-124a beacon into P19 cells, and acquisition of activated fluorescence signal measured by confocal microscope can be conducted approximately within 6 h.

Key words microRNA, Molecular beacon, Imaging, Neurogenesis

1 Introduction

The investigation of the expression levels of endogenous microRNA (miRNA, miR), a single-stranded noncoding RNA molecule responsible for regulating gene expression, has been occupied a vital position for the understanding of a wide range of biological processes such as cellular proliferation and differentiation. Currently, in order to detect the cellular distribution and expression level of intracellular miRNAs, real-time PCR, Northern blot analysis, and fluorescence in situ hybridization (FISH) analysis

Zdravka Medarova (ed.), *RNA Imaging: Methods and Protocols*, Methods in Molecular Biology, vol. 1372,
DOI 10.1007/978-1-4939-3148-4_11,

have been widely used at the cellular level [1–3]. However, these methods require the cell destruction and do not provide time course information of miRNA expression in living organisms [4, 5]. Therefore, the development of the detection method that tracks intracellular miRNAs is required in living cells.

Recently, a 3′ untranslated region (UTR)-based reporter gene imaging system has been successfully developed to monitor the expression patterns of mature miRNAs [6–9]. However, due to the miRNA function that binds to the sequences which are partially or completely complementary to mature miRNAs and that degrades mRNA or inhibits translation, the reporter gene-based miRNA detection system is accompanied with signal off results of reporter gene by interaction of miRNA with 3′ UTR of reporter gene, which it is difficult to distinguish whether the shown signaling-off data results from substantial miRNA expression or only from cell death in vivo. Therefore, a signal-on imaging system is technically demanded to monitor intracellular miRNAs overcoming the shortcoming of the conventional signal-off reporter imaging system.

Molecular beacon is a single-strand hairpin loop-structured probes to be composed of quenching molecule and fluorescence dye at the end of each oligonucleotide. Molecular beacon tools have been recently shown to be a powerful approach to real time visualization of specific endogenous mRNAs and simultaneous monitoring of gene expression in cancer cells [10–14]. Therefore, a molecular beacon strategy might be suitable for the detection of the expression levels of endogenous small molecules in living subjects. The quencher-based molecular beacon system, with an on/off fluorescence signal, is easily controlled by sequence-sequence matching and is well suited for the detection of the expression profiles of endogenous miRNAs.

Here, we describe a standard protocol for the fluorescence imaging detection of miRNA using a signal tunable molecular beacon technique in living cells. We targeted miR-124a known to be specifically and highly expressed in neurons, and its expression profile is well established during neuronal development [6, 7, 15]. In our system shown in Fig. 1, in the absence of miR-124a, the miR-124a beacon forms a hairpin loop structure that quencher and fluorescence dye are located in adjacent region to each other. Therefore, few fluorescence signals are observed. In contrast, the presence of miR-124a makes the quencher molecules separated from the miR-124a beacon, resulting in a bright fluorescence signal (Fig. 1). This miR-124a beacon system represented the enhanced fluorescence intensity after induction of exogenous miR-124a. Also, miR-124a beacon system exhibited stronger fluorescence signal after progression of neuronal development in P19 cells, which is capable of measuring endogenous miR-124a expression level in living cells.

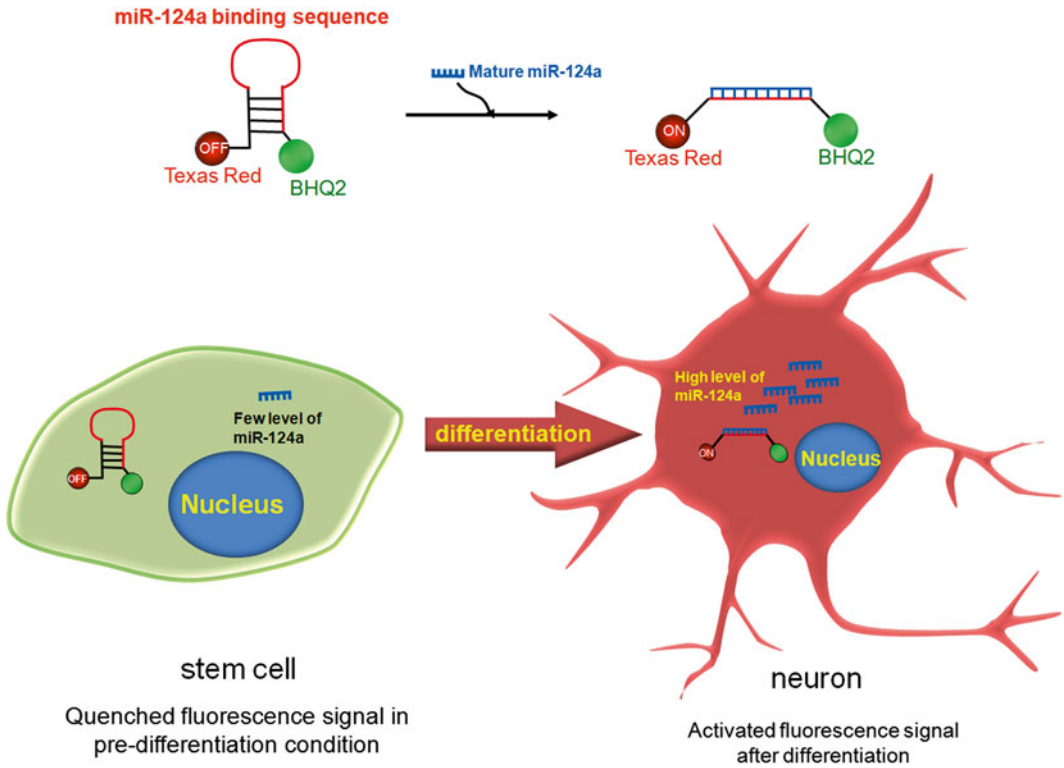

Fig. 1 A schematic diagram of the step for miR-124a beacon. The single-stranded hairpin loop oligonucleotide miR-124a beacon consisting of Texas Red fluorescence dye (emission wavelength 617 nm) attached at the 5′ end and quenching molecule at the 3′ end was designed to target mature miR-124a, partial miR-124a-binding sequences were contained in both hairpin loop and partial stem section of full molecular beacon sequence, which was designated as the miR-124a beacon. When the mature miR-124a is hybridized with the miR-124a-binding region in the miR-124a beacon, the quencher molecules and the Texas Red were separated from each other, resulting in an increase in the fluorescence signal. In the undifferentiated stem cell condition, weak fluorescence signal quenched by quenching molecule in miR-124a beacon will be observed due to few expression of miR-124a. When stem cells are differentiated into neuron, a large amount of produced miR-124a will make quenched fluorescence signal in miR-124a beacon activated

Figure 2 shows a flowchart of this protocol. This miR-124a beacon strategy could provide valuable information by monitoring endogenous miR-124a expression during neurogenesis. Furthermore, we expect that the miRNA beacon strategy could be applied to high throughput imaging system for the molecular network of cellular developments and diseases by simultaneously monitoring a variety of endogenous miRNAs using multiple fluorescence-based molecular beacon system in living subjects.

2 Materials

Use analytical grade reagents and ultrapure water (18 MΩ dH_2O) when preparing all solutions. All reagents should be stored at –20 °C, unless otherwise stated.

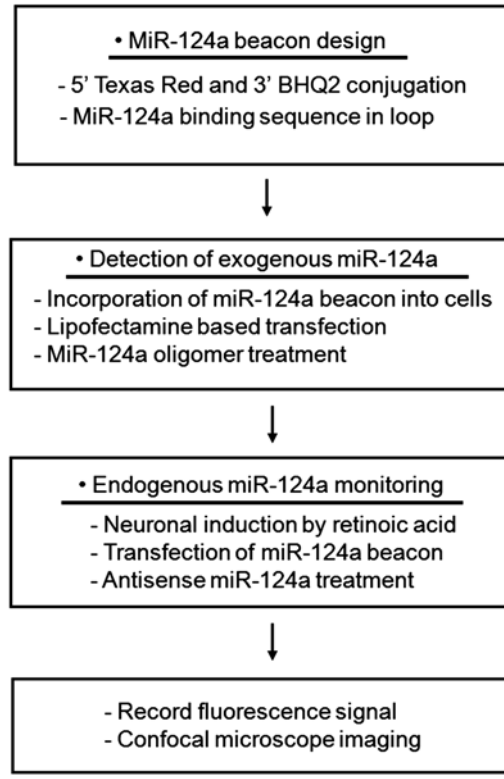

Fig. 2 Flow diagram of whole protocols

2.1 Design and Fluorescence Recovery Test of miR-124a

1. MiR-124a beacon: Texas Red-5′ ATTCCGTGCGCCAC TTACGGGGAAT 3′-BHQ2 (Bioneer).
2. MiR-124a (phosphorothioate-modified, Bioneer).
3. Phosphate-buffered saline (PBS). Store at 4 °C.
4. Fluorescence imager.

2.2 Fluorescence Activation of miR-124a Beacon

1. HeLa cells (human cervical cancer cell line, KCLB).
2. Dulbecco's modified Eagle medium (DMEM). Store at 4 °C.
3. Fetal bovine serum (FBS).
4. Penicillin/Streptomycin solution. Store at 4 °C.
5. Culture medium: DMEM supplemented with 10 % FBS and 1 % penicillin/streptomycin solution. Store at 4 °C.
6. Antisense miR-124a (phosphorothioate-modified, Bioneer).
7. RIPA (Radio-immunoprecipitation assay) buffer.
8. Lipofectamine and Plus reagent. Store at 4 °C.
9. Opti-MEM medium. Store at 4 °C.
10. BCA Protein Assay kit.
11. 96-Well black microplate.

12. Bio Tek Fluorescent Microplate Fluorometer (Synergy Mx, BioTeck Ltd, VT).
13. Cell culture incubator (operated at 5 % CO_2 and 37 °C).

2.3 Detection of Endogenous miR-124a Expression Level

1. P19 cells (mouse embryonic carcinoma cell line, ATCC no. CRT-1825) (*see* **Notes 1** and **2**).
2. All-trans-retinoic acid (RA, 0.5 μM in absolute ethanol) (*see* **Note 3**).
3. Bovine calf serum (BCS). Store at 4 °C.
4. Minimal essential medium alpha (MEM-α). Store at 4 °C.
5. DMEM/F12 1:1 medium. Store at 4 °C.
6. Antibiotic-antimycotic solution (AA). Store at 4 °C.
7. Insulin-transferrin-selenium supplement (ITS, 100×). Store at 4 °C.
8. Culture medium: MEM-α supplemented with 7.5 % BCS, 2.5 % FBS, and 1 % AA solution. Store at 4 °C.
9. Neuronal differentiation medium: DMEM/F12 1:1 medium supplemented with 1 % ITS solution and 0.5 μM RA. Store at 4 °C.
10. 3.7 % formaldehyde solution in PBS. Store at 4 °C.
11. Mounting reagent containing 4′,6-diamidino-2-phenylindole dihydrochloride (DAPI) (*see* **Note 4**).
12. Gelatin.
13. Glass cover slip.
14. Trypan blue.
15. Hemocytometer.
16. Confocal microscopy with a laser scanning microscope.

3 Methods

3.1 Fluorescence Recovery Test of miR-124a Beacon in Tube

Hairpin loop-based molecular beacon was designed to enable the detection of miR-124a. Spectrally paired fluorescence dye and quencher were composed of Texas Red fluorescence dye (ex; 598 nm/em; 617 nm) at the 5′ end, and BHQ2 (black hole quencher) at the 3′ end that absorption spectra of which is around 600 nm wavelength. MiR-124a binding sequence in miR-124a beacon was partially contained in stem section to reduce a total beacon size.

1. Treat 200 pmol miR-124a beacon (labeled with Texas Red at the 5′ end, and labeled with BHQ2 at the 3′ end) into the Eppendorf tube containing 100 μl PBS.
2. Add the different amount of synthetic miR-124a oligomer (0.1, 0.5, 1 nmol) to the pretreated reaction sample in tube.

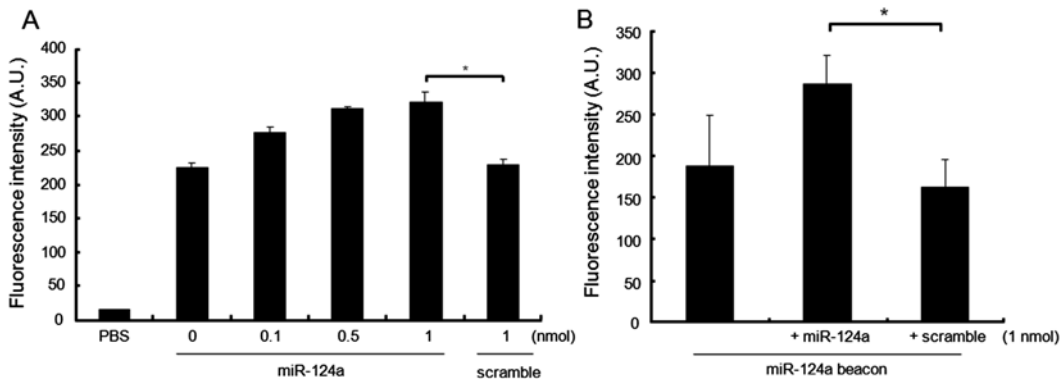

Fig. 3 (**a**) The fluorescence recovery effect of the miR-124a beacon after treatment of the synthetic mature miR-124a in the tube. The miR-124a beacon was treated with a synthetic oligomer of the mature miR-124a dose-dependently (0.1, 0.5, 1 nmol) or a scramble (1 nmol) for 1 h at RT. The quenched fluorescence intensity was gradually activated in the presence of the mature miR-124a. However, no fluorescence recovery was observed in the scramble-treated miR-124a beacon group (*$P < 0.05$). (**b**) The activation of fluorescence intensity of the miR-124a beacon in HeLa cells. The miR-124a beacon containing the miR-124 binding sequence and synthetic miR-124a modified with phosphorothioate (or scramble miRNA) was transfected into miR-124a-negative HeLa cells using lipofection method. The fluorescence signal from the quenched fluorescence dye in miR-124a beacon inside of HeLa cells was activated in the mature miR-124a-treated group (1 nmol), compared to the fluorescence intensity of the scramble-treated group (1 nmol) (*$P < 0.05$)

3. Incubate the mixture sample for 1 h at 25 °C.
4. Transfer the mixture sample to 96-well black microplate (*see* **Note 5**).
5. Measure the fluorescence signal of each mixture sample using microplate fluorometer (Fig. 3a).

3.2 Functional Action of miR-124a Beacon by Induction of Exogenous miR-124a in HeLa Cells

Because the designed miR-124a beacon is composed of oligonucleotide-based sequence, simple internalization protocol by lipofection method was conducted. MiR-124a beacon and synthetic miR-124a oligomer were transfected into cells with distinct time point, respectively to exclude the possibility that miR-124a oligomer might be pre-bound to miR-124a beacon due to existence of miR-124a oligomer and miR-124a beacon together in the same tube space. 2 h after pre-transfection of miR-124a beacon was performed in HeLa cells which are miR-124a-negative cell line, the lipofectamine-coated synthetic miR-124a oligomers are internalized into pre-transfected HeLa cells. Before transfection of miR-124a oligomer, several washing step using PBS should be performed to avoid the attachment of miR-124a oligomer with the retained miR-124a beacon in supernatant solution. To detach the cells from culture dish, RIPA buffer was used for protein normalization. The harvested cells are transferred into 96-well black plate for the acquisition of fluorescence signals.

1. One day prior to transfection of miR-124a beacon, incubate 1×10^5HeLa cells in the 12-well plate at 37 °C for overnight.

2. Transfect miR-124a beacon (0.5 nmol) first into the seeded HeLa cells through lipofectamine-based transfection method. Briefly, dilute the miR-124a beacon and Plus reagent (4 μl) into 35 μl serum-free OptiMEM medium and incubate at room temperature for 15 min after mixing gently. Transfer the miR-124a beacon and Plus reagent mixture into other mixture sample containing the Lipofectamine (1 μl) with OptiMEM solution and incubate for 20 min. During formation of liposome-DNA complexes, wash the prepared HeLa cells in the 12-well plates using PBS solution. Add 200 μl OptiMEM solution in each well. Transfect 70 μl mixture evenly into each well plate, and maintain the well plate for 3 h at 37 °C. All transfections were conducted in triplicate (*see* **Note 6**).
3. Prepare for the liposome-coated synthetic mature miR-124a oligomer (or miR-124a mutant, 1 nmol) by mixing phosphorothioate-modified miR-124a with lipofectamine reagent, one and half hour after transfection of miR-124a beacon. In brief, dilute miR-124a oligomer (or miR-124a mutant oligomer) with 4 μl Plus reagent and 35 μl serum-free OptiMEM medium. Mix gently and incubate for 15 min at room temperature. Transfer each mixture into other mixtures containing 1 μl Lipofectamine and OptiMEM medium and incubate for 20 min (*see* **Note 7**).
4. 2 h after transfection of miR-124a beacon, rinse the first transfected HeLa cells with PBS one time. Add 200 μl of OptiMEM medium in washed cell plate.
5. Transfect the prepared miR-124a oligomer into the HeLa cells, and incubate for 2 h at 37 °C.
6. Add serum-containing medium into the well plate, and incubate for 1 h at 37 °C more (*see* **Note 8**).
7. Wash the treated samples with PBS twice.
8. In order to measure the quantitative fluorescence signal, treat RIPA buffer and collect the lysates after verifying totally detached cells by bright field microscopy.
9. Measure the fluorescence intensities of each well using a microplate fluorometer (Fig. 3b).
10. Quantify the total protein of lysates for normalization study using BCA Protein Assay kit.

3.3 Detection of miR-124a Expression Level during Neuronal Differentiation in P19 Cells

To monitor the expression dynamics of the intracellular miRNA as progression of neuronal differentiation, P19 cells, embryonal teratocarcinoma cells that have easy differentiation procedure and that miRNA expression profile is well documented were chosen in this protocol. Many previous researches represented that P19 cells showed gradual increase expression pattern of miR-124a after treatment with retinoic acid (RA) to induce neuronal differentiation [16, 17].

1. For the preparation of neuronal differentiation study, plate 0.5×10^5P19 cells in 6-well plate after 6-well cover slip is placed on the each well plate (*see* **Note 9**).
2. To induce neuronal differentiation, prepare differentiation DMEM/F12 medium containing 1 % ITS solution and 0.5 μM RA. For the differentiation sample, rinse the seeded P19 cells using PBS twice, and add the prepared differentiation medium to cells. Change the old medium to new differentiation medium every 2 days.
3. Transfect the undifferentiated or differentiated P19 cells with miR-124a beacon under lipofectamine based transfection method.
4. In the case of antisense-miR-124a study, after induction of neuronal differentiation, 0.5 nmol miR-124a beacon and the 1 nmol antisense-miR-124a modified with phosphorothioate was co-transfected into P19 cells.
5. After transfection of miR-124a beacon, maintain P19 cells on transfected OptiMEM condition for 3 h, and add complete cell medium by incubating for 1 h more.
6. To acquire the confocal microscope image in P19 cells, aspirate the cell cultured medium and wash cells using PBS solution twice. Fix washed cells using 3.7 % formaldehyde solution by adding 1 ml of formaldehyde into each 6-well plate. Incubate fixed cells in mild shaking condition for 20 min at RT. Wash the cells using PBS each 10 min twice. Treat mounting reagent containing 4′,6-diamidino-2-phenylindole dihydrochloride (DAPI) solution onto slide glass, and place the cover slips from the 6-well plates onto a slide glass, followed by fixation of cover slip on slide glass using manicure-like substance (Fig. 4).

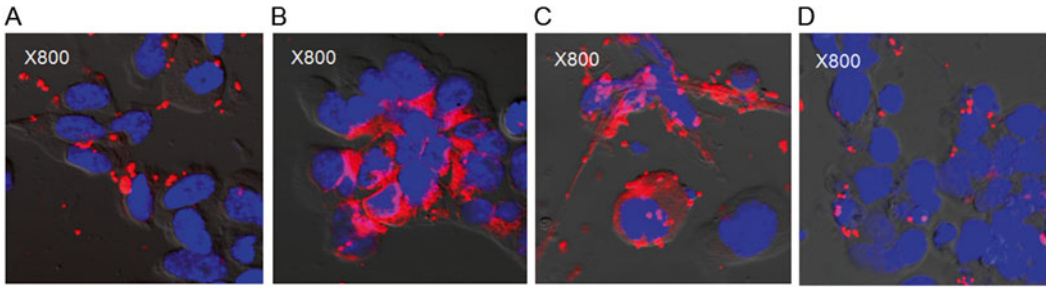

Fig. 4 The visualization of fluorescence recovery of the miR-124a beacon to detect endogenous miR-124a during neurogenesis. With making P19 cells induced into neuronal differentiation by 0.5 μM RA, miR-124a beacon was treated into both undifferentiated and differentiated P19 cells. Compared to fluorescence signal in undifferentiated P19 cells (**a**), activated fluorescence signal of miR-124a beacon was detected in cytoplasmic area of P19 cells 2 days (**b**) or 4 days (**c**) after the induction of neuronal differentiation by RA. Treatment of antisense miR-124a oligomer revealed that activated fluorescence signal was endogenous miR-124a specific (**d**), showing that quenched fluorescence signal was maintained by treatment of exogenous antisense miR-124a

4 Notes

1. Before P19 cells were seeded into proper well plate, the bottom of well plate should be coated with 0.1 % gelatin, followed by several rinsing step using PBS.
2. Growth medium can be prepared as follows: α-MEM supplemented with 7.5 % (v/v) BS, 2.5 % (v/v) FBS and 1 % (v/v) AA (10 U/ml penicillin, and 10 μg/ml streptomycin, which is stable for <3 month at a 5 % CO_2-humidified chamber at 37 °C). Next, 0.5×10^5P19 cells were seeded into a 6-well plate, and maintained in a 5 % CO_2-humidified chamber for 18 h before performing the designed experiments.Neuronal differentiation medium can be also prepared as follows [18]; DMEM/F12 medium supplemented with 1 % (v/v) ITS, 1 % (v/v) AA, and 0.5 μM RA (stored at 4 °C).
3. RA should be protected from light. To minimize light exposure, RA should be stored at −20 °C in aluminum foil-wrapped tube. Aliquot aluminum foil-wrapped RA into individual tubes.
4. Avoid light exposure and store at 4 °C.
5. Avoid the mixture sample to the light exposure for a long duration.
6. Because the co-transfection of miR-124a beacon with synthetic mature miR-124a might cause the unexpected functional reaction of miR-124a beacon with synthetic miRNA in the same solution space, transfect miR-124a beacon first, and then synthetic miR-124a oligomer in order.
7. To make synthetic miR-124a more stable inside of cells, phosphorothioate chemical modification is essential for cell study.
8. To put miR-124a beacon with minimal light exposure after transfection of fluorescence-labeled miR-124a beacon, wrap the well plate using aluminum foil during incubation.
9. It is important to note that P19 cells should be maintained at proper passage number and at optimal confluence for a successful cell growth. Excessive passage number can make self-renewal P19 cells more progressed to neuronal lineage. P19 cell passage should be conducted at 70–80 % confluency. Appropriate cell plating number is very important for the comparison study between undifferentiated and differentiated P19 group. Too much cell seeding number is unsuitable for differentiation study until 4 days, and also a low-amount cell plating number might influence on cell growth with less cell-to-cell interaction.

Acknowledgement

This work was supported by the Bio & Medical Technology Development Program of the National Research Foundation (NRF) funded by the Korean government (MEST) (No. 2013R1A2A2A01068140), the Next-Generation BioGreen 21 program (#PJ010002), Rural Development Administration and a grant of the Korean Health Technology R&D Project, Ministry of Health and Welfare (HI14C3297), and the Visiting Professor Program (VPP) at King Saud University, Kingdom of Saudi Arabia.

References

1. Silahtaroglu AN, Nolting D, Dyrskjøt L et al (2007) Detection of microRNAs in frozen tissue sections by fluorescence in situ hybridization using locked nucleic acid probes and tyramide signal amplification. Nat Protoc 2:2520–2528
2. Krichevsky AM, Sonntag KC, Isacson O et al (2006) Specific microRNAs modulate embryonic stem cell-derived neurogenesis. Stem Cells 24:857–864
3. Várallyay E, Burgyán J, Havelda Z (2008) MicroRNA detection by northern blotting using locked nucleic acid probes. Nat Protoc 3:190–196
4. Sempere LF, Freemantle S, Pitha-Rowe I et al (2006) Expression profiling of mammalian microRNAs uncovers a subset of brain-expressed microRNAs with possible roles in murine and human neuronal differentiation. Genome Biol 5:R13.1–13.11
5. Suh MR, Lee Y, Kim JY et al (2004) Human embryonic stem cells express a unique set of microRNAs. Dev Biol 15:488–498
6. Lee JY, Kim S, Hwang do W et al (2008) Development of a dual-luciferase reporter system for in vivo visualization of MicroRNA biogenesis and posttranscriptional regulation. J Nucl Med 49:285–294
7. Ko MH, Kim S, Hwang do W et al (2008) Bioimaging of the unbalanced expression of microRNA9 and microRNA9* during the neuronal differentiation of P19 cells. FEBS J 275:2605–2616
8. Kim HJ, Kim YH, Lee DS et al (2008) In vivo imaging of functional targeting of miR-221 in papillary thyroid carcinoma. J Nucl Med 49:1686–1693
9. Ko HY, Hwang do W, Lee DS et al (2009) A reporter gene imaging system for monitoring microRNA biogenesis. Nat Protoc 4:1663–1669
10. Peng XH, Cao ZH, Xia JT et al (2005) Real-time detection of gene expression in cancer cells using molecular beacon imaging: new strategies for cancer research. Cancer Res 65:1909–1917
11. Nitin N, Santangelo PJ, Kim G (2004) Peptide-linked molecular beacons for efficient delivery and rapid mRNA detection in living cells. Nucleic Acids Res 32:e58.1–e58.9
12. Narita A, Ogawa K, Sando S et al (2007) Cis-regulatory hairpin-shaped mRNA encoding a reporter protein: catalytic sensing of nucleic acid sequence at single nucleotide resolution. Nat Protoc 2:1105–1116
13. Mhlanga MM, Tyagi S (2006) Using tRNA-linked molecular beacons to image cytoplasmic mRNAs in live cells. Nat Protoc 1:1392–1398
14. Kim JK, Choi KJ, Lee M et al (2012) Molecular imaging of a cancer-targeting theragnostics probe using a nucleolin aptamer- and microRNA-221 molecular beacon-conjugated nanoparticle. Biomaterials 33:207–217
15. Hwang DW, Song IC, Lee DS et al (2010) Smart magnetic fluorescent nanoparticle imaging probes to monitor microRNAs. Small 6:81–88
16. Smirnova L, Gräfe A, Seiler A et al (2005) Regulation of miRNA expression during neural cell specification. Eur J Neurosci 21:1469–1477
17. Noh EY, Ko HY, Lee CH et al (2013) Carbon nanodot-based self-delivering microRNAs sensor to visualize microRNA124a expression during neurogenesis. J Mater Chem B 1:4438–4445
18. Huang B, Li W, Zhao B et al (2009) MicroRNA expression profiling during neural differentiation of mouse embryonic carcinoma P19 cells. Acta Biochim Biophys Sin 41:231–236

Chapter 12

Hypoxia-Responsive Copolymer for siRNA Delivery

Federico Perche, Swati Biswas, Niravkumar R. Patel, and Vladimir P. Torchilin

Abstract

A wide variety of nanomedicine has been designed for cancer therapy. Herein, we describe the synthesis and evaluation of a hypoxia-responsive copolymer for siRNA delivery (Perche et al., Angew Chem Int Ed Engl 53:3362–3366, 2014). The synthesis is achieved using established coupling chemistry and accessible purification procedures. A polyelectrolyte-lipid conjugate (polyethyleneimine 1.8 kDa-dioleyl-phosphatidylinositol, PEI-PE) and polyethylene glycol 2000 (PEG) were assembled via the hypoxia-sensitive azobenzene (Azo) unit to obtain the PEG-Azo-PEI-DOPE copolymer. This copolymer can condense siRNA and shows hypoxia-induced cellular internalization and reporter gene downregulation in vitro and tumor accumulation in vivo after parenteral administration (Perche et al., Angew Chem Int Ed Engl 53:3362–3366, 2014). We also detail procedures to evaluate hypoxia-targeted polymers both in monolayer cultures, cancer cell spheroids and in tumor xenografts murine models.

Key words siRNA delivery, Tumor hypoxia, Tumor targeting, Stimuli-sensitive, Azobenzene

1 Introduction

Self-assembled nanoparticles represent a promising class of drug delivery systems (DDS) for cancer therapy [1–6]. However, as most drug delivery systems, pharmaceutical polymers show limited (less than 10 % of administered dose) distribution to the tumor site and moderate increase in survival over conventional therapy, and cancer treatment remains an unmet challenge [7–13].

Administration of inactive assemblies has been proposed as a further step to increase dosage of therapeutic agent for enhanced therapeutic activity, with specific and localized conversion of the DDS to an active anticancer drug at the tumor site by physiological tumor stimuli [1, 14–20]. Physiopathological traits shared by most tumors such as acidosis, hypoxia, overexpressed proteases are employed as the stimuli [14]. In this chapter we focus on the preparation of a hypoxia-responsive polymer and its use for tumor targeting.

Zdravka Medarova (ed.), *RNA Imaging: Methods and Protocols*, Methods in Molecular Biology, vol. 1372,
DOI 10.1007/978-1-4939-3148-4_12,

We developed PEG-Azo-PEI-DOPE/siRNA nanoparticles which possess several features (Fig. 1). First, the PEI-DOPE conjugate is capable of siRNA condensation, protection against nucleases and endosomal escape [21–25]. Second, the hydrated PEG corona provides stability in the physiological fluids and assures specific internalization of the siRNA. Third, PEG and PEI-DOPE are connected via an azobenzene linker, a unit used in hypoxia-based cancer imaging applications [26–28].

Azobenzene is a nitroimidazole derivative (R-N=N-R′), subject to oxygen-dependent destabilization by successive reductions leading to cleavage of the unit [26–28]. The first reduction reaction (formation of the nitroanion radical) imparts hypoxia specificity as it is reversed by molecular oxygen, while reduction proceeds to cleavage or hypoxia-induced adducts formation under hypoxic conditions, with the established hypoxia probe Hydroxyprobe® as a representative [28]. Decrease in the oxygen levels causes increase in reductive stress. In brief, azobenzene derivatives are reduced to aromatic amine derivatives by reductases. In the first step of this reduction azobenzene derivatives takes up an electron in the

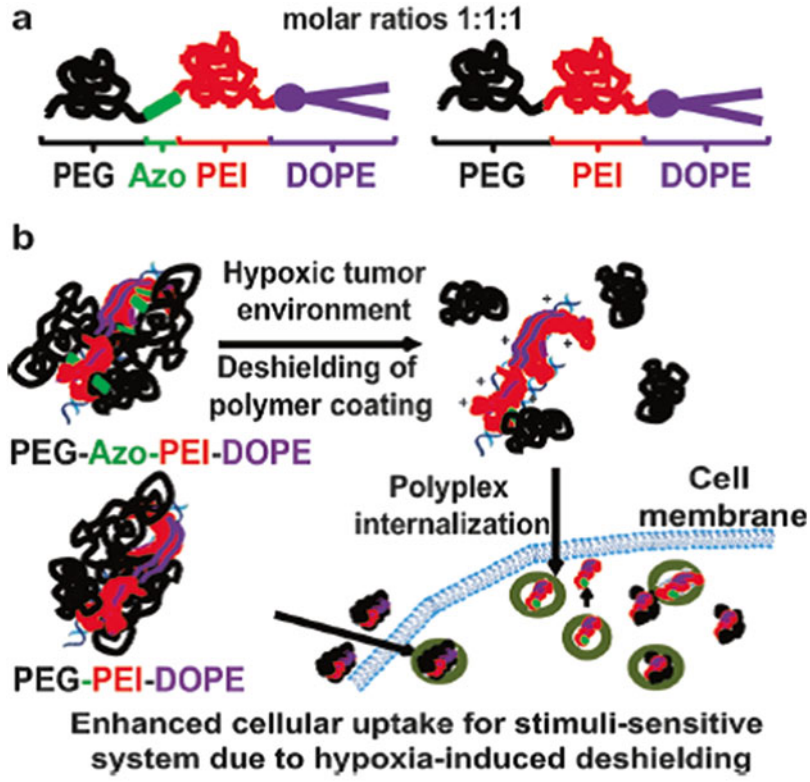

Fig. 1 Scheme of the Hypoxia responsive copolymer and suggested mechanism of hypoxia-induced activation. PEG-PEI-DOPE represents a non-hypoxia responsive control copolymer. Reproduced from ref. [29] with permission

environment and form the nitroanion radicals. This step is reversible and in the presence of oxygen, oxygen molecules take the electrons instead of the azobenzene bond and the back oxidation readily occurs. However, in the absence or low levels of oxygen, the nitroanion radicals will continue to gain electrons in a nonreversible way and the reduction will be completed by the cleavage of the azobenzene bond ($R\text{-}NH_2 + R'\text{-}NH_2$).

By linking a fluorophore to a quencher via an azobenezene unit the group of Pr. Nagano demonstrated oxygen-dependent fluorescence [26, 27]. Note that the oxygen sensitivity of azobenzene could be finely tuned to detect different oxygen tensions, with activation of fluorescence below either 5, 1 or 0.1 % oxygen [27].

It is the localized removal of the PEG corona in the hypoxic environment after azobenzene cleavage that leads to exposure of the positive charges of the PEI/siRNA polyion complex for cellular internalization and subsequent gene downregulation.

We describe the synthesis and evaluation of this hypoxia-targeted siRNA delivery formulation. The methods provided are appropriate for the evaluation of hypoxia-sensitive formulations both in monolayer cultures, cancer cell spheroids and tumor xenografts.

2 Materials

To avoid degradation of siRNA, RNAse-free tips and tubes should be used. Moreover, solutions should be prepared with RNAse free water.

2.1 Synthesis

1. 1,2-dioleoyl-*sn*-glycero-3-phosphoethanolamine-N-(glutaryl) (sodium salt) (NGPE) (Avanti Polar Lipids, AL, USA).
2. Chloroform ($CHCl_3$), deuterated chloroform ($CDCl_3$) for ^1H NMR.
3. *N*,*N*-dimethylformamide (DMF).
4. Pyridine.
5. 8 mL amber glass vials.
6. Cellulose ester membrane for dialysis of different molecular weight cutoff (MWCO of 1.0, 2.0, and 3.5 K).
7. *N*-(3-dimethylaminopropyl)-*N*′-ethylcarbodiimide HCl (EDC).
8. *N*-hydroxysuccinimide (NHS).
9. Triethylamine.
10. Deionized water (dH_2O).
11. Azobenzene-4,4′-dicarboxylic acid.
12. Dimethylaminopyridine (DMAP).
13. Methoxy-poly-(ethyleneglycol) (mPEG-NH_2, 2.0 K).

14. mPEG-NH_2, 1.8 K.
15. 0.2 μm syringe driven filters.
16. mPEG-SCM (Succinimidyl Carboxy Methyl ester) (Creative PEG Works, NC, USA).
17. Rhodamine B isothiocyanate.

2.2 In Vitro and In Cellulo Experiments

1. Cell culture medium: DMEM (Dulbecco's modified Eagle's medium) high glucose containing 10 % fetal bovine serum and penicillin–streptomycin antibiotics.
2. NCI-ADR-RES cells (National Cancer Institute Adriamycin Resistant) were obtained from the National Cancer Institute (Bethesda, MD, USA).
3. A NCI-ADR-RES cell line stably expressing the reporter gene GFP, NCI-ADR-RES/GFP cells was obtained by transfection with the pEGFP-N1 plasmid complexed with Lipofectamine (following manufacturer's instructions) followed by gentamicin selection at 0.5 mg/mL [29].
4. LabTek 8-well chambers with removable media chamber (Thermo Scientific).
5. Pimonidazole hydrochloride and mouse antibody against reduced pimonidazole adducts (Hydroxyprobe®, Inc., Burlington, MA).
6. Goat anti-mouse PE (phycoerythrin)-conjugated anti-mouse antibody (sc-3738, Santa Cruz Biotechnology, Santa Cruz, CA).
7. Goat anti-mouse TRITC-conjugated antibody (T-2762, Life Technologies, Carlsbad, CA).
8. Rabbit anti-mouse PErCP Cy5.5 (sc-358940, Santa Cruz Biotechnology, Santa Cruz, CA).
9. Rat liver microsomes.
10. Lipofectamine 2000.
11. High gelling temperature agarose (Invitrogen, Grand Island, NY).
12. Premixed calibration gas cylinders (21 or 0.5 % O_2, 5 % CO_2, nitrogen balanced mix) can be obtained from a medical gas supplier.
13. Anti-GFPsiRNA (5′-AUGAACUUCAGGGUCAGCUd TdT-3′, sense [30].
14. RNase Cocktail™ Enzyme Mix (Invitrogen, Carlsbad, CA).
15. Vectashield® mounting medium for fluorescence (Vector laboratories, Burlingame, CA).
16. Cell Titer Blue (Promega, Madison, WI).
17. Large-orifice pipet tips.

2.3 Animal Experiments

1. Female 6–8 weeks old C57BL/6 J and BALB/c nude mice (Charles River Laboratories, Willmington, MA).
2. BD Matrigel® matrix phenol red free (BD Biosciences, San Jose, CA).
3. Alanine aminotransferase and aspartate aminotransferase detection kit (Biomedical Research Service and Clinical Application, University at Buffalo, Buffalo, NY).

2.4 Instrumentation

1. Freeze-dryer.
2. Rotary evaporator.
3. Zeta potential analyzer.
4. Spectrophotofluorimeter plate reader.
5. Flow cytometer.
6. Confocal microscope.
7. Hypoxia chamber.
8. Cryomicrotome.
9. Kodak FX Imaging Station (Rochester, New York).
10. Varian 400 MHz FT NMR.
11. Waters 2545 HPLC equipped with a 2998 diode array detector (waters 3100 ESI-MS module), and XTerraMS C18 5 μm, 4.6 × 50 mm column.

3 Methods

We describe the synthesis of PAPD, composed of three components, the PEG shell, the azobenzene linker and PEI-DOPE. The synthesis is performed in three steps, synthesis of PEG–Azobenzene conjugate, PEG–Azobenzene–PEI conjugate, and coupling of DOPE to the PEI to obtain PEG–Azo–PEI–DOPE (Fig. 2) (*see* **Notes 1** and **2**).

3.1 Synthesis of PEI-DOPE

1. Activate NGPE (24.5 mg, 27.8 μM) in chloroform at a stock solution concentration of 25 mg/mL with *N*-(3-dimethylaminopropyl)-*N*′-ethylcarbodiimide HCl (EDC) (16 mg, 83.3 μM) and *N*-hydroxysuccinimide (NHS) (10 mg, 83.3 μM) in the presence of 15 μL of triethylamine for 4 h.
2. Dissolve 50 mg of 1.8 KDa PEI (27.8 μM) in 1.5 mL of chloroform in a 25 mL round bottom flask.
3. Add drop wise the activated acid solution into the PEI solution under stirring condition.
4. Stir for 18 h under nitrogen atmosphere.

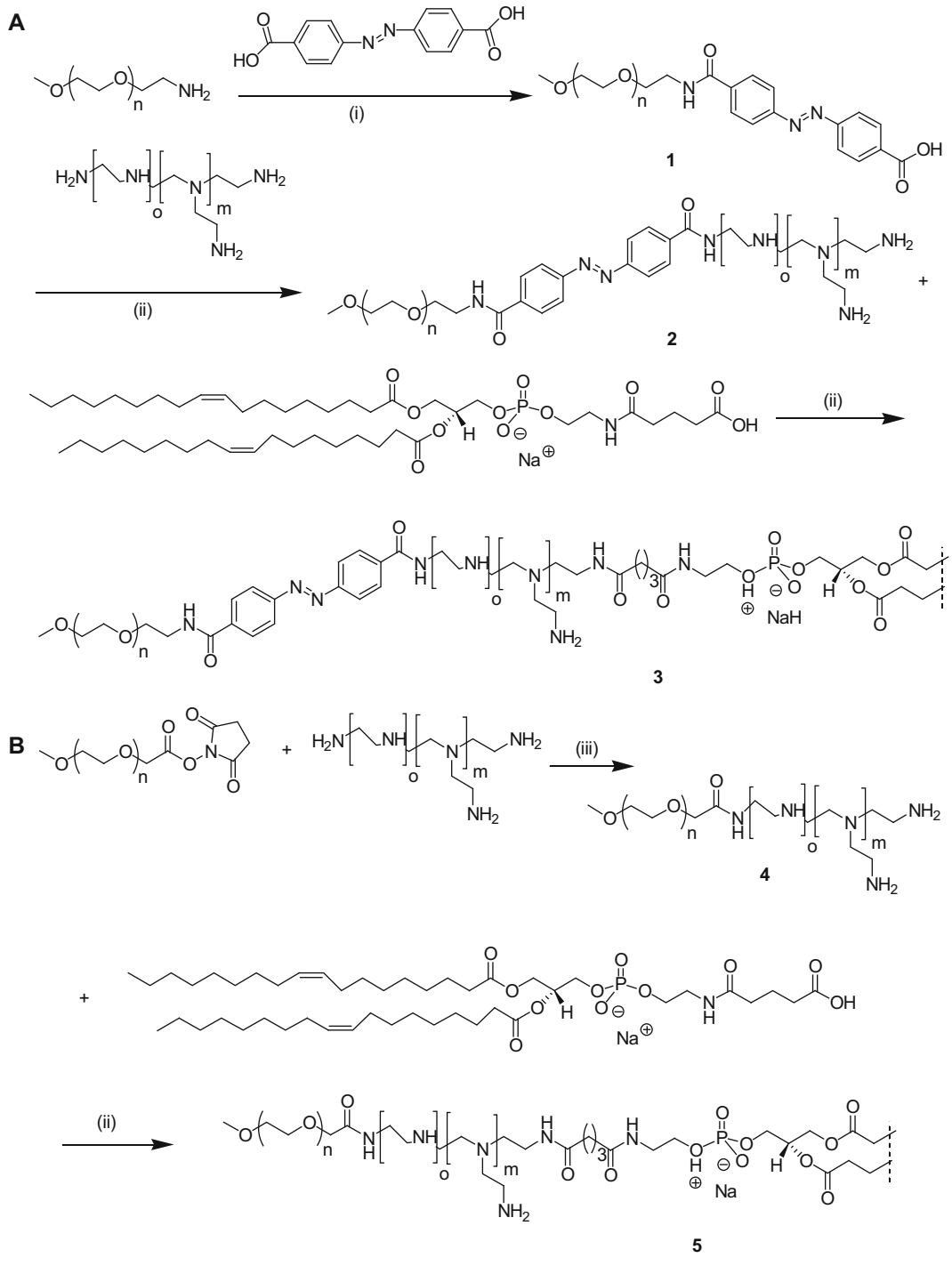

Fig. 2 Synthesis scheme of PEG-Azo-PEI-DOPE (**a**) and PEG-PEI-DOPE (**b**). (*i*) N-(3-Dimethylaminopropyl) N′-ethylcarbodiimide hydrochloride (EDCI), N-hydroxysuccinimide (NHS), pyridine, 4-dimethylaminopyridine, RT, overnight; (*ii*) EDCI, NHS, Triethylamine (TEA), $CHCl_3$, RT, overnight; (*iii*) TEA,$CHCl_3$, RT, overnight. Reproduced from ref. [29] with permission

5. Evaporate chloroform in the rotary evaporator under reduced pressure and freeze dry to remove traces of solvent, the same procedure is repeated for each solvent removal step.
6. Suspended the residue in 2 mL of deionized water (dH_2O) and purify by dialysis (MWCO 2.0 KDa) against 4 L of dH_2O overnight with one water change and freeze-dry.
7. Dissolve PEI-DOPE in $CDCl_3$ and characterize by ^1H NMR.

3.2 Synthesis of PAPD

3.2.1 Synthesis of PEG-Azo-Acid (1)

1. Dissolve Azobenzene-4,4′-dicarboxylic acid (5.4 mg, 20 μM) in 1 mL of pyridine in an amber glass vial (8 mL), and add EDC (5.4 mg, 20 μM), NHS (2.3 mg, 20 μM) and catalytic amount of dimethylaminopyridine (DMAP) under stirring. Stir for 1 h under nitrogen atmosphere.
2. Into this reagent mixture, add mPEG-NH_2 (MW. 2.0 K) (20 mg, 10 μM) dissolved in $CHCl_3$ drop wise. The reaction mixture is then stirred overnight.
3. The following day, remove solvent using rotary evaporator and freeze drying.
4. Suspend the crude reaction mix in 10 mL of water, vortex and centrifuge at $2000 \times g$ for 10 min.
5. Pass the supernatant through a 0.2 μM filter, dialyze against 4 L of water (MWCO. 1 K) for 2 days.
6. Freeze-dry the dialysate to obtain a fluffy yellow solid (1).

3.2.2 Synthesis of PEG-Azo-PEI (2)

1. Dissolve PEG-Azo-Acid (1) (12 mg, 5.3 μM) in 1 mL of a 1:1 mixture of $CDCl_3$ and Pyridine.
2. Into this solution, sequentially add EDC (2.0 mg, 10.6 μM), NHS (1.2 mg, 10.6 μM) and catalytic amount of dimethylaminopyridine (DMAP) under stirring condition. Stir 1 h under nitrogen.
3. This reagent mixture is added drop wise into a solution of poly ethyleneimine (PEI) (MW. 1.8 K) (11.5 mg, 5.3 μM) in $CHCl_3$. Stir overnight under nitrogen.
4. The following day, remove organic solvent and dissolve the reaction mixture in water, dialyze against water (cellulose ester membrane, MWCO. 3.5 K), and freeze-dry dialysate (2).

3.2.3 Synthesis of PEG-Azo-PEI-DOPE (3)

1. Add triethylamine (30 μL) to a solution of NGPE (6.6 mg, 7.44 μM), EDC (4.3 mg, 22.3 μM) and NHS (2.6 mg, 22.3 μM) in $CDCl_3$.
2. Stir 1 h before dropwise addition of PEG-Azo-PEI (30 mg, 7.44 μM) in $CHCl_3$. Stir overnight.
3. Remove organic solvent and dialyze the crude reaction mixture against water (cellulose ester membrane, MWCO. 3.5 K) overnight, followed by freeze-drying of the dialysate.

3.3 Synthesis of the Control Hypoxia Insensitive Copolymer PEG-PEI-DOPE

3.3.1 Synthesis of PEG-PEI (4)

1. Add mPEG-SCM (MW. 2.0 K) (50 mg, 25 μM) to a solution of PEI (MW. 1.8 K) (45 mg, 25 μM) and triethylamine (30 μL) in $CHCl_3$; stir overnight under nitrogen atmosphere.
2. On the following day, remove organic solvent and dialyze the crude reaction mixture against water (cellulose ester membrane, MWCO. 3.5 K) overnight and freeze dry.

3.3.2 Synthesis of PEG-PEI-DOPE (5)

1. PEG-PEI-DOPE is obtained following the protocol described for the synthesis of polymer *3*. EDC and NHS activated NGPE (7 mg, 7.9 μM) are added to a solution of polymer *4* (30 mg, 7.9 μM).
2. The reaction mixture is purified by dialysis against water during 3 days with several water changes.

3.4 Synthesis of Rhodamine-Labeled Polymers

The rhodamine-labeled polymers are synthesized following the above-mentioned procedure using Rhodamine-PEI instead of PEI. Rhodamine-PEI can be obtained as follows:

1. Rhodamine B isothiocyanate (59.6 mg, 111 μM) dissolved in DMF/$CHCl_3$ (1:1) (500 μL) is added drop wise to a solution of PEI (200 mg, 111 μm), and triethylamine (30 μL) in 1 mL of $CHCl_3$.
2. Stir overnight under a nitrogen atmosphere at room temperature.
3. The following day, remove organic solvents and dissolve the crude reaction mix in water. Dialyze against water (cellulose ester membrane, MWCO. 1.0 KDa) for 1 day. Freeze dry the dialysate.
4. For characterization of polymers using NMR spectroscopy, dissolve the polymers in $CDCl_3$ at a concentration of 10 mg/mL.

3.5 Cell Culture

3.5.1 Monolayers Cells Cultures

Cells were cultured in DMEM containing 10 % fetal bovine serum (FBS), 100 U/mL penicillin and 100 μg/mL streptomycin.

3.5.2 Culture of Cancer Cell Spheroids

As tumors are considered as semi-organs, evaluation of formulations in three-dimensional cell culture models, cancer cell spheroids, have been proposed as models of the tumor microenvironment, ability to penetrate spheroid cultures emerging as a critical parameter of anticancer activity [31, 32]. Spheroids of ~500 μm diameter are prepared by a liquid overlay method using agarose as the non-adherent substrate, according to [33] (Fig. 3).

1. Prepare and autoclave a solution of 1.5 % agarose in DMEM. Once prepared this solution can be stored at 4 °C and should be redissolved by heating in a water bath prior to use (*see* **Note 3**).

2. Dispense 50 µL of 1.5 % agarose in DMEM into 96-well plates to form a non-adherent layer using a multichannel pipette, avoid bubble formation both in the tips and in the wells.
3. Wait 30 min at RT for the agarose to solidify.
4. Add a cell suspension containing 8000–10,000 cells per 100 µL (we used A549 cells, NCI-ADR-RES cells and NCI-ADR-RES/GFP cells).
5. Centrifuge the plates for 15 min at 1500 × *g* without deceleration brake.
6. Transfer the plates in the incubator and monitor spheroid formation during 3–5 days by microscopy (Figs. 3 and 4).

3.6 Establishment of Tumor Models

3.6.1 B16F10 Syngeneic Tumors

1. Subcutaneously inject 10^6 B16F10 cells in 100 µL PBS to C57BL6/J anesthetized mice (*see* **Notes 4** and **5**).
2. For anesthesia with ketamine/xylazine, mix 1 mL of Imalgene® 1000, 0.5 mL Rompun® 2 % and 8.5 mL saline, and use 0.1 mL of solution per 10 g body weight.
3. Measure tumor growth in two perpendicular directions every 2 days using a caliper to estimate tumor volume (Volume = $0.5 \times L \times l^2$) where L and l are the longest and shortest axis, respectively. Monitor body weight at the same time.
4. Wait for the tumors to reach 400–500 mm^3 before treatment.

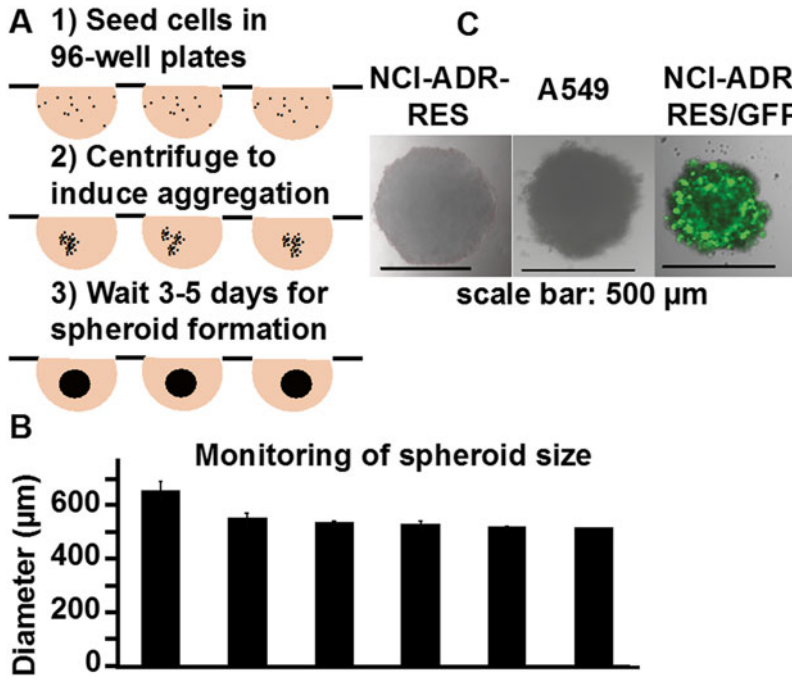

Fig. 3 Culture of spheroids. (**a**) scheme, (**b**) monitoring of diameter increase, (**c**) observation by confocal microscopy of spheroids

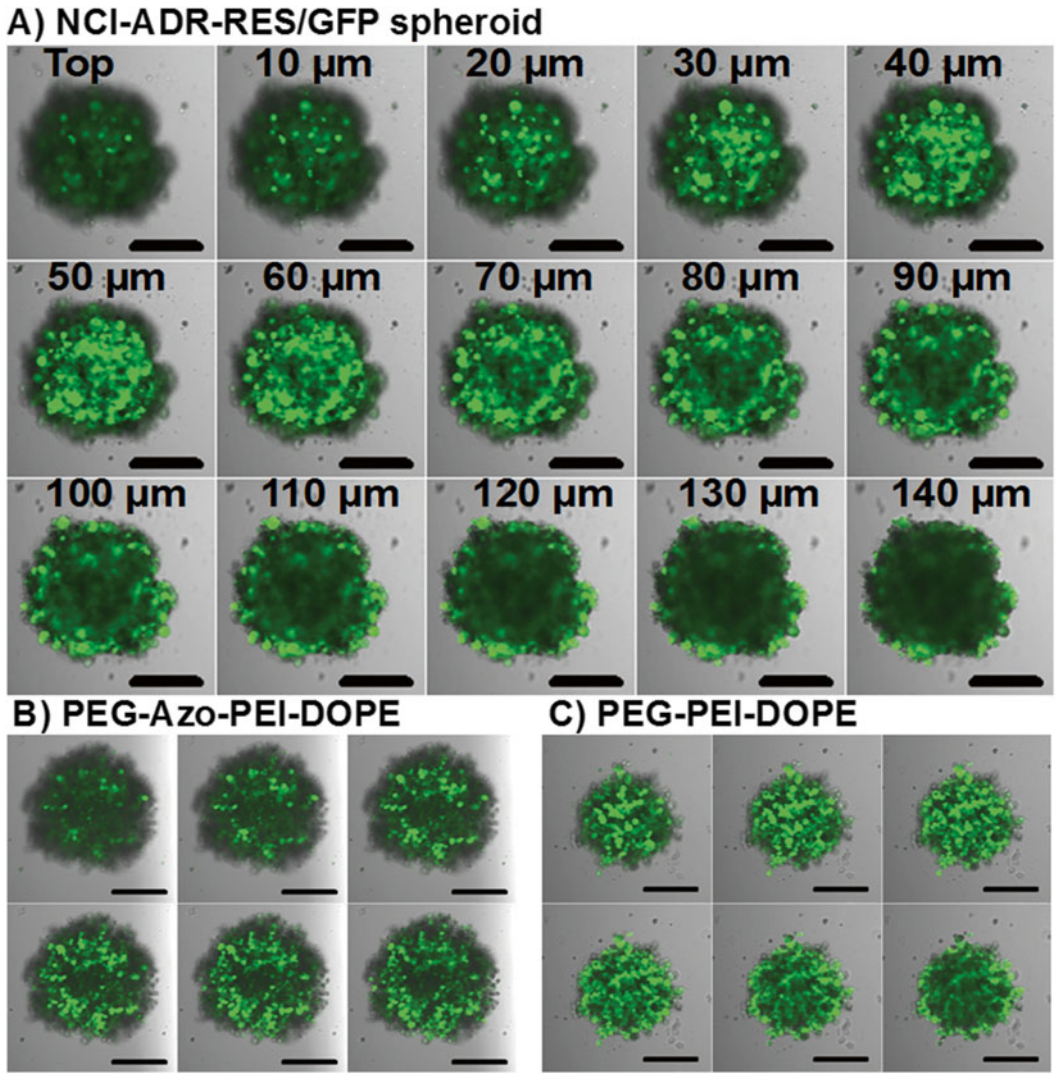

Fig. 4 GFP-expressing spheroid model for evaluation of reporter gene down-regulation. (**a**) NCI-ADR-RES/GFP spheroid, NCI-ADR-RES/GFP spheroid 48 h after transfection with 400 nM anti-GFP siRNA as PEG-Azo-PEI-DOPE/siRNA complexes (**b**) or PEG-PEI-DOPE/siRNA complexes (**c**). Scale bar represents 200 µm

3.6.2 A2780 Xenografts To obtain xenografts, human cancer cell lines should be implanted in a support basement membrane preparation (Matrigel®).

1. Matrigel® has a gel to liquid transition at temperatures above 4 °C. Tubes, solutions and syringes should be prechilled in ice before use.
2. Dispense 60 µL of Matrigel in as many 1.5 mL propylene tubes as your mice number.

3. Then, add 60 μL of your cell suspension at a twofold cell concentration (in PBS, 4 °C) to each tube and use it for subcutaneous tumor implantation, one syringe per animal.
4. As for syngeneic tumor models, monitor body weight and tumor growth.

3.7 Assessment of Polyion Complex Formation

Prepare polyion complexes between the polyelectrolytes and siRNA at increasing Nitrogen-to-Phosphate (N/P) ratios of polymer-to-siRNA in PBS. Complexation of siRNA is evaluated by exclusion of the ethidium bromide intercalate as well as decreased mobility of siRNA in an agarose gel after interaction with the copolymer (electrophoretic mobility shift assay).

3.7.1 Determination of N/P Ratio Allowing Complexation of siRNA

This assay is performed in 96-wells to use minute quantities of siRNA and copolymers. Black-walled 96-well plates are used to decrease background and signal crosstalk.

1. Prepare complexes with 0.5 μg siRNA at increasing N/P ratios in PBS, complexes should be prepared in duplicates.
2. Transfer complexes as well as free siRNA to the wells of the 96-well plate; wells with copolymer without siRNA should also be included to consider contribution to background.
3. Add ethidium bromide (EtBr, final concentration 20 μg/mL in PBS) and mix by pipetting.
4. Measure fluorescence with a spectrophotofluorimeter plate reader (λ_{ex}531/25 nm, λ_{em}620/10 nm).
5. Setting the fluorescence of free siRNA as 100 % determine the N/P ratio needed for maximal complexation of siRNA (i.e., with lowest EtBr fluorescence as in Fig. 5a). In the figure, siRNA was mixed with either PAPD (○) or PEI 1.8 kDa (◇) at increasing N/P ratios before determination of fluorescence. Maximal complexation was achieved at N/P 20 for PAPD with more than 80 % EtBr exclusion (*see* **Note 6**).
6. Add Heparin (in PBS, 2 mg/mL final concentration), mix by pipetting and measure the fluorescence again to evaluate recovery of nucleic acid fluorescence suggesting its integrity and intracellular polyplex dissociation. Fluorescence recovery after Heparin treatment is illustrated in Fig. 5a from PAPD/siRNA complexes (○) to heparin-treated PAPD/siRNA complexes (●).

3.7.2 Gel Electrophoresis

Gel electrophoresis is used to confirm the absence of free siRNA after complexation with the polyelectrolyte as well as integrity of siRNA (degraded siRNA will appear as a smear in the gel).

1. Prepare complexes in PBS with 1 μg siRNA and run on a 2 % agarose gel at 10 V/cm^2 during 20 min (*see* **Note 7**).
2. Compare the migration of complexed siRNA to that of free siRNA.

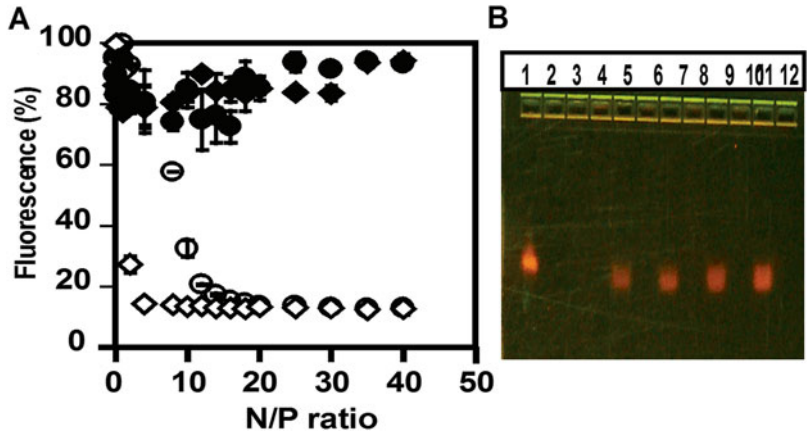

Fig. 5 siRNA complexation. (**a**) Ethidium bromide exclusion assay. (**b**) Electrophoretic mobility shift assay and RNAse protection. RNAse protection assay. *1*: untreated free siRNA, *2*: RNAse-treated free siRNA; *4*. PAPD polyplexes, N/P 40; *5*. PAPD polyplexes, N/P 40 treated with RNAse and heparin; *6*. PAPD polyplexes, N/P 60; *7*. PAPD polyplexes, N/P 60 treated with RNAse and heparin; *8*. PEG-PEI-DOPE (PPD) polyplexes, N/P 40; *9*. PPD polyplexes, N/P 40 treated with RNAse and heparin; *10*. PPD polyplexes, N/P 60; *11*. PPD polyplexes, N/P 60 treated with RNAse and heparin; wells 3 and 12 were unused. Adapted from ref. [29] with permission

3.7.3 RNAse Protection Assay

Degradation by nucleases is one of the main limitations of siRNA delivery [34]. Thus, evaluation of resistance to RNAse degradation is a critical assay before in vivo administration of complexes. RNAse protection assay is also evaluated by gel electrophoresis after incubation in the presence of RNAse.

1. Prepare the complexes in PBS with 1 µg siRNA in PBS, in a final volume of 5 µL.
2. Add RNAse (1 U/µg of siRNA, *see* **Note 8**) in a volume of 1–5 µL, incubate 1 h at 37 °C.
3. Add 1–5 µL of 10 mM EDTA (pH 8.0 in water, 1 mM final concentration) to inhibit RNAse and incubate 15 min at RT. EDTA chelates the di-cations that are cofactors of RNAse.
4. Add 5–10 µL of 500 KDa dextran sulfate (10 mg/mL in gel loading buffer) and incubate 15 min at RT to dissociate the complexes.
5. Run on a 2 % agarose gel during 20 min. RNA protected from degradation should be visualized on the gel whereas free RNA should have been degraded (Fig. 5b).

3.7.4 Reporter Gene Silencing Evaluation by Flow Cytometry

We evaluated the down-regulation of an exogenous reporter protein (GFP) stably expressed in cancer cell lines (*see* **Note 9**).

1. Grow cells to 60–70 % confluency in 24-well plates.
2. Incubate with polyplexes prepared using 200 nM siRNA (both targeted and control siRNA, *see* **Note 10**).

3. 48 h after transfection, wash with PBS, detach with trypsin and transfer to FACS tubes for analysis of cell-associated fluorescence, with acquisition of at least 10,000 events per sample.
4. The fluorescence of un-transfected cells cultured in the same conditions is set as 100 % reporter gene expression to evaluate gene down-regulation.

3.7.5 Evaluation of Gene Down-Regulation by Confocal Microscopy on Monolayers

1. Grow cells to 60–70 % confluency on LabTek chambers.
2. Incubate with polyplexes prepared using 200 nM siRNA (both targeted and control siRNA).
3. 48 h after transfection, wash with PBS, fix with 4 % PFA in PBS for 30 min at RT.
4. Wash with PBS and counterstain with Hoechst 33352 at 5 μM in PBS for 15 min at RT.
5. Finally, remove the polystyrene media chambers and mount with a cover glass and Vectashield®.
6. Seal slides with nail polish before storage at –20 °C or imaging (*see* **Note 11**).
7. Quantify the signal of at least ten cells per group using ImageJ [35].

3.7.6 Evaluation of Gene Down-Regulation by Confocal Microscopy on Spheroid Cultures

1. Prepare spheroids with GFP expressing cells, (we used NCI-ADR-RES/GFP cells) [36].
2. Transfect spheroids with anti-GFPsiRNA complexes (400 nM siRNA are used instead of 200 nM since gene silencing in 3D cultures is more challenging).
3. Image treated spheroids to evaluate GFP downregulation (Figs. 4b, c, *see* **Note 12**) [36].

3.8 Cellular Viability

Cellular viability after transfection is evaluated by a metabolic assay (Cell Titer blue). Nonfluorescent resazurin is reduced in the fluorescent resorufin (λ_{cm} 590 nm) by live cells.

1. Seed cells in 96-well plates to obtain a monolayer in 24 h, with 100 μL final volume.
2. Incubate cells with free copolymer and complexes.
3. At designated time points (8, 24, 48, 72 h after transfection) perform the metabolic assay:
4. Add 10 μL of Cell Titer Reagent per well and incubate 1–4 h at 37 °C (*see* **Note 13**).
5. Measure fluorescence at 590 nm using a spectrophotofluorimeter.
6. Setting the fluorescence of untreated cells cultured in the same conditions as 100 % viability, estimate the toxicity of your treatments.

3.9 Staining for Hypoxic Conditions

We used a hypoxia chamber to generate a hypoxic atmosphere, using an oxygen/carbon dioxide/nitrogen gas mix where oxygen is replaced by nitrogen (*see* **Note 14**). Confirmation of relevant hypoxic conditions is achieved using a Hydroxyprobe® kit [28, 37, 38]. In this assay, cells are first incubated with pimonidazole hydrochloride. Pimonidazole hydrochloride forms adducts with glutathione under hypoxia and these adducts are detected with a specific antibody provided in the kit. Formation of pimonidazole adducts can be detected both by flow cytometry and by microscopy.

3.9.1 Staining for Hypoxia in Monolayer Cell Cultures by Flow Cytometry

1. Seed cells in 24-well plates to form a monolayer over 24 h. The next day cells, incubate cells with 100 μM pimonidazole hydrochloride in media for 1–3 h at 37 °C in either normoxic (21 % O_2, 5 % CO_2) or hypoxic (0.5 % O_2, 5 % CO_2, nitrogen balanced) atmospheres.
2. Rinse wells with PBS, detach cells with trypsin and transfer them to flow cytometry tubes.
3. Wash once with PBS.
4. Resuspend the cells in 100 μL PBS and add 900 μL ice-cold methanol, vortex briefly and keep at −20 °C for 30 min.
5. Dilute with 2 mL ice-cold PBS, centrifuge, and wash twice with 500 μL PBS.
6. Resuspend cells in 30–50 μL PBS 1 % Bovine Serum Albumin containing antibody against reduced pimonidazole adducts at a 1/100th (HP-1 antibody, Hydroxyprobe) or an isotype-matched mouse antibody for 1 h at 4 °C.
7. Dilute with 500 μL PBS, centrifuge and resuspend in 30–50 μL of PBS 1 % BSA containing an optimized dilution of fluorophore-conjugated secondary antibody for 1 h at 4 °C. We obtained a good staining using either a secondary IgG PE-conjugated antibody at a 1/100th dilution (Fig. 6a) or PerCp Cy5.5-conjugated antibody at a 1/100th dilution.
8. Lastly, dilute with 300 μL before flow cytometry analysis with a FACSCalibur flow cytometer after live cells gating using forward and side scatter (Fig. 6a).

3.9.2 Staining for Hypoxia in Monolayer Cell Cultures Using Microscopy

1. Seed cells in 8-well chambers to form a monolayer over 24 h. The next day cells, incubate cells with 100 μM pimonidazole hydrochloride in media for 1–3 h at 37 °C in either normoxic (21 % O_2, 5 % CO_2) or hypoxic (0.5 % O_2, 5 % CO_2, nitrogen balanced) atmospheres.
2. Wash three times with PBS.
3. Fix cells with 4 % PFA in PBS for 30 min at RT.
4. Wash three times with PBS.

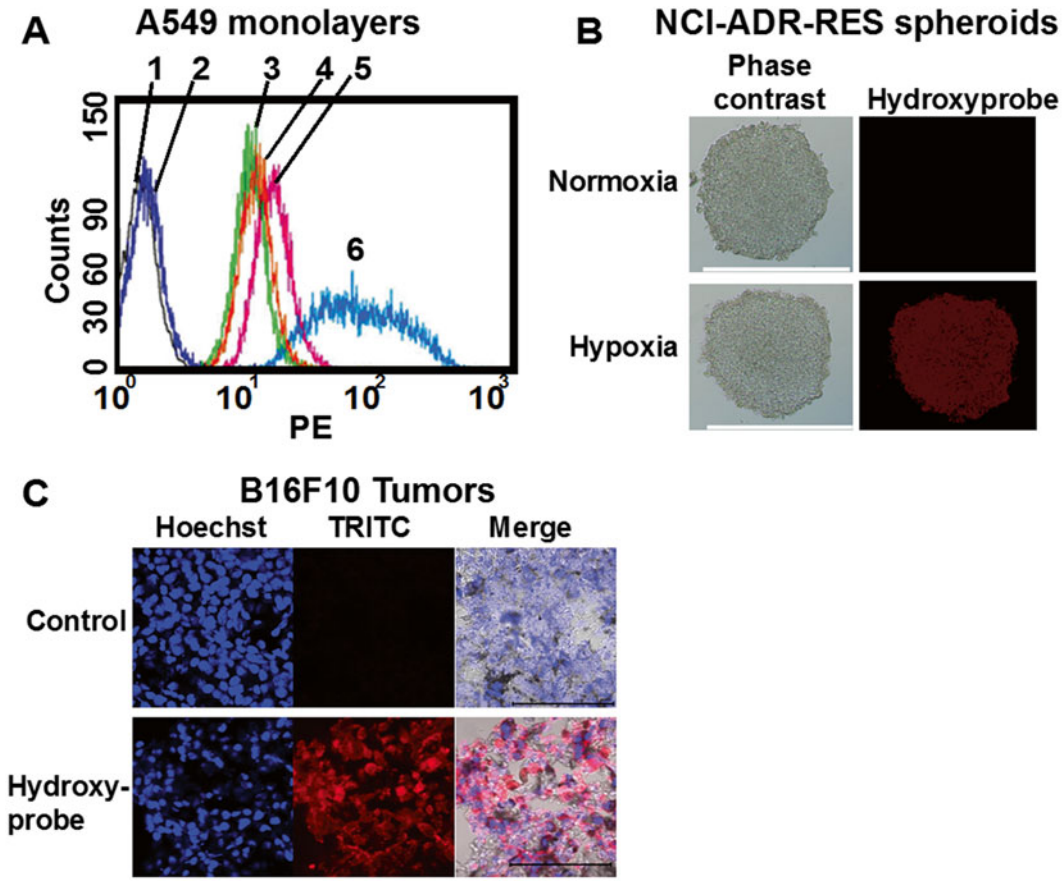

Fig. 6 Staining for hypoxic conditions. (**a**) Staining in monolayers followed by flow cytometry analysis. *1*: untreated cells in normoxia, *2*: untreated cells in hypoxia, *3*: control-matched isotype and secondary antibody in normoxia, *4*: control-matched antibody and secondary antibody in hypoxia, *5*: HP-1 antibody and secondary in normoxia, *6*: HP-1 antibody and secondary in hypoxia. (**b**) Staining for hypoxia in NCI-ADR-RES spheroids, scale bar represents 500 μm. (**c**) Staining for hypoxia in B16F10 tumors, scale bar represents 100 μm. Reproduced from ref. [29] with permission

5. Permeabilize cells with PBS 1 % BSA 0.2 % Triton X-100 for 2 min at RT.
6. Probe with 100 μL of PBS 1 % Bovine Serum Albumin containing antibody against reduced pimonidazole adducts at a 1/100th or control isotype for 1 h at 4 °C.
7. Counterstain with anti-mouse fluorophore conjugated antibody for 1 h at 4 °C, at optimized dilution. We used a TRITC-conjugated anti-mouse antibody at 1/100th for 1 h at 4 °C.
8. Finally, counterstain with Hoechst 33352 at 5 μM in PBS for 15–20 min at RT and mount with an aqueous mounting medium (Vetashield®).

3.9.3 Staining for Hypoxia in Spheroids

1. Incubate spheroid under normoxic or hypoxic atmospheres 3 h under with 100 μM pimonidazole hydrochloride.
2. Wash spheroids with PBS, fix with neutral-buffered formalin and cut in 15 μm sections.
3. Perform immunostaining as for monolayer cultures and image by microscopy (Fig.6b).

3.9.4 Staining for Hypoxia in Tissues

We followed the protocol developed by Kieda and coworkers [37].

1. Intravenously inject mice with 75 mg/kg of pimonidazole in PBS.
2. Sacrifice mice after1 h and fix tissues overnight at 4 °C in neutral-buffered formalin.
3. Cut 5–15 μm sections and perform immunostaining as indicated above for monolayer cultures followed by imaging (Fig. 6c).

3.10 Evaluation of Hypoxia-Dependent Cellular Uptake

1. Seed cells in 24-well plates to obtain monolayers in 24 h.
2. Incubate cells with complexes prepared with fluorophore-labeled siRNA or polymer for 4–24 h under normoxic and hypoxic atmospheres.

3.10.1 Hypoxia-Dependent Internalization

3. Measure cell-associated fluorescence with a flow cytometer. Typically, enhanced internalization is detected for hypoxia-responsive complexes under hypoxia whereas low uptake of PEGylated complexes is detected, as in Fig. 7a.

3.10.2 Hypoxia-Dependent Distribution of Polymer and/or siRNA in Spheroid Cultures

The penetration of spheroid cultures is evaluated with siRNA complexes prepared with fluorophore-labeled siRNA (siRNA coupled to DY547, siGLO transfection indicator, Thermo Scientific) or rhodamine-labeled polymers.

1. Incubate the spheroids with fluorophore-labeled hypoxia-sensitive and control formulations in the agarose-coated 96-well plates for 1–4 h.
2. After incubation carefully transfer spheroids to LabTek chambers using large-orifice pipet tips.
3. Wash three times with PBS and proceed to imaging with confocal microscopy using a 10× objective. Increase of fluorescence under hypoxia over normoxia should only be detected for the hypoxia-responsive formulation (Fig. 7b).
4. To further distinguish between intracellular accumulation in spheroids rather than distribution to the intercellular space, prepare sections from the imaged spheroids and image them at higher magnification (64×, as in [39]). In Fig. 7c, the penetration and intracellular accumulation of a matrix metalloprotease2 responsive TAT peptide-PEG1000-polyethylenimine-1, 2-dioleyl-phosphatidylethanolamine-peptide-paclitaxel (MMP2-responsive

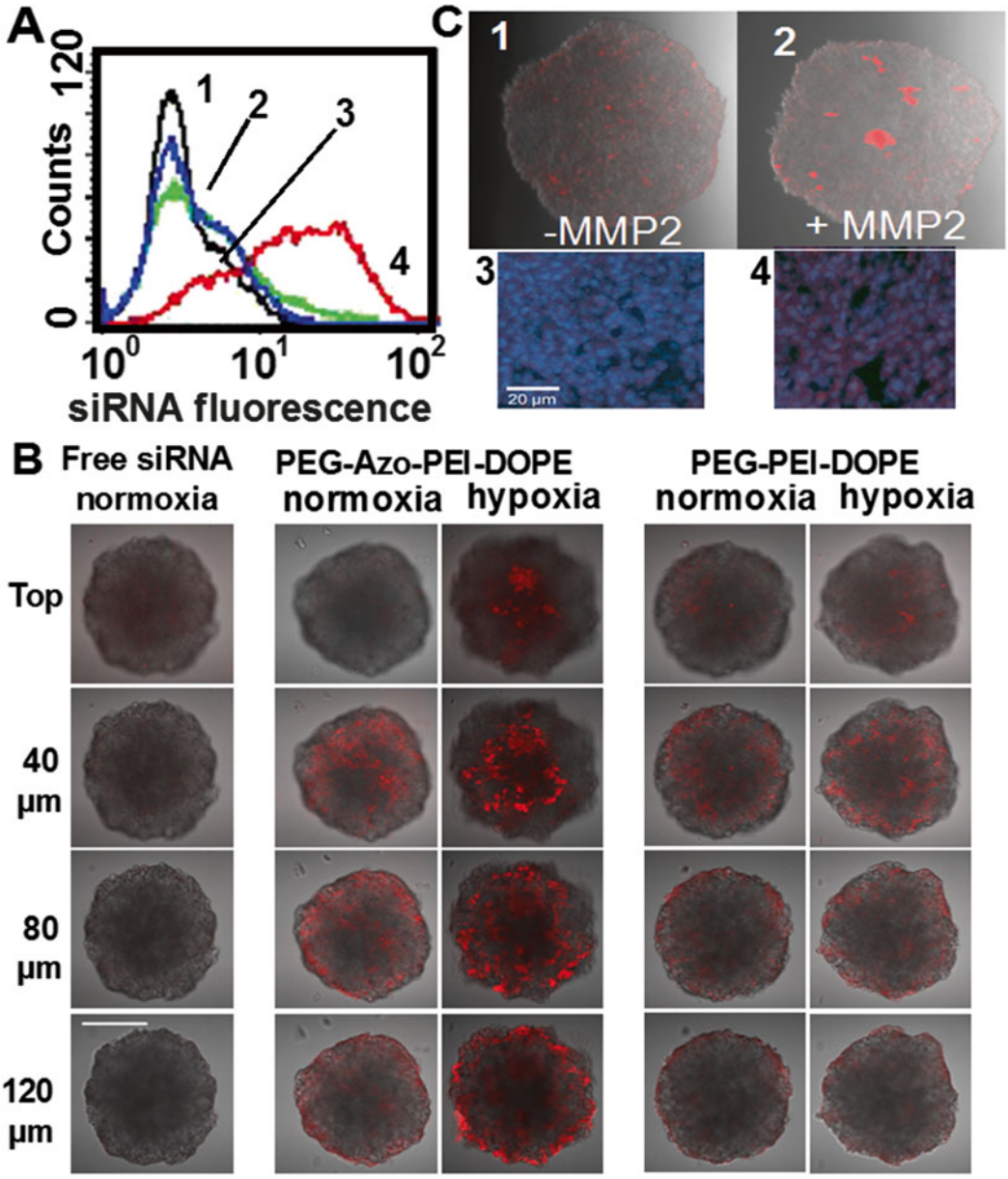

Fig. 7 Stimuli-dependent cellular internalization. (**a**) Hypoxia-dependent cellular uptake of DY547-labeled siRNA in monolayers. *1*: untreated cells, *2*: free siRNA, *3*: PEG-PEI-DOPE/siRNA, *4*: PEG-Azo-PEI-DOPE/siRNA. (**b**) Hypoxia-dependent siRNA uptake in NCI-ADR-RES spheroids. Scale bar: 200 μm. (**c**) Intracellular accumulation of MMP2-responsive TATp-PEG1000-PE/PEG2000-peptide-PTX in A549 spheroids. *1* and *2*: Enhanced spheroid penetration after incubation with recombinant MMP2. *3* and *4*: Intracellular accumulation in A549 spheroids. *3* and *4* are the sections from *1* to *2*. Scale bar represents 20 μm. Adapted from ref. [29, 39] with permission

TATp-PEG1000-PE/PEG2000-peptide-PTX) formulation was evaluated [39]. Enhanced penetration of spheroids is demonstrated after incubation with recombinant MMP2 (–MMP2 and +MMP2) and intracellular accumulation was demonstrated by sectioning of the spheroids, staining with Hoechst to delineate intracellular space, and imaging at higher magnification (inserts 3 and 4, scale bar of 20 μm instead of 200 μm for the whole spheroids) [39].

3.11 Biodistribution Evaluation

1. Inject mice with complexes prepared with rhodamine-PEI containing polymers.
2. Tissues are collected into 6-well plates using 1 well for each organ (tumor, liver, lungs, spleen, kidney, heart) and 1 plate per animal.
3. Fill each well with 2 mL of PBS.
4. At designated time points, collect organs into the designated wells and wash twice with PBS.
5. Divide tissue in two fractions with scalpel blades, one used for sectioning and imagery, the other for flow cytometry.

3.12 Biodistribution Evaluation on Tissue Sections

Sections are obtained and processed as indicated in Subheading 3.6.2 and imaged by microscopy (Fig. 8a).

3.12.1 Biodistribution Evaluation on Tissue Homogenates by Flow Cytometry

1. Using scalpel blades, mince tissues into 2–5 mm pieces.
2. Transfer pieces to flow cytometry tubes and incubate with 400 U/mL collagenase D solution in PBS for 30 min at 37 °C to dissociate cells (according to [40]).
3. Wash with PBS and resuspend in PBS at a cell concentration $<10^8$ cells/mL to avoid clogging of the flow cytometer (*see* **Note 15**).
4. Forward- and side-scatter as well as autofluorescence should be evaluated for each tissue.
5. Analyze 50,000–200,000 events per sample (Fig. 8b).
6. The flow cytometer should be washed between samples. To do this, run 1 mL of BD FACS Clean solution, prime, run 1 mL of BD FACS Rinse solution, prime, and run 1 mL of PBS. This should be performed until no remaining cells are detected.

3.13 In Vivo Silencing

Gene down-regulation in vivo is evaluated with mice bearing tumor stably expressing a reporter gene (GFP in our situation).

1. Intravenously inject siRNA complexes (1.5 mg/kg siRNA in 200 μL PBS) to mice bearing GFP-expressing tumors (*see* **Note 16**).

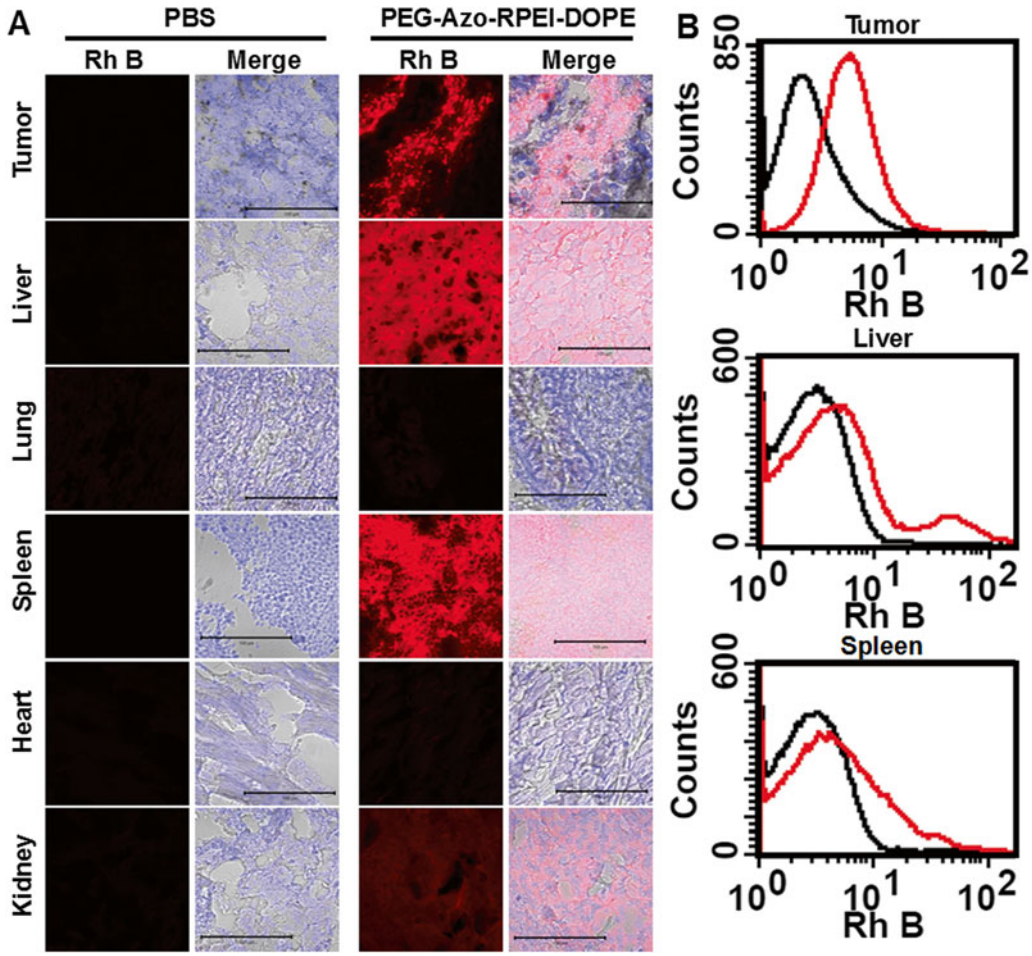

Fig. 8 Biodistribution. (**a**) Micrographs show fluorescence from tissue sections with rhodamine B (Rh B) on the left and merge of rhodamine B, Hoechst, and visible (Merge) on the *right*. Scale bar represents 100 μm. (**b**) Representative histogram plots of dissociated organs from mice treated with either PBS (*black*), or PEG-Azo-RPEI-DOPE (PARPD, *red*). Adapted from ref. [29] with permission

2. After 48 h, euthanize mice and image tumor fluorescence ex vivo using an imaging station (Fig. 9a, b). Data are presented as color-coated fluorescence (*see* **Note 17**).
3. Prepare homogenates from the tumors (as indicated in Subheading 5.1.2) to determine gene down-regulation by flow cytometry (Fig. 9c, d).

4 Notes

1. Chloroform, Triethylamine and pyridine are toxic both by contact and inhalation and should be manipulated under a chemical hood.

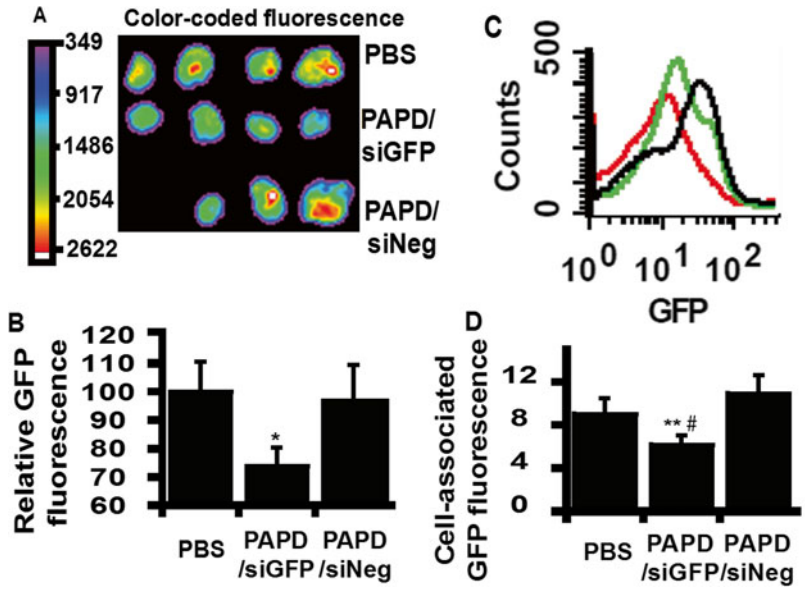

Fig. 9 In vivo silencing. (**a**) Quantitation of GFP emission from tumors ex vivo 48 h after intravenous injection of PBS ($n=4$), PEG-Azo-PEI-DOPE/anti-GFP siRNA complexes prepared with (PAPD/siGFP, $n=4$) and PEG-Azo-PEI-DOPE/negative siRNA complexes (PAPD/siNeg, $n=3$). (**b**) Relative GFP fluorescence from the ex vivo imaging of tumors in (**a**). Student's *t* test was performed, $*p<0.05$ compared to PBS or PAPD/siNeg. (**c**) Cell-associated fluorescence from dissociated tumors and representative histogram (**d**). *Green*: PBS, *red*: PAPD/siGFP, *black*: PAPD/siNeg. (Student's *t* test, $**p<0.01$ compared to PBS, $\#p<0.001$ compared to PAPD/siNeg). Reproduced from ref. [29] with permission

2. All synthesis reactions are performed at room temperature and under nitrogen atmosphere.
3. Commercially available reusable 3D Petri Dish® micro-molds (Sigma-Aldrich) filled with agarose may be used as an alternative non-adherent support.
4. Cell cultures used for tumor models should not be over confluent at the time of injection.
5. PBS 10×: 80 g NaCl, 2 g KCl, 28.9 g Na_2HPO_4 12 H_2O, 2 g KH_2PO_4,pH 7.4, distilled water sufficient for 1 L. 4 % PFA should be dissolved in PBS at 50–60 °C, since PFA and formaldehyde vapors are known carcinogens, PFA solution should be prepared in a chemical hood.
6. Plates can also be imaged with a UV trans-illuminator for fast screening of autofluorescence and complexation using the same device used to visualize EtBr-stained gels [41].
7. 2 % agarose gels may be prepared dissolving agarose in TAE (Tris Acetate EDTA buffer, TAE 50×: 242 g Tris base, 57.1 mL glacial acetic acid, 18.61 g EDTA, distilled water sufficient for 1 L). TAE 1× is also the running buffer for electrophoresis.

Agarose is dissolved by heating, typically in a microwave. When the solution has cooled down to 40–50 °C add ethidium bromide to a final concentration of 10–20 μg/mL and cast the gel. Precast 2 % agarose gels containing ethidium bromide can also be ordered (E-gel®, Invitrogen). Note that ethidium bromide may be a carcinogen and should be handled with PPE and discarded accordingly.

8. Whereas RNAse A alone can be used to evaluate protection against RNAse digestion, we used a RNAse mix (RNase Cocktail™ Enzyme Mix, Ambion) of RNAse A (cuts RNA after C and U) and RNAse T1 (cuts RNA after G) to obtain clearer bands on the electrophoresis gel.
9. If using a cell line stably expressing the reporter gene selected by antibiotic resistance, transfection should be performed in absence of selection antibiotic to avoid toxicity. Moreover, while we used NCI-ADR-RES/GFP cells prepared in the laboratory, the reader can also seed GFP expressing spheroids form commercially available A549/GFP cells (Cell Biolabs Inc.).
10. Whereas user-defined scrambled siRNA can be used, it is hard to predict off-target effects. For in vivo silencing, we used *Silencer*® Negative control siRNA (Ambion), guaranteed to have no significant effect on cellular homeostasis in human, mouse and rat cell lines.
11. We used confocal microscopy. A conventional microscope can also be used for imaging but it should be equipped with a monochromatic camera to be able to quantify signal.
12. For an accurate evaluation of reporter gene silencing, quantitative PCR should be performed as this method requires very low amounts of samples with established protocols with spheroids [42].
13. Although the manufacturer recommends using 20 μL of Reagent per 100 μL of cell culture media, we had good results with 10 μL of Reagent per 100 μL of media. Since dispensing and mixing of 10 μL is not accurate, prepare an intermediate dilution of reagent to add 50 μL per well.
14. We used an 850 LCM incubation chamber (PLAS Labs, Lansing, MI), flushed with cylinders of premixed calibration gas (0.5 % O_2, 5 % CO_2, nitrogen balanced), for 10 min before sealing and incubated at 37 °C for various time points. For long time exposures (24 h, 48 h), the chamber's atmosphere was changed three times a day. Note that a more precise control of the atmosphere can be achieved using an automated hypoxia chamber coupled to oxygen/carbon dioxide/nitrogen sensors such as the systems proposed by Biospherix (Lacona, NY).

15. To avoid clogging of the flow cytometer, samples may be drained through 40 μm cell strainer filters (BD Biosciences).
16. Mice should be imaged prior to their use for in vivo silencing to ensure that the average reporter gene expression is similar among groups prior to siRNA injection.
17. Acute toxicity may also be evaluated at the time of estimation of gene down-regulation by measuring the serum levels of alanine aminotransferase and aspartate aminotransferase.

Acknowledgments

This work was supported by grant U54CA151881 to Pr. Torchilin.

References

1. Schroeder A, Heller DA, Winslow MM, Dahlman JE, Pratt GW, Langer R, Jacks T, Anderson DG (2012) Treating metastatic cancer with nanotechnology. Nat Rev Cancer 12(1):39–50. doi:10.1038/nrc3180
2. Tabernero J, Shapiro GI, LoRusso PM, Cervantes A, Schwartz GK, Weiss GJ, Paz-Ares L, Cho DC, Infante JR, Alsina M, Gounder MM, Falzone R, Harrop J, White AC, Toudjarska I, Bumcrot D, Meyers RE, Hinkle G, Svrzikapa N, Hutabarat RM, Clausen VA, Cehelsky J, Nochur SV, Gamba-Vitalo C, Vaishnaw AK, Sah DW, Gollob JA, Burris HA 3rd (2013) First-in-humans trial of an RNA interference therapeutic targeting VEGF and KSP in cancer patients with liver involvement. Cancer Discov 3(4):406–417. doi:10.1158/2159-8290.CD-12-0429
3. Hrkach J, Von Hoff D, Mukkaram Ali M, Andrianova E, Auer J, Campbell T, De Witt D, Figa M, Figueiredo M, Horhota A, Low S, McDonnell K, Peeke E, Retnarajan B, Sabnis A, Schnipper E, Song JJ, Song YH, Summa J, Tompsett D, Troiano G, Van Geen HT, Wright J, LoRusso P, Kantoff PW, Bander NH, Sweeney C, Farokhzad OC, Langer R, Zale S (2012) Preclinical development and clinical translation of a PSMA-targeted docetaxel nanoparticle with a differentiated pharmacological profile. Sci Transl Med 4(128):128ra39. doi:10.1126/scitranslmed.3003651
4. Davis ME, Chen ZG, Shin DM (2008) Nanoparticle therapeutics: an emerging treatment modality for cancer. Nat Rev Drug Discov 7(9):771–782. doi:10.1038/nrd2614
5. Chow EK, Ho D (2013) Cancer nanomedicine: from drug delivery to imaging. Sci Transl Med 5(216):216. doi:10.1126/scitranslmed.3005872
6. Chauhan VP, Jain RK (2013) Strategies for advancing cancer nanomedicine. Nat Mater 12(11):958–962. doi:10.1038/nmat3792
7. Bertrand N, Wu J, Xu X, Kamaly N, Farokhzad OC (2014) Cancer nanotechnology: the impact of passive and active targeting in the era of modern cancer biology. Adv Drug Deliv Rev 66:2–25. doi:10.1016/j.addr.2013.11.009
8. Caron WP, Morgan KP, Zamboni BA, Zamboni WC (2013) A review of study designs and outcomes of phase I clinical studies of nanoparticle agents compared with small-molecule anticancer agents. Clin Cancer Res 19(12):3309–3315. doi:10.1158/1078-0432.CCR-12-3649
9. Cheng Z, Al Zaki A, Hui JZ, Muzykantov VR, Tsourkas A (2012) Multifunctional nanoparticles: cost versus benefit of adding targeting and imaging capabilities. Science 338(6109):903–910. doi:10.1126/science.1226338
10. Gill PS, Wernz J, Scadden DT, Cohen P, Mukwaya GM, von Roenn JH, Jacobs M, Kempin S, Silverberg I, Gonzales G, Rarick MU, Myers AM, Shepherd F, Sawka C, Pike MC, Ross ME (1996) Randomized phase III trial of liposomal daunorubicin versus doxorubicin, bleomycin, and vincristine in AIDS-related Kaposi's sarcoma. J Clin Oncol 14(8):2353–2364
11. Gradishar WJ, Tjulandin S, Davidson N, Shaw H, Desai N, Bhar P, Hawkins M, O'Shaughnessy

J (2005) Phase III trial of nanoparticle albumin-bound paclitaxel compared with polyethylated castor oil-based paclitaxel in women with breast cancer. J Clin Oncol 23(31):7794–7803. doi:10.1200/JCO.2005.04.937

12. Harrington KJ, Mohammadtaghi S, Uster PS, Glass D, Peters AM, Vile RG, Stewart JS (2001) Effective targeting of solid tumors in patients with locally advanced cancers by radiolabeled pegylated liposomes. Clin Cancer Res 7(2):243–254
13. Committee AACR, Sawyers CL, Abate-Shen C, Anderson KC, Barker A, Baselga J, Berger NA, Foti M, Jemal A, Lawrence TS, Li CI, Mardis ER, Neumann PJ, Pardoll DM, Prendergast GC, Reed JC, Weiner GJ (2013) AACR cancer progress report 2013. Clin Cancer Res 19(Suppl 20):S4–S98. doi:10.1158/1078-0432.CCR-13-2107
14. Chan A, Orme RP, Fricker RA, Roach P (2013) Remote and local control of stimuli responsive materials for therapeutic applications. Adv Drug Deliv Rev 65(4):497–514. doi:10.1016/j.addr.2012.07.007
15. Ge Z, Liu S (2013) Functional block copolymer assemblies responsive to tumor and intracellular microenvironments for site-specific drug delivery and enhanced imaging performance. Chem Soc Rev 42(17):7289–7325. doi:10.1039/c3cs60048c
16. Chen CY, Kim TH, Wu WC, Huang CM, Wei H, Mount CW, Tian Y, Jang SH, Pun SH, Jen AK (2013) pH-dependent, thermosensitive polymeric nanocarriers for drug delivery to solid tumors. Biomaterials 34(18):4501–4509. doi:10.1016/j.biomaterials.2013.02.049
17. Li Y, Xiao K, Zhu W, Deng W, Lam KS (2014) Stimuli-responsive cross-linked micelles for on-demand drug delivery against cancers. Adv Drug Deliv Rev 66:58–73. doi:10.1016/j.addr.2013.09.008
18. Mura S, Nicolas J, Couvreur P (2013) Stimuli-responsive nanocarriers for drug delivery. Nat Mater 12(11):991–1003. doi:10.1038/nmat3776
19. Nguyen QT, Olson ES, Aguilera TA, Jiang T, Scadeng M, Ellies LG, Tsien RY (2010) Surgery with molecular fluorescence imaging using activatable cell-penetrating peptides decreases residual cancer and improves survival. Proc Natl Acad Sci U S A 107(9):4317–4322. doi:10.1073/pnas.0910261107
20. Olson ES, Jiang T, Aguilera TA, Nguyen QT, Ellies LG, Scadeng M, Tsien RY (2010) Activatable cell penetrating peptides linked to nanoparticles as dual probes for in vivo fluorescence and MR imaging of proteases. Proc Natl Acad Sci U S A 107(9):4311–4316. doi:10.1073/pnas.0910283107
21. Navarro G, Essex S, Sawant RR, Biswas S, Nagesha D, Sridhar S, de ILarduya CT, Torchilin VP (2014) Phospholipid-modified polyethylenimine-based nanopreparations for siRNA-mediated gene silencing: implications for transfection and the role of lipid components. Nanomedicine 10(2):411–419. doi:10.1016/j.nano.2013.07.016
22. Navarro G, Sawant RR, Biswas S, Essex S, Tros de Ilarduya C, Torchilin VP (2012) P-glycoprotein silencing with siRNA delivered by DOPE-modified PEI overcomes doxorubicin resistance in breast cancer cells. Nanomedicine (Lond) 7(1):65–78. doi:10.2217/nnm.11.93
23. Navarro G, Sawant RR, Essex S, Tros de Ilarduya C, Torchilin VP (2011) Phospholipid-polyethylenimine conjugate-based micelle-like nanoparticles for siRNA delivery. Drug Deliv Transl Res 1(1):25–33. doi:10.1007/s13346-010-0004-0
24. Sawant RR, Torchilin VP (2010) Polymeric micelles: polyethylene glycol-phosphatidylethanolamine (PEG-PE)-based micelles as an example. Methods Mol Biol 624:131–149. doi:10.1007/978-1-60761-609-2_9
25. Zhu L, Perche F, Wang T, Torchilin VP (2014) Matrix metalloproteinase 2-sensitive multifunctional polymeric micelles for tumor-specific co-delivery of siRNA and hydrophobic drugs. Biomaterials 35(13):4213–4222. doi:10.1016/j.biomaterials.2014.01.060
26. Kiyose K, Hanaoka K, Oushiki D, Nakamura T, Kajimura M, Suematsu M, Nishimatsu H, Yamane T, Terai T, Hirata Y, Nagano T (2010) Hypoxia-sensitive fluorescent probes for in vivo real-time fluorescence imaging of acute ischemia. J Am Chem Soc 132(45):15846–15848. doi:10.1021/ja105937q
27. Piao W, Tsuda S, Tanaka Y, Maeda S, Liu F, Takahashi S, Kushida Y, Komatsu T, Ueno T, Terai T, Nakazawa T, Uchiyama M, Morokuma K, Nagano T, Hanaoka K (2013) Development of azo-based fluorescent probes to detect different levels of hypoxia. Angew Chem Int Ed Engl 52(49):13028–13032. doi:10.1002/anie.201305784
28. Krohn KA, Link JM, Mason RP (2008) Molecular imaging of hypoxia. J Nucl Med 49(Suppl 2):129S–148S. doi:10.2967/jnumed.107.045914
29. Perche F, Biswas S, Wang T, Zhu L, Torchilin VP (2014) Hypoxia-Targeted siRNA Delivery. Angew Chem Int Ed Engl 53(13):3362–3366. doi:10.1002/anie.201308368

30. Biswas S, Dodwadkar NS, Piroyan A, Torchilin VP (2012) Surface conjugation of triphenylphosphonium to target poly(amidoamine) dendrimers to mitochondria. Biomaterials 33(18):4773–4782. doi:10.1016/j.biomaterials.2012.03.032
31. Thoma CR, Zimmermann M, Agarkova I, Kelm JM, Krek W (2014) 3D cell culture systems modeling tumor growth determinants in cancer target discovery. Adv Drug Deliv Rev 69–70:29–41. doi:10.1016/j.addr.2014.03.001
32. Mehta G, Hsiao AY, Ingram M, Luker GD, Takayama S (2012) Opportunities and challenges for use of tumor spheroids as models to test drug delivery and efficacy. J Control Release 164(2):192–204. doi:10.1016/j.jconrel.2012.04.045
33. Perche F, Patel NR, Torchilin VP (2012) Accumulation and toxicity of antibody-targeted doxorubicin-loaded PEG-PE micelles in ovarian cancer cell spheroid model. J Control Release 164(1):95–102. doi:10.1016/j.jconrel.2012.09.003
34. Huang L, Liu Y (2011) In vivo delivery of RNAi with lipid-based nanoparticles. Annu Rev Biomed Eng 13:507–530. doi:10.1146/annurev-bioeng-071910-124709
35. Schneider CA, Rasband WS, Eliceiri KW (2012) NIH Image to ImageJ: 25 years of image analysis. Nat Methods 9(7):671–675
36. Waite CL, Roth CM (2009) PAMAM-RGD conjugates enhance siRNA delivery through a multicellular spheroid model of malignant glioma. Bioconjug Chem 20(10):1908–1916. doi:10.1021/bc900228m
37. Kieda C, El Hafny-Rahbi B, Collet G, Lamerant-Fayel N, Grillon C, Guichard A, Dulak J, Jozkowicz A, Kotlinowski J, Fylaktakidou KC, Vidal A, Auzeloux P, Miot-Noirault E, Beloeil JC, Lehn JM, Nicolau C (2013) Stable tumor vessel normalization with pO(2) increase and endothelial PTEN activation by inositol trispyrophosphate brings novel tumor treatment. J Mol Med (Berl) 91(7):883–899. doi:10.1007/s00109-013-0992-6
38. Tupper J, Greco O, Tozer GM, Dachs GU (2004) Analysis of the horseradish peroxidase/indole-3-acetic acid combination in a three-dimensional tumor model. Cancer Gene Ther 11(7):508–513. doi:10.1038/sj.cgt.7700713
39. Zhu L, Wang T, Perche F, Taigind A, Torchilin VP (2013) Enhanced anticancer activity of nanopreparation containing an MMP2-sensitive PEG-drug conjugate and cell-penetrating moiety. Proc Natl Acad Sci U S A 110(42):17047–17052. doi:10.1073/pnas.1304987110
40. Kortylewski M, Kujawski M, Wang T, Wei S, Zhang S, Pilon-Thomas S, Niu G, Kay H, Mule J, Kerr WG, Jove R, Pardoll D, Yu H (2005) Inhibiting Stat3 signaling in the hematopoietic system elicits multicomponent antitumor immunity. Nat Med 11(12):1314–1321. doi:10.1038/nm1325
41. Perche F, Lambert O, Berchel M, Jaffres PA, Pichon C, Midoux P (2012) Gene transfer by histidylated lipopolyplexes: a dehydration method allowing preservation of their physicochemical parameters and transfection efficiency. Int J Pharm 423(1):144–150. doi:10.1016/j.ijpharm.2011.04.009
42. Primon M, Huszthy PC, Motaln H, Talasila KM, Torkar A, Bjerkvig R, Lah Turnsek T (2013) Cathepsin L silencing enhances arsenic trioxide mediated in vitro cytotoxicity and apoptosis in glioblastoma U87MG spheroids. Exp Cell Res 319(17):2637–2648. doi:10.1016/j.yexcr.2013.08.011

Chapter 13

Controlling RNA Expression in Cancer Using Iron Oxide Nanoparticles Detectable by MRI and In Vivo Optical Imaging

Zdravka Medarova, Mustafa Balcioglu, and Mehmet V. Yigit

Abstract

Herein, we describe a protocol for the preparation of iron oxide nanoparticle-based contrast agents and drug delivery vehicles for noninvasive cancer imaging and therapy. In the first part of the chapter we describe the details of the contrast agent synthesis, functionalization, and characterization. In the second part we describe the methods for tumor imaging using the synthesized particles with noninvasive T2-weighted magnetic resonance imaging (MRI) and in vivo near infrared optical imaging.

Key words Contrast agent, MRI, Fluorescence, Optical imaging, Tumor, Nanoparticle, miRNA, siRNA, Antisense oligonucleotide, Iron oxide, Oncogene

1 Introduction

Magnetic Resonance Imaging (MRI) is a noninvasive imaging methodology, which provides remarkable information from deep tissues inside the body. MRI has numerous advantages for cancer diagnosis due to its ability to differentiate malignant tissues from healthy ones due to the differences in tissue compositions. MRI contrast agents have been used for creating contrast between healthy and malignant tissues due to higher cellular uptake of the contrast agents by tumor cells. Such detailed imaging with high spatial resolution and tissue characterization is combined with in vivo optical fluorescence imaging to provide quick whole body biodistribution of contrast agents [1]. Contrast agents with two imaging capabilities enable bimodal preclinical imaging for cancer diagnosis.

Contrast agents serve as platforms for therapy aside from their diagnostic properties. This is accomplished by functionalization with therapeutic materials such as anticancer drugs or therapeutic oligonucleotides [2–4]. In this chapter, we will focus on the synthesis and application of oligonucleotide functionalized theranostic

Zdravka Medarova (ed.), *RNA Imaging: Methods and Protocols*, Methods in Molecular Biology, vol. 1372,
DOI 10.1007/978-1-4939-3148-4_13,

magnetic nanoparticles. The tumoral uptake of the contrast agents is validated by noninvasive MRI and in vivo fluorescence imaging. The therapeutic oligonucleotide component can be double stranded siRNA molecules for silencing disease-causing mRNAs [5] or antisense synthetic oligonucleotides to inhibit miRNAs overexpressed in cancer—oncomiRs. Gene expression is dysregulated in cancer and controlling the activity of these oncogenes has important implications for cancer therapeutics [6]. Therefore, a contrast agent, which can provide information about disease status via bimodal noninvasive imaging methods and regulate the expression of oncogenes (miRNAs and/or mRNAs) can have significant impact on the fight against cancer.

In this chapter we will describe our methods [1, 7–11] for (1) constructing a multifunctional contrast agent based on superparamagnetic iron oxide nanoparticles with bimodal imaging and therapeutic capability and (2) imaging the tumoral uptake by MRI and in vivo optical imaging.

2 Materials

The buffers are prepared using ultrapure water by purifying water to attain a sensitivity of 18 MΩ cm at 25 °C and analytical grade chemicals. All the reagents are stored at room temperature unless indicated otherwise. Institutional regulations are followed for waste disposal of materials produced during the experiments. Cellular and animal experiments are performed according to institutional regulations. The entire nanoparticle and contrast agent synthesis is performed in a dedicated fume hood.

2.1 Reagents

1. Dextran T10 (powder, Pharmacosmos, Holbaek, Denmark).
2. Ferric chloride hexahydrate ($FeCl_3 \cdot 6H_2O$).
3. Ferrous chloride tetrahydrate ($FeCl_2 \cdot 4H_2O$).
4. Ammonium hydroxide (NH_4OH, 28 %).
5. Sodium hydroxide (NaOH).
6. Epichlorohydrin ((±)-2-(Chloromethyl)oxirane, 1-Chloro-2, 3-epoxypropane).
7. SPDP (*N*-Succinimidyl 3-(2-pyridyldithio)propionate, Pierce Biotechnology).
8. TCEP, (*tris*(2-carboxyethyl)phosphine powder).
9. Phosphate buffered saline (powder in packs, Pierce Biotechnology).
10. Hydrochloric acid (HCl).
11. Hydrogen peroxide (H_2O_2, 30 % in H_2O).
12. DMSO (dimethyl sulfoxide).

13. cy5.5 mono-reactive NHS ester (1 mg of dry compound, GE Healthcare Life Sciences).
14. Short thiolated antisense miRNA (LNAs, Exiqon, Inc.).
15. Thiolated siRNA molecules (Dharmacon, GE Healthcare Life Sciences).
16. Ammonium acetate ($CH_3CO_2NH_4$, molecular biology grade, ≥98 %,).
17. Ethyl alcohol (200 proof, molecular biology grade).
18. Isoflurane (250 mL, Baxter Healthcare Corporation).
19. d-luciferin (K^+ Salt Bioluminescent Substrate, Caliper Life Sciences).
20. DPBS (Dulbecco's Phosphate-Buffered Saline, Life Technologies).
21. 5 M sodium hydroxide (NaOH) stock solution is prepared with extreme caution by dissolving 200 g of NaOH pellets in 1 L of distilled water in a glass bottle. During this step the glass bottle can get very hot therefore safety precautions have to be taken.
22. 20 mM sodium citrate buffer (pH 8.0) is prepared by mixing 8 mL of 20 mM of citric acid monohydrate ($C_6H_8O_7 \cdot H_2O$, MWT = 210.14 g/mol) and 92 mL of 20 mM of trisodium citrate dihydrate ($C_6H_5O_7Na_3 \cdot 2H2O$, MWT = 294.12 g/mol). The pH is adjusted by concentrated 1 M NaOH.
23. Phosphate buffered saline buffer (PBS, pH 7.4) is prepared by dissolving the Phosphate Buffered Saline powder in 500 mL of distilled water.
24. 3 % TCEP (*tris*(2-carboxyethyl)phosphine) is prepared by dissolving 30 mg of TCEP crystals in 1 mL of H_2O.
25. 9.5 M ammonium acetate is prepared by dissolving 735 mg in 500 μL H_2O to a final volume of 1 mL.
26. Iron standards are prepared by dissolving ferric chloride hexahydrate ($FeCl_3 \cdot 6H_2O$) in 6 N hydrochloric acid (HCl) to final iron concentrations of 0.1, 0.5, 1.0, 2.0, 2.5, 3.0, 4.0, and 6.0 mg/mL.

2.2 Consumables

1. Amicon Ultra-15 centrifugal filter units (MWCO 30 kDa, EMD Millipore, MA, USA).
2. Amicon Ultra-0.5 mL Centrifugal Filters (0.5 mL, MWCO 100 kDa, EMD Millipore).
3. Dialysis bag (MWCO 12–14 kDa, Spectrum Laboratories, Inc.).
4. Disposable Sephadex PD-10 columns (GE Healthcare Life Sciences).

5. 0.22 μm sterile syringe filter units (EMD Millipore).
6. Disposable Sephadex PD-10 columns (GE Healthcare Life Sciences).
7. G-50 Sephadex disposable quick spin columns (Roche Applied Science).

2.3 Cells and Animals

1. MDA-MB-231-*luc*-D3H2LN metastatic breast cancer cell lines (Caliper Life Sciences, Hopkinton, MA).
2. Mice (nu/nu or NIH III nude, Charles River Laboratories, Wilmington, MA).

2.4 Equipment

1. Sorvall Primo R benchtop centrifuges (Thermo Scientific).
2. Microcentrifuge (Model 5424, Eppendorf).
3. Speed vacuum concentrator (Thermo Scientific Savant SpeedVac.).
4. Zetasizer Nano ZS (Malvern Instruments Ltd, Malvern, Worcestershire, UK).
5. UV/Vis Spectrophotometer (Lambda 25, Perkin Elmer).
6. Minispec relaxometer (mq20, Bruker Corporation).
7. 9.4 T MRI Bruker horizontal bore scanner with Para Vision 5.1 software (Bruker Biospin, Billerica, MA, USA).
8. Marevisi 3.5 software (Institute for Biodiagnostics, National Research Council, Canada).
9. Xenogen IVIS Spectrum in vivo imaging system (Caliper Life Sciences).
10. Gas anesthesia system (XGI-8 Gas Anesthesia Unit, Caliber Life Sciences).
11. Living Image 4.0 software (Caliper Life Sciences).

3 Methods

3.1 Synthesis of Iron Oxide Nanoparticle Based T2-Weighted MRI Contrast Agents

1. 500 g of technical quality Dextran T10 in powder form is used for nanoparticle synthesis. Dextran T10 is a high purity dextran fraction with an average molecular weight of 10 kDa. 9 g of Dextran T10 is first added into 30 mL of double-distilled water and mixed thoroughly.
2. This viscous solution is stirred at room temperature in a 250 mL round bottom flask using a magnetic stirrer until all the dextran dissolves. The resulting solution is colorless but slightly cloudy. Moderate heat can be applied to dissolve the dextran completely.

3. The dissolved solution is filtered using 0.22 μm syringe filter units to remove the impurities and large non-dissolved dextran fractions.
4. The dissolved solution in the round bottom flask is chilled in an ice bucket with constant stirring for 1 h on a magnetic stirrer.
5. 0.65 g of ferric chloride hexahydrate ($FeCl_3 \cdot 6H_2O$) is dissolved completely in 1 mL of distilled water resulting in a brown colored suspension.
6. Ferric chloride solution is added into the cold dextran solution and mixed for an hour under a constant argon or nitrogen flush in the flask. The neck of the round bottom is capped with a rubber stopper to prevent oxidation by minimizing air contact.
7. Later 0.4 g of ferrous chloride tetrahydrate ($FeCl_2 \cdot 4H_2O$) powder is dissolved completely in 0.5 mL of distilled water which was previously flushed with argon or nitrogen gas to prevent oxidation, (*see* **Note 1**).
8. The greenish ferrous chloride solution is added into the dextran and ferrous chloride mixture under constant stirring and argon or nitrogen flow. The reaction is run for half an hour.
9. Later 15 mL of concentrated cold (~4 °C) ammonium hydroxide (NH_4OH, 28 %) is added dropwise into the reaction mixture. The gas flow is stopped during the titration; however, air contact should be kept to a minimum. The reaction mixture initially becomes very viscous and slurry and obtains an army-green color. The viscosity is lost after the ammonium hydroxide titration is over.
10. The gas flow resumes after the titration is over. The ice bucket under the reaction mixture must stay and the stirring has to be maintained during the entire process.
11. Fifteen minutes later the ice bucket under the round bottom flask is removed and temperature is increased to between 75 and 85 °C for 90 min. After this step the gas flow is stopped and the solution is cooled to room temperature slowly. The formation of dextran coated magnetic nanoparticles should be achieved at the end of these series of reactions. The volume of the final solution is around 40 mL.
12. The resulting solution is purified from free unreacted dextran, iron salts and ammonium hydroxide with centrifugation using Amicon Ultra-15 centrifugal filter units (MWCO 30 kDa).
13. The nanoparticle suspension is first concentrated with centrifugation (~1500×*g* (RCF) for 30–45 min), which results in a highly concentrated nanoparticle suspension on the filter and a

nanoparticle-free elution under the filter unit. The eluent under the filter is discarded and the nanoparticle pellet is resuspended in distilled water and recentrifuged using the same filter unit. This step is repeated ~8 times to remove any side products and unreacted species completely. Initially removing the free dextran with centrifugation is time-consuming (~1 h) due to the viscosity of the solution, large size and the greater amount of unreacted free dextran in the mixture. However, after the first 3 or 4 centrifugation steps, most of the free dextran is removed, and resuspension and concentration of nanoparticles can be done in relatively short centrifugation steps.

14. The resulting purified solution of dextran coated super paramagnetic iron oxide nanoparticles is resuspended in 20 mL of distilled water.
15. The nanoparticles are cross-linked and aminated with a series of reaction steps using sodium hydroxide, epichlorohydrin and ammonium hydroxide, Fig. 1a, (*see* **Note 2**).
16. 35 mL of NaOH (5 M) is later added into the 20 mL of nanoparticle suspension in a 250 mL round bottom flask. The reaction mixture is stirred for 15 min without a gas flow.

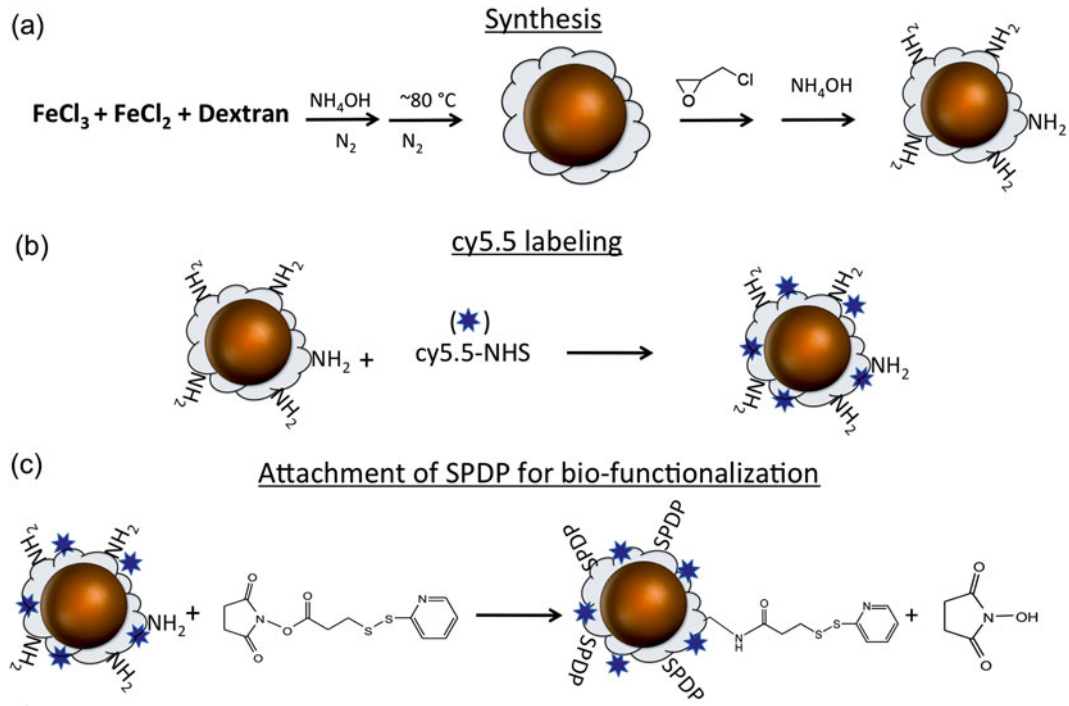

Fig. 1 Illustration represents the (**a**) synthesis and functionalization of aminated magnetic nanoprobe with (**b**) cy5.5 NIRF dye and (**c**) SPDP hetero-bifunctional linker

17. Later, 14 mL of epichlorohydrin is added into the reaction mixture. The resulting solution forms two liquid phases after the addition of epichlorohydrin which disappear after 8 h of stirring at room temperature, (*see* **Note 3**).
18. The resulting homogenous solution is then reacted with ammonium hydroxide to aminate the final nanoparticle composition. 60 mL of ammonium hydroxide (NH_4OH, 28 %) is added into the reaction. The reaction is stirred for 36 h at room temperature. The neck of the round bottom flask is capped with a rubber stopper to prevent ammonia from evaporating which is important for obtaining high-yield of amination.
19. After the reaction is over, the solution (~150 mL) is transferred into a dialysis bag (MWCO 12–14 kDa) and dialyzed against 4–6 L of distilled water in a beaker with constant stirring in a fume hood. Dialysis is repeated several times over 2 days to remove all the unreacted ammonium hydroxide and side products. After the dialysis against water is over, the ammonia smell from the dialysis bag disappears.
20. The resulting brown nanoparticle suspension is later concentrated to 20 mL using Amicon Ultra-15 centrifugal filter units (MWCO 30 kDa) in 20 mM of sodium citrate buffer at pH 8.0.
21. The size of the nanoparticle (~25 nm in diameter) is determined by dynamic light scattering using Zetasizer Nano ZS.
22. The iron content of the nanoparticles is calculated by the iron assay protocol described below.
23. The amination is quantified by SPDP (*N*-Succinimidyl 3-(2-pyridyldithio)propionate) conjugation and cleavage method. SPDP is a hetero-bifunctional linker reactive to amino and sulfhydryl groups. SPDP functionalized nanoparticles are cleaved by a reducing reagent (3 % TCEP) to release a detectable by product of pyridine-2-thione.
24. Quantification of pyridine-2-thione (P2T) is achieved by monitoring the maximum absorbance peak at 343 nm (extinction coefficient at 343 nm of 8.08×10^3/cm/M).
25. The number of P2T gives the number of reactive amine groups in the solution. The number of amine per nanoparticle can be calculated by the ratio of concentration of P2T versus nanoparticles.
26. Briefly an aliquot of nanoparticle suspension (100 μL) is diluted in 1000 μL of Phosphate Buffered Saline (PBS, pH 7.4)
27. The SPDP bottle is removed from freezer and equilibrated to room temperature before opening to avoid moisture accumulation in the bottle. This is important to prevent hydrolysis of the NHS ester of SPDP.

28. 1 mg of SPDP is dissolved in 100 μL of anhydrous DMSO. SPDP has limited water solubility therefore the nanoparticle solution is titrated into the SPDP solution (in DMSO) slowly in order to prevent crystallization of SPDP, (*see* **Note 4**).
29. After 24 h of incubation the nanoparticles are purified using disposable Sephadex PD-10 columns against PBS. The purified SPDP functionalized nanoparticles (~1000 μL) are incubated with 10 μL of 3 % TCEP to release pyridine-2-thione which is detectable by absorbance spectroscopy.
30. The nanoparticles are transferred into an Amicon filtration unit (0.5 mL, MWCO 100 kDa) and centrifuged in a microcentrifuge using ~10,000 × *g* (RCF) for 10 min. The eluent, containing the P2T, is recovered and used for amine quantification by UV–vis spectroscopy. The retained nanoparticle pellet on filter unit is discarded.
31. Typical number of amine terminals is determined to be between 60 and 90 per nanoparticle.
32. The amount of iron is determined using an iron assay described below using eight standard iron solutions and four samples.
33. 10 μL of iron standards and nanoparticle solution are added into 980 μL of 6 N HCl. 10 μL of hydrogen peroxide (H_2O_2, 30 % in H_2O) is added into each mixture. Blank sample is prepared by adding 10 μL of distilled water instead of iron standards into the 980 μL of 6 N HCl and 10 μL of H_2O_2. The iron oxide cores are digested during this process. The optical density (OD) at 410 nm values is determined by UV–vis spectroscopy. The calibration curve is obtained using the standards. The concentration of the iron content in the nanoparticle solution is determined using the obtained calibration curve.
34. The nanoparticle concentration is determined after measuring the iron concentration in the nanoparticle suspension by the assumption that each nanoparticle has an average of 2064 iron atoms per nanoparticle [12, 13]. The concentration is determined around 12 mg/mL which is equivalent to 100 μM nanoparticle solution.
35. The superparamagnetic iron oxide cores in the nanoparticles serve as T2-weightedMRI contrast agent. However, in order to provide in vivo fluorescence imaging modality, a near infrared fluorescent (NIRF) dye molecule is attached on the nanoparticle surface as described below.
36. The nanoparticles in PBS (pH 7.4) buffer are labeled with cy5.5 molecules (mono-reactive NHS ester), Fig. 1b.
37. Briefly, 1 mg of amine reactive cy5.5 mono-reactive NHS ester is dissolved completely in 100 μL of anhydrous DMSO and immediately added to the stock nanoparticle solution (10 mg

Fe, equivalent to ~1 mL) in 20 mM citrate buffer (pH 8.0). The solution is pipetted several times in order to obtain a homogenous solution mixture. The resulting blue colored mixture is left overnight in dark room on a rotator with constant rotation.

38. The nanoparticles are purified using disposable PD-10 columns against PBS (pH 7.4). Briefly ~1.1 mL of nanoparticles is added to PBS-equilibrated PD-10 column. After the nanoparticles are adsorbed by the column filter, PBS solution is added to elute the purified cy5.5 labeled nanoparticles. Formation of two green lanes in the column is the indication of the separation of cy5.5 conjugated nanoparticles and free cy5.5 in the mixture.
39. The first green elution containing labeled nanoparticles is collected and the second one with free dye is discarded.
40. After the cy5.5 conjugation the brownish colored nanoparticles gains a greenish color. The cy5.5 conjugation yield is quantified by measuring the optical density at 675 nm (extinction coefficient at 675 nm of 2.5×10^5/cm/M). Typically 4–5 cy5.5 molecules per nanoparticle is obtained after the conjugation step.
41. The purified nanoparticles are later conjugated to SPDP in order to provide thiol reactive terminals to nanoparticles for further conjugation steps, Fig. 1c.
42. The SPDP bottle is removed from freezer and equilibrated to room temperature before opening the bottle to avoid moisture accumulation in the bottle as indicated above.
43. 10 mg of SPDP is dissolved in 500 μL of anhydrous DMSO and used immediately. The cy5.5 labeled nanoparticle solution is titrated into the SPDP solution slowly. Fresh SPDP solution has to be prepared for each time since it hydrolyzes quickly.
44. After 24 h of incubation in the dark the nanoparticles are purified using disposable PD-10 column against PBS (pH 7.4) to remove free unreacted SPDP molecules.
45. The concentration of final nanoparticle solution is calculated using absorbance spectroscopy by monitoring the cy5.5 signals or performing iron assay.
46. The nanoparticles with thiol reactive ends are ready to be conjugated to the targeting peptide molecules with cysteine residue terminals or thiolated oligonucleotides, (*see* **Note 5**).
47. For instance; attachment of a cRGD peptide ~4.5 mg of cyclo (Arg-Gly-Asp-D-Phe-Lys-PEG-Cys) peptide is dissolved in 100 μL of PBS buffer and added to the cy5.5 and SPDP labeled nanoparticles. The solution is incubated at room temperature for 2 h.

48. The nanoparticles are purified by disposable PD-10 columns against PBS (pH 7.4).
49. Finally, the nanoparticles are attached to the thiolated siRNA or anti sense miRNA therapeutic oligonucleotides as described below.
50. The thiolated oligonucleotides are dissolved in nuclease-free water to a final concentration of 1 mM. The oligonucleotides are then treated with 3 % TCEP in order to activate the thiol groups by cleaving the protecting disulfide bonds in the oligonucleotide construct.
51. The 3 % TCEP is prepared freshly before each use. 100 μL of TCEP solution is added to the 1000 μL of oligonucleotide stock solution (1 mM) and incubated for a few minutes. Later the oligonucleotides are purified using ammonium acetate/ethanol precipitation method.
52. Briefly, 500 μL of 9.5 M ammonium acetate is added to the oligonucleotide mixture. Later, 2300 μL of cold ethanol (200 proof, molecular biology grade) is added to the mixture. The white cloudy oligonucleotide precipitation is observed in the tube. The solution is then left at −80 °C for 1 h.
53. Later, the oligonucleotide mixture is centrifuged at 4 °C for 15 min at 20,000 × *g* (RCF). A white oligonucleotide pellet forms at the bottom of the tube after the end of the centrifugation. The supernatant is discarded and the pellet is washed several times with 70 % ethanol.
54. The pellet is later dried by speed vacuum concentrator and resuspended in PBS (pH 7.4) to a final concentration of 1 mM.
55. The nanoparticles are mixed and incubated with activated oligonucleotides with a 1:10 or 1:8 M ratio in the cold room on a rotator at least 1 day.
56. The nanoparticle solution is filtered with a 0.22 μm syringe filter to remove any large contaminants.
57. For in vitro or in vivo studies, 100 μL of nanoparticles are purified using a G-50 Sephadex disposable quick spin columns in PBS (pH 7.4).
58. The concentration, size, magnetization, and oligonucleotide loading of the resulting MRI and fluorescently active therapeutic iron oxide nanoprobes are characterized using optical spectroscopy, dynamic light scattering, magnetic relaxometry, and gel electrophoresis.
59. The nanoparticles are concentrated using 0.5 mL Amicon filtration units (MWCO 100 kDa, Amicon Ultra-0.5 mL Centrifugal Filters) with centrifugation if necessary for in vivo studies.

3.2 Administration of Contrast Agents to Animals Bearing Breast Tumor

1. For animal studies 6-week-old female mice (nu/nu or NIH III nude) are housed in the animal facilities few days before performing any experiments.
2. MDA-MB-231-*luc*-D3H2LN metastatic breast cancer cell line is used for animal studies. MDA-MB-231-*luc*-D3H2LN cell line is derived from MDA-MB-231 human adenocarcinoma cells and transfected with the North American Firefly Luciferase gene for applications with in vivo bioluminescence imaging. The cell line is derived from lymph node metastasis from a D3H1 mammary fat pad tumor and used for orthotopic model for breast cancer metastasis.
3. The cell line is maintained and prepared for orthotopic injection according to the instructions of the supplier.
4. The tumor is implanted orthotopically by injecting ~2 million MDA-MB-231-*luc*-D3H2LN cells in 50 μL of PBS in the upper right mammary fat pad of the mice. The animals are anesthetized during this procedure.
5. After the tumor implant, the animals are housed in the animal facility of the institution and monitored daily for tumor growth by professional personnel. Any animal with discomfort and significant weight loss has to be euthanized.
6. Intravenous nanoparticle administration is performed 14 days after the tumor implant when the size of the tumor is approximately 5 mm in diameter.
7. The siRNA or antisense miRNA functionalized, cy5.5 labeled, magnetic nanoparticles (MN-cy5.5-oligo, ~100 μL of 2.5 mg Fe/mL in PBS pH 7.4, 10 mg Fe/kg body weight) are injected through the tail vein of the mice under anesthesia by professional animal specialist. The injection is repeated once a week for 4 weeks.
8. The animals are removed from anesthesia and put back in their cage after injection. The imaging studies are performed 24 h after injection.

3.3 In Vivo MRIImaging

1. MRI studies are performed using a 9.4 T Bruker horizontal bore scanner with Para Vision 5.1 software. This MRI scanner has high quality, high resolution anatomical imaging using various contrast mechanisms (T1, T2, diffusion, and perfusion). The imager is used primarily for rodent (rats and mice) studies, and has 9.4 T 21 cm diameter horizontal bore Magnex magnet, Magnex gradient coil set capable of 20 G/cm, and a Bruker BioSpin BioSpec/Avance dual RF channel multinuclear console. The scanner is equipped with a gas anesthesia unit that allows continuous administration of isoflurane gas for anesthetizing animals during the imaging.

2. MR Imaging is performed on animals before and 24 h after intravenous nanoparticle injection as described above. The animals are anesthetized before the imaging procedure. Afterwards the animals are placed in the RF coil engineered specifically for small animal studies. The MR imaging protocol with T2-weighted spin echo pulse sequences is used with the following parameters:

   Spin echo repetition time/echo time = 2000/[8, 16, 24, 32, 40, 48, 56, 64].

   Field of view (FOV) = 32×34 mm^2.

   Matrix size = 128×128 pixels.

   Slice thickness = 0.5 mm

   In plane resolution = 250×250 mm^2

3. The imaging of each animal is completed in approximately 30 min. The animals are placed in their cage after the imaging procedure is over and housed in the animal facility to recover from the stress that might occur during the imaging.
4. The T2-weightedMRI images of the tumor slices are constructed and analyzed using Marevisi 3.5 software before and after nanoparticle administration. Decrease in the T2 values (transverse relaxation time) is observed in the images of the tumor after nanoparticle injection suggesting accumulation of iron oxides in the tumor, Fig. 2.
5. T2-weightedMRIimage maps of the tumor are constructed by fitting the eight echo times (spin echo repetition time/echo time = 2000/[8, 16, 24, 32, 40, 48, 56, 64]) to a standard exponential decay curve.

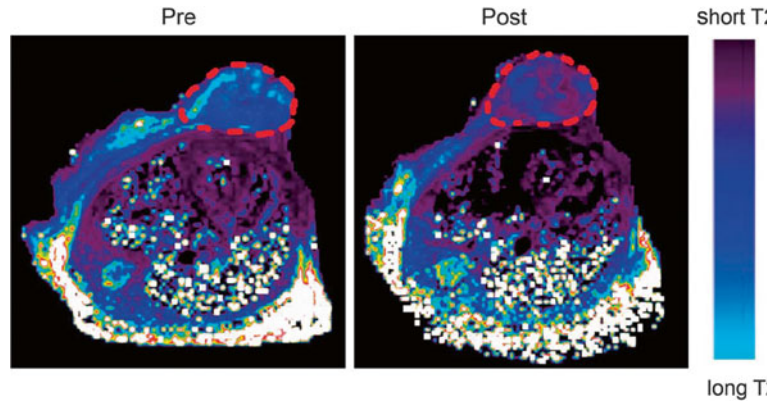

Fig. 2 T2-weighted color-coded transverse MRIimage of orthotopic MDA-MB-231-*luc*-D3H2LN tumor in mice before (pre) and after (post) nanoprobe administration. Shortening in the T2 values is an indication of nanoprobe accumulation in tumor. Reproduced from ref. 1 with permission from Nature Publishing Group

6. T2 values are calculated by manually selecting the tumor on MR images from each slice for each animal before (pre-injection) and after (post-injection) nanoparticle administration. Longitudinal relaxation rate ($R2 = 1/T2$) is calculated for each slice for pre- and post-injection. $\Delta R2$ is calculated by subtracting the R2 values of tumor images of pre- from post-injection.

3.4 In Vivo Fluorescence Optical Imaging

1. In vivo fluorescence optical imaging of whole body is performed using the Xenogen IVIS Spectrum in vivo imaging system. Quantitative in vivo optical imaging can be performed by monitoring of bioluminescent and/or fluorescent signals with this imaging system.
2. The imaging system allows noninvasive imaging of disease progression, cell migration and gene expression in living animals. The imaging system is also equipped with a gas anesthesia unit that allows continuous administration of isoflurane gas for anesthetizing animals during imaging.
3. The IVIS imaging system has 10 narrow band excitation filters (30 nm bandwidth) and 18 narrow band emission filters (20 nm bandwidth) that reduce autofluorescence through spectral scanning of filters and the use of spectral unmixing procedures. The imaging system is also equipped with Living Image 4.0 software which enables multicolor quantitative optical imaging.
4. Each animals is imaged with the IVIS imaging system before (pre-injection) and after (post-injection, 24 h later) nanoparticle administration right before or after the MR imaging, Fig. 3.
5. The animals are first anesthetized with isoflurane in the induction chamber of the gas anesthesia system (XGI-8 Gas Anesthesia Unit). The anesthesia system is composed of gas anesthesia module, induction chamber, and anesthesia manifold located in the IVIS system imaging chamber. The gas anesthesia module controls the gas flow in the induction chamber and manifold in the imaging chamber.
6. After the animals are anesthetized in the induction chamber, each animal is placed supine in the IVIS system imaging chamber with constant isoflurane flow. The temperature in the chamber is set to 37 °C for animal comfort.
7. The abdominal region of the animal is shielded with black paper or cloth in order to avoid interfering signal from internal organs predominantly from liver. Imaging is performed using 675 nm excitation and 720 nm emission filter suitable for the excitation and emission parameters of cy5.5 (Ex: 675 nm, Em: 695 nm) probe on the nanoparticle surface. The same set of

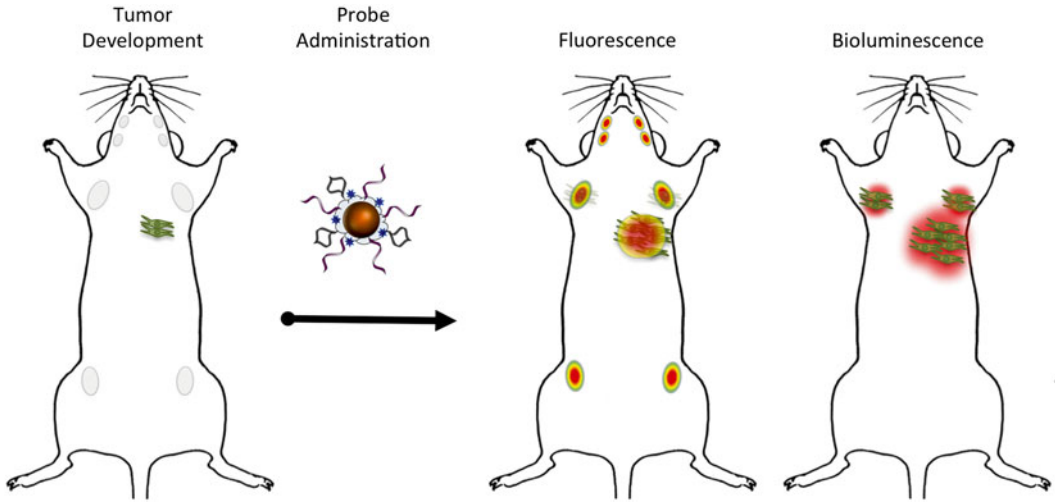

Fig. 3 Illustration of in vivo fluorescence and bioluminescence imaging of mice bearing orthotopic MDA-MB-231-*luc*-D3H2LN tumor after nanoprobe administration

parameters is used for pre- and post-injection when fluorescent images are acquired.

8. The fluorescent images and the grayscale photographs of mice are acquired and constructed after imaging is over using the Living Image 4.0 software, Fig. 4. The quantitation of the fluorescence reading is determined by segmenting out the tumor on the fluorescent images for each animal before and after nanoparticle injection.
9. The same imaging parameters and size of region of interest (ROI) are used for each animal for data analysis to ensure reliability and consistency in the results.
10. The animals are removed from the chamber and placed in their cage after the imaging is complete. Each animal scan takes approximately 10 min.

3.5 In Vivo Bioluminescence Imaging

1. In vivo whole body bioluminescence imaging is performed using the Xenogen IVIS Spectrum in vivo imaging system. The bioluminescence signals are generated by the luciferase expression in the MDA-MB-231-*luc*-D3H2LN cells.
2. In order to generate bioluminescence signal in the MDA-MB-231-*luc*-D3H2LN tumor, D-Luciferin bioluminescent substrate is needed.
3. D-Luciferin powder is dissolved in DPBS buffer (pH 7.4) to a final concentration of a 15 mg/mL and stored in the freezer as suggested by the supplier.
4. 200 μL of D-Luciferin (15 mg/mL) is injected in the lower left abdominal quadrant of the animals (150 mg D-Luciferin/kg

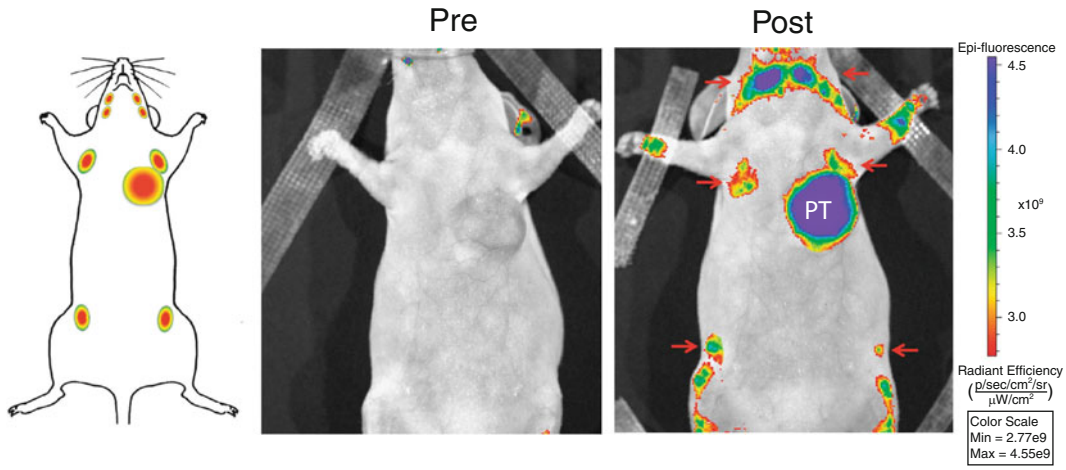

Fig. 4 In vivo fluorescence imaging of mice bearing orthotopic MDA-MB-231-*luc*-D3H2LN tumor before (pre) and after (post) nanoprobe administration. Reproduced from ref. 1 with permission from Nature Publishing Group

body weight) and the imaging was performed 10, 15 and 20 min after the D-Luciferin administration as suggested by the supplier in order to obtain maximum bioluminescence reading. According to instructions and our experience, imaging at minute 10 gives the optimum reading however the readings at other two time points are not significantly different, consistent with the supplier's instructions.

5. The bioluminescence readings are collected with the primary tumor however in order to determine the metastasis, migration and invasion of MDA-MB-231-*luc*-D3H2LN cells to the lymph node the primary tumor is shielded with a dark cloth or thick black paper and black tape to prevent signal leakage from primary tumor into the right brachial lymph nodes.
6. The bioluminescence imaging is performed with identical imaging settings (time = 30–60 s, F-stop = 2; binning = medium) and region of interest (ROI).
7. Total radiance flux of the signals are obtained from primary tumor and the lymph node with metastasis. Total radiance (photons/s) from the bioluminescence readings is used for signal quantification.
8. The bioluminescence images and the grayscale photographs of mice are acquired and constructed after imaging using the Living Image 4.0 software, Fig. 5.
9. The animals are sacrificed after the study according to the institutional regulations and instructions. Ex vivo studies are performed for characterization and quantification purposes however they are not described in this protocol.

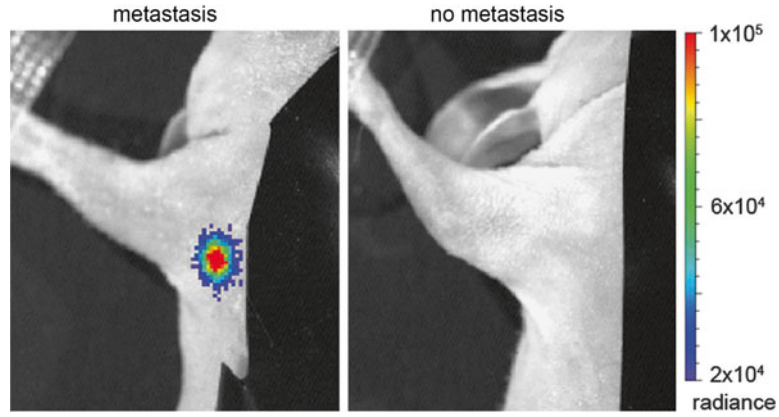

Fig. 5 In vivo bioluminescence lymph node imaging of mice bearing orthotopic MDA-MB-231-*luc*-D3H2LN tumor. The bioluminescence signal is an indication of metastasis, migration of MDA-MB-231-*luc*-D3H2LN cells to lymph nodes. Reproduced from ref. 1 with permission from Nature Publishing Group

4 Notes

1. The ferrous chloride tetrahydrate bottle has to be stored in a desiccator to minimize oxidation by air. The powder ferrous chloride should have a green color and formation of brown crystals in the bottle is an indication of iron oxidation—from Fe(II) to Fe(III)—which should be avoided for obtaining high quality superparamagnetic nanoparticles.
2. The experiments should be performed in a fume hood and safety precautions should be taken in order to minimize exposure to the chemicals used in the synthesis.
3. Health hazard information about epichlorohydrin should be read before its use.
4. Fresh SPDP solution has to be prepared each time.
5. It is important to avoid any disulfide reducing agents including DTT (dithiothreitol) or TCEP residues or contamination in the mixture to maintain the activity of SPDP on the nanoparticle.

References

1. Yigit MV, Ghosh SK, Kumar M, Petkova V, Kavishwar A, Moore A et al (2013) Context-dependent differences in miR-10b breast oncogenesis can be targeted for the prevention and arrest of lymph node metastasis. Oncogene 32:1530–1538
2. Laurent S, Saei AA, Behzadi S, Panahifar A, Mahmoudi M (2014) Superparamagnetic iron oxide nanoparticles for delivery of therapeutic agents: opportunities and challenges. Expert Opin Drug Deliv 11:1449–1470
3. Caruso F, Hyeon T, Rotello VM (2012) Nanomedicine. Chem Soc Rev 41:2537–2538
4. Yoo B, Ifediba MA, Ghosh S, Medarova Z, Moore A (2014) Combination treatment with theranostic nanoparticles for glioblastoma sensitization to TMZ. Mol Imaging Biol 16:680–689

5. Ifediba MA, Moore A (2012) In vivo imaging of the systemic delivery of small interfering RNA. Wiley Interdiscip Rev Nanomed Nanobiotechnol 4:428–437
6. Robertson NM, Yigit MV (2014) The role of microRNA in resistance to breast cancer therapy. Wiley Interdiscip Rev RNA 5:823–833
7. Ghosh SK, Yigit MV, Uchida M, Ross AW, Barteneva N, Moore A et al (2014) Sequence-dependent combination therapy with doxorubicin and a survivin-specific small interfering RNA nanodrug demonstrates efficacy in models of adenocarcinoma. Int J Cancer 134:1758–1766
8. Kumar M, Yigit M, Dai G, Moore A, Medarova Z (2010) Image-guided breast tumor therapy using a small interfering RNA nanodrug. Cancer Res 70:7553–7561
9. Wang P, Yigit MV, Medarova Z, Wei L, Dai G, Schuetz C et al (2011) Combined small interfering RNA therapy and in vivo magnetic resonance imaging in islet transplantation. Diabetes 60:565–571
10. Wang P, Yigit MV, Ran C, Ross A, Wei L, Dai G et al (2012) A theranostic small interfering RNA nanoprobe protects pancreatic islet grafts from adoptively transferred immune rejection. Diabetes 61:3247–3254
11. Yoo B, Ghosh SK, Kumar M, Moore A, Yigit MV, Medarova Z (2014) Design of nanodrugs for miRNA targeting in tumor cells. J Biomed Nanotechnol 10:1114–1122
12. Kircher MF, Mahmood U, King RS, Weissleder R, Josephson L (2003) A multimodal nanoparticle for preoperative magnetic resonance imaging and intraoperative optical brain tumor delineation. Cancer Res 63:8122–8125
13. Pittet MJ, Swirski FK, Reynolds F, Josephson L, Weissleder R (2006) Labeling of immune cells for in vivo imaging using magnetofluorescent nanoparticles. Nat Protoc 1:73–79

Chapter 14

Microvesicles: Isolation, Characterization for In Vitro and In Vivo Procedures

Karmele Valencia and Fernando Lecanda

Abstract

Microvesicles and exosomes are released to the extracellular milieu and are detectable in body fluids. They act as unique vehicles for cargo transfer to other cells/tissues. They contain a set of membrane receptors, intracellular proteins and nucleic acids. Here, we describe basic techniques for their isolation and characterization from cell culture media or body fluids. We also describe critical techniques for characterizing their cargo (miRNAs) and their protein content. Finally, we present labeling methods for their use in in vitro procedures and for their in vivo delivery and subsequent analysis of their cargo transfer to multiple cell types.

Key words Exosome, Microvesicle, Nanoparticle

1 Introduction

Exosomes are small (30–150 nm) membrane vesicles of endocytic origin that are released by a variety of cells to the extracellular milieu by fusion of multivesicular bodies with the plasma membrane [1, 2]. The composition of exosomes depends on the cell of origin, although the membrane composition remains distinct from its parental cell as a result of a selective process of assembly, enabling specialized functions [3]. Exosomes contain a set of nucleic acids including miRNAs and mRNAs which could be transferred to target cells [4] inducing regulatory changes [5] under physiological conditions. Current estimate of microvesicle concentration in the peripheral blood of healthy individuals is 5–50 μg/ml; the majority of it has its origin in platelets [6]. Yet, this process could be deeply altered in different pathological settings such as immune response, inflammation, tumor progression and tissue repair. Exosome-mediated cargo transfer to adjacent or remote cells could deeply influence disease progression. This mechanism of intercellular communication is especially relevant in cancer. Accumulated evidence

Zdravka Medarova (ed.), *RNA Imaging: Methods and Protocols*, Methods in Molecular Biology, vol. 1372,
DOI 10.1007/978-1-4939-3148-4_14,

indicates the potential role of exosomes as non-invasive biomarkers with prognostic or diagnostic role, as they can be detected in body fluids [7, 8].

A lot of information about exosome-specific signatures, especially disease related can be obtained from the ExoCarta complendium of exosomal proteins and RNA [9].

In this chapter we have assembled and adapted several protocols for (a) the isolation of exosomes from conditioned medium, (b) the characterization of their nucleic acid cargo and hallmark proteins, (c) the measurement of their size and particle number, and (d) the fluorescent labeling for in vitro and in vivo tracking purposes [10].

2 Materials

1. Ultracentrifuge plastic tubes were 25 × 89 mm, Ref. #326823 for a SW40 rotor of a Beckman Optima™ LE-80K ultracentrifuge. For the recovery of exosomes we used conical 35 ml ultracentrifuge tubes (Beckman Ref #358126) with their adaptors Ref #358156.
2. The transmission electron microscope was from Philips CM120 BioTwin. The copper grids carbon coated were EMS CF300-Cu from Aname.
3. The 4 μm latex beads were purchased from Invitrogen (Ref# A37304).
4. Prepare all solutions using ultrapure water (prepared by purifying deionized water to attain a resistivity of 18 MΩ cm at 25 °C) and analytical grade reagents.
5. DEPC water was obtained by dissolving for 12 h at 37 °C 0.1 g in 100 ml of deionized water and subsequently autoclaved.
6. PBS and molecular grade BSA were purchased from Sigma. To prepare PBS/5 % BSA solution, 5 g of BSA were dissolved in 100 mL of PBS prewarmed at 37 °C by gently stirring and filtered by 0.22 μm.
7. Penicillin/streptomycin solution (Sigma, Ref # P0781-100 ML).
8. RIPA lysis buffer 1×: for 50 mL: 5 ml of 10 % NP-40 detergent solution, 1.5 ml of 5 M NaCl, 2.5 ml of 1 M Tris pH:7.4, 200 μl of 0.25 M EDTA and ~41 ml of ultrapure H_2O. Add protease inhibitors as follows: 10 μl of PMSF (20 mg/ml), 10 μl of 0.5 M NaF, 5 μl of 200 mM $NaVO_3$, and a Protease inhibitor cocktail tablet (Roche, Ref# 11 836 170 001).
9. TRIZOL LS Reagent® was from Life Technologies.

10. Red Blood Lysis Buffer, MINI26 cell linker kit and PKH67 Green Fluorescent Cell Linker Mini Kit (ref #MINI67) were purchased from Sigma.
11. Glycogen was from Ambion.
12. ExoQuick™ was from Systems Biosciences.
13. Phycoeritrin was purchased from Jackson Inmuno Research, (cat# 016110-084).
14. Anti-CD63 anti-human antibody was purchased from BD Biosciences (Ref #556019).
15. Anti-IG2 goat biotinylated anti-mouse antibody was from Dako.
16. INMMUNO solution was contained PBS, 1 % BSA, 0.1 % Tween 20 and 0.2 % DAPI.
17. Vectashield® was purchased from Vector Laboratories.
18. Automacs buffer was obtained by dissolving 2.5 ml FBS, 2.5 ml of 0.5 M EDTA, 5 ml of penicillin/streptomycin solution (Sigma, Ref # P0781-100 ML) in 500 ml of PBS.

3 Methods

3.1 Isolation of Exosomes from Cells in Culture

3.1.1 Preparation of Exosome-Depleted Medium

Work under sterile conditions all along these procedures (*see* **Note 1**).

1. Thaw 50 ml aliquot of complement inactive fetal calf serum (FCS) and mix it with 160 ml of regular serum-free medium used in cell culture. This will allow filling six tubes (35 ml per tube).
2. Use the Beckman plastic tubes.
3. Complete to 35 ml each tube and equilibrate with a balance.
4. Centrifuge 110,000 × *g* at 4 °C overnight (12–16 h) on an ultracentrifuge (*see* **Note 2**).
5. Recover carefully the supernatant. The pellet is invisible.
6. Filter through a 0.22 μm filter on sterile conditions.
7. Add serum-free medium and antibiotics (if needed) to obtain the regular complete medium used in cell culture.

This complete medium is used to culture the cells and can be stored at 4 °C for 1 month.

3.1.2 Purification of Exosomes from Cultured Cells (Fig. 1) (See Note 3)

1. Cells should be growing exponentially until 80 % confluence. The medium should contain exosome-free FCS prepared as previously described in Subheading 3.1.1. Use the best culture conditions to minimize cellular debris as much as possible (*see* **Notes 4** and **5**).

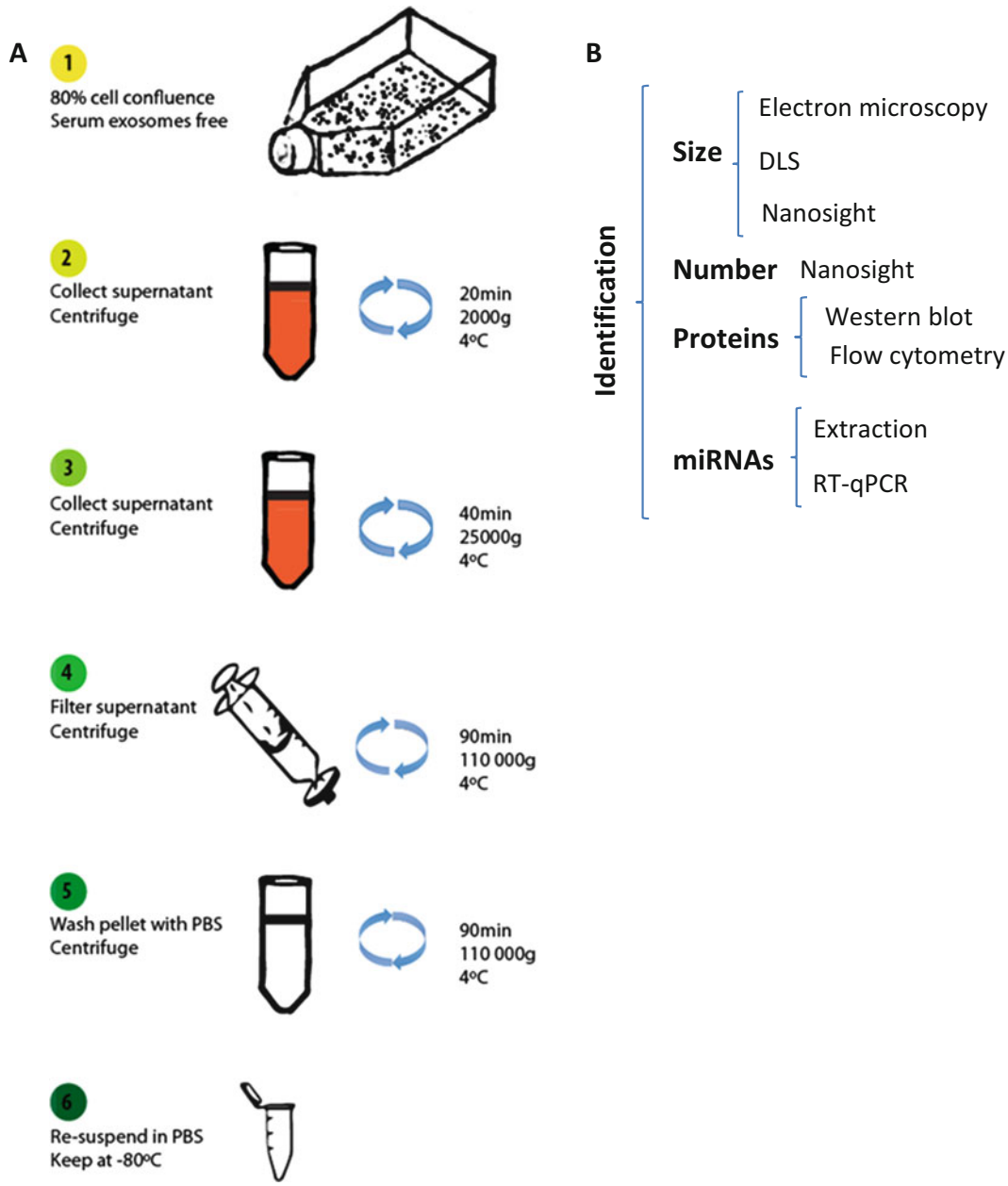

Fig. 1 Procedure for exosome isolation and characterization techniques. (**a**) Schematic of exosome isolation. (**b**) Basic techniques required for the physical characterization and their miRNA and protein cargo

2. Collect 48–96 h -supernatant after the last medium change performed in complete medium. We use 10 ml per T-75 flask. Usually we collect six T-75 flasks to obtain 60 ml of conditioned medium (*see* **Note 6**).
3. Centrifuge supernatant at 2000 × *g* for 20 min at 4 °C to spin down cell debris and death cells.

4. Recover supernatant.
5. Ultracentrifuge supernatant at 25,000 × *g* for 40 min at 4 °C to eliminate large microvesicles on an SW40 rotor or similar (*see* **Note 7**).
6. Recover and filter the supernatant through 0.22 μm pore filters.
7. Ultracentrifuge supernatant at 110,000 × *g*, 90 min, 4 °C using conical tubes and adaptors. This is crucial to ensure a good recovery of the invisible pellet.
8. Discard supernatant and wash the pellet with PBS, first resuspend in 1 ml and then add 29 ml. Note that the pellet is not visible.
9. Ultracentrifuge supernatant at 110,000 × *g*, 90 min, at 4 °C.
10. Discard supernatant and resuspend pellet in 50–100 μl of sterile PBS in each tube and the collect the content of exosomes from six tubes on a regular 1.5 ml tube.
11. Store and keep at −80 °C (**Notes 7** and **8**).

3.1.3 Micorvesicle Imaging by TEM

1. Use transmission electronic microscopy (TEM) copper grids carbon coated.
2. Perform vacuum electrical discharge (glow discharge technique) so grids become temporarily hydrophilic.
3. Put a 5 μl drop of each sample at the right concentration on a parafilm and invert grid on it.
4. Leave 1 min at room temperature to allow adherence.
5. Dry the drop with a Whatman paper and invert the grid over a 5 μl drop of 2 % uranyl acetate.
6. Leave 30 s at room temperature.
7. Repeat dye if necessary.
8. Remove uranyl acetate and let the grid dry.
9. Samples were assessed using a transmission electron microscope. Images were captured by a digital Olympus SIS camera.

3.1.4 Assessment of Particle Size and Number

A couple of techniques are important to measure the number and the size of the particles. It is important to carefully measure the exact number of cells and/protein from which exosomes were isolated for normalization purposes. These measurements are becoming mandatory in any research involving microvesicles or exosomes.

Step 1: Dynamic light scattering (DLS) and zeta potential determinations can be performed using a Zetasizer nanoseries instrument (Malvern Nano-Zetasizer). Add always same exosome concentration diluted in PBS (around 50 ng/μl). * Pick should appear between 30 and 120 nm (Fig. 1).

Step 2: Nanoparticle tracking analysis (NTA) measurements can be performed with a NanoSight LM20 instrument (NanoSight). The samples should be diluted at 2–5 ng/ ml and injected with a sterile syringe until the liquid reaches the tip of the nozzle.

3.2 Exosome Characterization

This protocol should be performed at 4 °C (*see* **Note 9**).

3.2.1 By Flow Cytometry: CD63

1. 5 μl exosomes + 5 μl latex beads 4 % w/v. *Less amount of exosomes is possible. Keep [exosome: bead] at 1:1 ratio.
2. Incubate 30 min and resuspend every 5 min by gentle pipetting.
3. Add 400 μl of [PBS/5 % BSA] solution.
4. Incubate 30 min and resuspend every 5 min by gentle pipetting.
5. Centrifuge 1000 × *g* for 10 min at 4 °C.
6. Discard supernatant and resuspend pellet in 50 μl de [PBS/5 % BSA] solution.
7. Incubate with first antibody diluted at 1/50 1 h, 4 °C (anti-CD63 anti-human antibody).
8. Wash twice with 400 μl [PBS/5 % BSA] solution.
9. Centrifuge at 1000 × *g* for 10 min at 4 °C.
10. Discard supernatant and leave exosomes with beads resuspended in 200 μl of PBS/5 % BSA.
11. Incubate with secondary biotinylated antibody diluted at 1/200 for 30 min at 4 °C (anti-IG2 goat biotinylated anti-mouse antibody).
12. Wash twice with 400 μl [PBS/5 % BSA] solution.
13. Centrifuge at 1000 × *g* for 10 min at 4 °C.
14. Discard supernatant and resuspend pellet in 50 μl solution [PBS/5 % BSA].
15. Add streptavidin with phycoerythrin (×28) 1/50 and incubate for 30 min in darkness.
16. Wash twice with 400 μl PBS (without BSA).
17. Centrifuge at 1000 × *g* for 10 min at 4 °C.
18. Resuspend in 300 μl PBS and perform FACS analysis.

3.2.2 By Western Blot

Use 25 μg of proteins from the isolated exosomes and add 10× RIPA buffer to a final 1× concentration. Add protein loading buffer, boil the samples, and run a regular SDS-PAGE gel.

3.2.3 miRNA Extraction from Conditioned Media

Before engaging into large experiments, we suggest comparing the protocol below with other commercially available extraction methods such as ExoQuick™ (*see* **Note 10**)

Similarly, the analysis of total miRNAs in the conditioned medium should be compared with the miRNA cargo of isolated exosomes. In our case, the free miRNA is negligible as compared to the miRNA cargo in exosomes.

Here, we describe the analysis in the conditioned media.

1. Use 15 ml tubes for the miRNA extraction of 48–96-h cultured cells as previously stated. Use three tubes per cultured sample, and add 1.6 ml conditioned medium in each tube.
2. Add 2 ml of TRIZOL LS Reagent®. Vortex and leave 5 min at room temperature.
3. Add 2 μl spike for each miRNA (each miRNA at 25 fmol concentration) of three different miRNAs per sample for normalization purposes. A total 6 μl per tube.
4. Add two volumes of chloroform (400 μl per tube) and leave for 3 min at room temperature.
5. Centrifuge at 3500 × *g* for 15 min at 4 °C.
6. Carefully take the upper aqueous phase (~2 ml) to another clean 15 ml tube.
7. Add 3 μl of glycogen at a concentration of 5 mg/ml in RNase-free water.
8. Add one volume of isopropanol (2 ml).
9. Mix and distribute in 1.5 ml tubes.
10. Centrifuge 12,000 × *g* for 10 min at 4 °C.
11. Wash the pellet with 1 ml of cold ethanol 75 % and spin for 5 min, 7500 × *g* at 4 °C.
12. Discard the supernatant.
13. Dry the pellet at room temperature.
14. For each original sample (which is distributed in three tubes), resuspend in 30 μl of DEPC water and store at −80 °C (*see* **Note 11**).

3.3 Tracking Microvesicles in Functional Assays (Fig. 2)

For in vitro applications, we use the MINI26 cell linker kit, which incorporates a red fluorescent dye into lipid regions of the cell membrane.

Perform the protocol after **step 7**, Subheading 3.1.2, right before PBS washing step (*see* **Note 12**).

3.3.1 Fluorescence Microvesicle Labeling

Method 1: Exosome Labeling with PKH 26

1. Add diluent C to exosomes to reach a final concentration 2×10^7 particles/ml, i.e., derived from 1×10^6 cells and add 50 μl diluent C.
2. Immediately prior to staining, prepare a volume of 2× PKH26 (4×10^{-6} M) in diluent C.
3. Rapidly add volume of 2× Dye to exosomes.

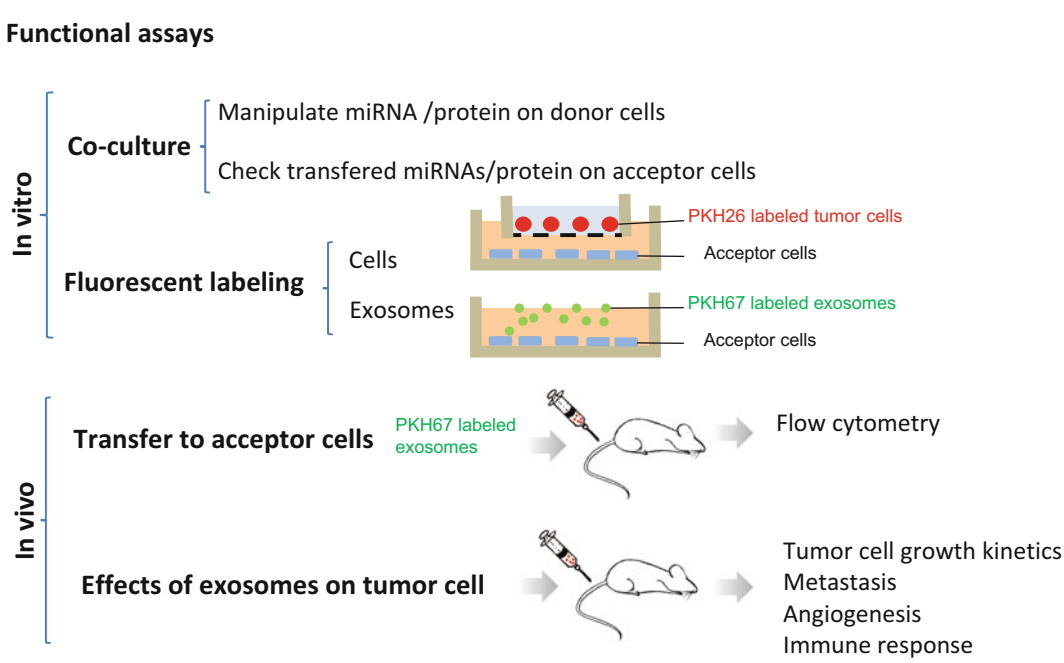

Fig. 2 In vitro and in vivo functional assays for donor–acceptor transfer

4. Final concentration: particles: 2×10^7 exosomes/ml PKH26: 2×10^{-6} M.
5. Immediately mix the sample by pipetting. Rapid and homogeneous mixing is critical for uniform labeling because staining is nearly instantaneous.
6. Incubate at room temperature for 7 min in the darkness.
7. Stop the staining reaction by adding an equal volume of serum or compatible protein solution (i.e., 1 % BSA). Incubate 1 min.
8. Add complete medium to the top of the tube.
9. Centrifuge exosomes at 11,000 × g for 90 min at 4 °C.
10. Discard supernatant and wash pellet with PBS.
11. Centrifuge exosomes at 11,000 × g for 90 min at 4 °C.
12. Discard supernatant and resuspend stained exosomes in 50 µl de PBS.
    Keep exosomes at −80 °C.

Method 2: Exosome Labeling with PKH67

We use the PKH67 Green Fluorescent Cell Linker Mini Kit.

Perform the protocol after **step 7**, Subheading 3.1.2, right before PBS washing step (*see* **Note 12**).

1. Take 100 µl resuspended exosomes in PBS.
2. Add 500 µl of solution C [2 µl PKH67 + 448 µl solution C].

3. Add PKH67 to exosomes and mix by pipetting up and down.
4. Incubate for 2 min at room temperature.
5. Neutralize with 1 ml [PBS/20 % BSA].
6. Incubate for 1 min at room temperature.
7. Add PBS to fill the centrifuge tube (~25 ml) in conical tubes and adaptors recommended.
8. Centrifuge 11,000 × *g* for 90 min at 4 °C.
9. Remove supernatant.
10. Wash with PBS.
11. Centrifuge at 11,000 × *g* for 90 min at 4 °C.
12. Remove supernatant.
13. Resuspend exosomes in 100 μl.
14. Store exosomes at −80 °C.

3.3.2 Evaluation of In Vitro Uptake of Exosomes

1. Treat a rounded cover slide for a p-24 with 0.2 % gelatin over 20 min at 37 °C.
2. Remove gelatin and let dry under the hood.

Day 1

3. Plate 2×10^5 of recipient cells per well.

Day 2

1. Treat cells with 5–10 μg exosomes for 24 h (or other timing: 1, 5, 24 h).

Day 3

1. Carefully wash the cells twice with PBS by slowly dropping the PBS through the tissue culture wall and fix them in 1 % paraformaldehyde for 15 min.
2. Wash twice with PBS and plate can be kept for 1 week at 4 °C.
3. Incubate for 30 min at 4 °C with INMUNO solution in dark 40 μl Immuno solution drops on a parafilm®.
4. Wash cover slide twice with PBS.
5. Mount with Vectashield®. Evaluate experiment on a fluorescence microscope.

3.3.3 Evaluation of In Vivo Uptake of Exosomes

After in vivo injection of exosomes, we used this protocol to evaluate the fluorescent in vivo uptake into several cell subpopulations of the bone marrow (Fig. 2) (*see* **Note 13**).

1. Label exosomes with PKH67, as detailed previously.
2. Quantify exosome protein of isolated exosomes.
3. Intravenously inject (i.v.) the mice with 10 μg in 100 μl fluorescently labeled exosomes and wait 4 h. Control mice will be i.v. injected with 100 μl PBS.

4. Sacrifice mice and isolate the bone marrow by bone marrow "flushing" technique as follows:
   (a) Damped briefly death mice in ethanol 70 %.
   (b) Excised long bones from the hind limbs, perfectly clean from surrounding tissue and keep bones on α-MEM with no FCS.
   (c) Cut with scissors both bone ends. Handle the bones with tweezers.
   (d) Use a 27 G needle for flushing the bone marrow with a syringe containing 5 ml of serum-free α-MEM medium and collect it on a 50 ml tube. The bone will appear as a vivid white color.
   (e) Spin cells to 600 × *g* for 10 min at 4 °C and discard supernatant.
   (f) Gently resuspend the pelleted cells in complete medium [α-MEM/10 % FBS/1 % penicillin/streptomycin solution] ten times with a 18 G needle to disaggregate cell clumps, and filter the cell suspension through a 70 μm cell strainer to retain cellular debris.
   (g) Spin cells at 600 × *g* for 10 min at 4 °C.
5. Resuspend cells on 5 mL of red blood lysis buffer and leave 5 min at 37 °C.
6. Neutralize lysing buffer with 5 mL complete medium.
7. Spin cells at 600 × *g* for 10 min at 4 °C.
8. Resuspend cells in PBS and count the cells.
9. Spin cells to 900 × *g* for 10 min at 4 °C.
10. Resuspend in Automacs Buffer and maintain at 4 °C until use.
11. For different subpopulation sorting, plate 100 μl (2×10^6 cells) in a U-bottom 96-well plate.
12. Add diluted antibody that works for flow cytometry (*see* **Note 14**).
13. Incubate for 15 min at 4 °C in the dark.
14. Centrifuge at 800 × *g* for 2 min at 4 °C.
15. Discard supernatant and resuspend pellet in 100 μl Automacs buffer.
16. Take volume to a cytometer tube and raise volume to 300 μl.
17. Use flow cytometer.

4 Notes

1. Sterilize ultracentrifuge tubes and adaptors under UV light for 15 min. To avoid contamination be careful with the tissue culture technique. Serum used to complement cell medium used all along this procedure must be exosome-depleted.
2. Before operating the centrifuge, operators should be carefully instructed on its use. Several key points should scrupulously be observed. For instance, the way of handling the rotor, the type of tubes to be used, filling the tubes almost to the top, and the equilibration of the tubes using a balance are critical measures to be taken before each ultracentrifugation.
3. Before choosing the cell line of study it is worthy to check the amount of exosomes secreted by each cell line. Please note that the amount of secreted exosomes is cell-line dependent.
4. Since stress conditions could increase the exosome secretion, it is important to keep and regularly check that all cell culture conditions (CO_2, humidity, pH, mycoplasma-free, etc.) are exquisitely maintained all along different extraction procedures.
5. We use a six conical 35 ml ultracentrifuge tubes (Beckman Ref #358126) with their adaptors Ref #358156. We distributed 60 ml of CM, leaving 30 ml of conditioned medium per tube.
6. The amount of T-75 flasks will depend on the amount of exosomes secreted by the chosen cell line. For some cell lines, one flask could be enough.
7. It is recommended to check the quality of the exosome purification with other methods commercially available such as ExoQuick® or Dynabeads®.
8. It is recommended to perform protein quantification with small aliquot in each round of isolation (we used 3 μl of exosome suspension).
9. Use a negative control running the same protocol but skipping **step 7**.
10. Before starting to work with RNA, clean all the bench surfaces with ethanol 70 % and an RNase solution (RNase away, Molecular BioProducts). Special care should be put during isolation and analysis of miRNA. All solutions should be prepared using RNase-free glassware, autoclaved water and chemicals reserved to work with RNA. Disposable gloves should be worn all along these procedures. Diligently follow all waste disposal regulations when disposing waste materials. DEPC should be handled with care in a fume hood.

11. For each sample, add the DEPC water in the first tube, resuspend and transfer to the second tube, and resuspend and pass to the third tube.
12. Work in low light conditions since fluorescent dyes are photosensitive.
13. This protocol could be adapted to other cell types as long as the antibody specific of this cellular phenotype works on flow cytometry.
14. The dilution of each antibody should experimentally adjusted.

Acknowledgment

This work was supported by the Spanish Ministry of Economy and Competitiveness SAF2012-40056 to F.L, "UTE project FIMA" agreement, the Cancer Research Thematic Network of the Health Institute Carlos III (RTICC RD12/0036/0066), European Regional Development Fund (ERDF) "Una manera de hacer Europa."

References

1. Simons M, Raposo G (2009) Exosomes: vesicular carriers for intercellular communication. Curr Opin Cell Biol 21(4):575–581. doi:10.1016/j.ceb.2009.03.007
2. Mittelbrunn M, Sanchez-Madrid F (2012) Intercellular communication: diverse structures for exchange of genetic information. Nat Rev Mol Cell Biol 13(5):328–335. doi:10.1038/nrm3335
3. Muralidharan-Chari V, Clancy JW, Sedgwick A, D'Souza-Schorey C (2010) Microvesicles: mediators of extracellular communication during cancer progression. J Cell Sci 123(Pt 10):1603–1611. doi:10.1242/jcs.064386
4. Valadi H, Ekstrom K, Bossios A, Sjostrand M, Lee JJ, Lotvall JO (2007) Exosome-mediated transfer of mRNAs and microRNAs is a novel mechanism of genetic exchange between cells. Nat Cell Biol 9(6):654–659. doi:10.1038/ncb1596
5. Ratajczak J, Miekus K, Kucia M, Zhang J, Reca R, Dvorak P, Ratajczak MZ (2006) Embryonic stem cell-derived microvesicles reprogram hematopoietic progenitors: evidence for horizontal transfer of mRNA and protein delivery. Leukemia 20(5):847–856. doi:10.1038/sj.leu.2404132
6. Hunter MP, Ismail N, Zhang X, Aguda BD, Lee EJ, Yu L, Xiao T, Schafer J, Lee ML, Schmittgen TD, Nana-Sinkam SP, Jarjoura D, Marsh CB (2008) Detection of microRNA expression in human peripheral blood microvesicles. PLoS One 3(11):e3694. doi:10.1371/journal.pone.0003694
7. Yu L, Todd NW, Xing L, Xie Y, Zhang H, Liu Z, Fang H, Zhang J, Katz RL, Jiang F (2010) Early detection of lung adenocarcinoma in sputum by a panel of microRNA markers. Int J Cancer 127(12):2870–2878. doi:10.1002/ijc.25289
8. Zen K, Zhang CY (2012) Circulating microRNAs: a novel class of biomarkers to diagnose and monitor human cancers. Med Res Rev 32(2):326–348. doi:10.1002/med.20215
9. Mathivanan S, Fahner CJ, Reid GE, Simpson RJ (2012) ExoCarta 2012: database of exosomal proteins, RNA and lipids. Nucleic Acids Res 40(Database issue):D1241–D1244. doi:10.1093/nar/gkr828
10. Valencia K, Luis-Ravelo D, Bovy N, Anton I, Martinez-Canarias S, Zandueta C, Ormazabal C, Struman I, Tabruyn S, Rebmann V, De Las RJ, Guruceaga E, Bandres E, Lecanda F (2014) miRNA cargo within exosome-like vesicle transfer influences metastatic bone colonization. Mol Oncol 8(3):689–703. doi:10.1016/j.molonc.2014.01.012

Chapter 15

Positive Bioluminescence Imaging of MicroRNA Expression in Small Animal Models Using an Engineered Genetic-Switch Expression System, RILES

Patrick Baril and Chantal Pichon

Abstract

MicroRNAs (miRNAs) are a class of small, noncoding RNAs which regulate gene expression by directing their target mRNA for degradation or translational repression. Since their discovery in the early 1990s, miRNAs have emerged as key components in the posttranscriptional regulation of gene networks, shaping many biological processes from development, morphogenesis, differentiation, proliferation and apoptosis. Although understanding of the molecular basis of miRNA biology is improving, methods to monitor the dynamic and the spatiotemporal aspects of miRNA expression under physiopathological conditions are required. However, monitoring of miRNAs is difficult due to their small size, low abundance, high degree of sequence similarity, and their dynamic expression pattern which is subjected to tight transcriptional and post-transcriptional controls. Recently, we developed a miRNA monitoring system called RILES, standing for RNAi-inducible expression system, which relies on an engineered regulatable expression system, to switch on the expression of the luciferase gene when the targeted miRNA is expressed in cells. We demonstrated that RILES is a specific, sensitive, and robust method to determine the fine-tuning of miRNA expression during the development of an experimental pathological process in mice. Because RILES offers the possibility for longitudinal studies on individual subjects, sharper insights into miRNA regulation can be generated, with applications in physiology, pathophysiology and development of RNAi-based therapies. This chapter describes methods and protocols to monitor the expression of myomiR-206, -1, and -133 in the tibialis anterior muscle of mice. These protocols can be used and adapted to monitor the expression of other miRNAs in other biological processes.

Key words microRNA, Molecular imaging, Bioluminescence study, Spatiotemporal regulation, RILES (RNAi-inducible luciferase expression system)

1 Introduction

MiRNAs are a class of noncoding RNA molecules that control the expression of target genes at the posttranscriptional level [1]. In the canonical miRNA pathway, miRNA genes are transcribed by polymerase II and/or III from endogenous genes either from individual transcriptional units (intergenic miRNAs) or in frame with host genes (intronic miRNAs). They are processed in the

Zdravka Medarova (ed.), *RNA Imaging: Methods and Protocols*, Methods in Molecular Biology, vol. 1372,
DOI 10.1007/978-1-4939-3148-4_15,

nucleus as long primary miRNA (pri-miRNA) transcripts before being shortened as precursor (pre-miRNA) transcripts of approximately 70 nucleotides by a first endoribonuclease complex consisting of Drosha and DGCR8. The pre-miRNAs are exported into the cytoplasm by the Exportin-5/Ran-GTP complex and then cleaved by a second endoribonuclease complex, DICER/TRBP, to produce a 20–22-nucleotide-long duplex RNA molecule. This miRNA duplex consists of the mature miRNA, called the guide strand and a less thermostable strand, called the passenger strand which is believed to be degraded. The single-stranded mature miRNA interacts with Argonaute proteins before being loaded in the RLC (RISC loading complex) composed of DICER/TRBP and Argonaute 2 bound to the mature miRNA. In the RLC complex, the miRNA binds to the mRNA target sequence through a perfect (100 % homology) or imperfect (less than 100 % homology) complementary base pairing mechanism, often located on the 3′-UTR part of the target mRNAs. According to the degree of homology, the mRNA is either degraded or the translational machinery is blocked inducing mRNA deadenylation and/or decapping [1].

Research in the field of noncoding RNA has advanced rapidly since the discovery of miRNA in the early 1990s [2]. It is known that the human genome encodes for at least 1200 miRNA genes and that at least 60 % of the transcriptome is under the control of miRNAs. Therefore, it is not surprising that almost all biological processes are directly or indirectly influenced by miRNAs [3] and that deregulated expression of miRNAs has also been found to be associated with human diseases, thus paving the way for novel therapeutic interventions [4].

An important aspect of miRNA function is that their regulation is highly dynamic, subject to tight, spatial, and temporal transcriptional controls which in turn fine-tune the expression of gene networks [5, 6]. The underestimation of these features results in the loss of important information linking miRNA expression to cell function. It is therefore crucial to know the repertoire of miRNAs and how their expression changes in response to cellular environments in order to improve understanding of their biological functions.

Several detection methods have been developed to monitor miRNA expression. These include Northern-blot, real-time PCR, microarray, in situ hybridization, and more recently deep sequencing and biochemical pull-down approaches [7]. At the same time, over the last 10 years, noninvasive molecular imaging methods have been developed to monitor the expression of miRNAs, in real time and noninvasively in small animal models. These methods can be subtyped into two classes according to the nature of the probes used. The first class includes synthetic probes composed mainly of molecular beacons, consisting in fluorescent oligonucleotide

sequences, which on binding to a complementary mature miRNA sequence can emit fluorescence. The second class includes fluorescent or bioluminescent reporter genes which once expressed in cells have their light-emission properties modulated by miRNAs. For the latter, the miR-OFF system is based on extinction of reporter gene expression by miRNA binding to miRNA target sequences cloned in the 3′-UTR of the reporter gene [8]. Nowadays, this miR-OFF system is widely used in vitro for functional studies to confirm the presence of potential miRNA binding sequences in the 3′-UTR or 5′-UTR of target mRNA. This system has also been found to be successful in monitoring biogenesis and miRNA activity during neuronal differentiation [9] and tumor development [8, 10] for instance. It has also been employed as a functional screening platform to identify miRNA candidates involved in regulation of tumor-associated mRNA [11].

More recently, we [12] have developed an alternative approach, a miR-ON system, to monitor positively the endogenous expression pattern of miRNAs in cells, tissues, and small animal models. In the strategy developed, the expression of the reporter gene is not suppressed by the miRNA but is instead induced. Therefore miRNA expression in cells is signed by the emission of optical signals which can be detected by standard fluorescence or bioluminescence equipment. The overall strategy relies on engineered regulatable expression systems, also known as genetic switches [13], such as the Tet-Krab, Tet R and the Cumate gene-switch systems [14]. The system is designed so that the transcriptional regulator molecule controlling the expression of a transgene driven by an inducible promoter is placed under control of a miRNA of interest. We engineered the Cumate operon system by subcloning in the 3′-UTR of the CymR transcriptional repressorcDNA, four complementary block sequences of a given miRNA (Fig. 1) [12]. Therefore, when the miRNA of interest is expressed in cells, it binds to the CymR mRNA inducing its degradation through the RLC machinery. In the absence of CymR repressor protein, the second transcription cassette, encoding for the luciferase gene, is transcribed, generating bioluminescence signals in cells. We recently demonstrated that this RNAi-inducing-luciferase expression system, which we named RILES, enabled the monitoring of ectopic and endogenously expressed miRNAs in cell lines and also in tissues of live anesthetized animals. We monitored the expression of miRNA-122 in the liver of mice and the differential expression pattern of myomiRs-133, -1 and -206 expressed in the skeletal muscle of anterior tibialis of naive mice. Furthermore, we established for the first time in mice, the kinetic of a miRNA during the development of a pathological process over a period of 35 days without repeated administration of RILES probes. Using a model of muscular atrophy we were able to determine the kinetic of miRNA-206 expression during the muscle regeneration phase of muscle atrophy. The bioluminescence data

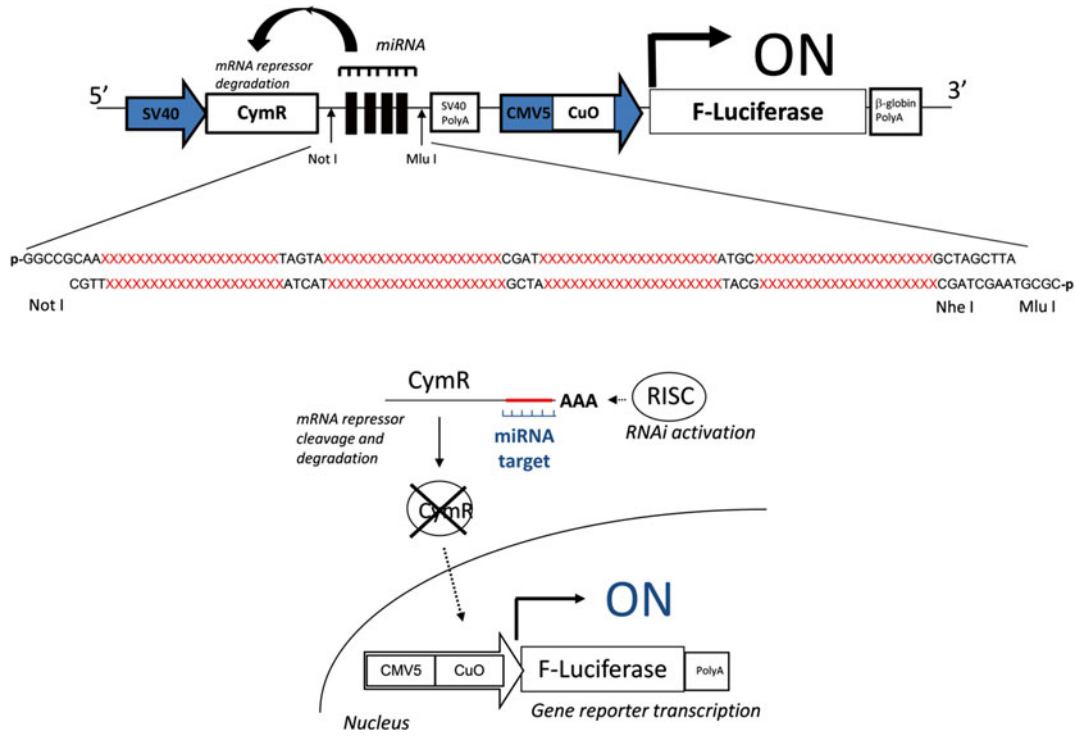

Fig. 1 Schematic representation of the RILES method. When present in cells, target miRNA binds to the four complementary-block sequences located in the 3′-untranslated region of the CymR repressor transcript and activates the RNAi silencing complex (RISC) machinery. The CymR mRNA is then cleaved and degraded, resulting in lack of repressor production. The luciferase expression system is thus switched on, generating a positive bioluminescence signal. Reprinted and adapted from [12]

indicated that the expression of miRNA-206 is individual dependent, finely regulated in a time-dependent manner, and characterized by individual heterogeneity during development of the pathology. When compared with data generated from conventional quantitative RT-PCR, miRNA-206 expression was also found to be over expressed but its expression remained constant for 7 days before returning to the basal level. This discrepancy between the two approaches is explained by the invasive nature of the quantitative RT-PCR method that generates a set of information from a heterogeneous population collected at different time points. This invasive method, in contrast to RILES, lacks temporal resolution at the individual level and thus undervalues the crucial significance of the temporal regulation of miRNA expression in response to biological processes [12].

In this chapter we describe in detail methods used to produce the RILES expression plasmid in a context of monitoring the expression of myomiR-206, -133, and -1 in the tibialis skeletal muscle of naïve mice and, as a control, the expression of miRNA-

122, a liver-specific miRNA not expressed in skeletal muscle tissue. The protocols described include the preparation of the RILES plasmids, from the cloning of the miR targeting sequence in the 3′-UTR of the CymR transcriptional repressor to the functional validation of the RILES plasmids in HEK 293 cells. Finally, we describe the procedure to monitor the expression of myomiRs in the skeletal tibialis muscle of mice following the intramuscular injections of RILES plasmids. These protocols can be adapted to monitor any other miRNA in vitro or in vivo in other tissues as long as the RILES can be transfected to the tissue of interest.

2 Materials

2.1 RILESPlasmid Design and Production

1. The RILES plasmid originates from the Cumate gene-switch, first described by Mullick et al. [14]. We prepared [12] an "all-in-one system" by assembling into a single plasmid unit, the expression cassette encoding for the CymR transcriptional repressor driven by the SV40 promoter and the inducible expression cassette encoding for the luciferase gene reporter driven by the CMV5(Cuo) inducible promoter. A multiple cloning site containing Mlu I and Not I restriction sites was inserted into the 3′-UTR of CymR cDNA, after the stop codon and before the polyadenylation site (Fig. 1) to insert a block of four perfect-match complementary sequences to miRNA (*see* **Note 1**). This block sequence, consisting of a double-stranded oligonucleotide, is called miR T sequence, standing for miRNA target sequence. Upon cloning, the RILES plasmid is denoted, for example pRILES/206T or pRILES/133T when the miR T sequence contained complementary block sequences to detect miRNA-206 or miRNA-133 respectively (Table 1).
2. To prepare the specific miR T sequences to monitor myomiR-206, -133, -1, and miRNA-122 as a control (Table 1), synthetic oligonucleotides are designed to contain, in addition to the miRNA T (*see* **Note 2**), four different nucleotide sequences, located in between the four block sequences of the miR T cassette, to ensure optimal annealing sequence match between the sense and antisense oligonucleotides. The oligonucleotides are also flanked at the 3′-end by a compatible, overhanging, phosphorylated Not I sequence, and at the 5′-end by a compatible, overhanging, phosphorylated Mlu I sequence. The sense and antisense single-stranded oligonucleotides are obtained commercially (Eurogentec, Seraing, Belgium), PAGE purified (polyacrylamide gel purification method), and coupled with a phosphate group at the 5′-end of each oligonucleotides (*see* **Note 3**). The purified oligonucleotides are resuspended in nuclease-free water to generate a 100 μM stock solution and conserved at −20 °C.

Table 1
Nucleotide sequences of the miR target subcloned in the RILES plasmids

RILES plasmids	Name	miR targeting sequence subcloned in the 3′UTR of CymR cDNA
RILES	pRILES	No RNAi targeting sequence
RILES/miR 122T	pRILES/122T	*GGCCGCAA* **CAAACACCATTGTCACACTCCA** TAGTA**CAAACACCATTGTCACACTCCA**CGAT**CAAACACCATTGTCACACTCCA**ATGC**CAAACACCATTGTCACACTCCA** *GCTAGCTTA*
RILES/miR 133T	pRILES/133T	*GGCCGCAA* **ACAGCTGGTTGAAGGGGACCAA**TAGTA**ACAGCTGGTTGAAGGGGACCAA**CGAT**ACAGCTGGTTGAAGGGGACCAA**ATGC**ACAGCTGGTTGAAGGGGACCAA** *GCTAGCTTA*
RILES/miR 2006T	pRILES/206T	*GGCCGCAA* **CCACACACTTCCTTACATTCCA**TAGTA**CCACACACTTCCTTACATTCCA**CGAT**CCACACACTTCCTTACATTCCA**ATGC**CCACACACTTCCTTACATTCCA** *GCTAGCTTA*
RILES/miR 1T	pRILES/1T	*GGCCGCAA* **TACATACTTCTTTACATTCCA**TAGTA**TACATACTTCTTTACATTCCA**CG AT**TACATACTTCTTTACATTCCA**ATGC**TACATACTTCTTTACATTCCA** *GCTAGCTTA*
RILES/miR 221T	pRILES/221T	*GGCCGCAA* **GAAACCCAGCAGACAATGTAGCT**TAGTA**GAAACCCAGCAGACAATGTAGCT**CGAT**GAAACCCAGCAGACAATGTAGCT**ATGC**GAAACCCAGCAGACAATGTAGCT** *GCTAGCTTA*

Reprinted and adapted from [12]
Bold and underlined: The four-block sequence complementary to the miRNA mature sequence of interest. Italic: *left* overhanging Not I sequence and *right* overhanging, Mlu I sequence. The other uppercase sequences correspond to the spacer sequence located in between the four block sequences of the miR T cassette

3. 10× annealing buffer: 100 mM Tris–HCl pH7.5, 1 M NaCl, 10 mM EDTA.
4. Water bath at 37 °C.
5. T4 DNA ligase with buffer, Not I and Mlu restriction enzymes (NEB, Hitchin; UK).
6. DH5 calcium-chloride-competent bacteria cells (stored at −80 °C) (NEB, Hitchin; UK).
7. LB broth and LB agar plates containing 100 μg/ml ampicillin (Life Technologies SAS, St. Aubin, France).
8. NucleoBond Xtra Mini and Maxi endotoxin-free extraction kits (Macherey-Nagel, Düren, Germany).
9. Electrophoresis grade agarose (Sigma Aldrich, St. Louis, USA), agarose gel electrophoresis equipment (Biorad, Hercules, CA, USA), ethidium bromide solution 50 μg/ml (Sigma Aldrich, St. Louis, USA).
10. 10× gel loading buffer (0.25 % bromophenol bleu, 0.25 % xylene cyanol FF, 50 % glycerol), 1 kb and 100 bp ladders (NEB, Hitchin UK), 50× TAE buffer (Sigma Aldrich, St. Louis, USA) for agarose gel, Gel Doc™ XR+ gel imaging System (Biorad, Hercules, CA, USA).

2.2 Tissue Culture and Transfection

1. HEK 293 cells (human embryonic kidney cell line, ATCC, CRL-1573) (*see* **Note 4**).
2. Complete growth media: Dulbecco's Modified Eagle Medium (DMEM, 4 g/l glucose, Life Technologies SAS, St. Aubin, France), supplemented with 10 % (vol/vol) of heat-inactivated fetal bovine serum (Life Technologies SAS, St. Aubin, France) and 100 I.U./ml penicillin and 100 μg/ml streptomycin (Life Technologies SAS, St. Aubin, France).
3. 2.5 % (vol/vol) Trypsin-EDTA, phosphate-buffered saline solution, opti-MEM medium and Trypan bleu 0.4 % (Life Technologies SAS, St. Aubin, France).
4. Tissue culture flask (25 cm^2), 24-well flat-bottom tissue culture plates, serological sterile polystyrene pipets, conical sterile polypropylene centrifuge tubes, hemocytometer (Starsted, Nümbrecht, Germany).
5. ICAFectin™ 441 (In-cell-Art, Nantes, France, or Eurogentec France SASU, Angers, France).
6. 5 nmol of synthetic miRNA precursor (Pre-miR™ miRNA precursor, AM 17100, Life Technologies SAS, St. Aubin, France) specific to miRNA-133a (PM 10412), miRNA-122 (PM 17100) and miRNA-221 (PM 12613). Theses miRNA precursors are resuspended in 1 ml of nuclease-free water to obtain a 5 μM final stock solution (*see* **Note 5**).

7. pQE30 plasmid (QIAGEN S.A.S, Courtaboeuf, France) (*see* **Note 6**).
8. Luciferase Assay System with Reporter Lysis Buffer kit (Promega France, Charbonniere, France).
9. AutoLumat LB 953 Multi-tube luminometer (Berthol France, Thoiry, France).
10. Pierce™ BCA Protein Assay Kit (Life Technologies SAS, St. Aubin, France).

2.3 Animal Experiments and Bioluminescence Imaging

1. 8-week-old female Swiss or BALB/C mice (Harlan laboratories, Paris, France).
2. Specific pathogen free (SPF) animal facility, litter, neutral pH water, individual ventilated cages, self-contained isoflurane-based anesthesia unit (FUJIFILM VisualSonics, Ontario, Canada), animal identification via ear notch (FUJIFILM VisualSonics, Ontario, Canada).
3. Amphiphilic block copolymer 704 as in vivo transfection reagent [15].
4. Tyrode salt solution (endotoxin free, Sigma Aldrich, St. Louis, USA).
5. In vivo-grade luciferin substrate (VivoGLo, Promega France, Charbonniere, France).
6. NightOWL LB in vivo imaging system (Berthol France, Thoiry, France) coupled with isoflurane-based anesthesia induction.

3 Methods

3.1 Molecular Cloning of myomiR T Sequences and Production of Recombinant RILESPlasmids

1. To anneal the miR T sequence, in a 1.5 ml Eppendorf tube, mix 0.5 nmol of sense oligonucleotides with 0.5 nmol of antisense oligonucleotides in a 20 µl final reaction volume of 1× annealing buffer. Heat the sample for 5 min at 95 °C and allow the reaction mixture to cool down to 37 °C for 30 min. The annealed miR T oligonucleotide products can be visualized on agarose gel (*see* **Note 7**) before being stored at −20 °C.
2. Digest 5 µg of RILES plasmids with 10 U of Not I and Mlu I restriction digest enzymes in a 50 µl reaction volume for 2 h at 37 °C. Gel purified the digested 6.2 kb RILES plasmid of 6.2 kb and measure absorbance at 260 nm using a spectrophotometer. A DNA band of 120 base pairs corresponding to the miR T sequence should also be detectable on the agarose gel.
3. Ligate 50 ng of purified, digested RILES plasmids with the 2 µl of a 1/250 dilution of miR T oligonucleotides from **step 1** in a 20 µl reaction volume containing 2.5 U of T4 DNA ligase.

Incubate the ligation mixture for 30 min at 25 °C (*see* **Note 8**). Stop the reaction by inactivating the ligase at 65 °C for 10 min.

4. Transform 50 μl of competent DH5a cells (2.5×10^6 pfu cells) with 5 μl of the ligation product from **step 3** according to the manufacturer's instructions (NEB, Hitchin UK). Incubate transformed bacteria on an LB agar ampicillin plate for 16 h at 37 °C.
5. The following day, pick ten individual recombinant colonies and grow each in 3 ml of LB containing 50 μg/ml of ampicillin for 16 h at 37 °C with agitation using an orbital shaker. Extract and purify the pRILES plasmids using the standard alkaline lysis method (NucleoBond Xtra Mini kit, Macherey-Nagel).
6. To identify the recombinant pRILES plasmids, containing the miR T sequence, from the parental, non-recombinant plasmid, digest 1 μg of plasmid from **step 5** with 5 U of Not I and Mlu I restriction enzymes for 1 h at 37 °C in 20 μl reaction volume. Analyse the digestion product on a 1 % agarose electrophoresis gel. A DNA band of 120 base pairs corresponding to the miR T cassette should be visible among the digested RILESplasmid DNA of 6.2 kb.
7. Amplify the corresponding positive colonies in 250 ml of LB containing ampicillin at 50 μg/ml for 16 h at 37 °C with agitation.
8. Extract the pRILES using endotoxin NucleoBond Xtra Maxi kit (Macherey-Nagel) and measure absorbance at 260 and 280 nm to estimate the concentration of the pRILES and the purity of the preparation. The RILES plasmids can be stored at −20 °C for at least 1 year without loss of activity. An aliquot is used for sequencing the plasmid to ensure specificity of oligonucleotide miR T sequences cloned in the RILES.

3.2 In Vitro Functional Validation Study Using Synthetic miRNA Mimics

1. HEK 293 cell are grown in complete medium at 37 °C, 5 % CO2, in a humidified atmosphere (tissue culture incubator). It is important that the cells are split at least twice at constant cell density to ensure optimal transfection efficiency.
2. One day before transfection, plate 1.5×10^5 cells into wells of a 24-well plate and incubate overnight in the tissue culture incubator.
3. The following day, ensure that the adherent cells have reached at least 80 % confluence. Renew the cell culture media in wells with 400 μl of serum-free media and return the plate to the tissue culture incubator.
4. Prepare the pRILES/ICAFectin complexes, according to a transfection ratio of 1/2 (μg pDNA/μl ICAfectin) (*see* **Note 9**) as recommended by the manufacturer (In Cell Art). The

following protocol is for the transfection of pRILES into 1 well of the 24-well plate. In a first Eppendorf tube (A) add 0.5 µg RILES plasmids *plus* the desired amount of miRNA precursor (*see* **Note 10**) and complete the total amount of nucleic acids to 2 µg using the pQE30 carrier plasmid (*see* **Note 6**). Adjust the final volume to 50 µl with OptiMEN medium. In a second Eppendorf tube (B) add 2 µl of ICAfectin 441 and adjust the final volume to 50 µl with OptiMEN medium. Equilibrate the tubes for 5 min at room temperature. Then add the content of tube B to tube A and homogenate the solution thoroughly by pipetting up and down at least five times. Incubate for 30 min at room temperature to allow the formation of the pRILES/ICAfectin 441 complexes.

5. Add the 100 µl complexes from **step 4** drop-by-drop into the well of the 24-well plate. Transfect the cells for 4 h in the tissue culture incubator. Thereafter, the transfection media is replaced with 500 µl of complete medium.
6. Incubate the 24-well plate for an additional 48 h in the tissue culture incubator.
7. Determine expression of the luciferase gene using the Luciferase Assay System with Reporter Lysis Buffer kit following the manufacturer's recommendations (Promega). Briefly, the cell monolayer is washed once with PBS, and dried completely before adding 100 µl of cell culture lysis reagent (CCLR). The cell monolayer is then scraped carefully using a cell scraper or alternatively using a 200 µl TIPS incurved manually to produce a right angle. The resulting cell lysate is incubated on ice for 10 min and pre-cleared by a centrifugation step at 6000 × *g* for 5 min. An aliquot of 20 µl of cell supernatant is transferred to a luminometer tube and 100 µl of Luciferase Assay Reagent containing the luciferin substrate is added to the tube using an automatic luminometer. The light emitted from the catalyzed luciferin product is recorded for a 2-s integration time. Each sample is read in duplicate to ensure accurate and reproducible results.
8. A 10 µl aliquot of pre-cleared lysate from **step 7** is used to determine the protein content in sample using the standardized BCA method (Pierce™ BCA Protein Assay Kit).
9. Relative luciferase activities (RLU) are normalized to protein content and expressed as RLU/mg of protein. The final data are represented as fold of luciferase induction relative to control cells, transfected with the RILES/miR T plasmid alone or transfected in the presence of irrelevant synthetic miRNAs, set to the arbitral value of 1. A typical example of results that can be generated is shown in Fig. 2.

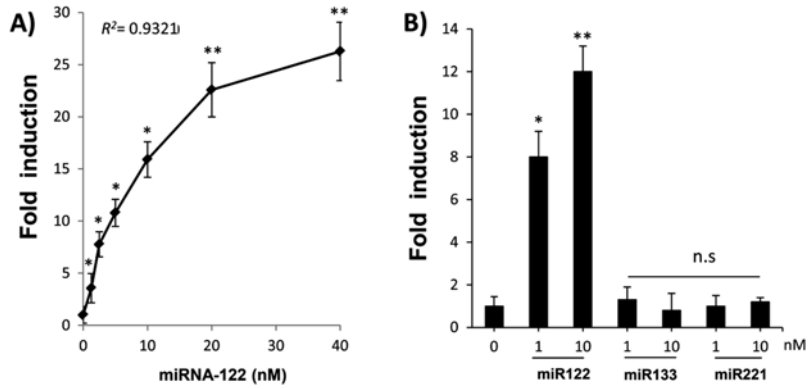

Fig. 2 Dose–response study of luciferase induction in HEK 293 cells transfected with pRILES/122 T. (**a**) The HEK 293 cells are transfected with pRILES/122 T in presence of increasing concentrations of synthetic miRNA-122 precursor. (**b**) Selective luciferase expression in HEK 293 cells transfected either with pRILES/122T in the presence of two concentrations of synthetic miRNA-122 precursor and as a control of specificity with the irrelevant synthetic miRNA-133 and miRNA-221. The luciferase expression in cells was determined 48 h post-transfection, and expressed as fold of luciferase induction relative to control cells transfected with the control pRILES plasmids, not regulated by miRNA and set to the arbitral value of 1. Data shown are the mean +/– SD of one representative experiment performed in triplicate and reproduced at least three times. Statistics using the two-tailed *t*-test, $*p<0.05$; $**p<0.01$, *n.s.* (no statistically significant difference) compared to control cells. Reprinted and adapted from [12]

3.3 In Vivo Bioluminescence Imaging of myomiRS Expression in the Tibialis Anterior Skeletal Muscles of Mice

1. Adult, 8-week-old female Swiss mice (Harlam) are housed in a specific pathogen-free (SPF) animal facility in accordance with the European Ethical Conduct and Animal Recommendation guidelines (CARE, directive 2010/63/EU).
2. A total of 15 mice are randomly separated into five groups as follows: RILES (control, non-regulated miRNA plasmid), RILES/1T (RILES plasmid containing the miRNA-1 targeting cassette), RILES/206T (RILES plasmid containing the miRNA-206 targeting cassette), RILES/133T (RILES plasmid containing the miRNA-133 targeting cassette), and the RILES/1T (RILES plasmid containing the miRNA-1 targeting cassette).
3. Two days before the intramuscular injection of RILES plasmids, the mice are anesthetized with 2.5 % isoflurane/02 (oxygen) at a flow rate of 1 l/min. Then the fur on the tibialis anterior muscles of each mouse is shaved using either a razor or an epilator cream to guide latter the intramuscular injection.
4. The day of the intramuscular injection, the pRILES/amphiphilic block copolymer 704 complexes are prepared before the mice are anesthetized. The general principle involves injecting 50 µl of solution containing 10 µg of pRILES formulated with 3 % (w/v) of amphiphilic block copolymer 704. Alternatively, the Lutrol block copolymer F-66 transfection reagent (Sigma

Aldrich, St. Louis, USA) can also be used with same results. The following protocol is for eight intramuscular injections (1 group of mice plus 2 extra volumes). In a first Eppendorf tube (A) add 200 µl of 6 % (w/v) amphiphilic block copolymer 704 (*see* **Note 11**) prepared in tyrode solution at pH 7.6. In a second Eppendorf tube (B) add 80 µg of pRILES and complete the volume to 200 µl using the tyrode solution at pH 7.6. Equilibrate the tubes for 5 min at room temperature. Then add the content of tube B to tube A and homogenate the solution thoroughly by pipetting up and down at least five times. Incubate for 30 min at room temperature to allow the formation of pRILES/amphiphilic block copolymer 704 complexes. The complexes are stable for at least 2 h at room temperature.

5. Before the intramuscular injection of the pRILES/amphiphilic block copolymer 704 complexes, the mice are first anesthetized as described in **step 3**. The intramuscular injection involves a rapid injection 50 µl of pRILES/amphiphilic block copolymer 704 complexes (*see* **Note 12**) at one site in the proximal region of the tendon tibialis (*see* **Note 12**). The injection is performed using a microfine insulin syringe (U100). Thereafter, the mice are returned to the cage and placed under surveillance until their behavior returns to normal.
6. Six days (*see* **Note 13**) later the mice are injected intraperitoneally with the luciferin substrate (1.5 mg/mouse prepared in PBS). Five minutes after the injection (*see* **Note 14**), the mice are anesthetized with isoflurane as described in **step 3** and placed in the bioluminescence scanner, connected to an isoflurane ventilation system to maintain constant anaesthesia. The first bioluminescence scan starts exactly 10 min after the injection of luciferin. The acquisition parameters are as follows: 2 min integration time, F/Stop, binin 8. At the end of the scan, a picture of the mouse is taken to enable bioluminescence images to be superposed. Final data are expressed as photons/second/pixel from reconstructed superposed images. A typical example of results generated is shown in Fig. 3.

4 Notes

1. The nucleotide sequence of mature miRNAs can be found from the miRNA data base as miR base (http://www.mirbase.org/). It is important to specify the species of miRNA. MiRNA nucleotide sequences from the same annotated miRNA can vary slightly from species to species, for instance from human to mice.
2. The number of the miR T block sequence can be adjusted from 2 to 8. Previous reports have demonstrated that a minimum of two block sequences are sufficient to repress expres-

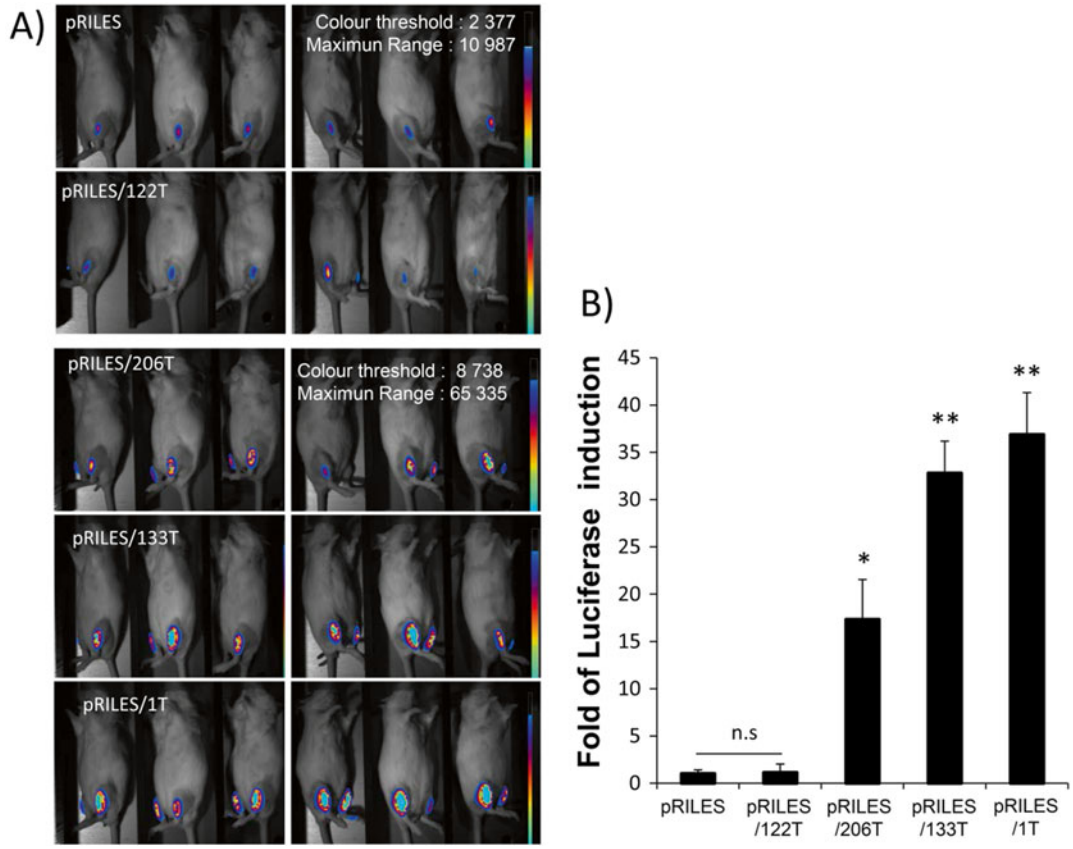

Fig. 3 Noninvasive bioluminescence imaging of the muscle-specific myomiRs-206, -133, and -1 in mice. 8 μg pRILES/133T, pRILES/1T, and pRILES/206T were formulated with the amphiphilic block polymer 704 transfection reagent and intramuscularly injected in the left and right tibialis anterior to transfect the skeletal muscles of Swiss mice. Negative control included the pRILES, not regulated by miRNA and the pRILES/122T, regulated by the miRNA-122, a liver specific miRNA not expressed in the mouse tibialis skeletal muscle. Bioluminescence imaging was performed 6 days later and light emission quantified using regions of interest covering the lower legs of the mice. (**a**) Representative bioluminescence images collected in the lower left legs of mice. (**b**) Quantitative bioluminescence values detected in the mice described in (**a**) and expressed as luciferase induction relative to the control pRILES group of animals set arbitrarily to the value of 1. Error bars in (**b**), mean +/− SEM ($n=6$) of one representative experiment repeated at least three times. Statistics using the two-tailed *t*-test, *$p<0.05$; **$p<0.01$ *n.s.* (no statistically significant difference) compared with the pRILES control group. Reprinted and adapted from [12]

sion of the target gene [16, 17]. In our study, we found that four complementary block sequences of a miRNA were optimal to switch on the RILES in cells.

3. Sense and antisense oligonucleotides are chemically synthesized with a 5′-end phosphate group to allow the direct ligation of the annealed miR T oligonucleotide to the digested RILES plasmid.
4. HEK 293 cells are easy to transfect enabling both efficient expression of the RILES plasmids and delivery of miRNA mimics in a large proportion of the same cells. We recommend

determining the endogenous expression level of the studied miRNAs in these cells by quantitative RT-PCR. Elevated endogenous expression of miRNAs in these cells will in turn elevate the basal expression level of luciferase gene in the cells transfected with the pRILES/miR T plasmid alone. This could compromise the dose response study carried out with increasing doses of synthetic miRNA precursors.

5. There are two types of commercially available synthetic miRNA agonists developed by Ambion and distributed by Life technology. The first generation consists in the miR precursor (Pre-mir™ miRNA Precursor) and the second (latest generation) consists in the miR mimics (*mir*Vana® miRNA mimic). Recently (unpublished data), we found that the miR mimics are up to ten times more potent in switching on the RILES than the miR precursors at the same final concentration.
6. We usually normalize our transfection condition to a final amount of 2 μg of nucleic acids (RILES*plus* synthetic miRNA precursors) to ensure that all formulated nucleic acids are the same from well to well. The amount and nature of nucleic acids formulated with the transfection reagent impact directly on the size and charge of nanoparticles formed after complexation and consequently on the transfection efficiency. This normalization procedure could also be carried out with the widely used "empty plasmid" or "mock plasmid".
7. One aliquot of the annealed double-stranded miR T oligonucleotides can be analyzed on 3 % TAE/agarose gel to differentiate the double-stranded oligonucleotides from the single-stranded, non-annealed oligonucleotides. Upon electrophoretic migration, the double-stranded oligonucleotides migrate the same distance to the 200 bp DNA band of a 1 kb ladder, while the single-stranded oligonucleotides migrate the same distance to the 100 bp DNA of the 1 kb ladder.
8. A negative control of this experiment includes the commonly used "self-ligation product" which is obtained by carrying out the same procedure, but without adding the miR T oligonucleotides in the reaction volume. This step is not strictly necessary but allows the efficiency of the ligation reaction to be predicted, enabling an estimation of the total number of bacterial colonies which need to be screened to identify colonies containing the recombinant pRILES plasmid.
9. Other transfection reagent such as Lipofectamine 2000 (Life Technologies SAS, St. Aubin, France) could also be used.
10. We recommend that each experiment includes the following samples in triplicate: (1) HEK 293 cells transfected with pRILES/122T alone, (2) HEK 293 cells transfected with

pRILES/122T *plus* 4 μl (20 μmol) of stock miRNA 122 precursor solution to generate a final concentration of miRNA-122 precursor of 40 nM during the transfection procedure (*see* **step 5** from Subheading 3), (3) HEK 293 cells transfected with pRILES/122T *plus* 2 μl (10 μmol) of stock miRNA 122 precursor solution to generate a final concentration of miRNA-122 precursor of 20 nM during the transfection procedure, (4) HEK 293 cells transfected with pRILES/122T *plus* 1 μl (5 μmol) of stock miRNA 122 precursor solution to generate a final concentration of miRNA-122 precursor of 10 nM during the transfection procedure, (5) HEK 293 cells transfected with pRILES/122T *plus* 0.5 μl (0.25 μmol) of stock miRNA 122 precursor solution to generate a final concentration of miRNA-122 precursor of 0.5 nM during the transfection procedure, (6) HEK 293 cells transfected with pRILES/122T *plus* 0.25 μl (0.125 μmol) of stock miRNA 122 mimic solution to a final concentration of miRNA-122 mimics of 0.25 nM during the transfection procedure, and (7) HEK 293 cells transfected with pRILES/122T *plus* 0.125 μl (0.625 μmol) of stock miRNA 122 mimic solution to generate a final concentration of miRNA-122 mimics of 0.125 nM during the transfection procedure. As a control, the HEK 293 cells are transfected with pRILES/122T *plus* 1 or 10 nM final concentration of irrelevant miRNA such as miRNA-133 precursor or miRNA-206 precursor (*see* Fig. 2).

11. We recommend preparing the amphiphilic block copolymer 704 solution the day before the intramuscular injection and leaving the solution at 4 °C overnight. We noticed that the transfection efficacy of the tibialis anterior skeletal muscle is optimal under this condition.
12. A rapid intramuscular injection (approximately 3 s) of the formulated RILES plasmids in the tibialis anterior muscle increases the efficacy of gene transfer in the skeletal muscle tissue. This procedure aims to mimic the principle of hydrodynamic injection of pDNA as described in detail in [18].
13. Optimal gene expression of pRILES is detected 6 days after the intramuscular injection although a minimum of 2 days is sufficient to detect significant bioluminescent signals in the tibialis skeletal muscle of the mice.
14. It is recommended to administrate the luciferin substrate to non-anesthetized mice to allow optimal diffusion of the substrate in the whole-body animal tissue. Moreover, to ensure equal and homogenate diffusion of the luciferin in all the group of mice, the scanning of the mice should start exactly 10 min after the intraperitonial injection of the luciferin substrate.

Acknowledgments

This work was supported by *La ligue Contre leCancerdu Loiret*, *Région Centre*. We would like thank the staff of the CIPA animal facility (TAAM/CIPA, CNRS UPS 44, Orléans) for their technical assistance and access to the Lumina Bioluminescence scanner. In addition, we would like to thank Dr. Lily Mijouin for helping in the preparation of the manuscript for this chapter.

References

1. Winter J, Jung S, Keller S, Gregory RI, Diederichs S (2009) Many roads to maturity: microRNA biogenesis pathways and their regulation. Nat Cell Biol 11:228–234
2. Lee RC, Feinbaum RL, Ambros V (1993) The C. elegans heterochronic gene lin-4 encodes small RNAs with antisense complementarity to lin-14. Cell 75:843–854
3. Berezikov E (2011) Evolution of microRNA diversity and regulation in animals. Nat Rev Genet 12:846–860
4. Kole R, Krainer AR, Altman S (2012) RNA therapeutics: beyond RNA interference and antisense oligonucleotides. Nat Rev Drug Discov 11:125–140
5. Kloosterman WP, Plasterk RH (2006) The diverse functions of microRNAs in animal development and disease. Dev Cell 11:441–450
6. Sayed D, Abdellatif M (2011) MicroRNAs in development and disease. Physiol Rev 91:827–887
7. Dong H, Lei J, Ding L, Wen Y, Ju H, Zhang X (2013) MicroRNA: function, detection, and bioanalysis. Chem Rev 113:6207–6233
8. Ko HY, Lee YS, Kim S (2014) Bioluminescence reporter gene-based detection of microRNAs. Methods Mol Biol 1098:85–95
9. Ko MH, Kim S, Hwang do W, Ko HY, Kim YH, Lee DS (2008) Bioimaging of the unbalanced expression of microRNA9 and microRNA9* during the neuronal differentiation of P19 cells. FEBS J 275:2605–2616
10. Kim HJ, Kim YH, Lee DS, Chung JK, Kim S (2008) In vivo imaging of functional targeting of miR-221 in papillary thyroid carcinoma. J Nucl Med 49:1686–1693
11. Maurel M, Jalvy S, Ladeiro Y, Combe C, Vachet L, Sagliocco F, Bioulac-Sage P, Pitard V, Jacquemin-Sablon H, Zucman-Rossi J, Laloo B, Grosset CF (2013) A functional screening identifies five microRNAs controlling glypican-3: role of miR-1271 down-regulation in hepatocellular carcinoma. Hepatology 57:195–204
12. Ezzine S, Vassaux G, Pitard B, Barteau B, Malinge JM, Midoux P, Pichon C, Baril P (2013) RILES, a novel method for temporal analysis of the in vivo regulation of miRNA expression. Nucleic Acids Res 41, e192
13. Stieger K, Belbellaa B, Le Guiner C, Moullier P, Rolling F (2009) In vivo gene regulation using tetracycline-regulatable systems. Adv Drug Deliv Rev 61:527–541
14. Mullick A, Xu Y, Warren R, Koutroumanis M, Guilbault C, Broussau S, Malenfant F, Bourget L, Lamoureux L, Lo R, Caron AW, Pilotte A, Massie B (2006) The cumate gene-switch: a system for regulated expression in mammalian cells. BMC Biotechnol 6:43
15. Chevre R, Le Bihan O, Beilvert F, Chatin B, Barteau B, Mevel M, Lambert O, Pitard B (2011) Amphiphilic block copolymers enhance the cellular uptake of DNA molecules through a facilitated plasma membrane transport. Nucleic Acids Res 39:1610–1622
16. Brown BD, Venneri MA, Zingale A, Sergi Sergi L, Naldini L (2006) Endogenous microRNA regulation suppresses transgene expression in hematopoietic lineages and enables stable gene transfer. Nat Med 12:585–591
17. Brown BD, Gentner B, Cantore A, Colleoni S, Amendola M, Zingale A, Baccarini A, Lazzari G, Galli C, Naldini L (2007) Endogenous microRNA can be broadly exploited to regulate transgene expression according to tissue, lineage and differentiation state. Nat Biotechnol 25:1457–1467
18. Suda T, Liu D (2007) Hydrodynamic gene delivery: its principles and applications. Mol Ther 15:2063–2069

Chapter 16

MicroRNA Imaging in Combination with Diagnostic Ultrasound and Bubble Liposomes for MicroRNA Delivery

Yoko Endo-Takahashi, Yoichi Negishi, Ryo Suzuki, Kazuo Maruyama, and Yukihiko Aramaki

Abstract

MicroRNA (miRNA) is expected to play an important role in the diagnosis and therapy of various diseases. In miRNA therapy, the development of delivery tools to the target site is considered to be essential. By using a delivery tool possessing imaging ability, miRNA colocalized with the carrier could be visualized after administration. We prepared polyethylene glycol (PEG)-modified liposomes containing echo-contrast gas, "Bubble liposomes" (BLs), and confirmed that BLs containing cationic lipid were capable of loading miRNA. Furthermore, we also achieved the imaging and delivery of systemically injected miRNA to target site in combination with ultrasound exposure. MiRNA-loaded BLs could be a useful tool for imaging and therapy.

Key words miRNA, Liposome, Ultrasound imaging

1 Introduction

MicroRNA (miRNA) is an endogenous noncoding small RNA that negatively regulates gene expression at the posttranscriptional level in various processes. MiRNA is considered to play a crucial role in development, differentiation, proliferation, and survival. It is becoming increasingly clear that the abnormal expression of miRNA is causally related to a variety of disease states. Therefore, miRNA is expected to have great potential in disease diagnosis. Furthermore, miRNA-based therapies are considered to have great promise. In miRNA therapy, however, the development of a delivery tool to the target site is necessary, as are therapies with other nucleic acids.

We previously developed polyethylene glycol (PEG)-modified liposomes containing echo-contrast gas, "Bubble liposomes" (BLs). We reported that BLs could function as a plasmid DNA (pDNA) and small interfering RNA (siRNA) delivery tool in combination with ultrasound (US) exposure in vitro and in vivo [1–5].

Zdravka Medarova (ed.), *RNA Imaging: Methods and Protocols*, Methods in Molecular Biology, vol. 1372,
DOI 10.1007/978-1-4939-3148-4_16,

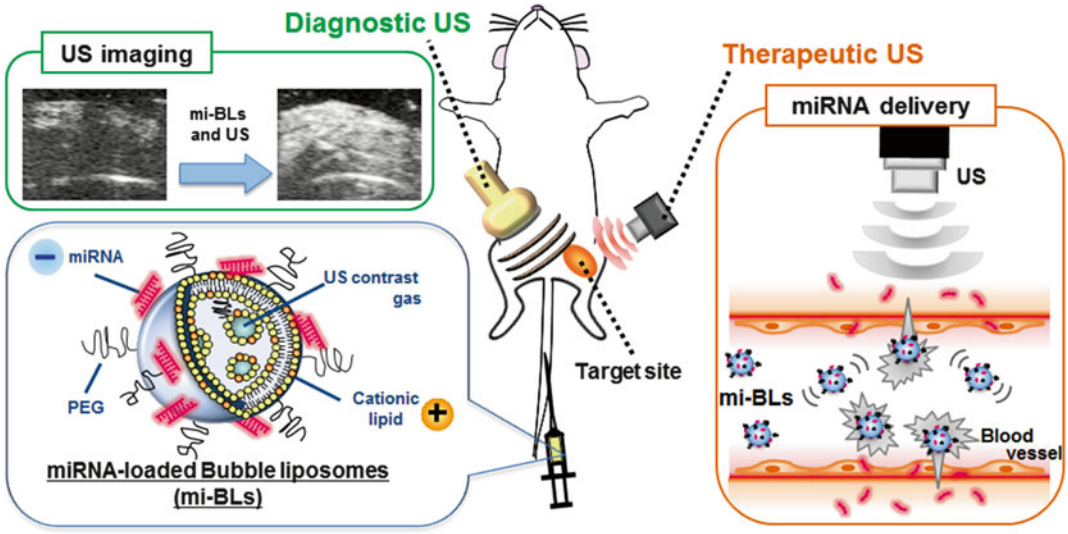

Fig. 1 Scheme of miRNA-loaded Bubble liposomes (mi-BLs) for the imaging and delivery of miRNA

Furthermore, to increase the efficiency of nucleic acid delivery via systemic administration, we prepared pDNA-loaded BLs (p-BLs) and siRNA-loaded BLs (si-BLs) using a cationic lipid [6–8]. These types of BLs could colocalize with nucleic acids in blood vessels after intravenous administration and improve the stability of nucleic acids in the presence of serum. BLs could also function as a US contrast agent. Therefore, nucleic acid-loaded BLs allow not only effective gene delivery and but also US imaging for delineating the process of gene delivery.

The term "theranostics," which is derived from "therapeutics" and "diagnostics," refers to a therapeutic strategy combined with a diagnostic examination and a specific therapy based on the examination results. BLs could also be effective tools for diagnosis. The combination of BLs and US has strong potential to become a theranostic agent and to have beneficial clinical applications for various diseases.

We prepared miRNA-loaded BLs (mi-BLs) [9]. The interaction of BLs with miRNA could be confirmed by analyzing with flow cytometry and measuring optical density. Several tens of seconds after administration, mi-BLs could be visualized as a USimage at our target site of the hindlimb by diagnostic US. In fact, the effect of miRNA delivery could also be seen when applying therapeutic US exposure (Fig. 1). This method is useful for miRNA imaging to confirm the accessibility to the target site.

2 Materials

2.1 Liposomes and BLs

1. Lipids: 1,2-Distearoylphosphatidylethanolamine-methoxy-polyethylene glycol (PEG_{2000}) and 1,2-distearoyl-sn-glycero-phosphatidylcholine (DSPC) were purchased from NOF Corporation (Tokyo, Japan). Cationic lipid and 1,2-distearoyl-3-dimethylammonium-propane (DSDAP) were purchased from Avanti Polar Lipids (Alabaster, AL) (*see* **Note 1**).
2. HEPES-buffered glucose (HBG buffer): 5 % Glucose, 10 mM HEPES, pH 7.0.
3. Filter: Sizing filter (Nuclepore Track-Etch Membrane, 200-nm pore size; Whatman plc, Kent, UK) and 0.45 μm syringe filter (Asahi Techno Glass Co., Chiba, Japan).
4. 5 mL vial (Maruemu Co., Osaka, Japan).
5. Ultrasound imaging gas: Perfluoropropane gas (Takachiho Chemical Inc. Co. Ltd., Tokyo, Japan).
6. Color solution: 6 mL HCl, 0.266 g $(NH_4)_6Mo_7O_{24} \cdot 4H_2O$, 1 g ascorbic acid in 100 mL (*see* **Note 2**).

2.2 miRNA

1. miRNA: FITC-labeled miRNA and non-labeled miRNA were purchased from BONAC Corporation (Fukuoka, Japan) (*see* **Note 3**).

2.3 USImaging

1. DiagnosticUS machine: Aplio80 (Toshiba Medical Systems, Tokyo, Japan) and 12 MHz transducer (*see* **Note 4**).

3 Methods

3.1 Preparation of Liposomes and Bubble Liposomes

1. Mix DSPC, DSDAP, and PEG_{2000} at a molar ratio of 64:30:6 and dissolve in 1:1 (v/v) chloroform/diisopropylether. Add HBG buffer to the lipid solution and sonicate the mixture for 4 min (*see* **Note 5**). Then evaporate and completely remove the organic solvent. Adjust the size of the liposomes to less than 200 nm using extrusion equipment and a sizing filter. After sizing, sterilize the liposomes using a 0.45 μm syringe filter.
2. The liposome concentration was determined using a phosphorus assay. Add 25 μL H_2SO_4 and HNO_3 to 50 μL standards (0–4.0 mM KH_2PO_4) or diluted samples. Heat at 200 °C for 1 h. Add 3 mL color solution and incubate at 60 °C for 2 min. Place samples in ice water to stop the reaction. Measure the absorbance of samples at a wavelength of 820 nm.

3. Add 2 mL liposome suspension (total lipid concentration: 1 mg/mL) to a 5 mL sterilized vial with perfluoropropane gas. Cap the vial and pressurize with 7.5 mL perfluoropropane gas. Sonicate the vial in a bath sonicator (42 kHz, 100 W; Bransonic 2510J-DTH; Branson Ultrasonics Co., Danbury, CT) for 5 min to form BLs (*see* **Note 6**).

3.2 Preparation of miRNA-Loaded Bubble Liposomes (mi-BLs)

1. Add 50 pmol FITC-miRNA to 60 μg BLs and mix gently.
2. Suspend mi-BLs in 500 μL HBG buffer and analyze the fluorescence intensity using a FACSCanto (Becton Dickinson, San Jose, CA) to examine the interaction between miRNA and BLs.
3. Centrifuge the solution of mi-BLs at 650 *g* for 1 min and remove the unbound miRNA as previously reported [10] (*see* **Note 7**). Boil the BL solution and aqueous solution containing unbound miRNA for 5 min to solubilize the BLs and prevent background scattering. Measure the optical density at 260 nm using a spectrophotometer to quantify the amount of miRNA loaded onto the BL surfaces.

3.3 USImaging

1. Anesthetize 5-week-old male ICR mice, shave the hair on the hindlimb, and coat the site with US gel.
2. Inject 200 μL mi-BL solution into the tail vein (*see* **Note 8**).
3. Place a 12 MHz ultrasound transducer on the hindlimb and examine using an Aplio80 with contrast harmonic imaging at a mechanical index of 0.27 (*see* **Note 9**).

4 Notes

1. Each lipid should be substituted with nitrogen gas to avoid oxidation.
2. Ascorbic acid should be added after complete dissolution of ammonium molybdate and the color solution should be prepared just before use.
3. When dealing with miRNA, sterile and disposable instruments should be used to maintain an RNase-free environment.
4. Frequency of the US transducer should be appropriate to the target site.
5. Sonication should continue until the organic phase has homogenously mixed with the aqueous phase.
6. The vials need to be kept under high pressure to avoid degassing the solution of BLs. Therefore, BLs should be prepared from liposomes just before use.

7. Point of Pasteur pipette was sealed by heating with a gas burner. The solution of mi-BLs was placed in the pipette and centrifuged, protecting the pipette against breaking, at approximately 650 × g for 1 min.
8. Volume and concentration of mi-BL solution should be appropriate to the target site.
9. Several tens of seconds after administration, mi-BLs could be visualized for approximately 10–20 min. If enhanced brightness is undetectable, encapsulation of echo-contrast gas in liposomes might be inadequate.

References

1. Suzuki R, Takizawa T, Negishi Y et al (2007) Gene delivery by combination of novel liposomal bubbles with perfluoropropane and ultrasound. J Control Release 117: 130–136
2. Suzuki R, Takizawa T, Negishi Y et al (2008) Tumor specific ultrasound enhanced gene transfer in vivo with novel liposomal bubbles. J Control Release 125:137–144
3. Suzuki R, Takizawa T, Negishi Y et al (2008) Effective gene delivery with novel liposomal bubbles and ultrasonic destruction technology. Int J Pharm 354:49–55
4. Negishi Y, Endo Y, Fukuyama T et al (2008) Delivery of siRNA into the cytoplasm by liposomal bubbles and ultrasound. J Control Release 132:124–130
5. Negishi Y, Omata D, Iijima H et al (2010) Enhanced laminin-derived peptide AG73-mediated liposomal gene transfer by bubble liposomes and ultrasound. Mol Pharm 7:217–226
6. Negishi Y, Endo-Takahashi Y, Matsuki Y et al (2012) Systemic delivery systems of angiogenic gene by novel bubble liposomes containing cationic lipid and ultrasound exposure. Mol Pharm 9:1834–1840
7. Endo-Takahashi Y, Negishi Y, Kato Y et al (2012) Efficient siRNA delivery using novel siRNA-loaded Bubble liposomes and ultrasound. Int J Pharm 422:504–509
8. Endo-Takahashi Y, Negishi Y, Nakamura A et al (2013) pDNA-loaded Bubble liposomes as potential ultrasound imaging and gene delivery agents. Biomaterials 34:2807–2813
9. Endo-Takahashi Y (2014) Systemic delivery of miR-126 by miRNA-loaded Bubble liposomes for the treatment of hindlimb ischemia. Sci Rep 4:3883
10. Haag P, Frauscher F, Gradl J et al (2006) Microbubble-enhanced ultrasound to deliver an antisense oligodeoxynucleotide targeting the human androgen receptor into prostate tumours. J Steroid Biochem Mol Biol 102:103–113

INDEX

Zdravka Medarova (ed.), *RNA Imaging: Methods and Protocols*, Methods in Molecular Biology, vol. 1372,
DOI 10.1007/978-1-4939-3148-4, © Springer Science+Business Media New York 2016

F

G

H

I

K

L

M

N

O

P

Q

R

S

T

U

V

W

X